Sustainable and Green Composite Functional Hydrogels: Synthesis, Characterization and Performance Evaluation

A Thesis
Submitted in Partial Fulfillment of the Requirements for the Degree of

DOCTOR OF PHILOSOPHY

By

Kajal Ingtipi

Department of Chemical Engineering
Indian Institute of Technology Guwahati
Guwahati –781039, India

May 2023

Dedicated

to

Almighty, My Family,

and My Mentor

Department of Chemical Engineering
Indian Institute of Technology Guwahati
Guwahati –781039, India

STATEMENT

I hereby declare that the content embodied in this thesis entitled "**Sustainable and Green Composite Functional Hydrogels: Synthesis, Characterization and Performance Evaluation**" is the result of investigation carried out by me in the Department of Chemical Engineering, Indian Institute of Technology Guwahati, Assam, India, under the guidance of **Prof. V. S. Moholkar**.

In keeping with the general practice of reporting scientific observations, due acknowledgment have been made wherever the work describe is based on the findings of other investigators.

May, 2023

Kajal Ingtipi
(Roll no. 166107029)

Department of Chemical Engineering
Indian Institute of Technology Guwahati
Guwahati –781039, India

CERTIFICATE

It is certified that the work contained in the thesis entitled "**Sustainable and Green Composite Functional Hydrogels: Synthesis, Characterization and Performance Evaluation**" by **Kajal Ingtipi (Roll no. 166107029)** has been carried out under my supervision in the Department of Chemical Engineering, Indian Institute of Technology Guwahati, Assam, India and this work has not been submitted elsewhere for a degree.

May, 2023

Prof. Vijayanand S. Moholkar
HAG Professor
Department of Chemical Engineering and
School of Energy Science and Engineering
Indian Institute of Technology Guwahati
Assam, India – 781 039

ACKNOWLEDGEMENTS

This thesis marks the end of my cherished memories at IIT Guwahati. Is gives me immense pleasure to express my deepest gratitude to everyone who made this possible and constantly encouraged me during my research work.

First and foremost, I express my deep sense of gratitude to my thesis supervisor ***Prof. Vijayanand S. Moholkar*** for his valuable suggestions, encouragement and constant support throughout my research work. He has provided an intriguing environment to work with freedom which cultivated my interest towards the topic. His illustrious guidance and effusive co-operation, encouraging interactions has always been a driving force for me in this project.

I would like to acknowledge my sincere gratitude to my doctoral committee members, ***Prof. G. Pugazhenthi***, ***Prof. P. Ghosh***, and ***Prof. S. Kanagraj*** for their insightful advices and suggestions throughout the research.

I am grateful to the faculty and staff members of Department of Chemical Engineering and Central Instruments Facilities (CIF) for providing various analytical facilities to carry out my research work. I am also thankful to the Indian Institute of Technology Guwahati for providing me with the state of the art infrastructure for advance level of research.

I would like to acknowledge Ahmedabad Textile Industry's Research Association (ATIRA) for providing limiting oxygen index (LOI) and cone calorimetry facility. I also acknowledge the CHNS elemental analysis facility provided by the Research and development Indian Institute of Technology Kanpur and Guwahati Biotech Park.

I am thankful to my seniors (*Dr. Ritesh Malani, Dr. Arup Bora, Dr. Kuldeep Roy, Dr, Amit Batghare, Dr. Neha Singh, and Dr. Niharika Kashyap*) for their valuable suggestions. I extend my thanks and gratitude to my colleagues (*Dr. Bhaskar, Udangshree, Karan, Aradhana, Pushpita, Rishiraj, Avinash, Komal, Umesh*) for their help and enthusiastic company. I am thankful to my special friends(my extended

family) Dr. Jinesh, *Dr. Sushma, Dr. Surabhi, Dr. Sutapa, Dr. Siddharth, Dr. Piyal and Nilanjana* for their precious companionship and support throughout this journey.

My final words go to my beloved family for their support, care, and encouragement. I am highly indebted to my ***Family*** whose endless love and blessing has made me come this far.

Kajal Ingtipi

Abstract

Hydrogels are the most versatile multifaceted polymer material which is widely applied in biomedical devices, bioelectronics, drug delivery, water remediation, and recently as fire retardants. The demand for low carbon footprint encourages the world to develop environmentally friendly and sustainable hydrogels. To achieve sustainability, the idea of valorizing waste biomass to formulate biomass-based hydrogel has become the primary focus of many researches. In this thesis, we have tried to valorize extracted components of *Arundo donax* namely, cellulose and lignin to formulate biomass-based hydrogels. The lignin extracted was irregular shaped and difficult to disperse in water. This particular problem was resolved by reducing the size of the lignin particles. Two different methods were opted to synthesize nano sized lignin particles. In the first method, lignin was ultrasonicated to produce nano sized lignin (10 to 50 nm). In the second method acetone–water cosolvent method (coprecipitation) was opted to produce core and shell structured spherical lignin particles (50–200 nm). These lignin particles were doped in PVA–Chitosan (CS) and PVA–xanthan gum (XG) blends respectively to formulate biopolymer based hydrogels. These lignin particles act as reinforcements and substantially improved the elastic moduli (G′) of the formulated hydrogels. Ultrasonicated lignin was further utilized to disperse multiwalled carbon nanotubes (MWCNT) in water and incorporated in PVA–CS blend to developed physically crosslinked conducting hydrogel. The conductivity of the formulated hydrogel was determined by electrochemical impedance spectroscopy (EIS) measurement. The conductivity of the formulated hydrogel was estimated at around 8.22 mS cm^{-1} for 1% MWCNT incorporation. The spherical lignin obtained as a result of the coprecipitation method was doped in basified PVA–XG and crosslinked by $Na_2B_4O_7$. This hydrogels was regenerated on cotton fabric to obtain PVA–XG–LNP hydrogel coating which substantially reduced the flammability of cotton cloth. Cellulose, another component extracted from biomass is extremely susceptible to fire. To improve its fire retardancy cellulose hydrogel was formulated by dissolving cellulose in NaOH/Urea mixture and crosslinking it with methylene bisacrylamide (MBA). To further improve the fire retardancy kaolin was added to the hydrogel matrix. The cellulose hydrogels were regenerated on cotton fabric to impart fire retardancy to cotton fabric. The efficacy of fire retardancy was validated by performing a cone calorimetry test (CCT),

vertical flammability test (VFT), open fire test (OFT), and measuring the limiting oxygen index (LOI). Further, the swelling and water retention ability of the fire retardant hydrogels were measured to check the water encapsulating and retaining potency. The network parameter of the hydrogels (mesh size, crosslinking density, and molecular weight between crosslinks) was also estimated using the results from the swelling test and elastic moduli (estimated by rheological studies). The results state that incorporation of 20% v/v LNPs in 2% w/v NaOH PVA–XG solution and 0.4% w/v $Na_2B_4O_7$ crosslinker induced substantial crosslinking and hence increment in moduli and reduction in swelling ability and water retention ability was observed. Similarly, the incorporation of 2% w/v kaolin and a high amount of MBA followed similar findings. Performing thermal analysis of the hydrogels confirmed that the hydrogel formulated were highly thermally stable and high char producing (34.61 wt.% for PVA–XG–20% v/v LNPs hydrogel and 63 wt% for 2% w/v kaolin incorporated cellulose hydrogel). All these results postulate the successful synthesis of biomass extracted component based hydrogel and its application as conducting hydrogel and hydrogel fire retardants.

CONTENTS

LIST OF TABLES

LIST OF FIGURES

ABBREVIATIONS

AD	*Arundo donax*
AIL	Acid insoluble lignin
ASL	Acid soluble lignin
CCT	Cone calorimetry test
CNT	Carbon nanotube
CS	Chitosan
EDX	Energy-dispersive X-ray analysis
EIS	Electrochemical impedance spectroscopy
FESEM	Field Emission Scanning electron microscopy
FETEM	Field Emission Transmission electron microscopy
FTIR	Fourier transform infrared spectroscopy
GPC	Gel permeation chromatography
HPLC	High-performance liquid chromatography
LOI	Limiting oxygen index
LNP	Lignin nanoparticles
MBA	Methylene bisacrylamide
MWCNT	Multi wall carbon nanotube
NREL	National Renewable Energy Laboratory
OFT	Open fire test
PEG	Poly ethylene glycol
PVA	poly(vinyl alcohol)
THF	Tetrahydrofuran
TGA	Thermogravimetric analysis
VFT	Vertical flammability test
XG	Xanthan gum
XRD	X-ray diffraction
XPS	X-ray photoelectron spectroscopy

भारतीय प्रौद्योगिकी संस्थान गुवाहाटी
Indian Institute of Technology Guwahati

CHAPTER 1

Introduction and Literature Review

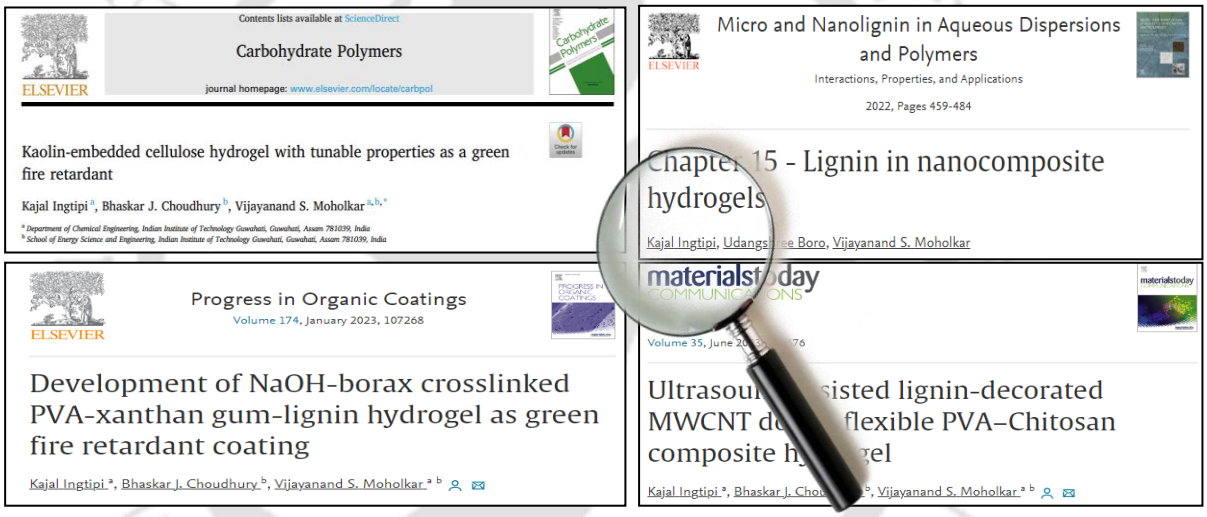

CHAPTER 1

INTRODUCTION AND LITERATURE REVIEW

1.1 Sustainable and green hydrogel

Environmental pollution and contamination is a major issue in the present world. The use of non-biodegradable and nonrenewable materials poses a hindrance in attaining sustainability as well as achieving a lesser carbon footprint. This predicament steers a continuous demand for sustainable and environmentally friendly materials. Hydrogels are modern-day smart materials that find applications in diverse fields. To satiate this demand, research in developing innovative crosslinked hydrogels based on renewable resources is increasing day by day.[1] Recent years have seen the world opting for more sustainable materials and routes for hydrogel synthesis. Nature is an abundant source of sustainable and renewable material. Rigorous research and development portray plant (cellulose, hemicellulose and lignin) and biomass (seaweed, bacteria, crab shell, gum, protein etc.) as an excellent source to produce biopolymers (viz. agarose, alginate, xanthan gum, chitosan, guar gum, gellan gum, starch etc.). These biopolymers are biodegradable, biocompatible, and widely exploited to develop sustainable gels and hydrogels.[2] Gels are 3D crosslinked networks of polymers in a fluid that are capable of retaining their shape under the action of their own weight.[3] Developed in 1960 by Wichterle and Lim[4], hydrogels are crosslinked hydrophilic gels with water as its main constituent. It has an enormous water-absorbing ability, imparted by numerous hydrophilic functional groups (viz. –$CONH_2$, –CONH, –OH, –COOH, and –SO_3H). Also, the degree of polymer crosslinking, osmotic pressure, and capillary action encourages hydrogel to absorb

and hold a substantial amount of water.[5] This also restricts the dissolution of the polymer network in the solvent.[6] Additionally, hydrogels are biocompatible materials with easily tunable properties. All these traits make hydrogels a multifunctional material. Hence, these materials are suitable for a wide range of applications, such as biomedical, agriculture, tissue engineering, water remediation, bioelectronics, and flexible electronics, and recently as hydrogel fire retardants.

In this thesis, we have reported our studies on the synthesis of composite hydrogels and attempted to resolve common problems faced during the synthesis of conducting hydrogels and fire retardant hydrogels. Conducting hydrogels possessed high water content and electroconductivity imparted by conducting polymer and/or other conducting fillers. CNTs are widely used conductive fillers owing to their excellent conductive and thermal properties, high mechanical and specific area, and low mass density.[7] However, like most conducting filler/polymers, CNTs are hydrophobic in nature and pose a challenge to disperse them in hydrophilic systems. To curb these challenges, we have valorized lignin (extracted from perennial grass, *Arundo donax*) as a dispersant to dispersed multiwalled carbon nanotubes (CNT). Lignin is abundantly available in nature and is an underutilized by-product of the paper industry. CNTs are known to be toxic in nature, and therefore they are incorporated in small doses in hydrogel (polyvinyl alcohol, PVA, and chitosan, CS) network to synthesize conductive hydrogels.

Conventional flame retardants are toxic in nature. Most widely used flame retardants are halogenated compounds, namely polybromodiphenylether (PBDE), tetrabromobisphenol A (TBBPA), tetrabromophthalic anhydride (TBPA), and hexabromocyclododecane (HBCD).[8] Replacing these conventional flame retardants with nontoxic flame retardants is the need of the hour. Fire can be doused by water

since it absorbs large amount of heat and water possess high latent heat of vaporization.[9,10] However, the retention time for the water used during fire fighting operations to put out the fire is low. Hydrogels are known for encapsulating large amounts of water in their network and can act as water-holding vessels. The hydrogels can absorb large amounts of heat due to the presence of water, and gradual evaporation of water keeps the underneath surface temperature lower.[11] Hence, hydrogels successfully delay the fire from igniting the surface and hinder the fire from spreading. The working mechanism of hydrogel fire retardants is shown in **Figure 1.1**.

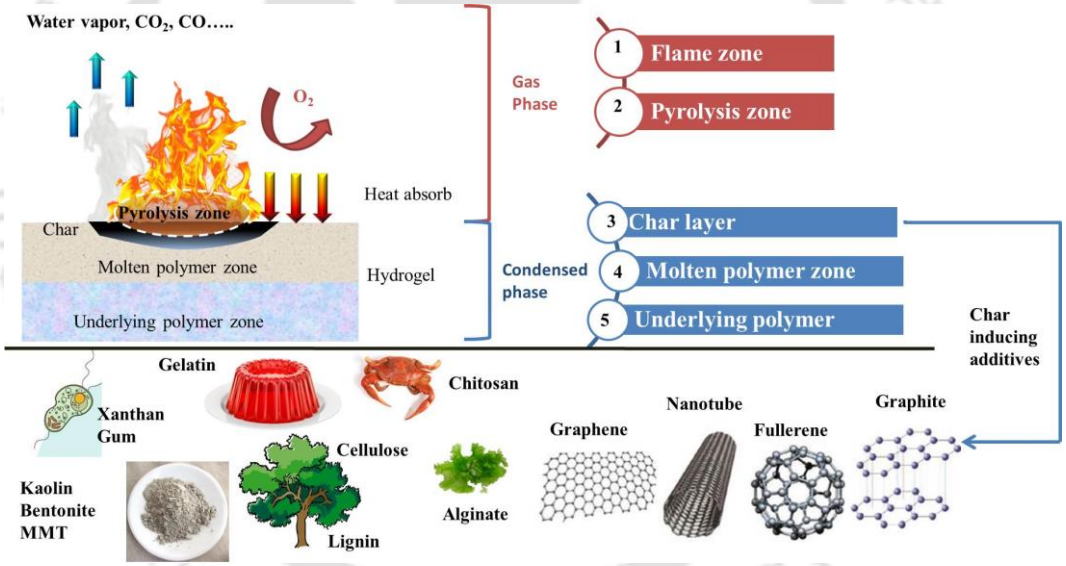

Figure 1.1 Fire retardant mechanism and different char inducing materials

Combustion is a complex phenomenon involving several simultaneous physical and chemical processes. Generally, gas and condensed phases are effective mechanisms of flame retardancy.[12] Several zones are identified in both phases. In gas phase, two types zones are observed namely, flame zone and pyrolysis zone. In pyrolysis zone, the polymer materials degrade and form char. In flame zone, the

volatiles from polymer degradation react with oxygen, subsequently generating radicals and releasing heat. The char layer is the critical zone in polymer combustion because it controls mass and heat transfer between the gas and condensed phase. In the molten polymer, also called the thermal decomposition zone, the decomposition volatiles first generate in this zone and then migrate towards the flame zone through the microporous char layer. The underlying polymer zone is in direct contact with the molten polymer zone but remains intact. The hydrogel on ignition forms a protective layer of char, preventing the underlying area from ignition (**Figure 1.1**). Further, hydrogels synthesized using high char forming biopolymer (chitosan, xanthan gum, starch, lignin and cellulose)[13,14] and clay particles[15,16] are beneficial for providing flame retardancy. Hence, the synergistic effect of water encapsulated in the hydrogel network and the layer of char provide flame retardancy. In recent times, extensive research has been carried out to formulate bio-based composite hydrogels as fire retardants.

This work aims to valorize lignin and cellulose extracted from *Arundo donax* to produce and characterize multifunctional hybrid composite materials as high-performing conductive hydrogels and fire-retardant hydrogels.

1.2 Fundamentals of hydrogel

The key aspects of a hydrogel are its physico-chemical features which are highly influenced by the crosslinked polymer chains. Hydrogels possess water permeability, high water retention ability, swelling–deswelling ability, mechanical stability, responsiveness, biocompatibility, and biodegradability. These properties can be tuned as desired by proper selection of hydrogel components (monomer/polymer

type), and synthesis route, varying the degree of crosslinking, and lastly via incorporation of nanoparticles.

1.2.1 Crosslinking of hydrogel

Hydrogels are made up of hydrophilic polymer chains which are intertwined/ interlinked, also termed as crosslinking of polymer chains. Crosslinking process increases the molecular weight of the polymer chains as well as restricts its motion.[17] Hence, impeding the solubility of the polymer chains. However, in presence of suitable fluid or water, the polymer chains swell and absorb large quantity of fluid/water.[18] Crosslinking of polymer chains affects the mechanical properties, swelling degree, molecular mass, heat, and solvent resistance.[19] The novel methods of crosslinking to design hydrogel are described below. The chemical method involves covalent interactions between the polymer chains, whereas physical interactions are established in case of the physical method.

1.2.1.1 Chemical methods of hydrogel crosslinking

Chemical methods involve the formation of strong covalent bonds between the polymers, bestowing excellent mechanical stability, tunable degradability and enhanced stability under physiological conditions.[20] Copolymerization of multifunctional monomers in presence of chemical initiators and under the influence of chemical reactions of crosslinkers, and/or high energy radiation promotes the development of such covalent bonds. This type of crosslinking requires agents which induce or enhance the interaction between the polymer chains. The major drawback of using such agents is that it may react with other substances. Also, they can be toxic in nature like aldehydes, boron atoms, and epoxide. However, many natural crosslinking agents, like genpin and citric acid, are now used to achieve a more sustainable and

ecofriendly approach.[21] Chemical crosslinking methods include radical polymerization, high energy radiation, chemical reaction of complementary groups and enzymatic crosslinking,[22] which is discussed in detail in the upcoming section.

Radical polymerization: Wichterle and Lim[23] chemical crosslinked low molecular weight monomer, poly(2-hydroxyethyl methacrylate) (pHEMA) using suitable crosslinker, ethylene glycol dimethacrylate, by radical polymerization. This was the first hydrogel synthesized using radical polymerization. Several other vinyl monomer based hydrogels have been formulated using similar procedures.[24,25] Besides vinyl monomers, acrylates, amide monomers, along with some water soluble polymers (both natural and synthetic) have been chemically crosslinked via radical polymerization. One such polymer of interest is the low molecular weight (Mw between 40 and 100 kDa) bacterial polysaccharide dextran. Edman et al.[26] pioneered the research on glycidylacrylate derivatized water soluble dextran, which participated in radical polymerization of vinyl monomers as crosslinkers. Similarly, albumin[27], starch[28], polyvinyl alcohol[29], hyaluronic acid[30], insulin[31] and sucrose[32] were modified by (meth)acrylic groups to introduce vinyl groups for participation as crosslinker in polymerization to obtain hydrogels. Additionally, acrylic acid and acrylamide are the most commonly used monomers for hydrogel synthesis via free radical polymerization.[33] This method of polymerization includes propagation, chain transfer, initiation, and termination steps. The process initiates with the decay of initiator to produce free radicals, which activate the monomers for polymerization. The polymerization process stops by deactivating active sites in the termination steps.[34]

High energy radiation polymerization: Unsaturated monomers can be crosslinked using gamma and electron bean type high energy radiation. Monofunctional acrylate with suitable crosslinker and water soluble polymers can be irradiated to initiate polymerization and crosslinking to obtain hydrogel. During irradiation, radicals are formed in the polymer chains due to the scission of C–H bonds. Further, irradiation of water also produces hydroxyl radicals, which attack the polymer chains, forming macroradicals.[35] These macroradicals recombine to form covalent bonds, subsequently forming crosslinked structures. Polyvinyl alcohol,[36,37] polyethylene glycol,[38] and poly acrylic acid[39,40] are some of the well-known polymers that can be crosslinked via irradiation. The advantage of this crosslinking technique is that the degree of crosslinking and pore formation can be tuned by varying the irradiation dose. Additionally, the process requires mild experimental conditions (ambient temperature with physiological pH) and can be carried out without using any crosslinker.

Crosslinking by chemical reaction of complementary groups: Establishment of covalent linkage can be achieved by crosslinking the functional groups of polymer chains with complementary groups such as aldehydes and ketones. Water soluble polymers with hydroxyl groups and amine containing polymers can be crosslinked using glutaraldehyde.[41] Several synthetic and natural polymers, such as proteins, have been crosslinked using this technique. However, glutaraldehyde is toxic in nature. Further, an addition reaction in the presence of bis or higher crosslinker can convert the water soluble polymers to hydrogel. Polysaccharides can be crosslinked with 1,6-hexamethylenediisocyanate, divinylsulfone , or 1,6-hexanedibromide, and many other reagents. However, the crosslinking reactions need to be performed in organic solvent because water may react with the crosslinker. The major disadvantage of this

crosslinking technique is the usage of toxic crosslinkers, which demands its removal from the formed gels. Crosslinking of hydroxyl or amines with carboxylic acid via condensation reaction is applied to produce hydrogels. Gelatin was crosslinked by N,N-(3-dimethylaminopropyl)-N-ethyl carbodiimide (EDC) reagent. Similarly, alginate and PEG-diamines were crosslinked using EDC. Additionally, carboxylic acid and an aldehyde or ketone are condensed with an isocyanide to yield an α-(acryloxy)amide. The reactions can be performed at ambient conditions. However, high pH of 9 can disintegrate the hydrogel at ambient temperature.

Crosslinking by enzyme: Poly(ethylene glycol) (PEG) based hydrogels can also be crosslinked using an enzyme, transglutaminase, which catalyzes the reaction to yield amide linkage between the polymer.[42,43] The gelation kinetics depended on the macromer structure and composition, the ratio of the reactants and the enzyme concentration. The gelation times typically were between 5 and 30 min. The gel formation occurs under very mild conditions and since the gelation kinetics can be well controlled, these systems are very suitable as *in situ* gelling systems.

1.2.1.2 Physically crosslinked hydrogels

Recent years have seen growing interest in development of physically crosslinked hydrogels. The advantage of not using any toxic crosslinking agent for gellification is to investigate more in hydrogels formed via physical crosslinking. Several techniques of physical crosslinking via ionic interaction, crystallization, formation of stereocomplex, and hydrogel bonding have been followed in formulation of hydrogels.

***Crosslinking by ionic* interaction**: Alginate can be crosslinked using Ca ions as a chelating agent to form hydrogels. These reactions can be performed under ambient conditions and physiological pH. Interestingly, polycations can be crosslinked with anions. Chitosan-based hydrogel, which is a cationic polysaccharide, was crosslinked with glycerol-phosphate disodium salt. Additionally, presence of potassium ions and sulfate ions induces gelation of dextran and carrageenan, respectively. The ionic radius of potassium ions was found to be a perfect fit for the cage established by six oxygen atoms of glucose units of three polymer chains, thereby forming a microstructure. However, the gels formed were unstable in ambient condition. Similar to cationic polymers, anionic polymers were crosslinked with metallic ions, hydrogels can also be obtained by complexation of polyanions with polycations. Xanthan gum helps in gellification of chitosan via inotropic interactions.

***Crosslinking by crystallization*:** Freeze–thawing method promotes the formation of crystalline microstructures. This method is straightforward and does not need any crosslinking agent. However, the performance of hydrogel may vary based on the number of freezing and thawing cycle. Aqueous PVA gradually transforms into gel when stored in ambient condition. However, the gel obtained is poor in mechanical properties. Interestingly, the same PVA solution produces mechanically stable hydrogels after a few cycles of freeze thaw (depending upon its polymer concentration, polymer molecular weight, time, temperature and duration of freeze thaw cycles). Gel formation is ascribed to the formation of PVA crystallites, which act as physical crosslinking sites in the network. Additionally, dextran 6000 spontaneously forms gel when stored at room temperature, which can be ascribed to the crystallization due to association of chains through hydrogen bonding, induced in concentrated dextran 6000 solutions.

***Crosslinking by hydrogen bonding*:** Hydrogen bond interaction primarily synthesizes reversible hydrogel. Hydrogen bonds are formed between O, N, and H, which cease to exist in harsh conditions of increasing temperature or pH change. These interactions play an essential role in increasing and decreasing the swelling of hydrogels.

***Crosslinking by formation of stereocomplex*:** Stereocomplexation refers to when two polymers have the same composition, but due to van der Waals forces, polymers crosslink to form a hydrogel. For such kind of in situ hydrogel formation, a very high elastic nature of polymer is required. High molecular weight PLA, with two stereoisomer PLLA and PDLA form hydrogel through stereo-complexation and was first observed by Ikada et al. Another system, stereocomplex formation by enantiomeric oligo(lactic acid) side chains grafted onto pHEMA (poly(HEMA-g-oligolactate)s) was prepared by Lim et al.[23]

1.2.2 Structure of hydrogel

As discussed elaborately in the previous section, the degree of crosslinking of the polymer is the utmost important parameter of the hydrogel. The internal structure of a hydrogel is defined by the networks formed by physical or chemical crosslinking of polymer chains. These structures are the controlling factors for determining and carefully tailoring hydrogel properties. At the molecular level, mesh size and molecular weight of polymer chains between the crosslinks define hydrogel structure characteristics. Mesh size (ξ) or correlation length is defined as the linear distance between two adjacent crosslinks. However, the mesh size should not be confused with pore size. Pores are typically large void in the hydrogel structure with a diameter in μm scale but positively correlates with mesh size.[44,45] The rubber elastic theory could predict the mesh size of the hydrogel.

1.2.3 Swelling behavior of hydrogel

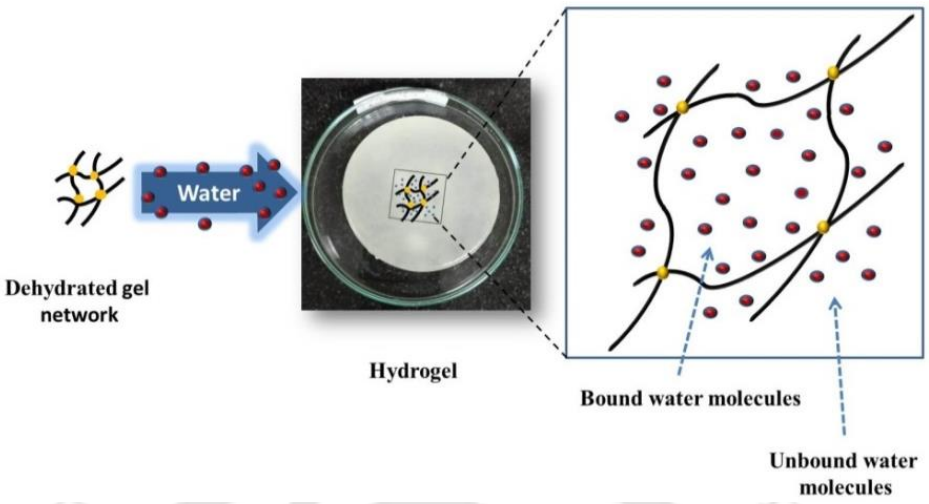

Figure 1.2 Illustration of swelling phenomena of hydrogel

Swelling ability is an important trait of a hydrogel. The process transpires according to the following three steps: (a) osmotic pressure driven diffusion of water molecules into the hydrogel network, (b) hydration and relaxation of polymer chains, and lastly, (c) expansion (swelling) of polymeric network.[46] This swelling is possible due to elastic stretching of the polymer chain strands between the crosslinking points. On the other hand, the expansion of polymer strands increases the elastic retractive force, which counters the network expansion. The balance between these two forces finally leads to equilibrium volume of the polymer network.[47] During the initial stages of water absorption (step a and b), the water molecules are taken up by the polar and hydrophobic moieties of the polymeric network and are termed as bound water (**Figure 1.2**). Addition of more water leads to the network imbibed with free water molecules. Finally, at infinite dilution equilibrium water content is reached. The equilibrium swelling behavior of hydrogel network is well represented by Flory–Rehner Theory, which combines rubber elastic theory and thermodynamic theory.[48]

Post swelling, most conventional hydrogels exhibit inadequate mechanical properties that impede their performance in applications like biomedical, bioelectronics, water treatment, etc. In addition, the popularity of hydrogels demands a superior tailored multifunctional characteristic in conventional hydrogel. Such limitations can be overcome by incorporating nanomaterials or fillers into conventional hydrogels, which are termed as nanocomposite hydrogels. Introducing suitable nanomaterials (nanofiber, nanosheet, nanowire, and nanoparticles) or fillers into conventional hydrogels matrix helps enhance hydrogels functionality by keeping the biocompatibility of the polymeric system intact.[49] Numerous inorganic (viz. clay, metals, ceramic particles, carbon nanotubes (CNT), and graphene) and organic (i.e., cellulose and lignin) fillers have been utilized to developed hydrogels.[50] Over the past two decades, numerous studies were carried out to understand the properties of hydrogel and their possible utilization in numerous applications.

1.3 Classification of hydrogel

Hydrogels can be categorized based on several criteria, as shown in **Figure 1.3**.

1.3.1 Based on source

Depending on source of polymer/monomer(s) used in the development of hydrogels, it can be classified as natural, synthetic, and hybrid. Polysaccharides such as alginate[51,52], peptides and proteins (including collagen, lipids, gelatin, and fibrin)[53,54], guar gum[55,56], chitosan[57,58], and xanthan gum[59,60] are some of the naturally available polymers that are extensively used in hydrogel development. These hydrogels are safe, biodegradable, and biocompatible. However, poor mechanical strength is a major concern with natural hydrogels.[61,62] Contrary, hydrogels developed with synthetic polymers viz. polylactic acid (PLA), poly(vinyl) alcohol

(PVA), and polyethylene glycol (PEG), polyacrylamide (PAM), and polyacrylic acid (PAC) can modify the mechanical strength, durability, and can be easily tailored as per requirements.[63] The major demerit of using synthetic polymer is its low biodegradability and toxicity imposed by the usage of crosslinking agents. Such limitations can be curbed by blending natural and synthetic polymers to form a hybrid hydrogel. These kinds of hydrogels have recently been gaining a lot of attention among researchers due to their multifunctionality and possibly modulation of their properties, viz. cross-linking density, swelling ability, and water retention.[46,64]

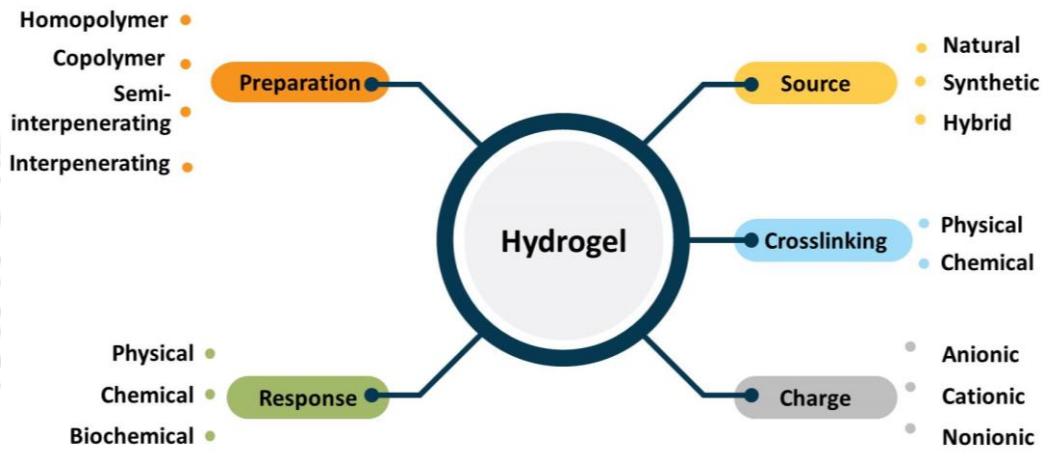

Figure 1.3 Classification of hydrogel

1.3.2 Based on the synthesis methods

Hydrogels can be classified based on the development methods into chemically and physically-crosslinked. Chemical crosslinking can be achieved by the addition of chemical crosslinkers to induce covalent bonding among the polymeric chains. Covalent bonding can be established through photo crosslinking,[65–67] radical polymerization,[24,68] interaction between the functional groups,[20,69] high energy radiation,[70–72] and enzyme-induced chemical reaction.[73–75] Physical crosslinking, on

the other hand, can be achieved with numerous techniques such as freeze–thaw,[76] ionic interaction,[77,78] hydrogen bonding,[79–81] thermogelation,[82] and stereo-complexation.[83] The details on these methods are discussed in section 1.2.1.

1.3.3 Based on the charge of polymeric network

Hydrogels can also be categorized as ionic (i.e., anionic, cationic, and zwitterionic) and nonionic based on the charge present in the polymeric network. Xanthan gum, Na alginate, and carboxymethylpullulan are examples of an anionic polymer based hydrogel. Chitosan and carboxymethyl cellulose based hydrogels are commonly synthesized cationic hydrogel. Poly(sulfobetaine methacrylate) hydrogels is an example of zwitterionic hydrogel.[84]

1.3.4 Based on hydrogel response to stimuli

According to the response of hydrogel to physical stimuli (temperature, electric fields, magnetic field, light, and pressure) or chemical stimuli (pH, ionic strength, and solvent composition) hydrogels are classified as physical, chemical or biochemical responsive hydrogel.

1.3.5 Based on polymeric compositions

Hydrogels can be classified as homopolymeric, copolymeric, and multipolymeric. As the name suggests, homopolymeric and copolymeric hydrogels can be developed with single and double (or more) definite sets monomer(s), respectively.[85,86] Multipolymeric hydrogels, also known as interpenetrating polymer networks (IPNs), mainly involve two (or more) networks, among which at least one is synthesized and/or cross-linked within the company of the other, without any covalent

bonds between them. IPNs synthesized without any crosslinking agent are called as semi-IPN.

1.4 Characterization techniques

1.4.1 Swelling ratio and water retention of hydrogel

A dry hydrogel (also termed xerogel), when placed in water, swells and absorbs water. By definition, water constitutes 10% of the weight of the material to be termed as a hydrogel. However, a hydrogel absorbs more than 10% of water and sometimes exceeds 95% of total weight or volume, termed as a superabsorbents. Hence, depending on the application, the properties of the hydrogel can be tuned and synthesized accordingly. To understand and quantify the swelling ability, the degree of swelling or swelling ratio of the hydrogel is estimated according to the equation 1.1.

$$swelling\ ratio = \frac{(wet\ weight - dry\ weight)}{dry\ weight} \times 100\% \quad 1.1$$

$$water\ retention = 1 - \frac{weight\ of\ swollen\ hydrogel - weight\ of\ dehydrated\ hydrogel}{weight\ of\ dehydrated\ hydrogel} \quad 1.2$$

The swelling kinetics demonstrates the amount of water uptake of a dry hydrogel. Additionally, the diffusion of solute through the hydrogel, mechanical properties of the hydrogel, surface properties, and degree of crosslinking can also be evaluated. An increase in crosslinking of the hydrogels restricts the water uptake and decreases the swelling ability of the hydrogel. These two counteracting forces act simultaneously and reach equilibrium after some point, leading to hydrogel swelling up to a certain limit. In a hydrogel kept in an ambient atmosphere, water tends to evaporate from the swollen hydrogel with the progress of time. Hence, similar to swelling kinetics, water

retention kinetics reveals the water holding capacity of fully swollen hydrogels (equation 1.2).

1.4.2 Rheology

Rheology is the study of deformation of the material. The viscoelastic behavior of the hydrogel can be characterized by performing different rheological tests. When forces are applied on a viscoelastic material, it deforms and on releasing the forces the material recoils. Viscosity is measured in case of viscous or the materials which flow under deformation. In case of materials that do not flow, the stiffness of the material is measured in terms of shear modulus, G. Viscoelastic material displays both elastic and viscous behavior. Oscillatory measurements identify just how much viscous or elastic in nature the material is. The oscillatory measurement involves oscillating the material in a sinusoidal manner around a fixed point. The oscillations provided are so small that the inherent structures in a sample are measured without being perturbed. The ratio of the applied stress (or strain) to the measured strain (or stress) gives the complex modulus (G*), which is a quantitative measure of material stiffness or resistance to deformation and can be described as follows:

$$G^* = G' + iG'' \qquad 1.3$$

G′ represents the storage modulus and G″ represents the loss modulus. The following conditions are to be noted for declaring the material as viscous or elastic (**Table 1.1**).

1.4.2.1 Amplitude sweep

To perform the oscillatory (dynamic) test, the first step to be performed is amplitude sweep. Here the amplitude is ramped while keeping frequency and temperature constant. The results are expressed in terms of G′ and G″ moduli. G′ also gives insight

into the Newtonian behavior or the linear viscoelastic region (LVR) of the material. The LVR of the hydrogels occurs at low shear stress, during which the moduli are independent of the increasing stress. Moreover, as the stress increases, the G′ and G″ crossover point potentially reaches the point where the gel-sol transformation occurs, and the material starts to behave like a fluid.[87] The main purpose of strain sweep testing is to determine the linear viscoelastic region (LVR) of the hydrogels.

Table 1.1 Conditions for a material to be elastic/solid or liquid.

Condition	Remark	
G″ >> G′	Liquid like structure	
G″ > G′	Liquid like structure	Viscoelastic liquid
G″ = G′	Gel point	
G′ > G″	Gel like structure	
G′ >> G″	Gel like structure	Viscoelastic solid

1.4.2.2 Frequency sweep

After determining the LVR region, the next step is to perform frequency sweep. This test characterizes the hydrogel with respect to ramping frequency and draws a relationship between the frequency and the moduli. Moreover, it gives insight into the viscoelastic properties and state of a material by comparing the two G' and G" values over the frequency range.[88] The impact of the degree of crosslinking can be easily characterized using this test.

These two tests are the most common test performed to characterize the hydrogel. These tests also give us an idea about the mechanical stability and crosslinking of the hydrogel. As crosslinking of the hydrogel tends to increase the weight of the material, the shear modulus also increases.

1.4.3 Estimation of structural parameter

The principal structural parameters of a hydrogel are: average molecular weight between crosslinks ($\overline{M_c}$), crosslinking density (V_e), and mesh size (ξ). These parameters are determined using rheological measurements (elastic and viscous modulus G'') and swelling tests. In general, the number of moles of elastic chains per unit volume (ν) and the number of moles of elastic junctions (cross-links) per unit volume of the network (μ) are used to describe the cross-link density of the polymer network. Consequently, ν and μ determine the average molecular weight between the junctions (M_c)[89]. The functionality of the junctions (*f*), being the number of chains leaving from one junction, determines the relation between ν and μ as shown in equation 1.1. Swelling experiments and rheological studies are carried out to determine ν, μ and *f*. The values of ν, μ and *f* thus obtained are rather estimates than accurate values, as the models are developed for ideal polymer systems, ignoring the defects like nonelastic dangling ends, loops and chains not attached to the network, no trapped entanglements (contributing to the elastic properties), nor heterogeneous regions.

$$\mu = \frac{2\nu}{f} \qquad 1.4$$

An important consideration in the development and interpretation of theoretical molecular models is the difference between affine networks and phantom networks. In an affine network, it is assumed that the junctions of the network do not fluctuate and that they transform affinely (linearly) with the macroscopic deformation. For an affine network, it is assumed that only the network chains contribute to the decrease of entropy of the network (which gives rise to the elastic force) upon deformation. For a phantom network it is assumed that the junctions do fluctuate over time. Real

networks are expected to show characteristics that lie somewhere between the properties of both affine and phantom models. This phenomenon was treated by Flory and Erman in the constrained junction model, which allows for this intermediate behavior. Based on rubber elasticity theory (RET) for homogeneous Gaussian chains network parameters, these structural parameters can be calculated using the following equations[90,91]:

$$\frac{1}{V_{2m}} = 1 + \left[\frac{\rho}{\rho_w} \left(\frac{1}{Z} - 1 \right) \right] \tag{1.5}$$

$$\frac{1}{V_{2r}} = 1 + \left[\frac{\rho}{\rho_w \left(\frac{1}{m} - 1 \right)} \right] \tag{1.6}$$

$$G' = A \frac{\rho}{M_c} RT (V_{2r})^{2/3} (V_{2m})^{1/3} \tag{1.7}$$

$$V_e = \frac{\rho}{M_c} \tag{1.8}$$

$$\xi = \left(\frac{G' N_A}{RT} \right)^{-1/3} \tag{1.9}$$

$$\rho = \frac{w}{S \times t} \tag{1.10}$$

Various notations are: ρ_w = density of water, m = weight of the dry hydrogel, Z = weight of the hydrogel at equilibrium, V_{2m} = polymer volume fraction of crosslinked polymer in equilibrium with swollen gel, V_{2r} = polymer volume fraction after crosslinking but before swelling, ρ = density of dry hydrogel, R = universal gas constant, T = temperature, N_A = Avogadro number, t = thickness of the sample, A = pre-factor (with value as 1 for the affine network model and $1-\frac{2}{\varphi}$ for the phantom

network model, where φ = number of branches originating from crosslinking site). As per constrained junction theory, the phantom network model is followed by the real network, and value of $\varphi = 3$.[91–93]

1.4.4 Thermal analysis

Thermogravimetric analysis (TGA) is employed to characterize the thermal properties of the hydrogel. In this technique, the mass of the material is monitored over a range of temperatures at a fixed rate under a controlled atmosphere. The material may gain weight in case of oxidation, absorption, or adsorption. Similarly, the material may experience weight loss in case of decomposition, evaporation of volatiles matters, reduction (interaction of sample to a reducing atmosphere), and desorption. TGA instrument consists of a pan that is supported by a precision balance. The pan resides inside a furnace and is heated or cooled during the experiment. A sample purge gas controls the environment. This gas may be inert or a reactive gas that flows over the sample and exits through an exhaust. Generally, the test is performed in an inert environment. Mostly nitrogen or argon is used so that the sample only reacts to temperature during decomposition.

The sample for TGA should be dried properly in an oven. The sample amount should be between 2 to 50 mg. The sample pan can be ceramic or platinum, accommodating solids or crystals, liquid, powders, and films. The weight % with respect to time or temperature can be calculated as follows:

$$\frac{m}{t} = \frac{m_i - m_{(i-1)}}{t_i - t_{(i-1)}} \qquad 1.11$$

where m_i represents the initial weight of the sample and *i* represent the weight loss at particular temperature.

To estimate the thermal conversion (or decomposition) of the hydrogels, kinetic parameters are determined. In a typical experiment, a crucible is filled with sample and heated over a temperature range in three or more linear heating rates in controlled atmosphere. The thermal decomposition can be expressed as follows:

$$\frac{d\alpha}{dt} = kf(\alpha) \qquad 1.12$$

$$\alpha = \frac{m_i - m_t}{m_i - m_f} \qquad 1.13$$

where $f(\alpha)$ is a function, the type of which depends on the reaction mechanism. α is the degree of conversion. m_i is the initial mass of the sample. m_f is the final mass of the sample. m_t is the sample mass at any temperature T. k is the temperature dependent rate constant, usually described by Arrhenius equation[94].

$$k = Ae^{-\frac{E}{RT}} \qquad 1.14$$

where A is the pre-exponential or frequency factor. E is the activation energy of the decomposition reaction. R is the universal gas constant. T is the absolute temperature. Inserting equation 1.14 in 1.12 we get

$$\frac{d\alpha}{dt} = -Ae^{-(\frac{E}{RT})} f(\alpha) \qquad 1.15$$

$$\frac{d\alpha}{dt} = -Ae^{-(\frac{E}{RT})} (1-\alpha)^n \qquad 1.16$$

Replacing $f = (1-\alpha)^n$ according to uniform kinetic of reaction where n is the order of reaction. In case of non-isothermal TGA experiments, the heating rate is varied as a function of time as follows:

$$\frac{d\alpha}{dT} = \frac{d\alpha}{dt} \times \frac{dT}{dt} \qquad 1.17$$

For non-isothermal measurements with linear heating rate: β = dT/dt. Hence, equation 1.16 can be rewritten as

$$\frac{d\alpha}{dT} = \frac{A}{\beta} e^{-(\frac{E}{RT})}(1-\alpha)^n \qquad 1.17$$

For calculating the activation energy, Opfermann et al.[95] suggested use of model free (isoconversional) kinetic analysis. Common model free methods used by researchers are listed in **Table 1.2**, and these are the most reliable and powerful tools for calculation of activation energies of thermally activated reactions[96,97].

Table 1.2 Model equations for the isoconversional method.

Isoconversional method	Expression
Friedman method	$\ln \beta \frac{d\alpha}{dT} = \ln(Af(\beta)) - \frac{E}{RT}$
Flynn-Wall-Ozawa method	$\ln \beta = \ln \frac{AE}{Rg(\alpha)} - 5.331 - 1.052 \frac{E}{RT}$
Kissinger method	$\ln \frac{\beta}{T_{max}^2} = \ln \frac{AR}{E} - \frac{E}{RT_{max}}$
Kissinger-Akahira-Sunrose method	$\ln \frac{\beta}{T^2} = \ln \frac{AR}{Eg(\alpha)} - \frac{E}{RT}$

1.4.5 Fourier Transform Infrared (FTIR) analysis

FTIR is majorly used to identify the functional groups in organic, polymeric, and, in some cases, inorganic materials. FTIR spectroscopy has been applied for blend studies because the physical properties of polymer blends are affected by the structures of the molecular chains. Depending on the nature of the blending, different polymer blends can exhibit different types of interactions and configurations, which can help predict their mechanical and physical properties.[98]

1.4.6 Morphological analysis

To characterize the surface morphology of the hydrogel, field emission electron microscope (FESEM) and high-resolution transmission electron microscopy (HRTEM) is used. The field emission scanning electron microscope (FESEM) is suitable for observing structures as small as 1 nm on the surface of the material. In order to be observed in SEM, objects are first made conductive. This can be done by coating them with an extremely thin layer (1.5–3.0 nm) of gold or gold palladium. Furthermore, objects must be able to sustain the high vacuum force and should not alter the vacuum, for example, by losing water molecules or gases.

HR-TEM is a powerful spectroscopy technique that offers information at the atomic level and reduces radiation damage at low accelerating voltages. In HRTEM, the accelerating voltage is highly stable of the range of one part per million (ppm) or higher.

1.5 Literature review

The focus of the present thesis is to valorize lignin and cellulose extracted from *Arundo donax*, and to synthesize sustainable composite hydrogels. Over the years, remarkable research on biopolymer hydrogel synthesis, characterization, and application has been published. Chitosan (CS) and xanthan gum (XG) are two commonly used biopolymers in environment-friendly hydrogel formulations. However, these biopolymers lack the mechanical strength required for application in flexible electrodes, as coatings. Hence, synthetic polymer PVA is blended with these biopolymers to incorporate adequate strength. Jin and Bai[99] formulated PVA–CS hydrogel bead where PVA was blended with CS to incorporate desirable mechanical and chemical properties in CS. The enhanced properties can be ascribed to the

hydrophobic side chain aggregation, and intermolecular and intramolecular hydrogen bonds between the two polymers.

Table 1.3 Summary of representative literature on PVA, CS, lignin/LNPs composites.

Composition	Remark	Reference
PVA–CS–Lignin nanoparticle (LNP)	•Enhancement in Young's modulus and tensile strength of PVA •LNP imparts high toughness in CS •High thermal stability	100
PVA–CS–Lignin nanoparticle (LNP)	•LNP promoted crosslinking •LNP limited deswelling of PVA •enhanced mechanical and thermal properties	101
PVA–LNP	•Toughening of hydrogel matrix •Thermal stabilization	102
PVA–CS	•mean tensile strength and percentage •elongation of CS–PVA blends decreases with decrease in PVA content	103
PVA–CS	•improvement in hydrophilicity of obtained films	104
CS–LNP	• Crosslinking of chitosan by lignin phenoxyl radicals •Synthesis/production lignin-crosslinked hydrogels •improvement in tensile strength, storage modulus, thermal degradation temperature and glass transition temperature of chitosan	105
Lignin decorated CNTs – PVA	•Lignin as CNT dispersant •Enhanced breaking stress and modulus •Superior antimicrobial properties	106
Lignin–nanofluid containing CNT	•Lignin as CNT dispersant •Viscosity and thermal conductivity enhancement with increasing LNPs	107
Lignin –PVA–CS	•enhanced mechanical strength •better protein absorption	108
Alkali lignin– CNT	•Lignin as CNT dispersant	109
Kraft lignin– CNT	•Lignin as CNT dispersant	110
PVA– CNT	•Fast water transport •Excellent environment tolerance •Excellent mechanical reversibility	111
O-carboxymethyl chitosan (O-CMCS)–PVA–CNT	•Rapid self-healing •Excellent antibacterial and tensile strength •Stable electrical conductivity	112

Another study reported by Dhiman and Agnihotri[113] used PVA–CS hydrogel for Ag nanoparticle immobilization, where PVA was blended to strengthen the poor mechanical properties of CS. Additionally, lignin particles have been incorporated in PVA and CS to curb the disadvantages of the CS biopolymer. Zhu et al.[114] incorporated lignin nanoparticles in carboxymethyl chitosan (CMC) to develop sprayable hydrogel. Morales et al.[115] developed physically crosslinked PVA lignin hydrogel with good mechanical and thermal properties. The addition of lignin also facilitated swelling of the formulated hydrogel up to 800% with 40–50% water retention. Zhang et al.[116] formulated PVA–CS hydrogel and added lignin nanoparticles (LNPs) to enhance the mechanical properties of PVA and CS. The reported tensile strength for PVA–CS–LNP hydrogel was 46.87 MPa. Also, during the synthesis of CNT based hydrogel, dispersion of CNTs in hydrophilic PVA and chitosan posed a challenge. This particular problem is resolved by using lignin particles to disperse CNTs. Literature on CNT based PVA–CS hydrogel is massive, but considering the scope of work, representative literature has been summarized in **Table 3.1**.

During the formulation of bio-based fire retardants, the main approach is to use high char-forming biopolymers. XG and cellulose are two such biopolymers that have recently gained attention as new bio-based fire retardants. The development of XG and cellulose based hydrogel has its own sets of disadvantages. Similarly to chitosan, XG is a non-gelling polymer displaying poor mechanical properties.[117] Hence, PVA is added to strengthen the mechanical stability as well as crosslink XG polymeric chains through freeze thaw. Zhang et al.[118] reported preparation of PVA–XG hydrogel via freeze thaw process. Presence of PVA strengthens the hydrogel and

reduced its compression properties due to strong hydrogen bonding formation. Additionally, presence of XG promoted a higher swelling ratio. Similarly, Bernal-Chávez et al.[119] reported increment of tensile strength from 9 to 87 kPa on blending PVA with XG. Also, presence of PVA imparted flexibility, crystallinity and resistance. Physical crosslinking or freeze thaw is an environmentally friendly method of crosslinking. However, with the incorporation of higher XG, the hydrogel produced lacked the desired properties. Hence, in the case of a higher percent of XG in the hydrogel crosslinking was done by using crosslinker. Oxalic acid, borax, and aldehydes (formaldehyde and glutaraldehyde) are generally used as crosslinkers. Enache et al.[120] reported dual crosslinking technique, physically crosslink via freeze thaw PVA–XG in presence of nontoxic oxalic acid as a chemical crosslinker. Alupei et al.[121] reported formulation of PVA –XG superabsorbent using epichlorohydrin as a crosslinker in basic medium. Similarly, in basic medium aldehydes are also used as crosslinker. Bhattacharya et al.[122] report synthesis of glutaraldehyde crosslinked PVA–XG superabsorbents under alkaline conditions. Saadatlou and Pircheraghi[123] crosslinked XG using tetra-functional crosslinker borax under alkaline conditions.

In addition to biopolymers, particles such as lignin and clay have been utilized as fire retardants by enhancing char formation.[124] Zhang et al.[125] utilized pristine lignin as fire retardant for PU foam. The flame retarding mechanism of lignin/PU foam was attributed to the fact that lignin could change the thermal degradation and burning behavior of PU foams in the condensed phase (char forming) and the gas phase (inert gas dilution) by radical quenching (phenolic groups) and S–N synergism. Lui et al.[126] synthesized functionalized lignin to impart fire retardancy to polypropylene wood. Similarly, clay particles have been incorporated to impart fire retardancy. Ullah et al.[15] used kaolin clay based intumescent fire retardant coating for

the protection of steel substrate. The weight residue at the end of the thermal analysis was estimated to be 49%. Fukushima et al.[127] established the effectiveness of expanded graphite/layered-silicate clay in increment of fire retardancy of poly lactic acid. Recent scientific reports have showcased a gradual increase in the formulation of halogen and other toxic chemical free bio-based fire retardants. Some recent literature is summarized in Table 1.4.

Table 1.4 Literatures on recent development in bio based fire retardants.

Composition	Remark	Reference
Lignin – polybutylene succinate (PBS)	• Reduction in peak heat release and total heat release of PBS by 27 and 31% • Reduction in weight loss by 33%	128
Polyacrylamide and alginate	• low heat transfer through hydrogel laminate • high heat protection until the hydrogel dries • dry hydrogel charred	129
Water soluble chitosan, sodium alginate and copper ions	• Self-extinguishes within 35s • Peak HRR 214.29 J g^{-1} and THR of 38.49 kJ g^{-1} • Mass residue obtained 8.7% to 6.1% (@650 ºC)	130
Sodium carboxymethyl cellulose–g– acrylic acid	• High heat resistant gel • High water absorption (equilibrium water absorption in 2–3 h) • Mass residue obtained (TGA) is 27.8%	131
Chitosan-grafted poly(acrylic acid-co-methacrylamide)	• Good water retention even at higher temperature • Mass residue obtained 55% to 70% @700ºC	132
Xanthan Gum and Resorcinol Bis(diphenyl phosphate)-Coated Starch	• Thick layer of char produced • Low heat transfer due to the layer of char	11
Kaolinite –Cellulose	• Showcased high strength of 37 MPa, and a modulus of 5.8 GPa with 35% nano–kaolinite and 14 wt% cellulose	133
MMT–CNF–cellulose	• Enhanced gas barrier property • Intense charring of polysaccharides • Intumescent behaviour observed	134
Expandable graphite flakes–cellulose	• Delay in ignition time • Increment in thermal stability of the composite	135

1.6 Thesis objectives

This thesis reports our studies in synthesizing composite hydrogels and put forth new methods for synthesizing conducting hydrogels and fire retardant hydrogels using sustainable sources. The following are the objectives of the thesis:

1. Investigation of the extractions process and products of *Arundo donax*
    a) Study the extraction process of lignin and cellulose derived from *Arundo donax.*
    b) Characterization of the extracted products (lignin and cellulose).
2. Ultrasound assisted lignin decorated MWCNT doped flexible PVA–Chitosan composite hydrogel
    a) Evaluate the process of ultrasonic dispersion of lignin and MWCNT.
    b) Formulation and characterization study of physically crosslinked PVA–CS hydrogel.
    c) Performance evaluation of the developed hydrogel through EIS measurement.
3. Development of NaOH-borax crosslinked PVA-XG-Lignin hydrogel as green fire retardant
    a) Synthesise of LNP using nanoprecipitation method
    b) Formulation and characterization study of PVA–XG–LNP hydrogel coating on cotton fabric.
    c) Performance evaluation of the developed hydrogel fire retardant.
4. Kaolin embedded cellulose hydrogel as green fire retardant
    a) Formulation and characterization study of Methylene bis acrylamide (MBA) crosslinked kaolin embedded cellulose hydrogel.

b) Performance evaluation as fire retardant

1.7 Thesis outline

On the basis of the above discussion, the thesis is organized in 6 chapters. A brief overview of the chapters is as follows:

Chapter 1: This chapter extensively discusses the background and fundamentals of hydrogels, their properties, and synthesis methods. The various theories related to hydrogel and different techniques involved in the characterization of hydrogels are also discussed elaborately. Sequentially, a review of the state-of-the-art literature on the various materials involved in hydrogel synthesis and the method adopted for hydrogel formulation is presented in this chapter. Finally, the broad scope and objectives of the present thesis have been outlined.

Chapter 2: Giant reed or *Arundo donax* is a perennial grass ubiquitously found in north-eastern region of India. This grass is an excellent resource of lignin and cellulose. This chapter discusses the compositional analysis of the biomass, pre-treatment process indulged, and the extraction process of lignin and cellulose. Lignin was extracted from the biomass via alkaline treatment (2 M NaOH). The solids obtained after lignin removal were bleached via sodium chlorite to obtain bleached cellulose. The standard NREL methods were followed to evaluate the compositional analysis of the biomass, and check the purity of the extracted products. The details of all the methods involved are described and discussed in this chapter.

Chapter 3: In this chapter, we have reported synthesis of physically crosslinked PVA–CS with LNP-dispersed-CNTs to produce conductive composite hydrogel. The thermal stability of hydrogels was characterized by TGA; rheological studies were carried out to test their mechanical strength. Post addition of nanoparticles, the CS–

PVA hydrogel revealed a significant increase in thermal stability. The conductive nature of the formulated hydrogels was verified by EIS analysis.

Chapter 4: This chapter reports synthesis, characterization, and testing of hydrogels comprising a biodegradable PVA matrix with two biomaterials additives, viz., xanthan gum and lignin nanoparticles (LNP). Nanoprecipitation from 7:3 acetone-water cosolvent was adopted to produce LNPs. The hydrogel network was achieved through crosslinking by borax and NaOH. Different hydrogels synthesized in this study with different combinations (or compositions) of the LNPs, borax, and NaOH revealed enhanced structural and fire retardant properties.

Chapter 5: In this chapter, we valorized the cellulose extracted from the waste perennial grass, Arundo Donax, to regenerate cellulose composite hydrogel on cotton fabric. Herein, we report synthesis of cellulose-kaolin composite hydrogels crosslinked using methylene bisacrylamide. The combustion behavior was evaluated by performing cone calorimeter test (CCT), limiting oxygen Index (LOI) test, vertical flammability test (VFT), and open fire test (OFT).

Chapter 6: This chapter summarized the findings of all the chapters of the thesis. The thesis has presented investigations in formulation of three types of hybrid composite hydrogels using biomass derived lignin nanoparticles or cellulose as hydrogel matrix for the generation of conductive hydrogels and fire retardant hydrogels. The formulated nanoparticles and composite hydrogels were extensively characterized using standard characterization techniques (viz. FTIR, FESEM, FETEM, and TGA). Further, conductivity of hydrogels was measured through EIS, and Fire retardants hydrogels was characterized by performing CCT, Vertical flammability tests (VFT),

Open fire test (OFT), and calculating the limiting oxygen index (LOI) of the hydrogel samples.

References

(1) Ciolacu, D. Sustainable Hydrogels from Renewable Resources. *Sustain. Biomass through Bio-based Chem.* **2021**, 161–189. https://doi.org/10.1201/9780429347993-6.

(2) Wang, Z.; Ganewatta, M. S.; Tang, C. Sustainable Polymers from Biomass: Bridging Chemistry with Materials and Processing. *Prog. Polym. Sci.* **2020**, *101*, 101197. https://doi.org/10.1016/J.PROGPOLYMSCI.2019.101197.

(3) Domínguez-Robles, J.; Tamminen, T.; Liitiä, T.; Peresin, M. S.; Rodríguez, A.; Jääskeläinen, A. S. Aqueous Acetone Fractionation of Kraft, Organosolv and Soda Lignins. *Int. J. Biol. Macromol.* **2018**, *106*, 979–987. https://doi.org/10.1016/J.IJBIOMAC.2017.08.102.

(4) Fan, H.; Gong, J. P. Fabrication of Bioinspired Hydrogels: Challenges and Opportunities. *Macromolecules* **2020**, *53* (8), 2769–2782. https://doi.org/https://doi.org/10.1021/acs.macromol.0c00238.

(5) Singhal, R.; Gupta, K. A Review: Tailor-Made Hydrogel Structures (Classifications and Synthesis Parameters). *Polym. Plast. Technol. Eng.* **2016**, *55* (1), 54–70. https://doi.org/10.1080/03602559.2015.1050520.

(6) Hoffman, A. S. Hydrogels for Biomedical Applications. *Adv. Drug Deliv. Rev.* **2012**, *64* (SUPPL.), 18–23. https://doi.org/10.1016/J.ADDR.2012.09.010.

(7) Mihajlovic, M.; Mihajlovic, M.; W Dankers, P. Y.; Masereeuw, R.; Sijbesma, R. P.; Mihajlovic, M.; Sijbesma, R. P.; W Dankers, P. Y.; Masereeuw, R. Carbon Nanotube Reinforced Supramolecular Hydrogels for Bioapplications. *Macromol. Biosci.* **2019**, *19* (1), 1800173. https://doi.org/10.1002/MABI.201800173.

(8) Yasmin, S.; Whalen, M. Flame Retardants, Hexabromocyclododecane (HCBD) and Tetrabromobisphenol A (TBBPA), Alter Secretion of Tumor Necrosis Factor Alpha (TNFα) from Human Immune Cells. *Arch. Toxicol.* **2018**, *92* (4), 1483. https://doi.org/10.1007/S00204-018-2156-5.

(9) Ye, Q. Super-Absorbent Polymer Based Fire Retardant, Johns Hopkins

University, 2021.

(10) Asako, Y.; Otaka, T.; Yamaguchi, Y. Fire Resistance Characteristics of Materials with Polymer Gels Which Absorb Aqueous Solution of Calcium Chloride. *Numer. Heat Transf. Part A Appl.* **2004**, *45* (1), 49–66. https://doi.org/10.1080/10407780490267 38.

(11) Xue, Y.; Yang, F.; Li, J.; Zuo, X.; Pan, B.; Li, M.; Quinto, L.; Mehta, J.; Stiefel, L.; Kimmey, C.; Eshed, Y.; Zussman, E.; Simon, M.; Rafailovich, M. Synthesis of an Effective Flame-Retardant Hydrogel for Skin Protection Using Xanthan Gum and Resorcinol Bis(Diphenyl Phosphate)-Coated Starch. *Biomacromolecules* **2021**, *22* (11), 4535–4543. https://doi.org/10.1021/acs.biomac.1c00804.

(12) Yang, H.; Yu, B.; Xu, X.; Bourbigot, S.; Wang, H.; Song, P. Lignin-Derived Bio-Based Flame Retardants toward High-Performance Sustainable Polymeric Materials. *Green Chem.* **2020**, *22* (7), 2129–2161. https://doi.org/10.1039/D0GC00449A.

(13) Maqsood, M.; Seide, G. Investigation of the Flammability and Thermal Stability of Halogen-Free Intumescent System in Biopolymer Composites Containing Biobased Carbonization Agent and Mechanism of Their Char Formation. *Polym. 2019, Vol. 11, Page 48* **2018**, *11* (1), 48. https://doi.org/10.3390/POLYM11010048.

(14) Muthuraj, R.; Hajee, M.; Horrocks, A. R.; Kandola, B. K. Biopolymer Blends from Hardwood Lignin and Bio-Polyamides: Compatibility and Miscibility. *Int. J. Biol. Macromol.* **2019**, *132*, 439–450. https://doi.org/10.1016/J.IJBIOMAC.2019.03.142.

(15) Ullah, S.; Ahmad, F.; Shariff, A. M.; Bustam, M. A. Synergistic Effects of Kaolin Clay on Intumescent Fire Retardant Coating Composition for Fire Protection of Structural Steel Substrate. *Polym. Degrad. Stab.* **2014**, *110*, 91–103. https://doi.org/10.1016/J.POLYMDEGRADSTAB.2014.08.017.

(16) Ur Rehman, Z.; Huh, S. H.; Ullah, Z.; Pan, Y. T.; Churchill, D. G.; Koo, B. H. LBL Generated Fire Retardant Nanocomposites on Cotton Fabric Using Cationized Starch-Clay-Nanoparticles Matrix. *Carbohydr. Polym.* **2021**, *274*, 118626. https://doi.org/10.1016/J.CARBPOL.2021.118626.

(17) Livshin, S.; Silverstein, M. S. Crystallinity and Cross-Linking in Porous Polymers Synthesized from Long Side Chain Monomers through Emulsion

Templating. *Macromolecules* **2008**, *41* (11), 3930–3938. https://doi.org/10.1021/MA800195W.

(18) Madduma-Bandarage, U. S. K.; Madihally, S. V. Synthetic Hydrogels: Synthesis, Novel Trends, and Applications. *J. Appl. Polym. Sci.* **2021**, *138* (19), 50376. https://doi.org/10.1002/APP.50376.

(19) Chamkouri, H.; Chamkouri, M. To Cite This Article: Hossein Chamkouri, Mahyodin Chamkouri. A Review of Hydrogels, Their Properties and Applications in Medicine. *Am J Biomed Sci Res* No. 6, 2021–2032. https://doi.org/10.34297/AJBSR.2021.11.001682.

(20) Hu, W.; Wang, Z.; Xiao, Y.; Zhang, S.; Wang, J. Advances in Crosslinking Strategies of Biomedical Hydrogels. *Biomater. Sci.* **2019**, *7* (3), 843–855. https://doi.org/10.1039/C8BM01246F.

(21) Nasution, H.; Harahap, H.; Dalimunthe, N. F.; Ginting, M. H. S.; Jaafar, M.; Tan, O. O. H.; Aruan, H. K.; Herfananda, A. L. Hydrogel and Effects of Crosslinking Agent on Cellulose-Based Hydrogels: A Review. *Gels 2022, Vol. 8, Page 568* **2022**, *8* (9), 568. https://doi.org/10.3390/GELS8090568.

(22) Deligkaris, K.; Tadele, T. S.; Olthuis, W.; van den Berg, A. Hydrogel-Based Devices for Biomedical Applications. *Sensors Actuators B Chem.* **2010**, *147* (2), 765–774. https://doi.org/10.1016/J.SNB.2010.03.083.

(23) Wichterle, O.; Lím, D. Hydrophilic Gels for Biological Use. *Nat. 1960 1854706* **1960**, *185* (4706), 117–118. https://doi.org/10.1038/185117a0.

(24) Ida, S. Structural Design of Vinyl Polymer Hydrogels Utilizing Precision Radical Polymerization. *Polym. J. 2019 519* **2019**, *51* (9), 803–812. https://doi.org/10.1038/s41428-019-0204-5.

(25) Gao, Y.; Zhou, D.; Lyu, J.; Sigen, A.; Xu, Q.; Newland, B.; Matyjaszewski, K.; Tai, H.; Wang, W. Complex Polymer Architectures through Free-Radical Polymerization of Multivinyl Monomers. *Nat. Rev. Chem. 2020 44* **2020**, *4* (4), 194–212. https://doi.org/10.1038/s41570-020-0170-7.

(26) Edman, P.; Ekman, B.; Sjöholm, I. Immobilization of Proteins in Microspheres of Biodegradable Polyacryldextran. *J. Pharm. Sci.* **1980**, *69* (7), 838–842. https://doi.org/10.1002/JPS.2600690725.

(27) Park, K. Enzyme-Digestible Swelling Hydrogels as Platforms for Long-Term Oral Drug Delivery: Synthesis and Characterization. *Biomaterials* **1988**, *9* (5), 435–441. https://doi.org/10.1016/0142-9612(88)90009-9.

(28) Artursson, P.; Edman, P.; Laakso, T.; Sjöholm, I. Characterization of Polyacryl Starch Microparticles as Carriers for Proteins and Drugs. *J. Pharm. Sci.* **1984**, *73* (11), 1507–1513. https://doi.org/10.1002/JPS.2600731103.

(29) Martens, P.; Holland, T.; Anseth, K. S. Synthesis and Characterization of Degradable Hydrogels Formed from Acrylate Modified Poly(Vinyl Alcohol) Macromers. *Polymer (Guildf).* **2002**, *43* (23), 6093–6100. https://doi.org/10.1016/S0032-3861(02)00561-X.

(30) Jin, Y.; Yamanaka, J.; Sato, S.; Miyata, I.; Yomota, C.; Yonese, M. Recyclable Characteristics of Hyaluronate–Polyhydroxyethyl Acrylate Blend Hydrogel for Controlled Releases. *J. Control. Release* **2001**, *73* (2–3), 173–181. https://doi.org/10.1016/S0168-3659(01)00234-6.

(31) Stubbe, B.; Maris, B.; … G. V. den M.-J. of controlled; 2001, undefined. The in Vitro Evaluation of "azo Containing Polysaccharide Gels" for Colon Delivery. *Elsevier*.

(32) Ferreira, L.; Vidal, M. M.; Geraldes, C. F. G. C.; Gil, M. H. Preparation and Characterisation of Gels Based on Sucrose Modified with Glycidyl Methacrylate. *Carbohydr. Polym.* **2000**, *41* (1), 15–24. https://doi.org/10.1016/S0144-8617(99)00064-8.

(33) Sennakesavan, G.; Mostakhdemin, M.; Dkhar, L. K.; Seyfoddin, A.; Fatihhi, S. J. Acrylic Acid/Acrylamide Based Hydrogels and Its Properties - A Review. *Polym. Degrad. Stab.* **2020**, *180*, 109308. https://doi.org/10.1016/J.POLYMDEGRADSTAB.2020.109308.

(34) Qamruzzaman, M.; Ahmed, F.; Mondal, M. I. H. An Overview on Starch-Based Sustainable Hydrogels: Potential Applications and Aspects. *J. Polym. Environ.* **2022**, *30* (1), 19–50. https://doi.org/10.1007/S10924-021-02180-9/FIGURES/11.

(35) Peppas, N. A.; Mikos, A. G. Preparation Methods and Structure of Hydrogels. *Hydrogels Med Pharm* **1986**, 1–26. https://doi.org/10.1201/9780429285097.

(36) Arab, M.; Jallab, M.; Ghaffari, M.; Moghbelli, E.; Saeb, M. R. Synthesis, Rheological Characterization, and Antibacterial Activity of Polyvinyl Alcohol (PVA)/ Zinc Oxide Nanoparticles Wound Dressing, Achieved under Electron Beam Irradiation. *Iran. Polym. J. (English Ed.* **2021**, *30* (10), 1019–1028. https://doi.org/10.1007/S13726-021-00952-7.

(37) Khozemy, E. E.; Nasef, S. M.; Mahmoud, G. A. Synthesis and Characterization

of Antimicrobial Nanocomposite Hydrogel Based on Wheat Flour and Poly (Vinyl Alcohol) Using γ-Irradiation. *Adv. Polym. Technol.* **2018**, *37* (8), 3252–3261. https://doi.org/10.1002/ADV.22094.

(38) Andrade, F.; Roca-Melendres, M. M.; Durán-Lara, E. F.; Rafael, D.; Schwartz, S. Stimuli-Responsive Hydrogels for Cancer Treatment: The Role of PH, Light, Ionic Strength and Magnetic Field. *Cancers 2021, Vol. 13, Page 1164* **2021**, *13* (5), 1164. https://doi.org/10.3390/CANCERS13051164.

(39) Passornraprasit, N.; Siripongpreda, T.; Ninlapruk, S.; Rodthongkum, N.; Potiyaraj, P. γ-Irradiation Crosslinking of Graphene Oxide/Cellulose Nanofiber/Poly (Acrylic Acid) Hydrogel as a Urea Sensing Patch. *Int. J. Biol. Macromol.* **2022**, *213*, 1037–1046. https://doi.org/10.1016/J.IJBIOMAC.2022.06.053.

(40) Jeong, J. O.; Park, J. S.; Kim, E. J.; Jeong, S. I.; Lee, J. Y.; Lim, Y. M. Preparation of Radiation Cross-Linked Poly(Acrylic Acid) Hydrogel Containing Metronidazole with Enhanced Antibacterial Activity. *Int. J. Mol. Sci.* **2019**, *21* (1), 187. https://doi.org/10.3390/IJMS21010187.

(41) Campos, E.; Coimbra, P.; Gil, M. H. An Improved Method for Preparing Glutaraldehyde Cross-Linked Chitosan-Poly(Vinyl Alcohol) Microparticles. *Polym. Bull.* **2013**, *70* (2), 549–561. https://doi.org/10.1007/S00289-012-0853-4.

(42) Wang, D.; Yang, X.; Liu, Q.; Yu, L.; Ding, J. Enzymatically Cross-Linked Hydrogels Based on a Linear Poly(Ethylene Glycol) Analogue for Controlled Protein Release and 3D Cell Culture. *J. Mater. Chem. B* **2018**, *6* (38), 6067–6079. https://doi.org/10.1039/C8TB01949E.

(43) Lai, E.; Bao, B.; Zhu, Y.; Lin, H. Transglutaminase-Catalyzed Bottom-Up Synthesis of Polymer Hydrogel. *Front. Bioeng. Biotechnol.* **2022**, *10*, 422. https://doi.org/10.3389/fbioe.2022.824747.

(44) Karvinen, J.; Ihalainen, T. O.; Calejo, M. T.; Jönkkäri, I.; Kellomäki, M. Characterization of the Microstructure of Hydrazone Crosslinked Polysaccharide-Based Hydrogels through Rheological and Diffusion Studies. *Mater. Sci. Eng. C* **2019**, *94*, 1056–1066. https://doi.org/10.1016/J.MSEC.2018.10.048.

(45) Aurand, E. R.; Lampe, K. J.; Bjugstad, K. B. Defining and Designing Polymers and Hydrogels for Neural Tissue Engineering. *Neurosci. Res.* **2012**, *72* (3),

199–213. https://doi.org/10.1016/J.NEURES.2011.12.005.

(46) Vasile, C.; Pamfil, D.; Stoleru, E.; Baican, M. New Developments in Medical Applications of Hybrid Hydrogels Containing Natural Polymers. *Molecules* **2020**, *25* (7), 1539. https://doi.org/10.3390/MOLECULES25071539.

(47) Tokarev, I.; Minko, S. Stimuli-Responsive Hydrogel Thin Films. *Soft Matter* **2009**, *5* (3), 511–524. https://doi.org/10.1039/B813827C.

(48) Richbourg, N. R.; Peppas, N. A. The Swollen Polymer Network Hypothesis: Quantitative Models of Hydrogel Swelling, Stiffness, and Solute Transport. *Prog. Polym. Sci.* **2020**, *105*, 101243. https://doi.org/10.1016/J.PROGPOLYMSCI.2020.101243.

(49) Cha, G. D.; Lee, W. H.; Lim, C.; Choi, M. K.; Kim, D. H. Materials Engineering, Processing, and Device Application of Hydrogel Nanocomposites. *Nanoscale* **2020**, *12* (19), 10456–10473. https://doi.org/10.1039/D0NR01456G.

(50) Rafieian, S.; Mirzadeh, H.; Mahdavi, H.; Masoumi, M. E. A Review on Nanocomposite Hydrogels and Their Biomedical Applications. *IEEE J. Sel. Top. Quantum Electron.* **2019**, *26* (1), 154–174. https://doi.org/10.1515/secm-2017-0161.

(51) Hernández-González, A. C.; Téllez-Jurado, L.; Rodríguez-Lorenzo, L. M. Alginate Hydrogels for Bone Tissue Engineering, from Injectables to Bioprinting: A Review. *Carbohydr. Polym.* **2020**, *229*, 115514. https://doi.org/10.1016/J.CARBPOL.2019.115514.

(52) Zhang, M.; Zhao, X. Alginate Hydrogel Dressings for Advanced Wound Management. *Int. J. Biol. Macromol.* **2020**, *162*, 1414–1428. https://doi.org/10.1016/J.IJBIOMAC.2020.07.311.

(53) Wang, Y.; Katyal, P.; Montclare, J. K. Protein-Engineered Functional Materials. *Adv. Healthc. Mater.* **2019**, *8* (11), 1801374. https://doi.org/10.1002/ADHM.201801374.

(54) Katyal, P.; Mahmoudinobar, F.; Montclare, J. K. Recent Trends in Peptide and Protein-Based Hydrogels. *Curr. Opin. Struct. Biol.* **2020**, *63*, 97–105. https://doi.org/10.1016/J.SBI.2020.04.007.

(55) Thakur, S.; Sharma, B.; Verma, A.; Chaudhary, J.; Tamulevicius, S.; Thakur, V. K. Recent Approaches in Guar Gum Hydrogel Synthesis for Water Purification. *https://doi.org/10.1080/1023666X.2018.1488661* **2018**, *23* (7),

621–632. https://doi.org/10.1080/1023666X.2018.1488661.

(56) Sharma, G.; Sharma, S.; Kumar, A.; Al-Muhtaseb, A. H.; Naushad, M.; Ghfar, A. A.; Mola, G. T.; Stadler, F. J. Guar Gum and Its Composites as Potential Materials for Diverse Applications: A Review. *Carbohydr. Polym.* **2018**, *199*, 534–545. https://doi.org/10.1016/J.CARBPOL.2018.07.053.

(57) Tian, B.; Hua, S.; Tian, Y.; Liu, J. Chemical and Physical Chitosan Hydrogels as Prospective Carriers for Drug Delivery: A Review. *J. Mater. Chem. B* **2020**, *8* (44), 10050–10064. https://doi.org/10.1039/D0TB01869D.

(58) Do, N. H. N.; Truong, Q. T.; Le, P. K.; Ha, A. C. Recent Developments in Chitosan Hydrogels Carrying Natural Bioactive Compounds. *Carbohydr. Polym.* **2022**, *294*, 119726. https://doi.org/10.1016/J.CARBPOL.2022.119726.

(59) Kaur, A.; Singh, D.; Sud, D. A Review on Grafted, Crosslinked and Composites of Biopolymer Xanthan Gum for Phasing out Synthetic Dyes and Toxic Metal Ions from Aqueous Solutions. *J. Polym. Res.* **2020**, *27* (10), 1–19. https://doi.org/10.1007/s10965-020-02271-6.

(60) Abu Elella, M. H.; Goda, E. S.; Gab-Allah, M. A.; Hong, S. E.; Pandit, B.; Lee, S.; Gamal, H.; Rehman, A. U.; Yoon, K. R. Xanthan Gum-Derived Materials for Applications in Environment and Eco-Friendly Materials: A Review. *J. Environ. Chem. Eng.* **2021**, *9* (1), 104702. https://doi.org/10.1016/J.JECE.2020.104702.

(61) Bao, Z.; Xian, C.; Yuan, Q.; Liu, G.; Wu, J. Natural Polymer-Based Hydrogels with Enhanced Mechanical Performances: Preparation, Structure, and Property. *Adv. Healthc. Mater.* **2019**, *8* (17), 1900670. https://doi.org/10.1002/ADHM.201900670.

(62) Catoira, M. C.; Fusaro, L.; Di Francesco, D.; Ramella, M.; Boccafoschi, F. Overview of Natural Hydrogels for Regenerative Medicine Applications. *J. Mater. Sci. Mater. Med.* **2019**, *30* (10), 1–10. https://doi.org/10.1007/s10856-019-6318-7.

(63) Gyles, D. A.; Castro, L. D.; Silva, J. O. C.; Ribeiro-Costa, R. M. A Review of the Designs and Prominent Biomedical Advances of Natural and Synthetic Hydrogel Formulations. *Eur. Polym. J.* **2017**, *88*, 373–392. https://doi.org/10.1016/J.EURPOLYMJ.2017.01.027.

(64) Singhal, R.; Gupta, K. A Review: Tailor-Made Hydrogel Structures (Classifications and Synthesis Parameters). *Polym. Plast. Technol. Eng.* **2016**,

55 (1), 54–70. https://doi.org/10.1080/03602559.2015.1050520.

(65) Wang, Y.; Ma, M.; Wang, J.; Zhang, W.; Lu, W.; Gao, Y.; Zhang, B.; Guo, Y. Development of a Photo-Crosslinking, Biodegradable GelMA/PEGDA Hydrogel for Guided Bone Regeneration Materials. *Mater. 2018, Vol. 11, Page 1345* **2018**, *11* (8), 1345. https://doi.org/10.3390/MA11081345.

(66) Zhang, J.; Zheng, Y.; Lee, J.; Hua, J.; Li, S.; Panchamukhi, A.; Yue, J.; Gou, X.; Xia, Z.; Zhu, L.; Wu, X. A Pulsatile Release Platform Based on Photo-Induced Imine-Crosslinking Hydrogel Promotes Scarless Wound Healing. *Nat. Commun. 2021 121* **2021**, *12* (1), 1–13. https://doi.org/10.1038/s41467-021-21964-0.

(67) Li, Z.; Wang, D.; Bai, H.; Zhang, S.; Ma, P.; Dong, W. Photo-Crosslinking Strategy Constructs Adhesive, Superabsorbent, and Tough PVA-Based Hydrogel through Controlling the Balance of Cohesion and Adhesion. *Macromol. Mater. Eng.* **2020**, *305* (1), 1900623. https://doi.org/10.1002/MAME.201900623.

(68) Das, D.; Pham, T. T. H.; Noh, I. Characterizations of Hyaluronate-Based Terpolymeric Hydrogel Synthesized via Free Radical Polymerization Mechanism for Biomedical Applications. *Colloids Surfaces B Biointerfaces* **2018**, *170*, 64–75. https://doi.org/10.1016/J.COLSURFB.2018.05.059.

(69) Khan, M. U. A.; Raza, M. A.; Razak, S. I. A.; Abdul Kadir, M. R.; Haider, A.; Shah, S. A.; Mohd Yusof, A. H.; Haider, S.; Shakir, I.; Aftab, S. Novel Functional Antimicrobial and Biocompatible Arabinoxylan/Guar Gum Hydrogel for Skin Wound Dressing Applications. *J. Tissue Eng. Regen. Med.* **2020**, *14* (10), 1488–1501. https://doi.org/10.1002/term.3115.

(70) Lin, T.; Bai, Q.; Peng, J.; Xu, L.; Li, J.; Zhai, M. One-Step Radiation Synthesis of Agarose/Polyacrylamide Double-Network Hydrogel with Extremely Excellent Mechanical Properties. *Carbohydr. Polym.* **2018**, *200*, 72–81. https://doi.org/10.1016/J.CARBPOL.2018.07.070.

(71) Afroz, S.; Afrose, F.; Alam, A. K. M. M.; Khan, R. A.; Alam, M. A. Synthesis and Characterization of Polyethylene Oxide (PEO)—N,N-Dimethylacrylamide (DMA) Hydrogel by Gamma Radiation. *Adv. Compos. Hybrid Mater.* **2019**, *2* (1), 133–141. https://doi.org/10.1007/s42114-018-0058-x.

(72) Alcântara, M. T. S.; Lincopan, N.; Santos, P. M.; Ramirez, P. A.; Brant, A. J. C.; Riella, H. G.; Lugão, A. B. Simultaneous Hydrogel Crosslinking and Silver

Nanoparticle Formation by Using Ionizing Radiation to Obtain Antimicrobial Hydrogels. *Radiat. Phys. Chem.* **2020**, *169*, 108777. https://doi.org/10.1016/j.radphyschem.2019.108369.

(73) Nezhad-Mokhtari, P.; Ghorbani, M.; Roshangar, L.; Soleimani Rad, J. Chemical Gelling of Hydrogels-Based Biological Macromolecules for Tissue Engineering: Photo- and Enzymatic-Crosslinking Methods. *Int. J. Biol. Macromol.* **2019**, *139*, 760–772. https://doi.org/10.1016/J.IJBIOMAC.2019.08.047.

(74) Kim, S. H.; Kim, K.; Kim, B. S.; An, Y. H.; Lee, U. J.; Lee, S. H.; Kim, S. L.; Kim, B. G.; Hwang, N. S. Fabrication of Polyphenol-Incorporated Anti-Inflammatory Hydrogel via High-Affinity Enzymatic Crosslinking for Wet Tissue Adhesion. *Biomaterials* **2020**, *242*, 119905. https://doi.org/10.1016/J.BIOMATERIALS.2020.119905.

(75) Zhong, Y.; Wang, J.; Yuan, Z.; Wang, Y.; Xi, Z.; Li, L.; Liu, Z.; Guo, X. A Mussel-Inspired Carboxymethyl Cellulose Hydrogel with Enhanced Adhesiveness through Enzymatic Crosslinking. *Colloids Surfaces B Biointerfaces* **2019**, *179*, 462–469. https://doi.org/10.1016/J.COLSURFB.2019.03.044.

(76) Adelnia, H.; Ensandoost, R.; Shebbrin Moonshi, S.; Gavgani, J. N.; Vasafi, E. I.; Ta, H. T. Freeze/Thawed Polyvinyl Alcohol Hydrogels: Present, Past and Future. *Eur. Polym. J.* **2022**, *164*, 110974. https://doi.org/10.1016/J.EURPOLYMJ.2021.110974.

(77) Deng, Z.; Wang, H.; Ma, P. X.; Guo, B. Self-Healing Conductive Hydrogels: Preparation, Properties and Applications. *Nanoscale* **2020**, *12* (3), 1224–1246. https://doi.org/10.1039/C9NR09283H.

(78) Banerjee, S. L.; Bhattacharya, K.; Samanta, S.; Singha, N. K. Self-Healable Antifouling Zwitterionic Hydrogel Based on Synergistic Phototriggered Dynamic Disulfide Metathesis Reaction and Ionic Interaction. *ACS Appl. Mater. Interfaces* **2018**, *10* (32), 27391–27406. https://doi.org/10.1021/acsami.8b10446.

(79) Chen, J.; Peng, Q.; Thundat, T.; Zeng, H. Stretchable, Injectable, and Self-Healing Conductive Hydrogel Enabled by Multiple Hydrogen Bonding toward Wearable Electronics. *Chem. Mater.* **2019**, *31* (12), 4553–4563. https://doi.org/10.1021/acs.chemmater.9b01239.

(80) Zhao, D.; Feng, M.; Zhang, L.; He, B.; Chen, X.; Sun, J. Facile Synthesis of Self-Healing and Layered Sodium Alginate/Polyacrylamide Hydrogel Promoted by Dynamic Hydrogen Bond. *Carbohydr. Polym.* **2021**, *256*, 117580. https://doi.org/10.1016/J.CARBPOL.2020.117580.

(81) Yu, H.; Rouelle, N.; Qiu, A.; Oh, J. A.; Kempaiah, D. M.; Whittle, J. D.; Aakyiir, M.; Xing, W.; Ma, J. Hydrogen Bonding-Reinforced Hydrogel Electrolyte for Flexible, Robust, and All-in-One Supercapacitor with Excellent Low-Temperature Tolerance. *ACS Appl. Mater. Interfaces* **2020**, *12* (34), 37977–37985. https://doi.org/10.1021/acsami.0c05454.

(82) Darge, H. F.; Andrgie, A. T.; Tsai, H. C.; Lai, J. Y. Polysaccharide and Polypeptide Based Injectable Thermo-Sensitive Hydrogels for Local Biomedical Applications. *Int. J. Biol. Macromol.* **2019**, *133*, 545–563. https://doi.org/10.1016/J.IJBIOMAC.2019.04.131.

(83) Hu, B.; Owh, C.; Chee, P. L.; Leow, W. R.; Liu, X.; Wu, Y. L.; Guo, P.; Loh, X. J.; Chen, X. Supramolecular Hydrogels for Antimicrobial Therapy. *Chem. Soc. Rev.* **2018**, *47* (18), 6917–6929. https://doi.org/10.1039/C8CS00128F.

(84) He, H.; Xiao, Z.; Zhou, Y.; Chen, A.; Xuan, X.; Li, Y.; Guo, X.; Zheng, J.; Xiao, J.; Wu, J. Zwitterionic Poly(Sulfobetaine Methacrylate) Hydrogels with Optimal Mechanical Properties for Improving Wound Healing in Vivo. *J. Mater. Chem. B* **2019**, *7* (10), 1697–1707. https://doi.org/10.1039/C8TB02590H.

(85) Iizawa, T.; Taketa, H.; Maruta, M.; Ishido, T.; Gotoh, T.; Sakohara, S. Synthesis of Porous Poly(N-Isopropylacrylamide) Gel Beads by Sedimentation Polymerization and Their Morphology. *J. Appl. Polym. Sci.* **2007**, *104* (2), 842–850. https://doi.org/10.1002/APP.25605.

(86) Said, H. M.; Alla, S. G. A.; El-Naggar, A. W. M. Synthesis and Characterization of Novel Gels Based on Carboxymethyl Cellulose/Acrylic Acid Prepared by Electron Beam Irradiation. *React. Funct. Polym.* **2004**, *61* (3), 397–404. https://doi.org/10.1016/J.REACTFUNCTPOLYM.2004.07.002.

(87) Mendoza, L.; Batchelor, W.; Tabor, R. F.; Garnier, G. Gelation Mechanism of Cellulose Nanofibre Gels: A Colloids and Interfacial Perspective. *J. Colloid Interface Sci.* **2018**, *509*, 39–46. https://doi.org/10.1016/J.JCIS.2017.08.101.

(88) Zhou, Y.; Zhao, S.; Zhang, C.; Liang, K.; Li, J.; Yang, H.; Gu, S.; Bai, Z.; Ye, D.; Xu, W. Photopolymerized Maleilated Chitosan/Thiol-Terminated Poly

(Vinyl Alcohol) Hydrogels as Potential Tissue Engineering Scaffolds. *Carbohydr. Polym.* **2018**, *184*, 383–389. https://doi.org/10.1016/J.CARBPOL.2018.01.009.

(89) De Smedt, S. C.; Lauwers, A.; Demeester, J.; Van Steenbergen, M. J.; Hennink, W. E.; Roefs, S. P. F. M. Characterization of the Network Structure of Dextran Glycidyl Methacrylate Hydrogels by Studying the Rheological and Swelling Behavior1". *Macromolecules* **1995**, *28*, 5082–5088.

(90) Richbourg, N. R.; Peppas, N. A. The Swollen Polymer Network Hypothesis: Quantitative Models of Hydrogel Swelling, Stiffness, and Solute Transport. *Prog. Polym. Sci.* **2020**, *105*, 101243. https://doi.org/10.1016/j.progpolymsci.2020.101243.

(91) Ben Ammar, N. E.; Saied, T. T.; Barbouche, M.; Hosni, F.; Hamzaoui, A. H.; Şen, M.; Elhouda, N.; Ammar, B.; Saied, T. T. A Comparative Study between Three Different Methods of Hydrogel Network Characterization: Effect of Composition on the Crosslinking Properties Using Sol–Gel, Rheological and Mechanical Analyses. *Polym. Bull.* **2018**, *75.9* (September), 3825–3841. https://doi.org/10.1007/s00289-017-2239-0.

(92) Sen, M.; Yakar, A.; Güven, O. Determination of Average Molecular Weight between Cross-Links ($\bar{M}$(c)) from Swelling Behaviours of Diprotic Acid-Containing Hydrogels. *Polymer (Guildf).* **1999**, *40* (11), 2969–2974. https://doi.org/10.1016/S0032-3861(98)00251-1.

(93) Gan, Y.; Li, P.; Wang, L.; Mo, X.; Song, L.; Xu, Y.; Zhao, C.; Ouyang, B.; Tu, B.; Luo, L.; Zhu, L.; Dong, S.; Li, F.; Zhou, Q. An Interpenetrating Network-Strengthened and Toughened Hydrogel That Supports Cell-Based Nucleus Pulposus Regeneration. *Biomaterials* **2017**, *136*, 12–28. https://doi.org/10.1016/j.biomaterials.2017.05.017.

(94) El-Sayed, S. A.; Mostafa, M. E. Pyrolysis Characteristics and Kinetic Parameters Determination of Biomass Fuel Powders by Differential Thermal Gravimetric Analysis (TGA/DTG). *Energy Convers. Manag.* **2014**, *85*, 165–172. https://doi.org/10.1016/J.ENCONMAN.2014.05.068.

(95) Opfermann, J. R.; Kaisersberger, E.; Flammersheim, H. J. Model-Free Analysis of Thermoanalytical Data-Advantages and Limitations. *Thermochim. Acta* **2002**, *391* (1–2), 119–127. https://doi.org/10.1016/S0040-6031(02)00169-7.

(96) Starink, M. J. The Determination of Activation Energy from Linear Heating

Rate Experiments: A Comparison of the Accuracy of Isoconversion Methods. *Thermochim. Acta* **2003**, *404* (1–2), 163–176. https://doi.org/10.1016/S0040-6031(03)00144-8.

(97) Jain, A. A.; Mehra, A.; Ranade, V. V. Processing of TGA Data: Analysis of Isoconversional and Model Fitting Methods. *Fuel* **2016**, *165*, 490–498. https://doi.org/10.1016/J.FUEL.2015.10.042.

(98) Riaz, U.; Ashraf, S. M. Characterization of Polymer Blends with FTIR Spectroscopy. *Charact. Polym. Blends Miscibility, Morphol. Interfaces* **2015**, *9783527331536*, 625–678. https://doi.org/10.1002/9783527645602.CH20.

(99) Jin, L.; Bai, R. Mechanisms of Lead Adsorption on Chitosan/PVA Hydrogel Beads. *Langmuir* **2002**, *18* (25), 9765–9770. https://doi.org/10.1021/la025917l.

(100) Yang, W.; Owczarek, J. S.; Fortunati, E.; Kozanecki, M.; Mazzaglia, A.; Balestra, G. M.; Kenny, J. M.; Torre, L.; Puglia, D. Antioxidant and Antibacterial Lignin Nanoparticles in Polyvinyl Alcohol/Chitosan Films for Active Packaging. *Ind. Crops Prod.* **2016**, *94*, 800–811. https://doi.org/10.1016/J.INDCROP.2016.09.061.

(101) Yang, W.; Fortunati, E.; Bertoglio, F.; Owczarek, J. S.; Bruni, G.; Kozanecki, M.; Kenny, J. M.; Torre, L.; Visai, L.; Puglia, D. Polyvinyl Alcohol/Chitosan Hydrogels with Enhanced Antioxidant and Antibacterial Properties Induced by Lignin Nanoparticles. *Carbohydr. Polym.* **2018**, *181*, 275–284. https://doi.org/10.1016/J.CARBPOL.2017.10.084.

(102) Hu, X. Q.; Ye, D. Z.; Tang, J. B.; Zhang, L. J.; Zhang, X. From Waste to Functional Additives: Thermal Stabilization and Toughening of PVA with Lignin. *RSC Adv.* **2016**, *6* (17), 13797–13802. https://doi.org/10.1039/C5RA26385A.

(103) Abraham, A.; Soloman, P. A.; Rejini, V. O. Preparation of Chitosan-Polyvinyl Alcohol Blends and Studies on Thermal and Mechanical Properties. *Procedia Technol.* **2016**, *24*, 741–748. https://doi.org/10.1016/J.PROTCY.2016.05.206.

(104) Kalantari, K.; Mostafavi, E.; Saleh, B.; Soltantabar, P.; Webster, T. J. Chitosan/PVA Hydrogels Incorporated with Green Synthesized Cerium Oxide Nanoparticles for Wound Healing Applications. *Eur. Polym. J.* **2020**, *134*, 109853. https://doi.org/10.1016/J.EURPOLYMJ.2020.109853.

(105) Beer, B.; Bartolome, M. J.; Berndorfer, L.; Bochmann, G.; Guebitz, G. M.; Nyanhongo, G. S. Controlled Enzymatic Hydrolysis and Synthesis of Lignin

Cross-Linked Chitosan Functional Hydrogels. *Int. J. Biol. Macromol.* **2020**, *161*, 1440–1446. https://doi.org/10.1016/J.IJBIOMAC.2020.08.030.

(106) Lee, E. S.; Kim, Y. O.; Ha, Y. M.; Lim, D.; Hwang, J. Y.; Kim, J.; Park, M.; Cho, J. W.; Jung, Y. C. Antimicrobial Properties of Lignin-Decorated Thin Multi-Walled Carbon Nanotubes in Poly(Vinyl Alcohol) Nanocomposites. *Eur. Polym. J.* **2018**, *105*, 79–84. https://doi.org/10.1016/j.eurpolymj.2018.05.014.

(107) Estellé, P.; Halelfadl, S.; Maré, T. Lignin as Dispersant for Water-Based Carbon Nanotubes Nanofluids: Impact on Viscosity and Thermal Conductivity. *Int. Commun. Heat Mass Transf.* **2014**, *57*, 8–12. https://doi.org/10.1016/J.ICHEATMASSTRANSFER.2014.07.012.

(108) Jaganathan, G.; Manivannan, K.; Lakshmanan, S.; Sithique, M. A. Fabrication and Characterization of Artocarpus Heterophyllus Waste Derived Lignin Added Chitosan Biocomposites for Wound Dressing Application. *Sustain. Chem. Pharm.* **2018**, *10*, 27–32. https://doi.org/10.1016/J.SCP.2018.08.002.

(109) Goodman, S. M.; Ferguson, N.; Dichiara, A. B. Lignin-Assisted Double Acoustic Irradiation for Concentrated Aqueous Dispersions of Carbon Nanotubes. *RSC Adv.* **2017**, *7* (9), 5488–5496. https://doi.org/10.1039/C6RA25986C.

(110) Sadeghifar, H.; Wells, T.; Le, R. K.; Sadeghifar, F.; Yuan, J. S.; Jonas Ragauskas, A. Fractionation of Organosolv Lignin Using Acetone:Water and Properties of the Obtained Fractions. *ACS Sustain. Chem. Eng.* **2017**, *5* (1), 580–587. https://doi.org/https://doi.org/10.1021/acssuschemeng.6b01955.

(111) Zhao, L.; Zhang, J.; Cao, P.; Kang, L.; Gong, Q.; Wang, J.; Zhang, Y.; Li, Q. Fast Water Transport Reversible CNT/PVA Hybrid Hydrogels with Highly Environmental Tolerance for Multifunctional Sport Headband. *Compos. Part B Eng.* **2021**, *211*, 108661. https://doi.org/10.1016/J.COMPOSITESB.2021.108661.

(112) Ren, Z.; Ke, T.; Ling, Q.; Zhao, L.; Gu, H. Rapid Self-Healing and Self-Adhesive Chitosan-Based Hydrogels by Host-Guest Interaction and Dynamic Covalent Bond as Flexible Sensor. *Carbohydr. Polym.* **2021**, *273*, 118533. https://doi.org/10.1016/J.CARBPOL.2021.118533.

(113) Dhiman, N. K.; Agnihotri, S. Hierarchically Aligned Nano Silver/Chitosan–PVA Hydrogel for Point-of-Use Water Disinfection: Contact-Active Mechanism Revealed. *Environ. Sci. Nano* **2020**, *7* (8), 2337–2350.

https://doi.org/10.1039/D0EN00405G.

(114) Zhu, W.; Lu, J.; Dai, L. Multifunctional PH-Responsive Sprayable Hydrogel Based on Chitosan and Lignin-Based Nanoparticles. *Part. Part. Syst. Charact.* **2018**, *35* (12), 1800145. https://doi.org/10.1002/PPSC.201800145.

(115) Morales, A.; Labidi, J.; Gullón, P. Assessment of Green Approaches for the Synthesis of Physically Crosslinked Lignin Hydrogels. *J. Ind. Eng. Chem.* **2020**, *81*, 475–487. https://doi.org/10.1016/J.JIEC.2019.09.037.

(116) Zhang, Y.; Jiang, M.; Zhang, Y.; Cao, Q.; Wang, X.; Han, Y.; Sun, G.; Li, Y.; Zhou, J. Novel Lignin–Chitosan–PVA Composite Hydrogel for Wound Dressing. *Mater. Sci. Eng. C* **2019**, *104*, 110002. https://doi.org/10.1016/J.MSEC.2019.110002.

(117) Byram, P. K.; Sunka, K. C.; Barik, A.; Kaushal, M.; Dhara, S.; Chakravorty, N. Biomimetic Silk Fibroin and Xanthan Gum Blended Hydrogels for Connective Tissue Regeneration. *Int. J. Biol. Macromol.* **2020**, *165*, 874–882. https://doi.org/10.1016/J.IJBIOMAC.2020.09.231.

(118) Zhang, Q.; Hu, X. M.; Wu, M. Y.; Wang, M. M.; Zhao, Y. Y.; Li, T. T. Synthesis and Performance Characterization of Poly(Vinyl Alcohol)-Xanthan Gum Composite Hydrogel. *React. Funct. Polym.* **2019**, *136*, 34–43. https://doi.org/10.1016/J.REACTFUNCTPOLYM.2019.01.002.

(119) Bernal-Chávez, S. A.; Alcalá-Alcalá, S.; Tapia-Guerrero, Y. S.; Magaña, J. J.; Del Prado-Audelo, M. L.; Leyva-Gómez, G. Cross-Linked Polyvinyl Alcohol-Xanthan Gum Hydrogel Fabricated by Freeze/Thaw Technique for Potential Application in Soft Tissue Engineering. *RSC Adv.* **2022**, *12* (34), 21713–21724. https://doi.org/10.1039/D2RA02295H.

(120) Enache, A. A.; Serbezeanu, D.; Vlad-Bubulac, T.; Ipate, A. M.; Suflet, D. M.; Drobotă, M.; Barbălată-Mândru, M.; Udrea, R. M.; Rîmbu, C. M. Tunable Properties via Composition Modulations of Poly(Vinyl Alcohol)/Xanthan Gum/Oxalic Acid Hydrogels. *Mater. 2022, Vol. 15, Page 2657* **2022**, *15* (7), 2657. https://doi.org/10.3390/MA15072657.

(121) Alupei, I. C.; Popa, M.; Hamcerencu, M.; Abadie, M. J. M. Superabsorbant Hydrogels Based on Xanthan and Poly(Vinyl Alcohol): 1. The Study of the Swelling Properties. *Eur. Polym. J.* **2002**, *38* (11), 2313–2320. https://doi.org/10.1016/S0014-3057(02)00106-4.

(122) Bhattacharya, S. S.; Mazahir, F.; Banerjee, S.; Verma, A.; Ghosh, A.

Preparation and in Vitro Evaluation of Xanthan Gum Facilitated Superabsorbent Polymeric Microspheres. *Carbohydr. Polym.* **2013**, *98* (1), 64–72. https://doi.org/10.1016/J.CARBPOL.2013.05.011.

(123) Saadatlou, G. A.; Pircheraghi, G. Concentrated Regimes of Xanthan-Based Hydrogels Crosslinked with Multifunctional Crosslinkers. *Carbohydr. Polym. Technol. Appl.* **2021**, *2*, 100047. https://doi.org/10.1016/J.CARPTA.2021.100047.

(124) Solihat, N. N.; Hidayat, A. F.; Taib, M. N. A. M.; Hussin, M. H.; Lee, S. H.; Ghani, M. A. A.; Edrus, S. S. A. O. Al; Vahabi, H.; Fatriasari, W. Recent Developments in Flame-Retardant Lignin-Based Biocomposite: Manufacturing, and Characterization. *J. Polym. Environ. 2022 3011* **2022**, *30* (11), 4517–4537. https://doi.org/10.1007/S10924-022-02494-2.

(125) Zhang, D.; Zeng, J.; Liu, W.; Qiu, X.; Qian, Y.; Zhang, H.; Yang, Y.; Liu, M.; Yang, D. Pristine Lignin as a Flame Retardant in Flexible PU Foam. *Green Chem.* **2021**, *23* (16), 5972–5980. https://doi.org/10.1039/D1GC01109J.

(126) Liu, L.; Qian, M.; Song, P.; Huang, G.; Yu, Y.; Fu, S. Fabrication of Green Lignin-Based Flame Retardants for Enhancing the Thermal and Fire Retardancy Properties of Polypropylene/Wood Composites. *ACS Sustain. Chem. Eng.* **2016**, *4* (4), 2422–2431. https://doi.org/10.1021/ACSSUSCHEMENG.6B00112.

(127) Fukushima, K.; Murariu, M.; Camino, G.; Dubois, P. Effect of Expanded Graphite/Layered-Silicate Clay on Thermal, Mechanical and Fire Retardant Properties of Poly(Lactic Acid). *Polym. Degrad. Stab.* **2010**, *95* (6), 1063–1076. https://doi.org/10.1016/J.POLYMDEGRADSTAB.2010.02.029.

(128) Chen, S.; Lin, S.; Hu, Y.; Ma, M.; Shi, Y.; Liu, J.; Zhu, F.; Wang, X. A Lignin-Based Flame Retardant for Improving Fire Behavior and Biodegradation Performance of Polybutylene Succinate. *Polym. Adv. Technol.* **2018**, *29* (12), 3142–3150. https://doi.org/10.1002/PAT.4436.

(129) Illeperuma, W. R. K.; Rothemund, P.; Suo, Z.; Vlassak, J. J. Fire-Resistant Hydrogel-Fabric Laminates: A Simple Concept That May Save Lives. *ACS Appl. Mater. Interfaces* **2016**, *8* (3), 2071–2077. https://doi.org/10.1021/acsami.5b10538.

(130) Liu, J.; Xiao, C. Fire-Retardant Multilayer Assembled on Polyester Fabric from Water-Soluble Chitosan, Sodium Alginate and Divalent Metal Ion. *Int. J. Biol.*

Macromol. **2018**, *119*, 1083–1089. https://doi.org/10.1016/J.IJBIOMAC.2018.08.043.

(131) Li, S.; Zhou, G.; Wang, Y.; Jing, B.; Qu, Y. Synthesis and Characteristics of Fire Extinguishing Gel with High Water Absorption for Coal Mines. *Process Saf. Environ. Prot.* **2019**, *125*, 207–218. https://doi.org/10.1016/J.PSEP.2019.03.022.

(132) Jiang, Z.; Dou, G. Preparation and Characterization of Chitosan Grafting Hydrogel for Mine-Fire Fighting. *ACS Omega* **2020**, *5* (5), 2303–2309. https://doi.org/https://doi.org/10.1021/acsomega.9b03551.

(133) Castro, D. O.; Karim, Z.; Medina, L.; Häggström, J. O.; Carosio, F.; Svedberg, A.; Wågberg, L.; Söderberg, D.; Berglund, L. A. The Use of a Pilot-Scale Continuous Paper Process for Fire Retardant Cellulose-Kaolinite Nanocomposites. *Compos. Sci. Technol.* **2018**, *162*, 215–224. https://doi.org/10.1016/J.COMPSCITECH.2018.04.032.

(134) Liu, A.; Berglund, L. A. Fire-Retardant and Ductile Clay Nanopaper Biocomposites Based on Montmorrilonite in Matrix of Cellulose Nanofibers and Carboxymethyl Cellulose. *Eur. Polym. J.* **2013**, *49* (4), 940–949. https://doi.org/10.1016/J.EURPOLYMJ.2012.12.017.

(135) Anielkis, B.; Wojciech, G.; Bartłomiej, M. Expandable Graphite Flakes as an Additive for a New Fire Retardant Coating for Wood and Cellulose Materials – Comparison Analysis. *Wood Fire Saf.* **2020**, 120–124. https://doi.org/10.1007/978-3-030-41235-7_18.

CHAPTER 2

EXTRACTION OF LIGNIN AND CELLULOSE FROM *Arundo Donax*

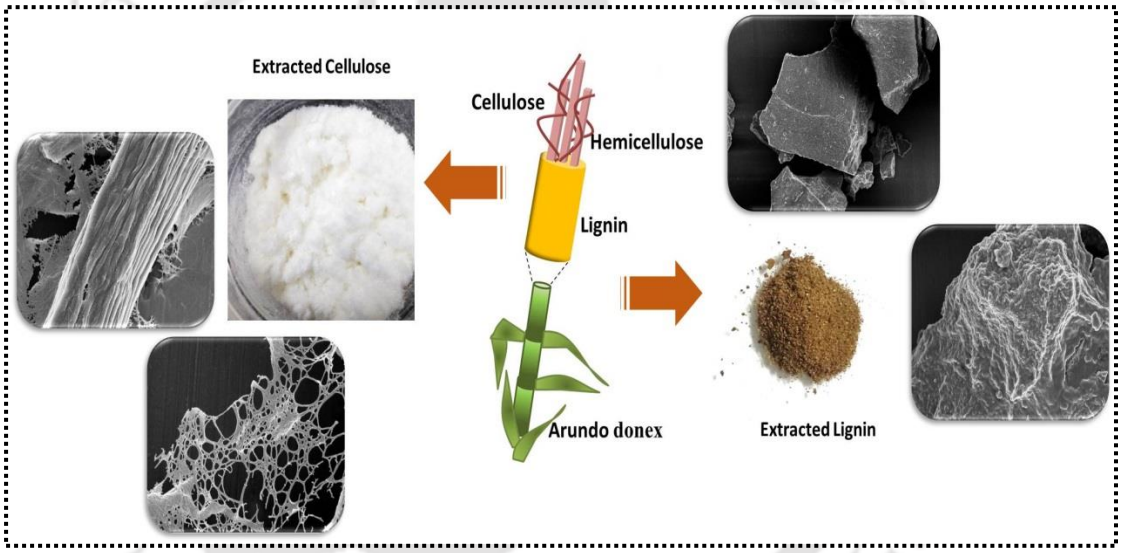

CHAPTER 2

EXTRACTION OF LIGNIN AND CELLULOSE FROM *Arundo Donax*

2.1 Introduction

Increasing population has increased consumption of raw materials and pollution. This situation demands for a low carbon life. Advocating and promoting renewable materials to achieve sustainability has become the new goal for both old and upcoming new industries and institutions. Lignocellulose biomass has emerged as potential renewable material due to availability and abundance in nature. Extensive efforts have been undertaken to develop sustainable materials from biomass. Biomass can be fractionated into its three major components, namely cellulose, hemicellulose, and lignin. Cellulose is a highly crystalline polysaccharide consisting of β-1,4 linked D-glucose units linear linkage. Cellulose can be extracted from both plants and bacteria. These are mostly found in packed microfibrils held together by intermolecular hydrogen bonding and weak van der Wall forces and play an important role in keeping the plant cell wall structure stable.[1] These are mainly used for the production of fibers and films. Similar to cellulose, hemicellulose is an integral part of plant cell wall, which immensely supports microfibrils cellulose. It is mainly composed of several different sugar units, viz. xylose, mannose, galactose, and arabinose.[2] Hemicellulose is mainly utilized for the production of biofuels. Similar to cellulose and hemicellulose, lignin is a highly crosslinked complex amorphous polysaccharide. It is made of syringyl (S), guaiacyl (G) and p-hydroxyphenyl (H)

moieties. This is mostly produced in the paper and pulp industry as a byproduct and incinerated to produce energy or discarded. Several research efforts have been going on to develop value added products, viz. vanillin from lignin. Recent advances report voluminous studies on synthesizing hydrogels from biomass components for various applications. Zhang et al.[3] reutilized bio-waste soybean dreg to develop low cost hydrogel adsorbents for removal of waste water remediation. Lin et al.[4] synthesized lignocellulose hydrogel evaporator for continuous production of fresh water from sea water. Introduction of lignin improved the hydrophilicity and maintain capillary channels in hydrogel and abet vaporization enthalpy of water. These environment friendly hydrogels were able to achieve sustainability as well as aid in solving global environmental problems.

Gaint reed or *Arundo donax* (AD) is an invasive perennial grass widely available in north east India. They belong to *Poaceae* family of the *Arundinae* tribe. These are segmented nodes and internodes tubular structured[5] (resembling bamboo) which can grow up to 6 m in height. They have long leaves with tapered tip and hairy base. Additionally, AD is a fast growing cane which can breed in different soil and climatic conditions. These are typically harvested for the production of biofuel, roof thatching, and as a source of fiber for printing paper. Its high biomass production makes it a great source of renewable material. AD has an interesting composition of cellulose, hemicellulose and lignin. Many studies have been reported on fractionation of high value products, viz. lignin, cellulose and hemicellulose, from AD. Shatalov and Pereira[6] reported extraction of lignin from AD using alkali method. Another study by Seca et al.[7] extracted lignin from nodes and internodes of AD and compared the chemical composition of the extracted lignins. Bessa et al.[8] extracted microcrystalline cellulose via acid hydrolysis from AD and reused the extract as reinforcement of

bisphenol A aniline based benzoxazine (BA-a). Shatalov and Pereira[9] extracted sulfur free cellulose from AD after selective removal of hemicellulose by dilute acid treatment. Candia et al.[10] valorized AD by extracting varying degree of cellulose fraction to formulate superabsorbent aerogels. Barana et al.[11] simultaneously fractionated lignin, cellulose and hemicellulose using alkaline method and further characterized the components.

This chapter reports the fractionation of cellulose and lignin from AD. Dilute acid hydrolysis was opted as the pretreatment process, followed by alkaline treatment to isolate lignin from biomass. Finally, the remaining biomass was treated with sodium chlorite to further remove the remaining lignin and hemicellulose to obtain highly crystalline cellulose. To maximize the utilization of the extracts, characterization was performed.

2.2 Experimental

2.2.1 Collection and processing of biomass

AD is widely available in Indian Institute of Technology Guwahati campus (Figure 2.1). The whole AD stem with leaves was collected, cut into pieces, and washed thoroughly to remove soil and unwanted foreign particles. Finally, it was dried at 45ºC in a hot air oven. Once dried the stem was fed to jaw crusher, to facilitate processing of AD nodes. After the biomass was fully crushed, a grinder was used to further reduce its size to pass through a sieve of 1000 μm and stored in an air tight container for the extraction process.

Figure 2.1 *Arundo donax* in IIT Guwahati campus

2.2.2 Compositional analysis of AD

Proximate were determined according to the standard protocol of NREL.[12] Ultimate analysis [C, H, N, S, O] was determined by elemental analysis [Elemental Analyzer (Exeter Analytical, CE 440)]. The methods followed to determine proximate analysis are mentioned in **Table 2.1**. The samples were first made free of extractives (nonstructural component of biomass viz. waxes, protein, chlorophyll etc.) by following the NREL/TP-510-42619 protocol. Extractive removal is an important step to avoid interference of extractive during further processing of samples. The protocol

states two step extractive removal processes. Initially, the ethanol soluble extractives were removed followed by removal of water soluble extractive. The solvent used for extractive removal were dicholomethane, ethanol and water (solvents mentioned in order of solvent used during extractive removal).[13] The extractives were determined gravimetrically.

Ash content, total dissolved solids and moisture content were determined using standard NREL protocol (**Table 2.1**) and were simultaneously performed along with extractive determination. To determine total dissolved solids and moisture, the sample was mix thoroughly first and weigh an appropriate amount to nearest 0.1mg. The measured sample was transferred to pre dried aluminum pan. The weight of the sample with the pan was recorded and then placed in an oven at 105± 3ºC for a minimum of four hours. At the end of four hours, the pan was removed and cooled in a desiccator and weight of the oven dried sample containing pan was recorded. The oven dried pan was placed back into the oven at 105 ± 3ºC and dry to constant weight. Constant weight is defined as ± 0.1% change in the weight percent solids upon one hour of re-heating the sample.

Table 2.1 Methods followed for proximate analysis

Analysis	Method
Extractives	NREL/TP-510-42619
Total dissolved solid, moisture content	NREL/TP-510-42621
Ash content	NREL/TP-510-42622
Structural carbohydrates and lignin	NREL/TP-510-42618

2.2.2.1 Estimation of lignin and carbohydrate content

To estimate the lignin and structural carbohydrate content NREL/TP-510-42618 procedure was followed. This is a two-step acid hydrolysis process, followed

by fractioned biomass for easier quantification of lignin and carbohydrates. Lignin fractionates into acid soluble and acid insoluble forms, which can be estimated gravimetrically and UV–Vis spectroscopy, respectively. Structural carbohydrates, during hydrolysis, break into their monomeric form, and HPLC is employed to quantify the different forms of carbohydrates.

Initially we weigh biomass in a tube and add 3 mL (or 4.92 g) of 72% H_2SO_4. The mixture was stirred for 1 min using a glass rod, placed in a water bath maintained at 30ºC and incubated for 1 h. The sample was stirred sporadically in 5 to 10 min without removing the tubes from water bath. After 1 h the sample was removed from the water bath and 86.73 mL of water was added to dilute the sample. The tube was sealed and shaken to mix the samples and then autoclaved the sample at 121ºC for 1 h. Allow the autoclaved sample to cool down at the end of 1 h. 10 mL of the sample was drawn into an aliquot for further processing and the remaining autoclaved sample was vacuum filtered to separate the filtrate and solids. The filtrate was transferred to a sample bottle which can be utilized to determine carbohydrates. The solids were washed with hot deionized water and dried at 105±3 ºC for 4 h. The residue that remained after drying is acid-insoluble lignin (AIL). Afterward, the residue was placed in the muffle furnace at 575±25 ºC for 24±6 h to determine the ash content of the residue.

To obtain the acid soluble lignin (ASL), UV–Vis absorption of the 10 mL of sample drawn in aliquot was performed. The samples were diluted with deionized water or sulfuric acid to bring the absorbance to 0.7 to 1.0 (the amount of dilution was recorded). The dilution solvent was used as blank (deionized water or sulfuric acid). This step was performed within 6h of biomass hydrolysis.

To quantify the carbohydrates of biomass HPLC was employed. Prepare a series of calibration of D-cellobiose, D(+)glucose, D(+)xylose, D(+)galactose, L(+)arabinose and D(+)mannose. Take the 50 mL of filtrate stored in sample bottle obtained after vacuum filtration and neutralized it using calcium carbonate. The addition of calcium carbonate was stopped after reaching 5 or 6 pH. The samples were allowed to settle, and the supernatant was decanted. The pH of the liquid after settling was recorded to be ~7. HPLC (mobile phase: HPLC grade water, Flow rate: 0.6 mL/min, Column temperature: 80–85 °C, was performed on the liquid obtained. The amount of glucose quantifies the cellulose content while the remaining component (xylose, galactose, arabinose and mannose) quantifies hemicellulose.[14] The amount of cellobiase detected is the result of over hydrolysis of the samples and indicates that the process must be repeated as some amount of carbohydrates was lost during hydrolysis.

2.2.3 Extraction of lignin and cellulose from *Arundo donax*

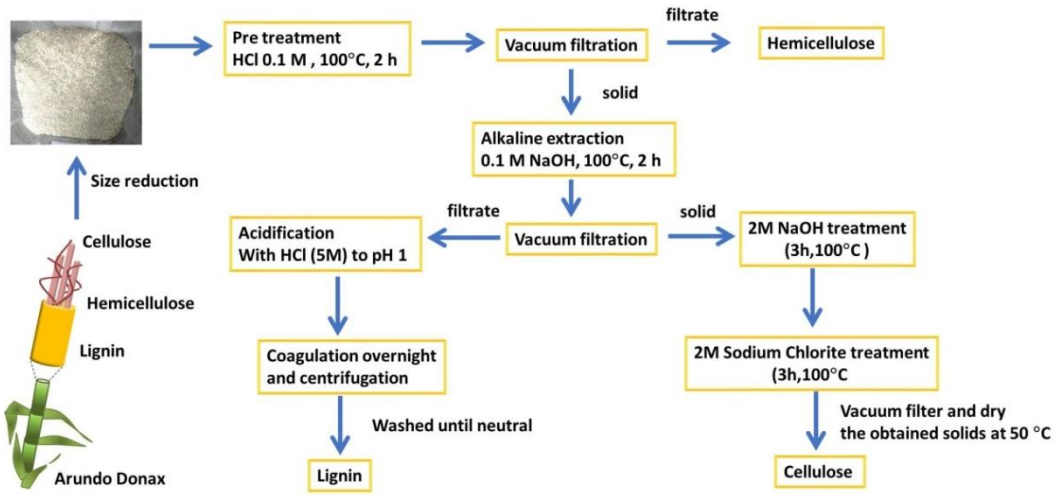

Figure 2.2 extraction process of lignin and cellulose

The extraction process of lignin and cellulose from *Arundo donax* is schematically represented in **Figure 2.2**. Prior to extraction process, the biomass was pretreated with dilute HCl (0.1 M) for 2 h to remove some part of hemicellulose. After 2 h the resultant was vacuum filtered to separate the filtrate and solid. The solid obtained was further process with 0.1 M NaOH for 2 h and vacuum filtered. The filtrate obtained is acidified with 5 M HCl to precipitate lignin. The precipitate was washed with deionized water until neutral. The solid obtained after vacuum filtration was further treated with 2 M NaOH for 3 h at 100ºC to remove any remaining hemicellulose and lignin in the solid. The solid obtained after 2 M alkaline treatment was treated with 2 M sodium chlorite to bleach the solid. This process was repeated until white solids or cellulose were obtained.

2.2.4 Characterization techniques

Crystallinity of cellulose was confirmed by X-ray diffractometer (XRD, Rigaku RINT 2500 TTRAX-III) equipped with Cu–Kα radiation (λ = 1.5406 Å) with nickel filter. Scans were recorded in the 2θ range of 10º to 70º. FTIR [Spectrum Two, PerkinElmer (USA)] was performed over the wavenumber range of 4000–400 cm^{-1} was to determine the chemical groups contributing in the structural formation of lignin and cellulose. FESEM [Sigma 300, Zeiss (USA)] enables to visualize the surface morphology of the extracted lignin and cellulose. The thermal decomposition profiles of biomass, lignin and cellulose were determined using TGA [TG 209 F1 Libra, Netzsch, Germany]. Gel permeation chromatography (GPC) [Agilent, G7820A], was employed to estimate the molecular weight of the extracted components. Tetrahydrofuran (THF) was used as eluent (injected at 1mL min^{-1} at 35ºC).

2.3 Results and discussion

2.3.1 Compositional analysis

Table 2.2 Proximate analysis of biomass

Characteristic	Value (%)
Moisture	9±0.05
Ash content	7±1
Cellulose	35±0.5
Hemicellulose	25±2
Lignin	14±0.35
Extractives	8.76±1.27

Table 2.3 Ultimate analysis of biomass, lignin and cellulose

	Biomass	Lignin	Cellulose
C (%)	56	55.32	39.78
H (%)	5.58	6.02	5.92
N (%)	1.64	0.79	0.04
S (%)	0.233	0.05	0.03
O (%)	36.54	37.82	54.23

Lignocellulose biomass consists primarily of polysaccharide cellulose and hemicellulose. The third primary component is lignin which is a phenolic polymer. Chemical composition of the biomass provides a better quantification of the carbohydrate and lignin content, enabling us to design an appropriate plan for the extraction and valorization of the extracted components. Also, the extractive content of the biomass can be quantified.

Extractive was removed from the biomass prior to hydrolysis. Three solvent, dichloromethane, ethanol and water, were refluxed in a soxhlet to carefully remove

the ethanol soluble and water soluble extractives. Ethanol extractives include waxes and chlorophyll whereas water soluble extractives include nonstructural sugars, inorganic materials and nitrogenous compounds[15]. The estimated total biomass extractives were around 8.76% (**Table 2.2**) consisting more water soluble extractives (4.12%) than the ethanol soluble extractives (3.26%).

Two step hydrolysis processes fractionate the biomass into its major component. During the first hydrolysis (72% H_2SO_4), undertaken at low temperature and short interval of time (30 ºC, 0.5 h) provide sufficient condition to solubilize C5 hemicellulose fraction. Meanwhile, a solid rich in cellulose and lignin is left behind. The second hydrolysis step performed at a higher temperature and longer period (121ºC, 1 h), fractionates the cellulose and lignin into more detectable monomers (sugars, acid soluble lignin and acid insoluble lignin). **Table 2.2** represents the result of the two step hydrolysis of biomass. The estimated values are 35% cellulose, 25% hemicellulose and 14% lignin. Elemental analysis of biomass reveals 56% of carbon, 36.54% oxygen, 5.58% hydrogen and 1.64% nitrogen and 0.223% sulfur. The results of extractive analysis corroborated with those of elemental analysis.

2.3.2 Extraction of lignin and cellulose

AD was acid–alkali treated to extract lignin and cellulose. Size reduced AD was pretreated with dilute HCl (0.1M) at 100ºC for 2 h to remove some part of hemicellulose. The solids obtained after dilute acid pretreatment was treated with 0.5 M NaOH at 100ºC for 2 h. This step solubilizes lignin and remaining hemicellulose sequentially, resulting in solids rich in cellulose. The filtrate obtained after vacuum filtration was allowed to precipitate to obtain lignin particles (**Figure 2.3a**) under acidic conditions (5 M HCl) by reducing the pH of the filtrate from pH 10 to 1. To remove traces of lignin and hemicellulose, the solids (from vacuum filtration) were

treated with 2 M NaOH at 100ºC for 2 h. To whiten the cellulose fibers the solids were treated with 2 M sodium chlorite at 100ºC for 2 h. This process was repeated at least two times to obtain bleached cellulose fibers (**Figure 2.3b**).

(a) (b)

Figure 2.3 Extracted (a)lignin and (b) cellulose

Table 2.4 Yield and purity of lignin

	NaOH	HCl+NaOH
Acid soluble lignin (ASL)	45.3±0.3	83.56±0.5
Acid insoluble lignin (AIL)	1.2±0.1	1.5±0.13
Ash	1.5±0.12	0.06±0.01
Purity(%)[a]	45	85
Yield(%)[b]	15	12

a purity of lignin was calculated as follows: ASL(wt%) +AIL(wt%)–Ash(wt%)[16]
b yield of lignin as follows: extracted lignin/lignin in biomass

Table 2.5 Yield and purity of cellulose

	1M Sodium Chlorite	2M Sodium Chlorite
Purity (%)	75	90
Yield (%)	48	55

The **Tables 2.4** and **2.5** represent the yield and purity of the extracted lignin and cellulose under different extraction conditions. Combination of dilute acid pretreatment with alkaline treatment yield lignin of higher purity.[11] Also, a low concentration of NaOH (0.5 M) facilitates extraction of high purity lignin. A higher alkali concentration (up to 2 M) resulted in more lignin extraction; however, the purity of the lignin extracted was compromised. In the case of cellulose, 2 M sodium chlorite yielded higher amount of high purity cellulose. HPLC was performed to validate the purity of the extracted cellulose.[17] To check the purity of the extracted cellulose, 3 g of the air dried cellulose sample was placed in 25ml of NaOH solution of 17.5 % (w/w).[18] Leaving the sample to swell for 5 mins, the pulp obtained was pressed. After pressing, another 25 ml of NaOH was added, and the sample was homogenized and left for 40 min. After 40 min, DI water was added and vacuum filtered. The sample was washed with DI water until the sample was neutral. After washing with DI water, 100 ml of 10% acetic acid was added to the sample for further washing, followed by DI water. The sample obtained after washing was oven dried at 105–106 ºC and weigh gravimetrically to estimate α cellulose. The purity of cellulose obtained was 90% (**Table 2.5**).

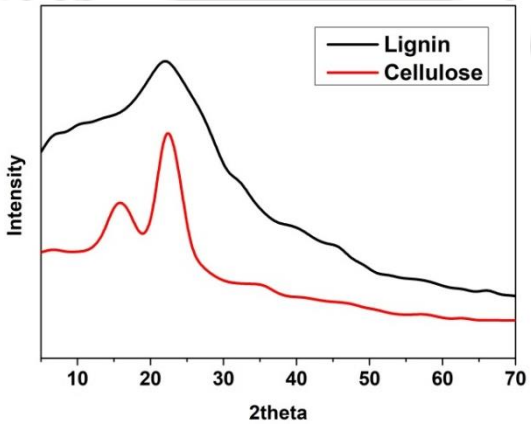

Figure 2.4 XRD of extracted lignin and cellulose

2.3.3 XRD to determine crystallinity of cellulose

Amorphous nature of lignin was evident by peak at 20º (**Figure 2.4**). XRD of cellulose reveals its crystalline nature with diffraction peaks at 16.3 and 22.6º that belong to (1 1 0) and (2 0 0) planes, which are the characteristic peaks of α-cellulose. Crystallinity index of cellulose was calculated from XRD using equation 2.1. Estimated crystallinity index (CI) was 52%.

$$CI = \frac{I_{200} - I_{110}}{I_{200}} \times 100 \qquad 2.1$$

where I_{200} and I_{110} represent the intensity at 200 and 110 planes.

2.3.4 FTIR of lignin and cellulose

FTIR analysis was performed to confirm the functional groups in lignin and cellulose. **Figure 2.5a** reveals the presence of hydroxyl groups (peaks at 3500, 3000 cm^{-1}). The sharp peak at 2925 cm^{-1} can be ascribed to C–H bending. C=O stretching vibration conjugated to the aromatic ring showed a peak at 1654 cm^{-1}. Peaks at 1591 and 1507 cm^{-1} can be ascribed to C=C aromatic vibration. Peaks from 1206 to 1026 cm^{-1} are due to C–O stretching vibrations in alcohol hydroxyl group. The peak at 828 cm^{-1} can be ascribed to C–H out-of-plane in positions 2, 5 and 6 of guaiacyl units. Similarly, for cellulose, **Figure 2.5b** reveals presence of hydroxyl groups (broad peak at 3391 cm^{-1}). Cellulose is made up of several glucose units and peaks at 2906 and 1375 cm^{-1} are due to C–H stretching of glucose unit. A small peak at 1061 cm^{-1} can is attributed to the –C–O group of secondary alcohols and ethers groups in the cellulose chain backbone. Peak at 828 cm^{-1} is due to bending vibration of –C–O bonds in cellulose.[19]

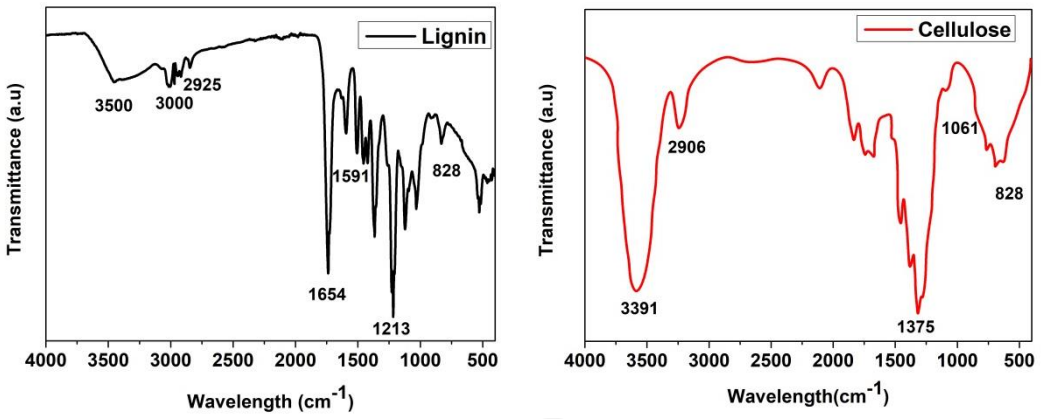

(a) **(b)**

Figure 2.5 FTIR spectra of (a) lignin and (b) cellulose

2.3.5 TGA of lignin and cellulose

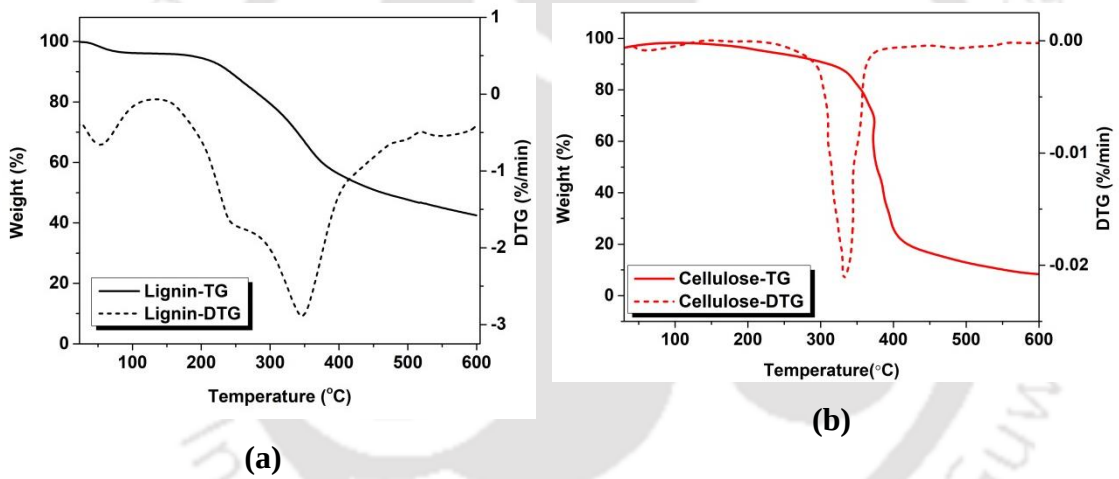

(a) **(b)**

Figure 2.6 TGA and DTG of (a) lignin and (b) cellulose

Performing thermal analysis on extracted components (lignin and cellulose) reveals the degradation profile and thermal stability of the material. The analysis was performed in the temperature range of 30–600ºC at 10ºC min^{-1} under nitrogen atmosphere. **Figure 2.6a and 2.6b** represent the TGA and DTG profile of lignin and cellulose respectively. **Figure 2.6a** shows a two-step degradation of lignin. Initial weight loss was observed in the temperature range of 30–150 ºC which is due to moisture loss. A major weight loss is observed in the temperature range of 200–500

ºC due to polymer backbone degradation. A small hump is observed at 234ºC due to degradation of phenylpropane side chains of lignin.[20] At the end of the analysis, 40% residue was observed. In the case of cellulose (Figure 2.6b), a single step degradation was observed between 220 and 480 ºC, mainly due to decomposition of carbon chains of cellulose.[21] At the end of the analysis, very less residue was obtained (~3%).

2.3.6 Estimation of molecular weight

Molecular weight is an integral property of a biomass component that strongly influences its interaction and valorization[22]. The molecular weight of the extracted lignin and cellulose were determined by GPC and represented in **Table 2.5** and **Figure 2.7**. Molecular weight of lignin was estimated by direct dissolution in THF and the estimated molecular weight of lignin was around 3357 g mol^{-1}. Direct dissolution of cellulose in THF is not possible. Hence, nitration of cellulose was adopted to produce THF soluble nitrocellulose. H_2SO_4:HNO_3 ratio of 50:50 at ambient temperature for 10 min. The nitration reaction was quenched by adding cold water. The obtained NC was neutralized with DI water at 100ºC. The cellulose structure and its derivative (nitrocellulose) have similar structures, but some hydroxyl groups get replaced by nitro groups in C2, C3 and C6 carbons. Thus, nitro groups can be joined at these positions giving a compound with the chemical formula $[C_6H_7O_2(OH)_{3-x}\ (ONO_2)]_n$, where x represent the nitro group replacing the hydroxyl group. The degree of substitution was calculated using the following equation 2.2.[23] The degree of substitution calculated was 1.7. Nitrogen content was calculated from the elemental analysis [Elemental analyzer Eurovector EA3100]. The amount of nitrogen estimated was 10.99 %. The molecular weight of cellulose was estimated to be 353470 g mol^{-1}.

$$DS = \frac{3.6 \times N\%}{31.13 - N\%} \qquad 2.2$$

Table 2.5 Elemental analysis of cellulose and nitrocellulose

Sample	C (wt. %)	H (wt. %)	N (wt. %)	S (wt. %)	O (wt. %)
Cellulose	39.78	5.92	0.04	0.02	54.26
Nitrocellulose	36.73	3.09	10.99	0.03	49.16

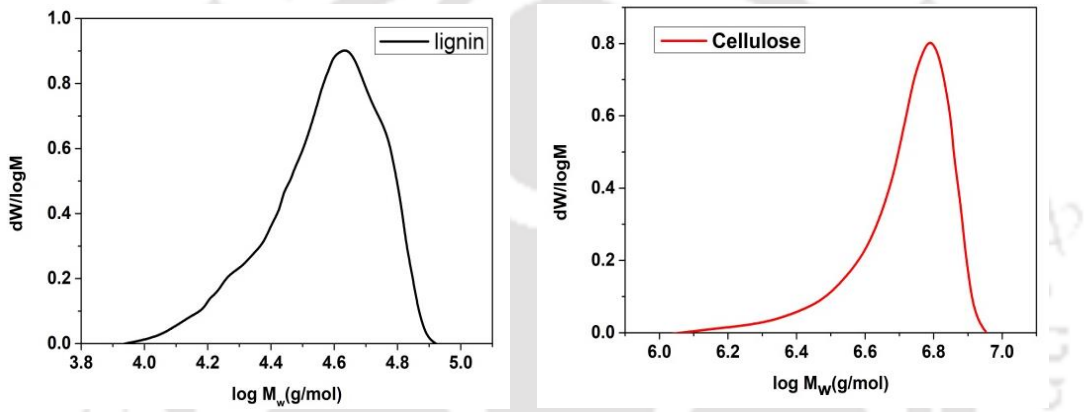

Figure 2.7 Molecular weight distribution of (a) lignin **(**b) cellulose

Table 2.6 Molecular weight of lignin and cellulose

Component	Mn (g/mol)	Mw (g/mol)
Lignin	1418	3357
Cellulose	81571	353470

2.3.7 FESEM of lignin and cellulose

The morphological features of the extracted lignin and cellulose are revealed by the FESEM images (**Figure 2.8**). **Figures 2.8a-c** shows the irregular sized lignin

particles extracted with sizes around 1000 µm. **Figures 2.8d-f** represents the FESEM images of cellulose fibers. The width of the fibers was around 10 to 80 µm.

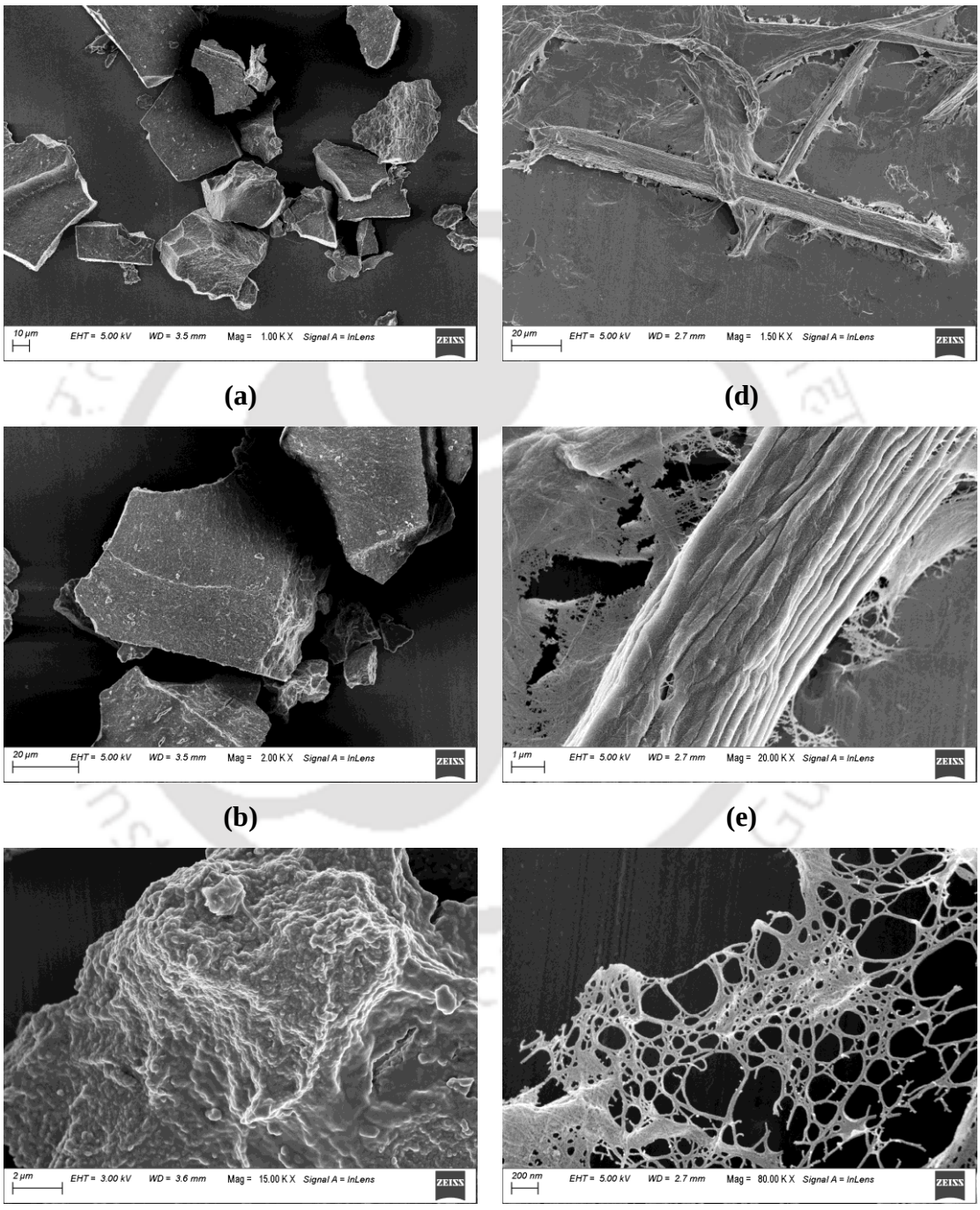

Figure 2.8 FESEM images of (a), (b) and (c) lignin and (d), (e) and (f) cellulose

2.4 Conclusions

In summary, we have successfully extracted lignin and cellulose from AD. Pretreatment and alkaline extraction methods yielded 12% lignin and 55% cellulose. Ultimate analysis of extracted components reveals high content of carbon and oxygen with smaller contents of nitrogen and sulfur. Additionally, the extracted lignin possessed a negligible amount of ash. Various techniques such as FTIR, FESEM, and TGA were used to characterize the extracted lignin and cellulose samples to reveal their functional groups, morphology, and thermal properties. At the end of the thermal analysis, the extracted lignin particles produced 40 wt.% of char, while the residue obtained for cellulose was –3wt. %. GPC analysis revealed the molecular weights of lignin and cellulose as 3357 g mol^{-1} and 353470 g mol^{-1}, respectively.

References

(1) Brigham, C. Biopolymers: Biodegradable Alternatives to Traditional Plastics. *Green Chem. An Incl. Approach* **2018**, 753–770. https://doi.org/10.1016/B978-0-12-809270-5.00027-3.

(2) Huang, L. Z.; Ma, M. G.; Ji, X. X.; Choi, S. E.; Si, C. Recent Developments and Applications of Hemicellulose From Wheat Straw: A Review. *Front. Bioeng. Biotechnol.* **2021**, *9*, 440. https://doi.org/10.3389/fbioe.2021.690773.

(3) Zhang, M.; Song, L.; Jiang, H.; Li, S.; Shao, Y.; Yang, J.; Li, J. Biomass Based Hydrogel as an Adsorbent for the Fast Removal of Heavy Metal Ions from Aqueous Solutions. *J. Mater. Chem. A* **2017**, *5* (7), 3434–3446. https://doi.org/10.1039/C6TA10513K.

(4) Lin, X.; Wang, P.; Hong, R.; Zhu, X.; Liu, Y.; Pan, X.; Qiu, X.; Qin, Y. Fully Lignocellulosic Biomass-Based Double-Layered Porous Hydrogel for Efficient Solar Steam Generation. *Adv. Funct. Mater.* **2022**, *32* (51), 2209262. https://doi.org/10.1002/ADFM.202209262.

(5) Shatalov, A. A.; Pereira, H. Influence of Stem Morphology on Pulp and Paper

Properties of Arundo Donax L. Reed. *Ind. Crops Prod.* **2002**, *15* (1), 77–83. https://doi.org/10.1016/S0926-6690(01)00098-X.

(6) Shatalov, A. A.; Pereira, H. Kinetics of Organosolv Delignification of Fibre Crop Arundo Donax L. *Ind. Crops Prod.* **2005**, *21* (2), 203–210. https://doi.org/10.1016/J.INDCROP.2004.04.010.

(7) Seca, A. M. L.; Cavaleiro, J. A. S.; Domingues, F. M. J.; Silvestre, A. J. D.; Evtuguin, D.; Neto, C. P. Structural Characterization of the Lignin from the Nodes and Internodes of Arundo Donax Reed. *J. Agric. Food Chem.* **2000**, *48* (3), 817–824. https://doi.org/10.1021/jf9910988.

(8) Bessa, W.; Tarchoun, A. F.; Trache, D.; Derradji, M. Preparation of Amino-Functionalized Microcrystalline Cellulose from Arundo Donax L. and Its Effect on the Curing Behavior of Bisphenol A–Based Benzoxazine. *Thermochim. Acta* **2021**, *698*, 178882. https://doi.org/10.1016/J.TCA.2021.178882.

(9) Shatalov, A. A.; Pereira, H. High-Grade Sulfur-Free Cellulose Fibers by Pre-Hydrolysis and Ethanol-Alkali Delignification of Giant Reed (Arundo Donax L.) Stems. *Ind. Crops Prod.* **2013**, *43* (1), 623–630. https://doi.org/10.1016/J.INDCROP.2012.08.003.

(10) Fontes-Candia, C.; Erboz, E.; Martínez-Abad, A.; López-Rubio, A.; Martínez-Sanz, M. Superabsorbent Food Packaging Bioactive Cellulose-Based Aerogels from Arundo Donax Waste Biomass. *Food Hydrocoll.* **2019**, *96*, 151–160. https://doi.org/10.1016/J.FOODHYD.2019.05.011.

(11) Barana, D.; Salanti, A.; Orlandi, M.; Ali, D. S.; Zoia, L. Biorefinery Process for the Simultaneous Recovery of Lignin, Hemicelluloses, Cellulose Nanocrystals and Silica from Rice Husk and Arundo Donax. *Ind. Crops Prod.* **2016**, *86*, 31–39. https://doi.org/10.1016/J.INDCROP.2016.03.029.

(12) Licursi, D.; Antonetti, C.; Bernardini, J.; Cinelli, P.; Coltelli, M. B.; Lazzeri, A.; Martinelli, M.; Galletti, A. M. R. Characterization of the Arundo Donax L. Solid Residue from Hydrothermal Conversion: Comparison with Technical Lignins and Application Perspectives. *Ind. Crops Prod.* **2015**, *76*, 1008–1024. https://doi.org/10.1016/J.INDCROP.2015.08.007.

(13) *Papermaking fibers from giant reed (Arundo donax L.) by advanced ecologically friendly pulping and bleaching technologies :: BioResources*. https://bioresources.cnr.ncsu.edu/resources/papermaking-fibers-from-giant-

reed-arundo-donax-l-by-advanced-ecologically-friendly-pulping-and-bleaching-technologies/ (accessed 2022-12-22).

(14) Garcia-Maraver, A.; Salvachúa, D.; Martínez, M. J.; Diaz, L. F.; Zamorano, M. Analysis of the Relation between the Cellulose, Hemicellulose and Lignin Content and the Thermal Behavior of Residual Biomass from Olive Trees. *Waste Manag.* **2013**, *33* (11), 2245–2249. https://doi.org/10.1016/J.WASMAN.2013.07.010.

(15) Pattiya, A. Fast Pyrolysis. *Direct Thermochem. Liq. Energy Appl.* **2018**, 3–28. https://doi.org/10.1016/B978-0-08-101029-7.00001-1.

(16) Yue, X.; Suopajärvi, T.; Sun, S.; Mankinen, O.; Mikkelson, A.; Huttunen, H.; Komulainen, S.; Romakkaniemi, I.; Ahola, J.; Telkki, V. V.; Liimatainen, H. High-Purity Lignin Fractions and Nanospheres Rich in Phenolic Hydroxyl and Carboxyl Groups Isolated with Alkaline Deep Eutectic Solvent from Wheat Straw. *Bioresour. Technol.* **2022**, *360*, 127570. https://doi.org/10.1016/J.BIORTECH.2022.127570.

(17) Yang, J.; Lu, X.; Liu, X.; Xu, J.; Zhou, Q.; Zhang, S. Rapid and Productive Extraction of High Purity Cellulose Material via Selective Depolymerization of the Lignin-Carbohydrate Complex at Mild Conditions. *Green Chem.* **2017**, *19* (9), 2234–2243. https://doi.org/10.1039/C7GC00493A.

(18) Handbook of Wood Chemistry and Wood Composites. *Handb. Wood Chem. Wood Compos.* **2005**. https://doi.org/10.1201/9780203492437.

(19) Hospodarova, V.; Singovszka, E.; Stevulova, N.; Hospodarova, V.; Singovszka, E.; Stevulova, N. Characterization of Cellulosic Fibers by FTIR Spectroscopy for Their Further Implementation to Building Materials. *Am. J. Anal. Chem.* **2018**, *9* (6), 303–310. https://doi.org/10.4236/AJAC.2018.96023.

(20) Ingtipi, K.; Moholkar, V. S. Sonochemically Synthesized Lignin Nanoparticles and Its Application in the Development of Nanocomposite Hydrogel. *Mater. Today Proc.* **2019**, *17*, 362–370. https://doi.org/10.1016/J.MATPR.2019.06.443.

(21) Leal, G. F.; Ramos, L. A.; Barrett, D. H.; Curvelo, A. A. S.; Rodella, C. B. A Thermogravimetric Analysis (TGA) Method to Determine the Catalytic Conversion of Cellulose from Carbon-Supported Hydrogenolysis Process. *Thermochim. Acta* **2015**, *616*, 9–13. https://doi.org/https://doi.org/10.1016/j.tca.2015.07.017.

(22) Tolbert, A.; Akinosho, H.; Khunsupat, R.; Naskar, A. K.; Ragauskas, A. J. Characterization and Analysis of the Molecular Weight of Lignin for Biorefi Ning Studies. *Biofuels, Bioprod. Bioref* **2014**. https://doi.org/10.1002/bbb.1500.

(23) Fernández De La Ossa, Á.; Torre, M.; García-Ruiz, C. Nitrocellulose in Propellants: Characteristics and Thermal Properties. *Adv. Mater. Sci. Res.* **2012**, 201–220.

भारतीय प्रौद्योगिकी संस्थान गुवाहाटी
Indian Institute of Technology Guwahati

CHAPTER 3

ULTRASOUND ASSISTED LIGNIN-DECORATED MWCNT DOPED FLEXIBLE PVA–CHITOSAN COMPOSITE HYDROGEL

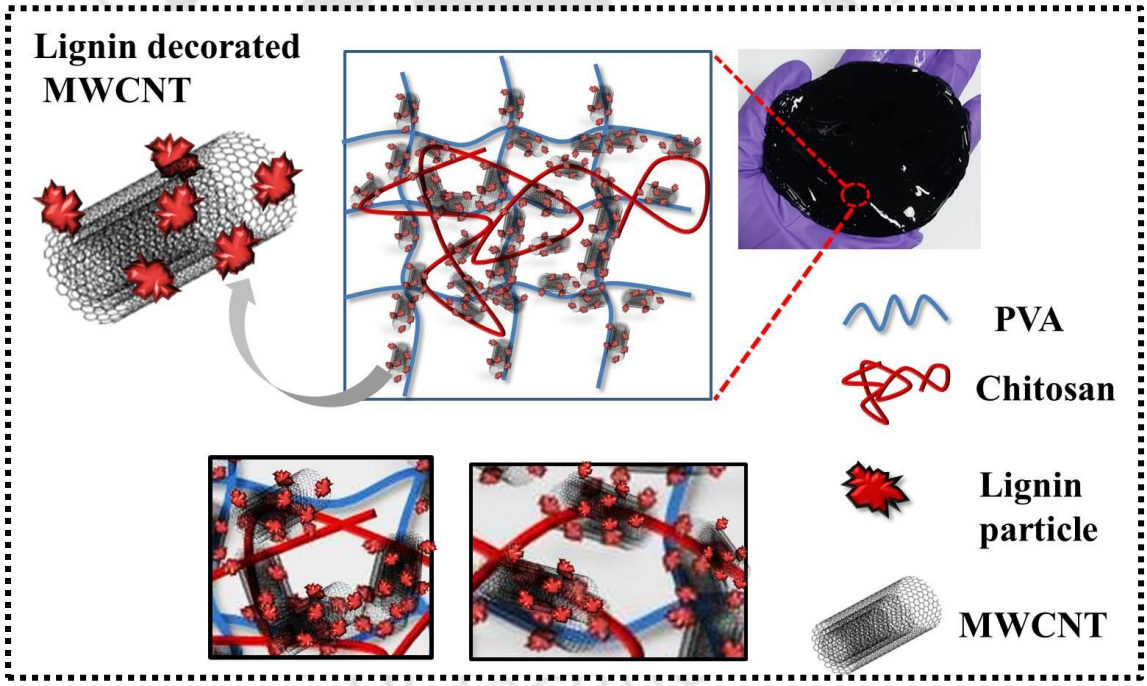

CHAPTER 3

ULTRASOUND ASSISTED LIGNIN-DECORATED MWCNT DOPED FLEXIBLE PVA–CHITOSAN COMPOSITE HYDROGEL

3.1 Introduction

Conductive hydrogels are soft, crosslinked polymer matter with tunable physical, chemical, and electrical properties. These are ideal as scaffolds in tissue engineering [1,2], bioelectronics [3,4], electrodes and electrolytes in supercapacitors and batteries [5,6], and ECG electrodes [7–9] owing to their conductivity and biocompatibility. Chitosan and PVA, by virtue of their biocompatibility and non-toxicity, have been widely used in the synthesis of these hydrogels.[10–12] Chitosan (CS) is a natural polysaccharide; however, it exhibits poor mechanical strength.[13,14] To overcome this shortcoming, PVA is blended with chitosan. PVA is a synthetic, water-soluble polymer that acts as the second matrix to CS, imparting mechanical support to the weak CS matrix.[11] Previous studies have shown that the electrical properties of PVA–CS hydrogel can be tuned via addition of numerous fillers or additives. Carbonaceous additives (CNT [15], graphene [16,17], carbon black [18], activated carbon [19,20]), liquid metal [21–23], and metal (Fe^{3+} [24,25], Al^{3+} [26] and ZnO [27]) have been widely exploited to impart as well as modify conductivity according to desired flexibility or stiffness of the polymer matrix. However, dispersion of CNT in water is tedious. CNTs tend to aggregate as a result of van der Waals forces between their sidewalls. This tube-to-tube contact results in the hydrophobic nature of CNTs, which is responsible for their poor solubility in water and incompatibility with most solvents. [28] As a result, CNTs tend to settle down in aqueous solution. These difficulties in manipulating CNTs in

aqueous medium limit the development of CNT-based devices or composites of interest for new applications. In order to obtain fine dispersion of CNTs in the selected solutions, especially water, it is important to break the cohesion of aggregated CNTs. This can be achieved by using ultrasound and the usage of different additives, such as surfactants (SDS, CTAB, and Triton X-100), organic solvents (DMF, acetone), and polymers. Rojas et al. [29] optimized ultrasound parameters to disperse multi-walled carbon nanotubes (MWCNT). Also, Triton X–100 (a non-ionic surfactant) was added to aid the dispersion of MWCNT in the aqueous medium. This technique of ultrasonication of CNTs in presence of surfactant produced debundled, unshortened and damage-free CNTs. Jung et al. [30] reported surfactant-aided and ultrasound-assisted dispersion of supercritical fluid-treated CNTs in aqueous medium. Results of Raman spectra validated the undamaging effect of the developed process. Bibi et al. [31] demonstrated that ultrasonication in very dilute acid could overcome the van der Waal forces of interaction between CNTs as well as modify its surfaces to obtain a fine dispersion. Jian et al. [32] studied the influence of sodium dodecylbenzene sulfonate (SDBS), SDS, and ultrasound on CNT dispersion. They reported that ultrasonication and surfactant could overcome the surface energy of CNTs and induce de-agglomeration. This process could effortlessly disperse small diameter CNTs whereas SDS dispersed larger diameter CNTs. Recently, Yuan et al. [33] reported ultrasound assisted aqueous dispersion of MWCNT. Further, organic solvents [34] such as acetone [35] and THF [36] have been used in dispersion of CNT. Bansal et al. [37] reported ultrasound assisted dispersion of CNT in presence of acetone. The acetone-aided fine dispersion was able to enhance the elastic modulus of the epoxy composite by 36% even with a small reinforcement of around 0.25 wt% of CNT.

Recently, valorisation of lignin has gained a lot of attention. Its application varied from polymer composite formulation, stabilizing pickering emulsion, dye absorbents, source of carbon, and as dispersants to name a few. However, hydrophobic nature of lignin limits its utilization in aqueous systems. Various methods have been employed for the alleviation of this impediment. In this case, as well, ultrasound offers a viable solution for dispersion of lignin in aqueous systems. In a liquid medium, ultrasound (US) induces nucleation of gas/vapor bubbles. US being a longitudinal wave moves through the liquid medium in the form of compression and rarefaction cycles. Propagation of ultrasound waves gives rise to bulk pressure variation in the liquid medium. This pressure variation gives rise to the phenomenon of cavitation, which is nucleation, growth, and transient collapse of gas/vapor bubbles. The phenomena of ultrasound wave propagation and cavitation induce intense convection in the system, which results in micro-mixing. Moreover, the cavitation bubbles also produce radical species on transient collapse, which induce chemical reactions in the system.[38] Prolonged exposure to sonication may lead to cleavage of phenyl ether α-O-4 and β-O-4 linkages in lignin macromolecule.[39] Simultaneously, radicals produced during cavitation oxidize the aromatic moieties (through hydroxylation) and also promote homolytic chain scission of the lignin macromolecules.[40–42] In the presence of additives such as surfactants and organic solvents, the time required for sonication can be significantly reduced.

This work is aimed at developing PVA-CS-MWCNT hydrogels. A peculiar feature of our synthesis methodology is that we have obtained the dispersion of MWCNT in water with the aid of lignin particles and acetone. The resultant dispersion of MWCNT in water was added to an aqueous mixture of PVA and CS. The crosslinking between PVA and CS was achieved through freeze-thaw cycles to

obtain composite hydrogels. The resultant hydrogels were characterized by standard techniques, viz. FTIR, TGA, FETEM, FESEM. The swelling ability of the hydrogels was also extensively evaluated. The conductivity of the hydrogels was measured using Electrochemical Impedance Spectroscopy (EIS) measurements.

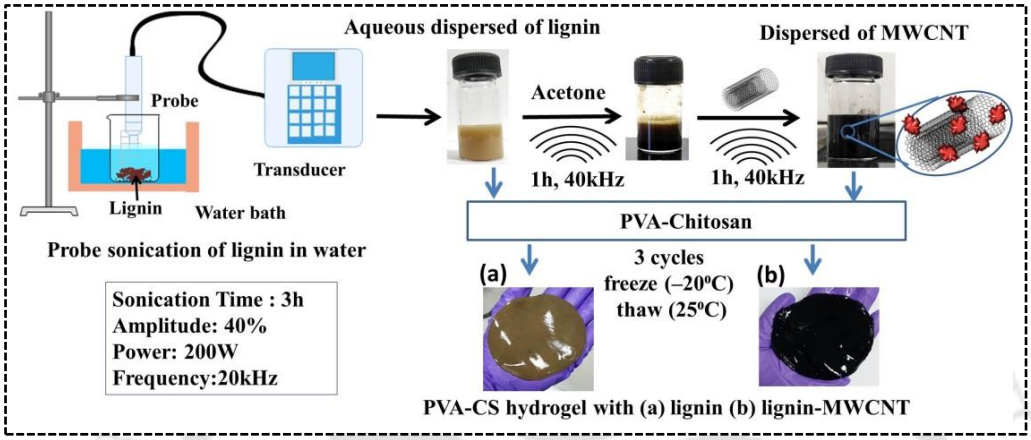

(a)

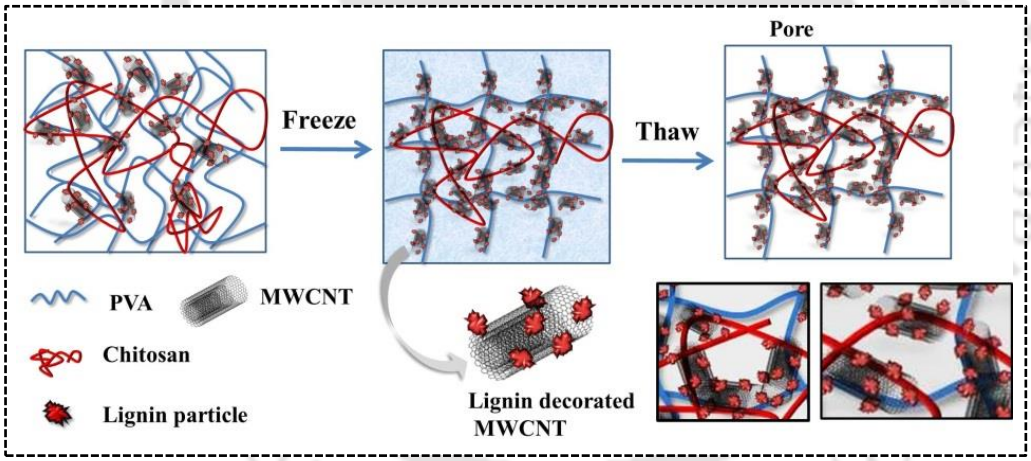

(b)

Figure 3.1 (a) Process followed for dispersion and formulation of hydrogels (b) Illustrative representation of physical crosslinking of the formulated hydrogel.

3.2 Experimental

3.2.1 Materials

PVA (Mw 89,000-98,000, 99+% hydrolyzed) and CS were purchased from Sigma Aldrich. MWCNT (outer diameter: 5–20 nm; inner diameter: 2–6 nm; length:

1–10 µm) was procured from Reinste Nano Ventures Ltd., India. Acetone (HPLC grade) was purchased from Merck. Lignin was extracted from *Arundo Donax* (AD) by alkaline treatment (0.1 M NaOH, 3 h) as previously described in chapter 2.[43,44]

3.2.2 Aqueous dispersion of MWCNT

Firstly, 1 g lignin in 45 ml water was sonicated using an ultrasound probe-type processor (Sonics and Materials VCX 500, 20 kHz, 200 W) for 3 h to obtain homogeneous lignin particle (LP) dispersion (**Figure 3.1a**). 5 ml acetone was added to this aqueous dispersion, followed by 1 h sonication in an ultrasound bath (Jeiotech, UC-10, 40 kHz, 300 W). Next, the desired quantity of MWCNT was added to this dispersion with further sonication for 1 h in the ultrasound bath.

3.2.3 Hydrogel formulation

Solutions of 10% w/v polyvinyl alcohol (PVA) and 2% w/v chitosan (CS) were separately prepared. Aqueous PVA solution was prepared by heating a mixture of 90 mL water and 10 g PVA powder for 20 min at 120^{o}C. Similarly, CS solution was prepared by adding 2 g CS in 98 ml of 1% v/v acetic acid solution. The resultant solution was centrifuged to remove any suspended undissolve particles. PVA and CS solutions were mixed at a volume ratio of 90:10, and this mixture was subjected to 3 freeze-thaw cycles (20 h freezing at –20 ºC, 4 h thaw at room temperature) to obtain PVA–CS hydrogels. Likewise, to prepare hydrogels containing MWCNT, an adequate amount of aqueous suspension of lignin and MWCNT (as described in the previous section) was added to PVA–CS solution and subjected to freeze-thaw cycles (**Figure 3.1b**). Five hydrogels with varying compositions were synthesized, as listed in **Table 3.1**.

Table 3.1 Composition of hydrogels

Composition	PVA (wt. %)	CS (wt. %)	Lignin (wt. %)	MWCNT (wt. %)
S1	10	2	--	--
S2	10	2	1	--
S3	10	2	2	--
S4	10	2	1	0.5
S5	10	2	2	1

3.2.4 Investigation of MWCNT dispersion by lignin

Particle sizes of LPs were measured by a particle size analyzer [Delsa Nano C, Beckman Coulter (Switzerland)]. FTIR of lignin and LPs were performed as mentioned in chapter 2. Dispersion of CNT by lignin is confirmed by UV-visible spectroscopy (Shimadzu, UV-2600, Japan), FETEM analysis (2100F, Jeol, Japan), zeta potential [Delsa Nano C, Beckman Coulter (Switzerland)] and surface tension (Kyowa, DY300) measurements. All the measurements for UV-visible analysis were performed in a quartz cuvette and dispersant samples were diluted to the same factor.

3.2.5 Characterization of PVA –CS hydrogel

Structural features of hydrogel were determined by FTIR and FESEM (Sigma 300, Zeiss, USA). Thermal stability of the freeze dried hydrogels was characterized using TGA [TG 209 F1 Libra, Netzsch (Germany)]. The swelling ability of the hydrogel was studied by immersing a sample of dimensions 1×1 cm^2 in distilled water followed by oven drying at 50ºC. The swelling ratio was calculated using equation 3.1.

$$SR = \frac{W_s - W_d}{W_s} \times 100 \qquad (3.1)$$

where, W_s and W_d denote the weight of the swollen hydrogel after time t and the weight of the dry gel, respectively.

The mechanical stability of formulated hydrogels was assessed by measurement of rheological properties (Anton Paar MCR 301). Dynamic strain sweep in the 0.01 to 100 Hz frequency range was performed to determine the linear viscoelastic region (LVR). Subsequently, for a constant strain % (the value of strain % taken half of the LVR), the dynamic frequency sweep was also performed. The mesh size of freeze dried hydrogels was calculated based on the following equation:

$$\xi = \left(\frac{G' N_A}{RT} \right)^{-1/3} \tag{3.2}$$

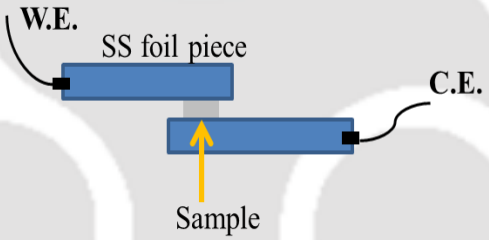

Figure 3.2 Experimental configuration for EIS of hydrogel between two SS foil pieces

3.2.6 Measurement of conductivity of the formulated hydrogel

The conductivity of hydrogels was measured in the frequency range of 100 kHz to 0.01 Hz using the EIS method [45] with M204 Potentiostat/Galvanostat (Metrohm Autolab). Individual hydrogels were equilibrated in DI water (pH 6). The hydrogels were sandwiched between two stainless steel (SS) plates tightly (1.0 cm × 1.0 cm), and an AC potential of 20 mV was applied (**Figure 3.2**). Since the gel thickness is fixed. The obtained EIS spectra were fit to equivalent circuit models. The

model includes inductors (L), resistors (R), constant phase element (CPE), and the finite Warburg diffusion impedance (W), which follows the certain impedance relationship as shown in equations 3.3–3.6. Then, the bulk resistance of the hydrogels was obtained, and the conductivity of the hydrogels was calculated following equation 3.7.

$$Z_L = i\omega L \tag{3.3}$$

$$Z_R = R \tag{3.4}$$

$$Z_{CPE} = \frac{1}{Y_0(i\omega)^{-1/2}} \tag{3.5}$$

$$Z_w = \sigma(i\omega)^{-1/2} \tag{3.6}$$

$$\sigma = \frac{l}{AR} \tag{3.7}$$

where l (mm) is the thickness of the hydrogel and A (cm^2) is the contact area of hydrogels and stainless steel plates.

3.3 Results and discussion

3.3.1 MWCNT dispersion by lignin

US was applied for dispersing as well as for size reduction of lignin particles. As previously reported in chapter 2, the initial size of the lignin particles extracted from *Arundo Donax* was 1000 μm (**Figure 3.3c**), US reduced the size of the lignin particles to 10–50 nm (**Figures 3.3a and 3.3d**).[43] Also, LP obtained after 3h sonication showed an increased presence of the C=O group, which is attributed to condensed aromatic groups. FTIR spectra of lignin and LPs confirmed peaks at 1700

and 1654, which are C=O non-conjugate stretching vibrations. Additionally, the increased intensity of the peak at 1118 is due to C–O stretching (**Figure 3.3b**).[42] These LPs, along with US and acetone, aided the dispersion of MWCNT in water. The dispersion of lignin, MWCNT is comprehensively characterized by measuring the UV absorption spectra, surface tension, zeta potential, and FETEM.

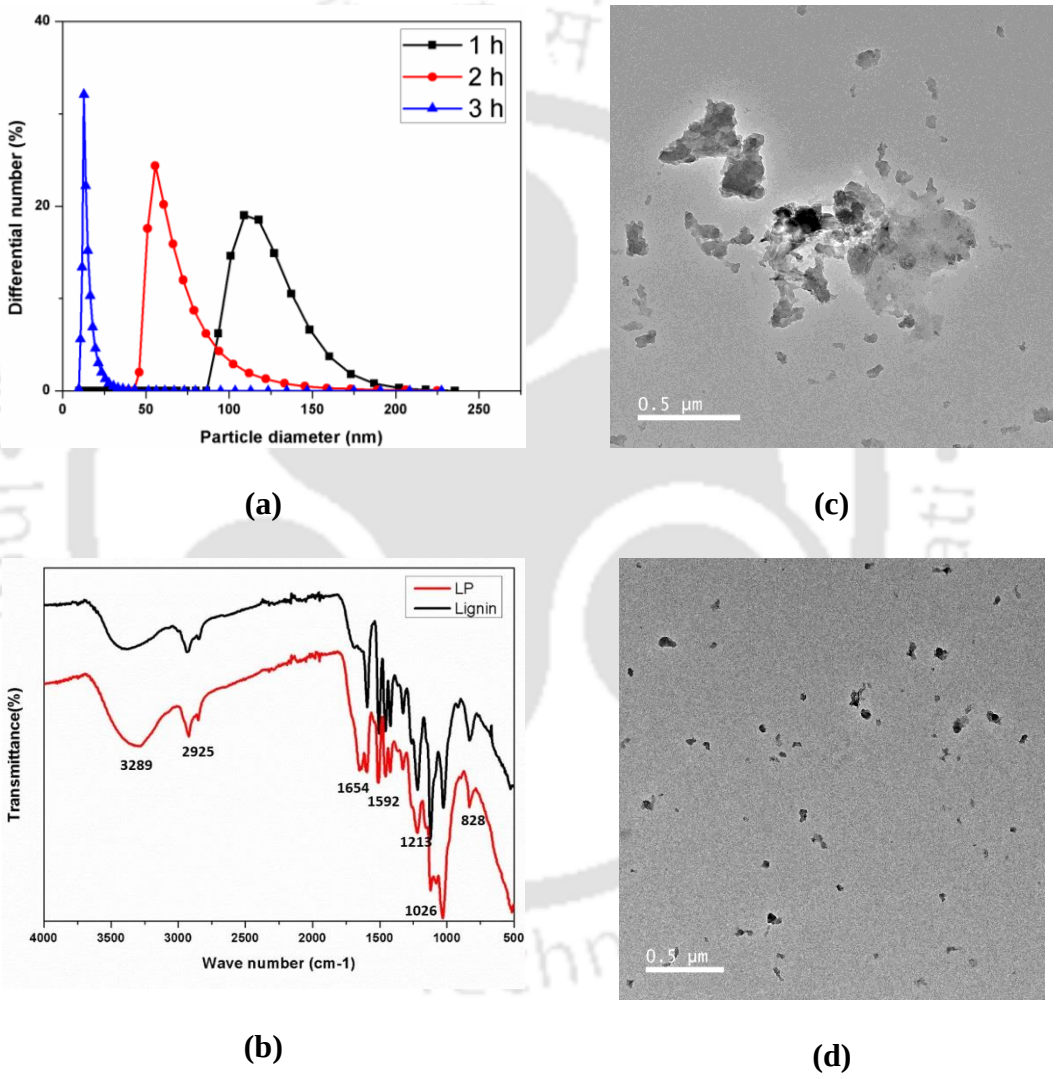

Figure 3.3 (a) Particle size of lignin particles post sonication. (b) FTIR spectra of lignin and lignin particles. FETEM images of lignin particles (c)before sonication and (d) post 3h sonication

Table 3.2 Zeta potential and surface tension of LP and MWCNT suspension

Composition	Zeta potential (mV)	Surface tension (mN m^{-1})
LP	- 46.00	26.83
2:1 LP:MWCNT	- 43.99	30.42
1:1 LP:MWCNT	-41.97	32.30
LP(acetone free)	-38.00	62.05

3.3.1.1 Effect of ultrasound and acetone on MWCNT dispersion

This section discusses the dispersion of MWCNT by lignin aided by acetone and US. Alkaline lignin is hydrophobic in nature, which tends to agglomerate and reduces its reactivity.[46] Hence, US is used for particle size reduction of lignin as well as to enhance its reactivity for improved dispersion of lignin and MWCNT. Dispersion of suspension obtained by US and the addition of acetone was confirmed by measuring the ς potential and surface tension (**Table 3.2**). For acetone-free LP suspension, the ς potential measured was higher (–38 mV) than the suspensions containing acetone obtained after US. As mentioned in the previous section 3.1 long hours of US results in oxidation of lignin by the radicals generated during US process.[47] Also, the large structure of lignin breaks up into smaller particles. This trait encourages improved dispersion of lignin particles, manifested in reduced ς potential (– 46 mV LP suspension aided by acetone and US). However, prolonged US may induce crosslinking of the phenolic hydroxyl groups of lignin. Hence, a shorter US time is always beneficial. To further aid the dispersion, acetone was added to the LP suspension. The dissolution of lignin due to addition of acetone is evident from the change of color of the suspension from light brown to dark brown (**Figure 3.1a**). The addition of acetone reduces the surface tension of the suspension due to formation of a hydrogen bond between the O atom of acetone and the H atom of water.[48] Hence, the

surface tension of the aqueous lignin suspension after sonication (62.05 mN m^{-1}) further decreases to 26.83 mN m^{-1} after addition of acetone (**Table 3.2**).

3.3.1.2 UV–vis spectroscopy

UV–vis spectroscopy is a common technique for characterizing the dispersion of CNT and lignin. Also, any structural changes in lignin induced by sonication can be determined from the UV spectra. Lignin consists of different chromophore functional groups, which absorb in UV or visible range.[49] Similarly, disentangled individual CNTs are active in UV–vis region and show characteristic spectra of absorption due to 1D van Hoff singularities.[50] However, bundled (or aggregated) CNTs tend to quench the photoluminescence usually detected in the range of 300–1200 nm, whereas non-dispersed LP may settle down due to gravity. Hence, uniform dispersion of lignin and debundled CNTs show higher UV absorption. **Figure 3.4** represents the absorption spectra of lignin and CNT suspension in acetone and acetone free solvent. The spectrum of lignin particle (LP) in acetone shows the highest absorption ratio (across entire wavelength range) as compared to acetone free solvent and MWCNT dispersed solvents. Acetone is a non–VOC solvent with a similar solubility parameter (Hildebrand and Hansen) for lignin.[51] Hence, lignin is moderately soluble in acetone owing to its high hydrogen bonding capacity.[52] **Figure 3.4** demonstrates that the suspension of LP dispersed by US alone had a lower absorption ratio, whereas the absorption increased with the addition of acetone to the suspension. For the suspension consisting of LP-aided MWCNT dispersion, the effect of ratio of LP to MWCNT was evident. 2:1 LP:MWCNT suspension performed better than the 1:1 LP:MWCNT suspension.[50,53] These trends in UV absorption spectra clearly suggest that dispersion of MWCNT in aqueous solution is promoted by lignin

nanoparticles, and this process is also assisted by sonication and the addition of acetone.

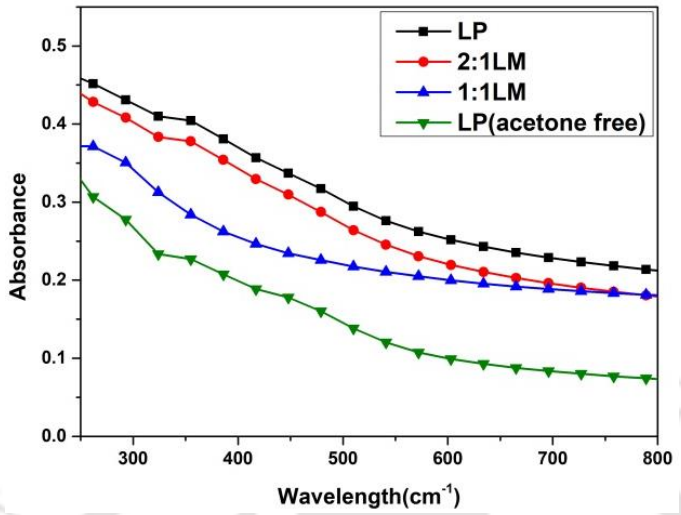

Figure 3.4 UV absorption of ultrasound assisted LP and LP– MWCNT suspension with and without addition of acetone.

3.3.1.3 Morphological analysis of dispersion

Further, FETEM was employed to validate the homogeneous dispersion of the suspension and the effect of US and acetone on lignin and MWCNT (**Figure 3.5**). Based on our previous findings, on the application of US alone to disperse lignin particles, the particle size obtained was in the range of 10–50 nm and the particles were irregular shaped.[43,54] These lignin particles were utilized to disperse the MWCNT in water (**Figures 3.5a, 3.5b, and 3.5c**). We observed that the MWCNTs were dispersed and the lignin particles adhere to the MWCNT which promoted the dispersion of MWCNT (**Figures 3.5b and 3.5c**). In the case of acetone aided dispersion, dissolution of lignin particles was seen cladded to MWCNT (**Figures 3.5e and 3.5f**). It can be said that acetone helped the adhesion of lignin to MWCNT, promoting better dispersion of MWCNT. The strong interaction between lignin and MWCNT is attributed to the presence of aromatic moieties which allowed π–π

interaction with MWCNT.[55] Acetone solubilized lignin provides more opportunity for lignin to strongly associate with MWCNT and clad onto its surface (**Figure 3.5d** and **3.5e**).

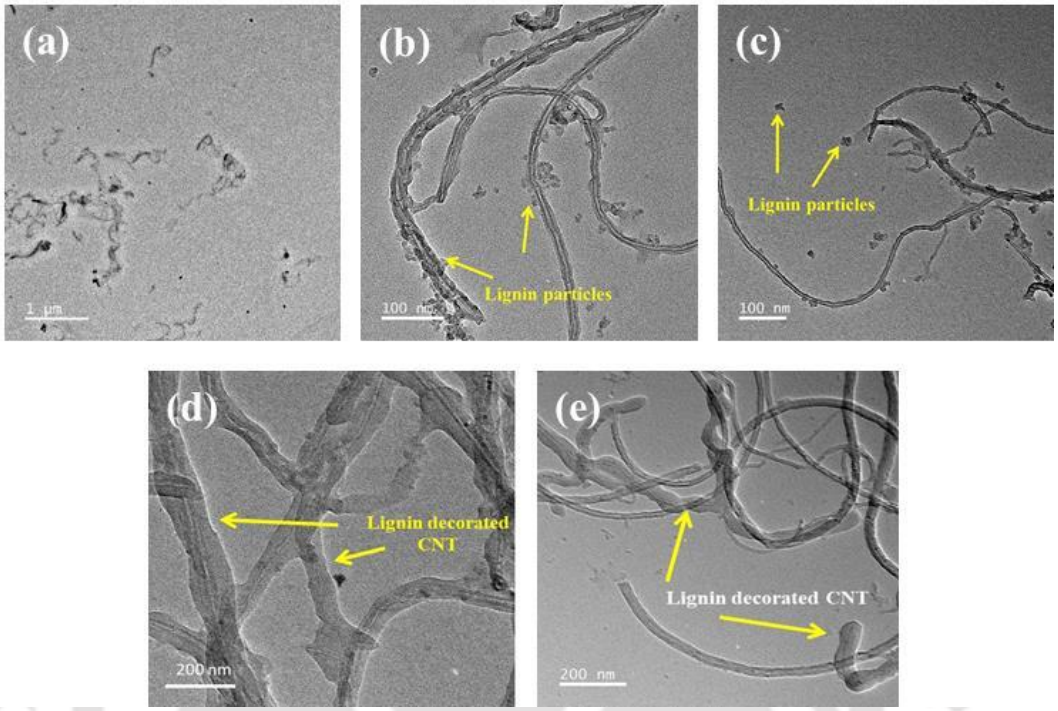

Figure 3.5 US assisted (a-c) LP and MWCNT dispersion in water (d and e) LP and MWCNT dispersion in presence of acetone

3.3.2 Characterization of formulated hydrogels

3.3.2.1 Physical crosslinking of hydrogel

Hydrogels were formulated by adopting physical gelation and solidification of the PVA via freeze−thaw method. Such a technique produces stable hydrogels that are physically crosslinked by the presence of crystalline regions in PVA.[56,57] FTIR was employed to confirm the formation of bonding between the polymers and fillers. From **Figure 3.6**, it can be clearly stated that with the increase in lignin particles and MWCNT, the strong broad peak between 3700 and 3000 cm^{-1} reduces to a weak and broad peak due to O−H stretching, suggesting an increase in intermolecular bonding

of hydrogels. Similarly, two peaks between 2700 and 3000 cm−1 are characteristic bands of $–CH_2$ and –CH vibrational stretching. Also, a significant reduction in peak intensity is observed at 1081 cm^{-1} which is a characteristic band of C−O stretching due to aliphatic ether and aliphatic alcohol. Hence, we can conclude a strong bond formation between lignin dispersed MWCNT and polymers matrix.

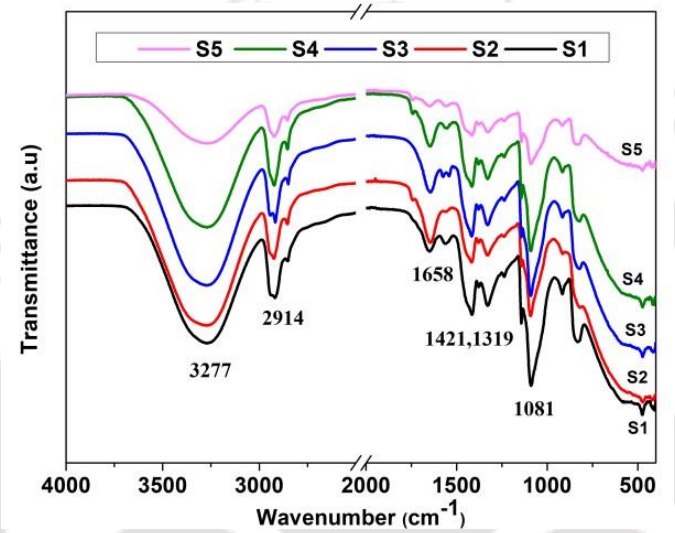

Figure 3.6 FTIR spectra of formulated hydrogel and schematic representation of the network formed in physically crosslinked hydrogels.

3.3.2.2 Investigation of thermal stability of the hydrogels

TGA was employed to investigate the thermal stability of the formulated hydrogel. **Figures 3.7a** and **3.7b** represent the TGA and DTG curves of hydrogels consisting of lignin and MWCNT. Three stages of degradation are observed. Initial degradation occurred until 200ºC, which can mainly be attributed to physically adsorbed water molecules. The second stage of degradation occurs around 300ºC, which can be ascribed to dehydration, decomposition, and chain scissioning of PVA, CS, and lignin. Dehydration of hydroxyl groups present in PVA, and the formation of volatile organic compounds and conjugated polyenes induce degradation of PVA. [58]

Chitosan degrades due to deacetylation and decomposition of glycosidic linkages. [59] The third stage of degradation is mainly due to decomposition of remaining thermally stable compounds, i.e. polyenes residue of PVA, pyranose ring of CS, and residue carbon. Further, from **Figure 3.7a**, it can be perceived that presence of lignin in PVA–CS has improved the thermal stability of the hydrogel. The addition of 1 wt% of lignin shifts the degradation peak from around 290ºC to 300ºC. This can be attributed to the pore forming ability of lignin, which delays removal of water molecules and residual acetic acid.[60] Further, lignin and MWCNT possess high thermal stability.[61,62] Hence, incorporation of lignin decorated MWCNT in PVA–CS matrix increased the thermal stability of the hydrogels and shift in the % degradation of the hydrogels.

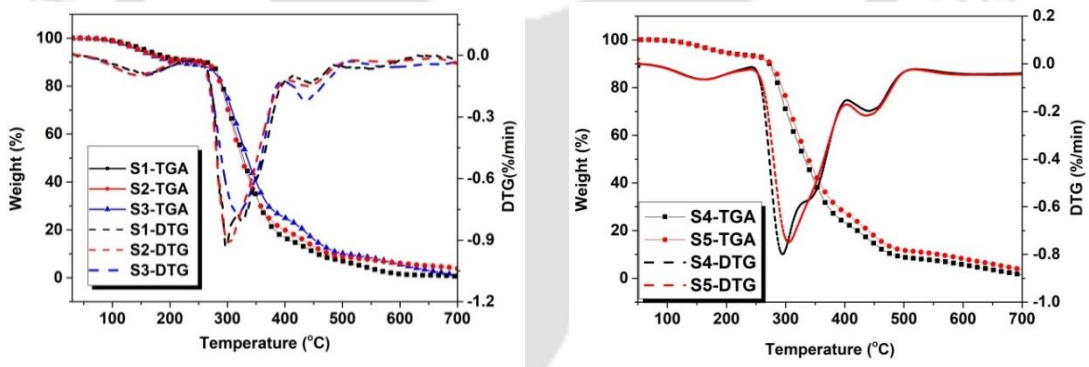

Figure 3.7 TGA and DTG curve of (a) S1 (control sample), S2 and S3 (lignin particle) hydrogel (b) S4 and S5 hydrogel consisting of MWCNT

Table 3.3 TGA of formulated hydrogels

Hydrogel	Stage I	Weight loss %	Stage II	Weight loss %	Stage III	Weight loss %	Residual weight % @700ºC
S1	30–210	10	230–350	80	360–450	7	3
S2	30–230	9	235–370	78	365–450	8	4
S3	30–235	9.5	240–375	50	370–455	15	15
S4	30–240	8	255–380	65	370–510	18	10
S5	30–247	9.7	256–380	55	372–512	17	12

Heating rate 10 ºC min^{-1}

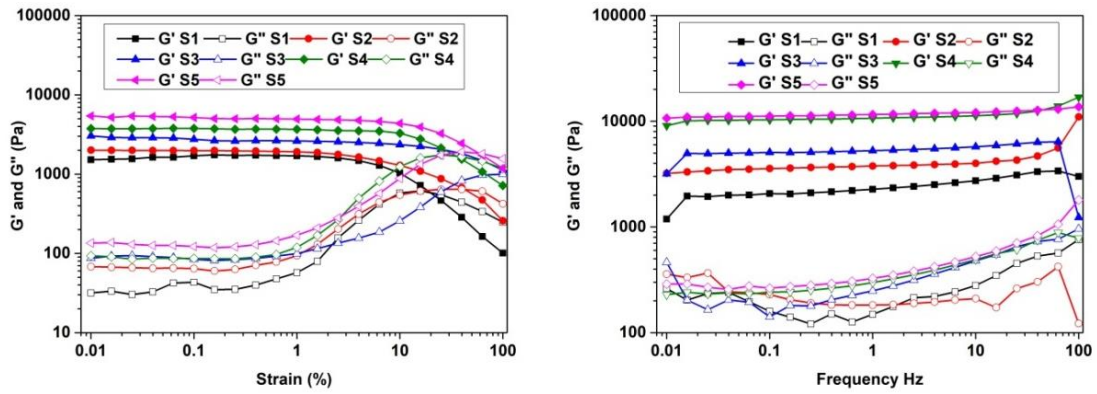

(a) **(b)**

Figure 3.8 (a) Amplitude sweep at constant 1 Hz frequency, (b) Frequency sweep at 1% strain.

3.3.2.3 Mechanical stability of hydrogels

Mechanical strength and viscoelastic behavior of the PVA–CS composite hydrogels were evaluated by performing oscillatory rheological measurements, i.e. amplitude sweep (**Figure 3.8a**) and frequency sweep (**Figure 3.8b**) to calculate G′ (storage modulus) and G″ (loss modulus). For the sol phase of the material, G″ > G′ whereas for the gel phase G′ > G″. Initially, amplitude sweep test was carried out over the wide range of strain (i.e., 0.01–100 %) and constant frequency to determine linear viscoelastic region (LVR) of hydrogel samples. Under this region, the kinetics of gelation was monitored by recording G′ and G″ which was achieved by maintaining the same experimental conditions while testing the samples. **Figure 3.8a** shows that for the low strain G′ and G'' the samples portray linear behavior. For higher strain%, G' decreases whereas G″ increases until cross over. The LVR was observed at 2% strain. Additionally, G′ dominated over G″ throughout the LVR. This suggests that physical crosslinking of PVA induces strong interaction with CS as well as with the additives (MWCNT and lignin particles), resulting in hydrogel formation. Considering the G′ > G″, the developed hydrogels confirm the viscoelastic solid-like

behavior, hence, confirming the formation of gel. **Figure 3.8b** demonstrates the influence of LP on the viscoelasticity of PVA–CS hydrogel. Addition of LP to the polymer mixture increased G' (sample S2 and S3) compared to pristine PVA–CS hydrogel (sample S1). The results clearly showcased the increment in G′ with increasing the concentration of lignin particles in PVA–CS hydrogel. The superior G′ over G″ throughout the frequency range confirms the formation of gel, post incorporation of lignin particles [63,64]. It is interesting to observe the improvement in the modulus of PVA–CS hydrogel by around 200% with 1% and 2% of lignin particles. This could be possible because of the strong interactions between PVA–CS and lignin particles.[60] The hydroxyl groups associated with PVA are responsible for inter- and intra- molecular hydrogen bonds. Similarly, **Figure 3.8b** unveils influence of MWCNT on the moduli of PVA–CS–lignin hydrogel, and results are shown as a function of frequency. Similar dominance of G′ over G″ was observed over the frequency range. In fact, addition of 1 wt% MWCNT increases the G′ of S3 by 235.45%. Also, any noteworthy degradation in the modulus was not witnessed post addition of MWCNT in PVA–CS–lignin hydrogel. This clearly justifies the robust gel-like and viscoelastic solid-like behavior of hydrogel. This could be possible because of the formation of physical crosslinking junction between lignin particles and MWCNT with PVA molecular chains.[63] MWCNT mostly restricts the movement of polymer chains and further acts as filler in PVA–CS hydrogel.[65]

Favorable mechanical property is of great significance for hydrogels in practical applications. The mechanical strength of the composite hydrogel was also characterized by measurement of the tensile strength of the dried composites as shown in **Figures 3.9a** and **3.9b**, and **Table 3.5** which clearly represent the positive influence of additives on the hydrogel. Compared to pristine PVA–CS hydrogel (sample S1),

addition of 2 wt% of lignin particles (sample S2) and 1 wt% MWCNT (sample S3) to the hydrogels imparts stiffness to the hydrogel.

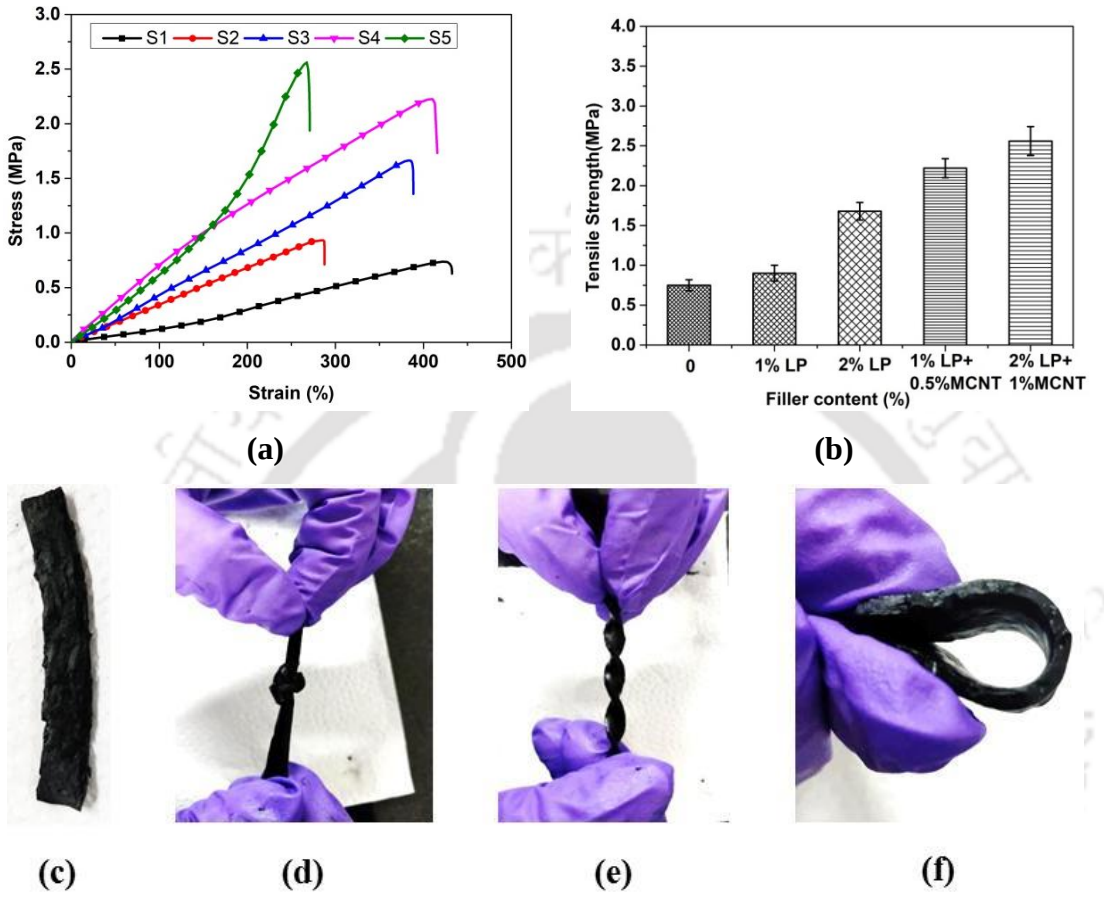

Figure 3.9 (a) Stress–strain curve of composite hydrogel (b) tensile strength with respect to the filler content of the hydrogel (c) rectangular shaped cut composite hydrogel and the rectangular hydrogel undergoing different physical deformation (d) knotting (e) convolving and (f) bending

It is observed that the neat PVA−CS exhibits extremely low tensile strength (0.75 MPa), which results in elastic behavior of the hydrogels. With the addition of lignin particles in the hydrogel matrix, a 93% increase in tensile strength (1.68 MPa) than the neat hydrogel is observed. However, elasticity of hydrogel was compromised. Similarly, addition of lignin particles dispersed MWCNT results in a 181% increase in tensile strength resulting in a much lower elastic value than the pristine PVA−CS

hydrogels (sample S1). This trait may be due to the fact that the presence of acetone encourages the lignin particles to adhere to MWCNT, which increases the interaction between fillers and polymers. Consequently, enhancement of the mechanical properties of the hydrogel was observed.

Table 3.4 Parameters calculated from rheological study of composite hydrogel

Hydrogel	Average G′ (Pa)	Average G″ (Pa)	Mesh size, ξ (nm)
S1	1100 ± 300	70 ± 20	15.52
S2	1710 ± 421	128 ± 50	13.40
S3	4198 ± 1644	227 ± 92	9.93
S4	11170 ± 1640	396 ± 205	7.17
S5	11757 ± 753	488 ± 369	7.05

Table 3.5 Mechanical properties of composite hydrogels

Hydrogel	Filler content	Elongation at break (%)	Tensile strength (MPa)	Young's modulus $\times 10^{-3}$(MPa)
S1	----	10 ± 1	0.75 ± 0.07	1.2 ± 0.5
S2	1% lignin	15 ± 0.5	0.90 ± 0.10	3.7 ± 1.0
S3	2% lignin	25 ± 0.5	1.68 ± 0.11	3.5 ± 0.7
S4	1% lignin, 0.5% MWCNT	30 ± 1.2	2.22 ± 0.12	5.4 ± 0.2
S5	2% lignin, 1% MWCNT	50 ± 1.5	2.56 ± 0.18	5.8 ± 0.5

3.3.2.4 Effect of morphology on swelling ability of hydrogel

The internal structure and morphology of the freeze dried hydrogels was assessed using FESEM micrographs. For this purpose, initially, the hydrogels were fully swollen by soaking in water, followed by freeze drying. PVA–CS hydrogels reveal sporadic and non-uniform porous structures (**Figures 3.10a** and **3.10b**). Post addition of lignin particles and MWCNT as the filler material, the structure became regular and compact (**Figure 3.10c–3.10f**). The uniformity and compactness of the hydrogel

structure improved proportionately with addition of the filler, as revealed in **Figures 3.10e** and **3.10f**. This could be due to the enhanced degree of crosslinking between the polymers and strong association of lignin and MWCNT with the polymers, which imparted a compact and regular porous structure to the hydrogel.

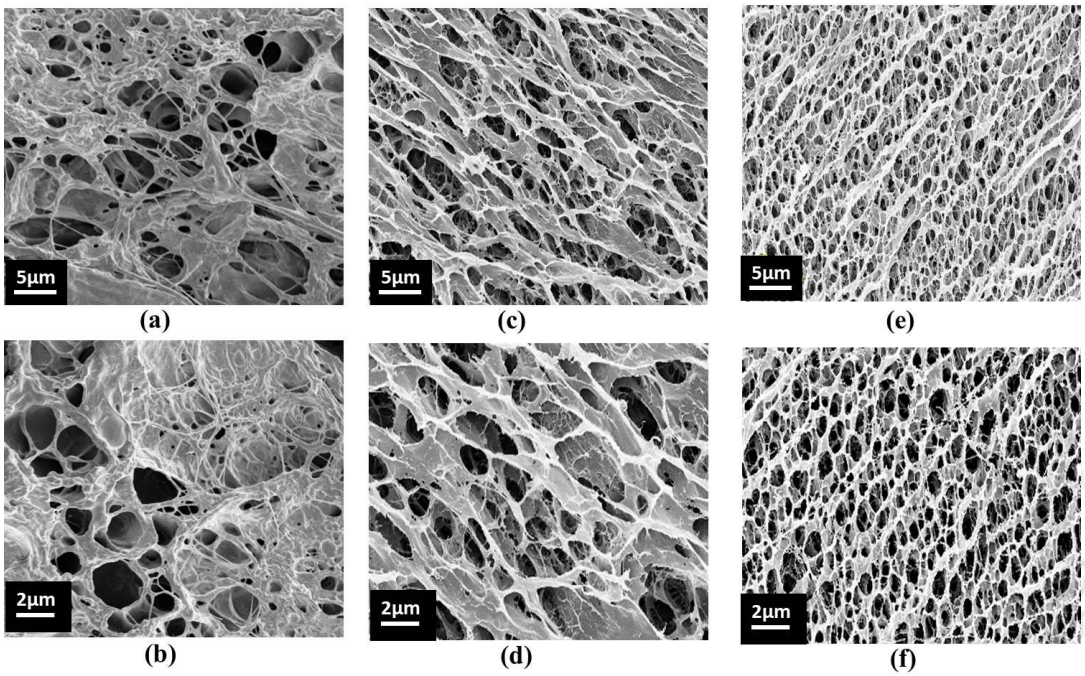

Figure 3.10 FESEM images of (a) and (b) S1 hydrogel, (c) and (d) S3 hydrogel and, (e) and (f) S5 hydrogels

The degree of crosslinking and internal structure of the hydrogel has an enormous impact on the swelling ability of the hydrogels (**Figure 3.11**). It was reported earlier that higher the amount of crosslinking, lower the swelling ability of the hydrogels owing to their compact internal structure.[44] The mesh size calculated from the rheology (**Table 3.4**) corroborates this result. Hence, a well-compact structure of hydrogel (S3, S4, and S5) resulted in low swelling ability whereas a sporadic porous structure was able to swell much higher (S1 and S2). The swelling ability of the hydrogel helps to determine the time required for the hydrogel to reach

equilibrium for constant EIS behavior. The formulated hydrogels reached their equilibrium after 6 h (**Figure 3.11**).

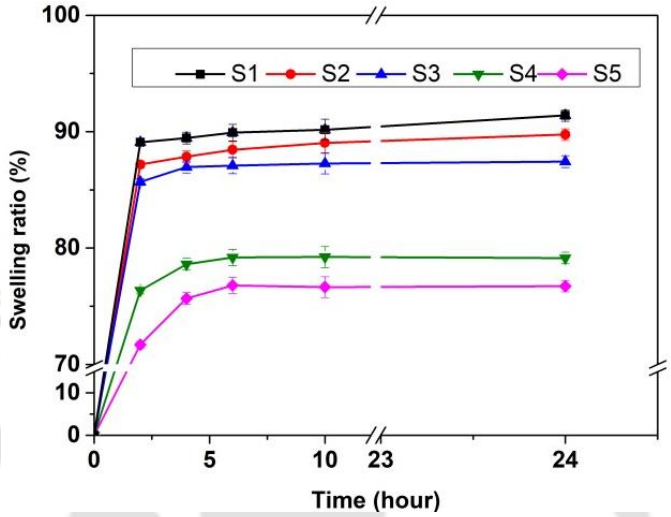

Figure 3.11 Swelling ratio of formulated hydrogels

3.3.2.5 Impedance measurement of hydrogel

EIS measurement for hydrogel equilibrated in DI water (pH 6) was recorded using the setup shown in **Figure 3.12b**. Results of EIS measurement are represented in the Nyquist plot (**Figure 3.12a**). The intercept in the horizontal axis of the Nyquist plot represents the interface impedance. The EIS spectra (**Figure 3.12a**) can be fitted using the equivalent circuit (**Figure 3.12**), which was a close fit to the experimental spectra obtained. Sequentially, using equation 3.7, the values obtained from the equivalent circuit were employed to evaluate the conductivity of the hydrogel sample. The calculated parameters, resistance (R), Warburg coefficient (Σ), and conductivity (σ), are stated in **Table 3.6**. The Warburg coefficient reflects the rate of diffusion through the hydrogel sample. **Table 3.6** summarizes the calculated conductivity of hydrogel. Presence of CNT enhanced the conductivity of the hydrogel, as evident from the measured values of 2.05 $mS \cdot cm^{-1}$ and 8.22 $mS \cdot cm^{-1}$ for 0.5% and 1%

MWCNT contents, respectively. An increment of 300% in conductivity was observed with a doubling of the MWCNT content of hydrogels. Uniform distribution of MWCNT in hydrogel matrix also contributes to a rise in conductivity. Also, we can conclude that the lignin particles do not have a negative effect on the MWCNT or its conducting nature.

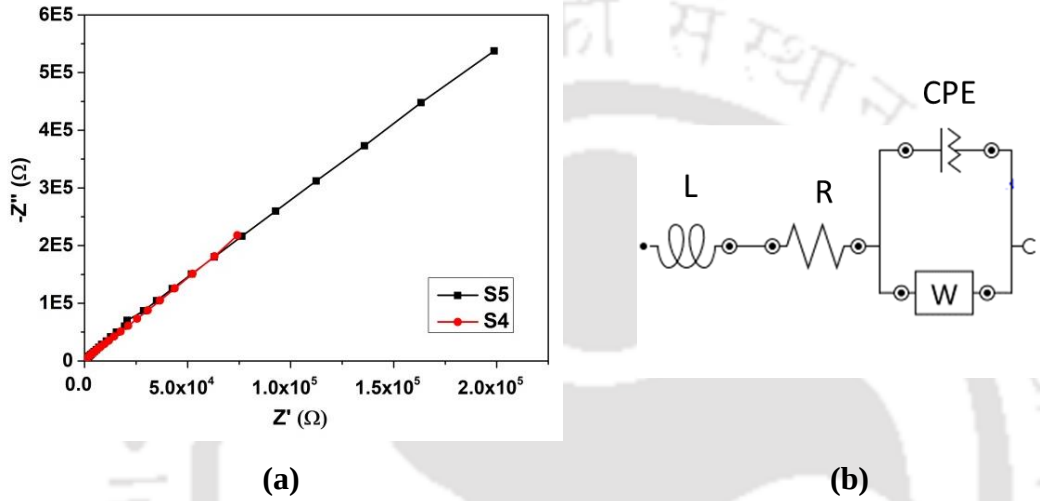

(a) **(b)**

Figure 3.12 (a) Nyquist(–Z″ vs. Z′) plots of composite hydrogel. (b) equivalent circuit used to fit EIS data. The circuit includes an instrumental inductance (L), the bulk gel resistance (R), a CPE for the double layer capacitance, and an infinite Warburg element (W).

Table 3.6 Calculated equivalent circuit parameters for composite hydrogel EIS spectra.

Hydrogel	Contact Area, A (cm^2)	R (Ω cm^2)	Σ ($n\Omega$ cm^2 $S^{-1/2}$)	σ (mS cm^{-1})
S4	1	2.47	937	2.05
S5	1	6.60	217	8.22

3.4 Conclusions

This study focuses on formulation of conductive PVA–CS hydrogels using ultrasonic assisted dispersion of MWCNT with lignin and acetone as additives. Dispersion of lignin and MWCNT was validated by UV–vis absorption spectra and zeta potential. Additionally, FETEM images confirmed that the presence of acetone assisted LP to adhere onto the surface of MWCNT, which facilitated easier dispersion of MWCNT. Presence of acetone also reduced the surface tension of the suspension, which further enhanced the dispersing ability of MWCNT with surface-attached LP in just 1 h of sonication. The mechanical properties of the hydrogel improved in presence of acetone. The elastic moduli (G′) of 0.5 and 1% MWCNT hydrogel samples were 11170 ± 1640 Pa and 11757 ± 753 Pa, respectively, which was an order of magnitude higher than G′ of PVA–CS hydrogel (1100 ± 300 Pa). Similarly, tensile strength also increased from 0.72 to 2.56 MPa. Finally, the conductivity of hydrogels with 1% MWCNT was determined as 8.22 mS cm^{-1}. These conductive hydrogels have potential applications as flexible electrodes and electrolytes for supercapacitors, ECG electrodes, and flexible sensors.

References

(1) Distler, T.; Boccaccini, A. R. 3D Printing of Electrically Conductive Hydrogels for Tissue Engineering and Biosensors – A Review. *Acta Biomater.* **2020**, *101*, 1–13. https://doi.org/10.1016/J.ACTBIO.2019.08.044.

(2) Serafin, A.; Murphy, C.; Rubio, M. C.; Collins, M. N. Printable Alginate/Gelatin Hydrogel Reinforced with Carbon Nanofibers as Electrically Conductive Scaffolds for Tissue Engineering. *Mater. Sci. Eng. C* **2021**, *122*, 111927. https://doi.org/10.1016/J.MSEC.2021.111927.

(3) Wang, T.; Song, J.; Liu, R.; Chan, S. Y.; Wang, K.; Su, Y.; Li, P.; Huang, W. Motion Detecting, Temperature Alarming, and Wireless Wearable

Bioelectronics Based on Intrinsically Antibacterial Conductive Hydrogels. *ACS Appl. Mater. Interfaces* **2022**, *14* (12), 14596–14606. https://doi.org/https://doi.org/10.1021/acsami.2c00713.

(4) Jia, M.; Rolandi, M. Soft and Ion-Conducting Materials in Bioelectronics: From Conducting Polymers to Hydrogels. *Adv. Healthc. Mater.* **2020**, *9* (5), 1901372. https://doi.org/10.1002/ADHM.201901372.

(5) Sardana, S.; Gupta, A.; Singh, K.; Maan, A. S.; Ohlan, A. Conducting Polymer Hydrogel Based Electrode Materials for Supercapacitor Applications. *J. Energy Storage* **2022**, *45*, 103510. https://doi.org/10.1016/J.EST.2021.103510.

(6) Khazaeli, A.; Godbille-Cardona, G.; J Barz, D. P.; Khazaeli, A.; Godbille-Cardona, G.; J Barz, D. P. A Novel Flexible Hybrid Battery–Supercapacitor Based on a Self-Assembled Vanadium-Graphene Hydrogel. *Adv. Funct. Mater.* **2020**, *30* (21), 1910738. https://doi.org/10.1002/ADFM.201910738.

(7) Li, T.; Liang, B.; Ye, Z.; Zhang, L.; Xu, S.; Tu, T.; Zhang, Y.; Cai, Y.; Zhang, B.; Fang, L.; Mao, X.; Zhang, S.; Wu, G.; Yang, Q.; Zhou, C.; Cai, X.; Ye, X. An Integrated and Conductive Hydrogel-Paper Patch for Simultaneous Sensing of Chemical–Electrophysiological Signals. *Biosens. Bioelectron.* **2022**, *198*, 113855. https://doi.org/10.1016/J.BIOS.2021.113855.

(8) Wang, Y.; Qu, Z.; Wang, W.; Yu, D. PVA/CMC/PEDOT:PSS Mixture Hydrogels with High Response and Low Impedance Electronic Signals for ECG Monitoring. *Colloids Surfaces B Biointerfaces* **2021**, *208*, 112088. https://doi.org/10.1016/J.COLSURFB.2021.112088.

(9) Chu, H.; Yang, C.; Xing, Y.; Li, J.; Liu, C. A Portable ECG Patch Monitor Based on Flexible Non-Hydrogel Electrode. *J. Med. Biol. Eng.* **2022**, *42* (3), 364–373. https://doi.org/https://doi.org/10.1007/s40846-022-00709-4.

(10) Khorasani, M. T.; Joorabloo, A.; Moghaddam, A.; Shamsi, H.; MansooriMoghadam, Z. Incorporation of ZnO Nanoparticles into Heparinised Polyvinyl Alcohol/Chitosan Hydrogels for Wound Dressing Application. *Int. J. Biol. Macromol.* **2018**, *114*, 1203–1215. https://doi.org/10.1016/J.IJBIOMAC.2018.04.010.

(11) Zhang, Y.; Jiang, M.; Zhang, Y.; Cao, Q.; Wang, X.; Han, Y.; Sun, G.; Li, Y.; Zhou, J. Novel Lignin–Chitosan–PVA Composite Hydrogel for Wound Dressing. *Mater. Sci. Eng. C* **2019**, *104*, 110002. https://doi.org/10.1016/J.MSEC.2019.110002.

(12) Luo, C.; Zhao, Y.; Sun, X.; Hu, B. Developing High Strength, Antiseptic and Swelling-Resistant Polyvinyl Alcohol/Chitosan Hydrogels for Tissue Engineering Material. *Mater. Lett.* **2020**, *280*, 128499. https://doi.org/10.1016/J.MATLET.2020.128499.

(13) Islam, M. M.; Shahruzzaman, M.; Biswas, S.; Nurus Sakib, M.; Rashid, T. U. Chitosan Based Bioactive Materials in Tissue Engineering Applications-A Review. *Bioact. Mater.* **2020**, *5* (1), 164–183. https://doi.org/10.1016/J.BIOACTMAT.2020.01.012.

(14) Yang, J.; Li, M.; Wang, Y.; Wu, H.; Zhen, T.; Xiong, L.; Sun, Q. Double Cross-Linked Chitosan Composite Films Developed with Oxidized Tannic Acid and Ferric Ions Exhibit High Strength and Excellent Water Resistance. *Biomacromolecules* **2019**, *20* (2), 801–812. https://doi.org/https://doi.org/10.1021/acs.biomac.8b01420.

(15) Cheng, P.; Gao, H.; Chen, X.; Chen, Y.; Han, M.; Xing, L.; Liu, P.; Wang, G. Flexible Monolithic Phase Change Material Based on Carbon Nanotubes/Chitosan/Poly(Vinyl Alcohol). *Chem. Eng. J.* **2020**, *397*, 125330. https://doi.org/10.1016/J.CEJ.2020.125330.

(16) Wu, L.; Huang, S.; Zheng, J.; Qiu, Z.; Lin, X.; Qin, Y. Synthesis and Characterization of Biomass Lignin-Based PVA Super-Absorbent Hydrogel. *Int. J. Biol. Macromol.* **2019**, *140*, 538–545. https://doi.org/10.1016/J.IJBIOMAC.2019.08.142.

(17) Yang, J. M.; Wang, S. A. Preparation of Graphene-Based Poly(Vinyl Alcohol)/Chitosan Nanocomposites Membrane for Alkaline Solid Electrolytes Membrane. *J. Memb. Sci.* **2015**, *477*, 49–57. https://doi.org/10.1016/J.MEMSCI.2014.12.028.

(18) Yu, D.; Teng, Y.; Feng, H.; Lin, X.; Li, J.; Wang, Q.; Xue, C. Multi-Responsive and Conductive Bilayer Hydrogel and Its Application in Flexible Devices. *RSC Adv.* **2022**, *12* (13), 7898–7905. https://doi.org/10.1039/D1RA09232D.

(19) Chen, Z.; Xu, Z.; Li, W.; Chen, C.; Yang, J.; Liu, J.; Gong, F.; Liao, J.; Wu, M. Cellulose-Hydrogel-Derived Self-Activated Carbon/SnO2 Nanocomposites for High-Performance Lithium Storage. *ACS Appl. Energy Mater.* **2019**, *2* (7), 5171–5182. https://doi.org/https://doi.org/10.1021/acsaem.9b00848.

(20) Chashiro, K.; Iwasaki, S.; Hasegawa, T.; Maruyama, J.; Maruyama, S.; Pal, A.;

Nandi, M.; Uyama, H. Integrating Polyacrylonitrile (PAN) Nanoparticles with Porous Bacterial Cellulose Hydrogel to Produce Activated Carbon Electrodes for Electric Double-Layer Capacitors. *Microporous Mesoporous Mater.* **2021**, *323*, 111209. https://doi.org/10.1016/J.MICROMESO.2021.111209.

(21) Merhebi, S.; Mayyas, M.; Abbasi, R.; Christoe, M. J.; Han, J.; Tang, J.; Rahim, M. A.; Yang, J.; Tan, T. T.; Chu, D.; Zhang, J.; Li, S.; Wang, C. H.; Kalantar-Zadeh, K.; Allioux, F. M. Magnetic and Conductive Liquid Metal Gels. *ACS Appl. Mater. Interfaces* **2020**, *12* (17), 20119–20128. https://doi.org/https://doi.org/10.1021/acsami.0c03166.

(22) Wang, M.; Feng, X.; Wang, X.; Hu, S.; Zhang, C.; Qi, H. Facile Gelation of a Fully Polymeric Conductive Hydrogel Activated by Liquid Metal Nanoparticles. *J. Mater. Chem. A* **2021**, *9* (43), 24539–24547. https://doi.org/10.1039/D1TA07254D.

(23) Xu, Y.; Rothe, R.; Voigt, D.; Hauser, S.; Cui, M.; Miyagawa, T.; Patino Gaillez, M.; Kurth, T.; Bornhäuser, M.; Pietzsch, J.; Zhang, Y. Convergent Synthesis of Diversified Reversible Network Leads to Liquid Metal-Containing Conductive Hydrogel Adhesives. *Nat. Commun. 2021 121* **2021**, *12* (1), 1–19. https://doi.org/10.1038/s41467-021-22675-2.

(24) Wang, D.; Qin, L.; Yang, W.; He, Y.; Zhang, S.; Yang, Y.; Xu, K.; Gao, P.; Yu, J.; Cai, K. A Conductive Hydrogel Based on GaIn and PVA/PAA/Fe3+for Strain Sensor and Physiological Signal Detection. *ACS Appl. Polym. Mater.* **2021**, *3* (10), 5268–5276. https://doi.org/https://doi.org/10.1021/acsapm.1c01063.

(25) Zhang, X.; Peng, Y.; Wang, X.; Ran, R. Melanin-Inspired Conductive Hydrogel Sensors with Ultrahigh Stretchable, Self-Healing, and Photothermal Capacities. *ACS Appl. Polym. Mater.* **2021**, *3* (4), 1899–1911. https://doi.org/https://doi.org/10.1021/acsapm.0c01430.

(26) Deng, Z.; Yu, R.; Guo, B. Stimuli-Responsive Conductive Hydrogels: Design, Properties, and Applications. *Mater. Chem. Front.* **2021**, *5* (5), 2092–2123. https://doi.org/10.1039/D0QM00868K.

(27) Yasin, A. S.; Yousef Mohamed, A.; Kim, D. H.; Luu Luyen Doan, T.; Chougule, S. S.; Jung, N.; Nam, S.; Lee, K. Design of Zinc Oxide Nanoparticles and Graphene Hydrogel Co-Incorporated Activated Carbon for Efficient Capacitive Deionization. *Sep. Purif. Technol.* **2021**, *277*, 119428.

https://doi.org/10.1016/J.SEPPUR.2021.119428.

(28) Maria, K. H.; Mieno, T. Production of Water Dispersible Carbon Nanotubes and Nanotube/Cellulose Composite. *Carbon Nanotub. - Recent Prog.* **2017**. https://doi.org/10.5772/INTECHOPEN.70543.

(29) Rojas, J. A.; Ardila-Rodríguez, L. A.; Diniz, M. F.; Gonçalves, M.; Ribeiro, B.; Rezende, M. C. Optimization of Triton X-100 Removal and Ultrasound Probe Parameters in the Preparation of Multiwalled Carbon Nanotube Buckypaper. *Mater. Des.* **2019**, *166*, 107612. https://doi.org/10.1016/J.MATDES.2019.107612.

(30) Jung, W. R.; Choi, J. H.; Lee, N.; Shin, K.; Moon, J. H.; Seo, Y. S. Reduced Damage to Carbon Nanotubes during Ultrasound-Assisted Dispersion as a Result of Supercritical-Fluid Treatment. *Carbon N. Y.* **2012**, *50* (2), 633–636. https://doi.org/10.1016/J.CARBON.2011.08.075.

(31) Bibi, S.; Jamil, A.; Yasin, T.; Rafiq, M. A.; Nawaz, M.; Price, G. J. Ultrasound Promoted Synthesis and Properties of Chitosan Nanocomposites Containing Carbon Nanotubes and Silver Nanoparticles. *Eur. Polym. J.* **2018**, *105*, 297–303. https://doi.org/10.1016/J.EURPOLYMJ.2018.06.004.

(32) Jiang, Y.; Song, H.; Xu, R. Research on the Dispersion of Carbon Nanotubes by Ultrasonic Oscillation, Surfactant and Centrifugation Respectively and Fiscal Policies for Its Industrial Development. *Ultrason. Sonochem.* **2018**, *48*, 30–38. https://doi.org/10.1016/J.ULTSONCH.2018.05.021.

(33) Yuan, Y.; Tang, X.; Jiang, L.; Yang, Y.; Zhou, Y.; Dong, Y. Convenient CNT-Paper Gas Sensors Prepared by a Household Inkjet Printer. *ACS Omega* **2020**, *5* (51), 32877–32882. https://doi.org/https://doi.org/10.1021/ie502339q.

(34) Berger, F. J.; Lüttgens, J.; Nowack, T.; Kutsch, T.; Lindenthal, S.; Kistner, L.; Müller, C. C.; Bongartz, L. M.; Lumsargis, V. A.; Zakharko, Y.; Zaumseil, J. Brightening of Long, Polymer-Wrapped Carbon Nanotubes by Sp3 Functionalization in Organic Solvents. *ACS Nano* **2019**, *13* (8), 9259–9269. https://doi.org/https://doi.org/10.1021/acsnano.9b03792.

(35) Słoma, M.; Wierzbicki, M.; Skalski, A. Composite Powders with Carbon Nanotubes for Laser Printing of Electronics. *Microelectron. Reliab.* **2022**, *136*, 114718. https://doi.org/10.1016/J.MICROREL.2022.114718.

(36) Damasceno, J. P. V.; Zarbin, A. J. G. A New Approach for the Achievement of Stable Aqueous Dispersions of Carbon Nanotubes. *Chem. Commun.* **2019**, *55*

(41), 5809–5812. https://doi.org/10.1039/C9CC01541H.

(37) Bansal, S. A.; Khanna, V.; Twinkle; Singh, A. P.; Kumar, S. Small Percentage Reinforcement of Carbon Nanotubes (CNTs) in Epoxy(Bisphenol-A) for Enhanced Mechanical Performance. *Mater. Today Proc.* **2022**, *61*, 275–279. https://doi.org/10.1016/J.MATPR.2021.09.225.

(38) Bubalo, M. C.; Sabotin, I.; Radoš, I.; Valentinčič, J.; Bosiljkov, T.; Brnčić, M.; Žnidaršič-Plazl, P. A Comparative Study of Ultrasound-, Microwave-, and Microreactor-Assisted Imidazolium-Based Ionic Liquid Synthesis. *Green Process. Synth.* **2013**, *2* (6), 579–590. https://doi.org/10.1515/GPS-2013-0086/MACHINEREADABLECITATION/RIS.

(39) Singh, S.; Bharadwaja, S. T. P.; Yadav, P. K.; Moholkar, V. S.; Goyal, A. Mechanistic Investigation in Ultrasound-Assisted (Alkaline) Delignification of Parthenium Hysterophorus Biomass. *Ind. Eng. Chem. Res.* **2014**, *53* (37), 14241–14252. https://doi.org/https://doi.org/10.1021/ie502339q.

(40) Subhedar, P. B.; Gogate, P. R. Alkaline and Ultrasound Assisted Alkaline Pretreatment for Intensification of Delignification Process from Sustainable Raw-Material. *Ultrason. Sonochem.* **2014**, *21* (1), 216–225. https://doi.org/10.1016/J.ULTSONCH.2013.08.001.

(41) Schieppati, D.; Dreux, A.; Gao, W.; Fatehi, P.; Boffito, D. C. Ultrasound-Assisted Carboxymethylation of LignoForce Kraft Lignin to Produce Biodispersants. *J. Clean. Prod.* **2022**, *366*, 132776. https://doi.org/10.1016/J.JCLEPRO.2022.132776.

(42) Gilca, I. A.; Popa, V. I.; Crestini, C. Obtaining Lignin Nanoparticles by Sonication. *Ultrason. Sonochem.* **2015**, *23*, 369–375. https://doi.org/10.1016/J.ULTSONCH.2014.08.021.

(43) Ingtipi, K.; Moholkar, V. S. Sonochemically Synthesized Lignin Nanoparticles and Its Application in the Development of Nanocomposite Hydrogel. *Mater. Today Proc.* **2019**, *17*, 362–370. https://doi.org/10.1016/J.MATPR.2019.06.443.

(44) Ingtipi, K.; Choudhury, B. J.; Moholkar, V. S. Development of NaOH-Borax Crosslinked PVA-Xanthan Gum-Lignin Hydrogel as Green Fire Retardant Coating. *Prog. Org. Coatings* **2023**, *174*, 107268. https://doi.org/10.1016/J.PORGCOAT.2022.107268.

(45) England, A. H.; Clare, T. L. Synthesis and Characterization of Flexible

Hydrogel Electrodes for Electrochemical Impedance Measurements of Protective Coatings on Metal Sculptures. *Electroanalysis* **2014**, *26* (5), 1059–1067. https://doi.org/10.1002/ELAN.201300653.

(46) Ou, J.; Kong, Z.; Yang, R.; Dai, Z. Synthesis of a Lignin-Based Alcohol Ether Carboxylate Surfactant and Its Application as Cotton Fiber Detergent. *J. Dispers. Sci. Technol.* **2021**. https://doi.org/https://doi.org/10.1080/01932691.2021.1956323.

(47) Tortora, M.; Cavalieri, F.; Mosesso, P.; Ciaffardini, F.; Melone, F.; Crestini, C. Ultrasound Driven Assembly of Lignin into Microcapsules for Storage and Delivery of Hydrophobic Molecules. *Biomacromolecules* **2014**, *15* (5), 1634–1643. https://doi.org/https://doi.org/10.1021/bm500015j.

(48) Wu, N.; Li, X.; Liu, S.; Zhang, M.; Ouyang, S. Effect of Hydrogen Bonding on the Surface Tension Properties of Binary Mixture (Acetone-Water) by Raman Spectroscopy. *Appl. Sci. 2019, Vol. 9, Page 1235* **2019**, *9* (6), 1235. https://doi.org/10.3390/APP9061235.

(49) Sadeghifar, H.; Ragauskas, A. Lignin as a UV Light Blocker—A Review. *Polym. 2020, Vol. 12, Page 1134* **2020**, *12* (5), 1134. https://doi.org/10.3390/POLYM12051134.

(50) Goodman, S. M.; Ferguson, N.; Dichiara, A. B. Lignin-Assisted Double Acoustic Irradiation for Concentrated Aqueous Dispersions of Carbon Nanotubes. *RSC Adv.* **2017**, *7* (9), 5488–5496. https://doi.org/10.1039/C6RA25986C.

(51) Arefmanesh, M.; Nikafshar, S.; Master, E. R.; Nejad, M. From Acetone Fractionation to Lignin-Based Phenolic and Polyurethane Resins. *Ind. Crops Prod.* **2022**, *178*, 114604. https://doi.org/10.1016/J.INDCROP.2022.114604.

(52) Li, X.; Shen, J.; Wang, B.; Feng, X.; Mao, Z.; Sui, X. Acetone/Water Cosolvent Approach to Lignin Nanoparticles with Controllable Size and Their Applications for Pickering Emulsions. *ACS Sustain. Chem. Eng.* **2021**, *9* (15), 5470–5480. https://doi.org/10.1021/acssuschemeng.1c01021.

(53) Lee, E. S.; Kim, Y. O.; Ha, Y. M.; Lim, D.; Hwang, J. Y.; Kim, J.; Park, M.; Cho, J. W.; Jung, Y. C. Antimicrobial Properties of Lignin-Decorated Thin Multi-Walled Carbon Nanotubes in Poly(Vinyl Alcohol) Nanocomposites. *Eur. Polym. J.* **2018**, *105*, 79–84. https://doi.org/10.1016/J.EURPOLYMJ.2018.05.014.

(54) Garcia Gonzalez, M. N.; Levi, M.; Turri, S.; Griffini, G. Lignin Nanoparticles by Ultrasonication and Their Incorporation in Waterborne Polymer Nanocomposites. *J. Appl. Polym. Sci.* **2017**, *134* (38), 45318. https://doi.org/10.1002/APP.45318.

(55) F. Graça, M. P.; Rudnitskaya, A.; Fernando, F. A.; Evtuguin, D. V.; Maria, M. T.; Joaõ, J. A.; C. Costa, L. Electrochemical Impedance Study of the Lignin-Derived Conducting Polymer. *Electrochim. Acta* **2012**, *76*, 69–76. https://doi.org/10.1016/J.ELECTACTA.2012.04.155.

(56) Hassan, C. M.; Peppas, N. A. Structure and Morphology of Freeze/Thawed PVA Hydrogels. *Macromolecules* **2000**, *33* (7), 2472–2479. https://doi.org/https://doi.org/10.1021/ma9907587.

(57) Adelnia, H.; Ensandoost, R.; Shebbrin Moonshi, S.; Gavgani, J. N.; Vasafi, E. I.; Ta, H. T. Freeze/Thawed Polyvinyl Alcohol Hydrogels: Present, Past and Future. *Eur. Polym. J.* **2022**, *164*, 110974. https://doi.org/10.1016/J.EURPOLYMJ.2021.110974.

(58) Li, M.; Tu, Q.; Long, X.; Zhang, Q.; Jiang, H.; Chen, C.; Wang, S.; Min, D. Flexible Conductive Hydrogel Fabricated with Polyvinyl Alcohol, Carboxymethyl Chitosan, Cellulose Nanofibrils, and Lignin-Based Carbon Applied as Strain and Pressure Sensor. *Int. J. Biol. Macromol.* **2021**, *166*, 1526–1534. https://doi.org/10.1016/J.IJBIOMAC.2020.11.032.

(59) Moussout, H.; Ahlafi, H.; Aazza, M.; Bourakhouadar, M. Kinetics and Mechanism of the Thermal Degradation of Biopolymers Chitin and Chitosan Using Thermogravimetric Analysis. *Polym. Degrad. Stab.* **2016**, *130*, 1–9. https://doi.org/10.1016/J.POLYMDEGRADSTAB.2016.05.016.

(60) Yang, W.; Fortunati, E.; Bertoglio, F.; Owczarek, J. S.; Bruni, G.; Kozanecki, M.; Kenny, J. M.; Torre, L.; Visai, L.; Puglia, D. Polyvinyl Alcohol/Chitosan Hydrogels with Enhanced Antioxidant and Antibacterial Properties Induced by Lignin Nanoparticles. *Carbohydr. Polym.* **2018**, *181*, 275–284. https://doi.org/10.1016/J.CARBPOL.2017.10.084.

(61) Collins, M. N.; Nechifor, M.; Tanasă, F.; Zănoagă, M.; McLoughlin, A.; Stróżyk, M. A.; Culebras, M.; Teacă, C. A. Valorization of Lignin in Polymer and Composite Systems for Advanced Engineering Applications – A Review. *Int. J. Biol. Macromol.* **2019**, *131*, 828–849. https://doi.org/10.1016/J.IJBIOMAC.2019.03.069.

(62) Kumar, D.; Jindal, P. Effect of Multi-Walled Carbon Nanotubes on Thermal Stability of Polyurethane Nanocomposites. *Mater. Res. Express* **2019**, *6* (10), 105336. https://doi.org/10.1088/2053-1591/AB3AD7.

(63) Yang, W.; Shao, B.; Liu, T.; Zhang, Y.; Huang, R.; Chen, F.; Fu, Q. Robust and Mechanically and Electrically Self-Healing Hydrogel for Efficient Electromagnetic Interference Shielding. *ACS Appl. Mater. Interfaces* **2018**, *10* (9), 8245–8257. https://doi.org/10.1021/ACSAMI.7B18700/ASSET/IMAGES/LARGE/AM-2017-187004_0004.JPEG.

(64) Karimi, A. R.; Khodadadi, A. Mechanically Robust 3D Nanostructure Chitosan-Based Hydrogels with Autonomic Self-Healing Properties. **2016**. https://doi.org/10.1021/ACSAMI.6B10375.

(65) Pirahmadi, P.; Kokabi, M.; Alamdarnejad, G. Polyvinyl Alcohol/Chitosan/Carbon Nanotubes Electroactive Shape Memory Nanocomposite Hydrogels. *J. Appl. Polym. Sci.* **2021**, *138* (11), 49995. https://doi.org/10.1002/APP.49995.

भारतीय प्रौद्योगिकी संस्थान गुवाहाटी
Indian Institute of Technology Guwahati

CHAPTER 4

DEVELOPMENT OF NaOH-BORAX CROSSLINKED PVA-XANTHAN GUM-LIGNIN HYDROGEL AS GREEN FIRE RETARDANT COATING

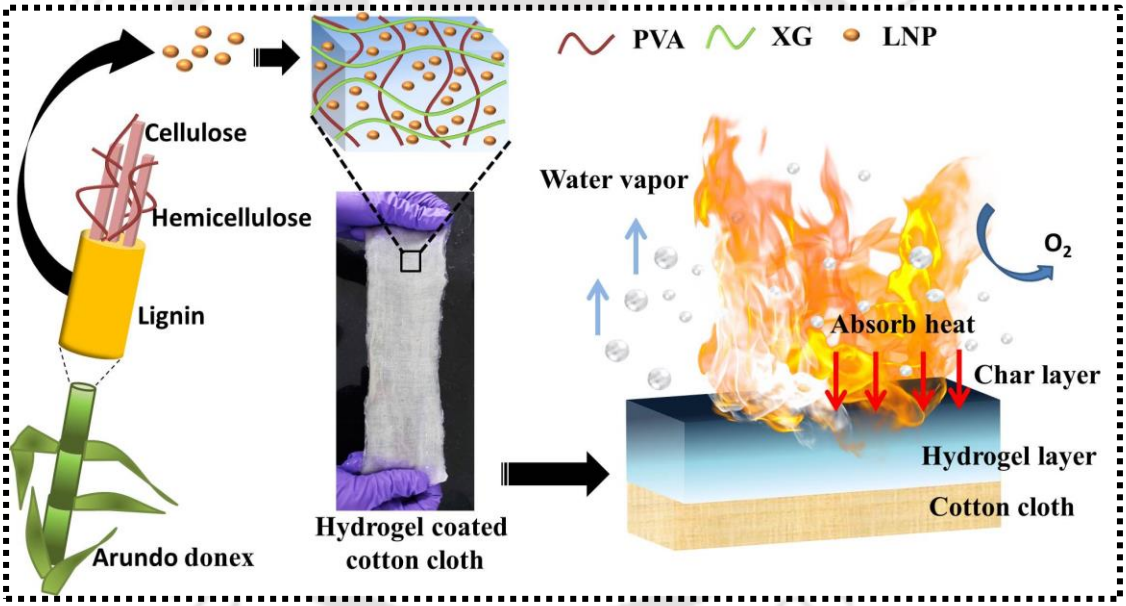

CHAPTER 4

DEVELOPMENT OF NaOH-BORAX CROSSLINKED PVA-XANTHAN GUM-LIGNIN HYDROGEL AS GREEN FIRE RETARDANT COATING

4.1 Introduction

A significant increase in forest fires and fire related accidents in residential areas and industrial sectors is a serious concern; hence, developing efficient fire resisting materials is becoming a pressing necessity. Conventionally, flame retardants (mostly halogens based) are added to flammable materials to improve their fire resistance. However, such compounds unveil serious health hazards and adverse environmental effects. Recent advances report the development of fire suppressant and fire retardant hydrogels, which can be coated over material surfaces such as fire resistant suits.[1,2] The hydrogels are hydrophilic, biodegradable, and biocompatible materials capable of retaining enormous quantities of water in their crosslinked polymer network.[3] When applied as coatings or sprayed on the surface of a substance, the hydrogels act as fire-suppressant and help in preventing the spread of fire.[4] Water is an effective fire extinguisher as it absorbs large amount of heat due to its high latent heat of vaporization and high specific heat.[5,6] Upon exposure to fire, gradual evaporation of entrapped water from the polymer network of hydrogel absorbs heat and delays the process of burning or spreading fire.[1] Further, a protective layer is formed on the surface post combustion, which prevents further burning. A significant amount of literature has been published on synthesis of different kinds of fire retardant hydrogels in the past several years.[7,8] We give herein a brief review of some

of the recent studies. Qin et al. [5] reported a sodium polyacrylate and sorbitan monooleate superabsorbent hydrogel composite for suppression of self-heating and combustion of coal. Similarly, Li et al. [9] developed expeditiously high water absorbing sodium carboxymethyl cellulose hydrogel for fire control in coal mines. This hydrogel possessed excellent salt tolerance in addition to high water retention at ambient and elevated temperatures. The gel mixed with coal samples formed a colloidal structure on the coal surface, which acted as a barrier between the surface and the atmospheric oxygen, and provided excellent resistance to fire. Further, fire susceptible fabrics (cotton, polyester) can be impregnated with water soluble polymer (chitosan, alginate) to bestow flame retardancy.[10] Further, polyacrylamide–alginate hydrogel, when sewn as laminates in firefighting clothes, provided thermal protection to the skin by acting as a barrier.[11]

Polyvinyl alcohol (PVA) is a biodegradable and easily tunable hydrophilic polymer. It possesses sturdy mechanical properties even in the swollen state, and hence, widely employed in biomedical, electronics, adhesive, and bio-remediation applications. However, PVA is substantially flammable when dehydrated and has low water retention capacity, which limits its usage as a fire retardant. Studies show that blending PVA with low flammable biopolymer and additives enhances its performance. A self-healing fire retardant coating on fabric was produced via amalgamation of water soluble chitosan (WC), PVA, acrylic acid, and Cu^{2+}.[12] It was observed that increasing the WC content and incorporation of Cu^{2+} substantially enhanced the thermal properties of the fabric. The gels also show a self-extinguishing nature. Ye et al. [13] and Yan et al. [14] crosslinked PVA with carrageenan and agarose, respectively, via hydrogen bonding to form an interpenetrating network hydrogel. Carrageenan is a biopolymer possessing flame retardant property that increases the

LOI value from 23% (pure PVA) to 30% (composite hydrogel). Similarly, Agarose, a naturally occurring algae gel, is a self-flame retardant that ensures a low heat release rate (HRR) and total heat release (THR) of the composites. In another study, Liu et al. added two biopolymers, viz. calcium alginate, and expandable graphite (intumescent additive) to the PVA matrix to increase its flame retardancy.[15] Calcium alginate with LOI of 48% promotes fire retardancy along with expandable graphite and formed a protective layer that inhibited further burning of the composite hydrogel. Yu et al. [2] formulated a triple network hydrogel that could be laminated on cotton fabric to prevent combustion of the highly flammable cotton cloth. The interpenetrating network mainly comprises PVA, sodium alginate, and thermosensitive poly (N-isopropylacrylamide) as the second and third networks, respectively. The hydrogel unveiled excellent swelling–deswelling performance, antibacterial activity, and flame retardancy. Banerjee et al. [16] customized PVA–MMT hydrogel actuators that could endure fire environments for an extended period of time.

Xanthan gum (XG) and lignin are two naturally occurring biopolymers possessing self–flame retardant property.[17,18] XG is an anionic polymer and widely used as a food thickening agent and suspension stabilizer due to its non-toxic nature. It is a rich source of carbon, thermally stable, and compatible with PVA.[19,20] Xue et al.[1] reported XG and starch based flame resisting hydrogel cream. This hydrogel comprised of resorcinol bis(diphenyl phosphate) (RDP) and produced a thick layer of char, which consequently prevented the chicken skin underneath from burning. After combustion, this hydrogel could provide three times more protection than conventional hydrogels. Similarly, lignin is a naturally occurring biopolymer mainly comprised of aromatic moieties. Lignin is known for its fire retardant nature due to char formation and high thermal stability. Its backbone constitutes coniferyl alcohol,

sinapyl alcohol, and ρ-coumaryl alcohol.[21] Mandlekar et al.[22] employed kraft lignin and lignosulphonate lignin as charring agents for polyamide 11. Shukla et al. [23] treated cotton cloth with 30 w/v % sodium lignin sulphonate to produce samples with 28.5% LOI and self-extinguishing behavior. Recently, Yang et al. [24] grafted phosphorus/nitrogen on lignin (TP-g-L) as a charring agent for PLA composites. A 5 wt% of TP-g-L satisfied industrial standards of UL94 V0 rating for flame retardancy as a result of balanced charring nature of the additive. However, it has been observed that incorporation of nano lignin delivered better thermal stability than pristine lignin.[25] Lignin nanoparticles also offer easier chemical modification and tunable morphological structure.[26,27] In summary, the previous literature clearly demonstrates the potential of biomaterials xanthan gum and lignin nanoparticles as additives to fire retardant hydrogels.

Herein, we report the synthesis of PVA composites with two biomaterials, viz. XG and lignin nanoparticles (LNP), to develop novel fire retardant hydrogels with enhanced properties. The blend of PVA, XG, and LNP was chemically crosslinked via NaOH (N)-borax (B) to form stable hydrogels. The nature of crosslinking and stability of the hydrogels were characterized by evaluating the swelling ratio, water retention ability and finally calculating the network parameters. The formulated hydrogel composites were utilized as green (or environment-friendly) coating on cotton cloths to bestow fire retardancy. These coatings can be utilized in manufacture of fire resistant suits for the firemen. The kinetic analysis of thermal decomposition (using TGA) of the nanocomposites was done using the Kissinger-Akahira-Sunose (KAS) isoconversional method. The fire retardant nature of the synthesized hydrogels was assessed using vertical flammability test (UL94), TGA, limiting oxygen index (LOI) and cone calorimeter test (CCT).

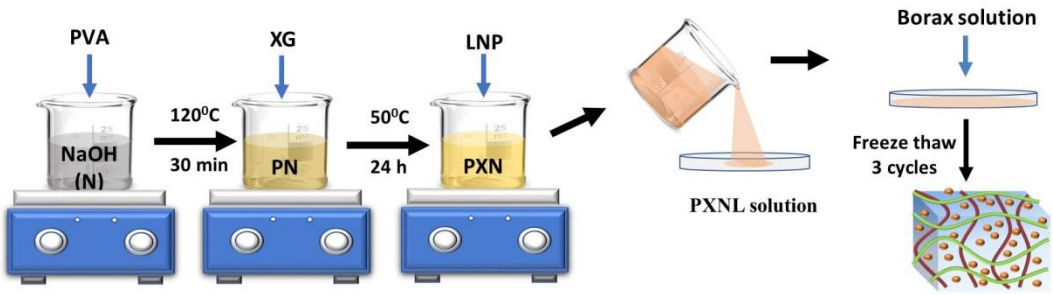

(a) Synthesis protocol of PBXNL hydrogel

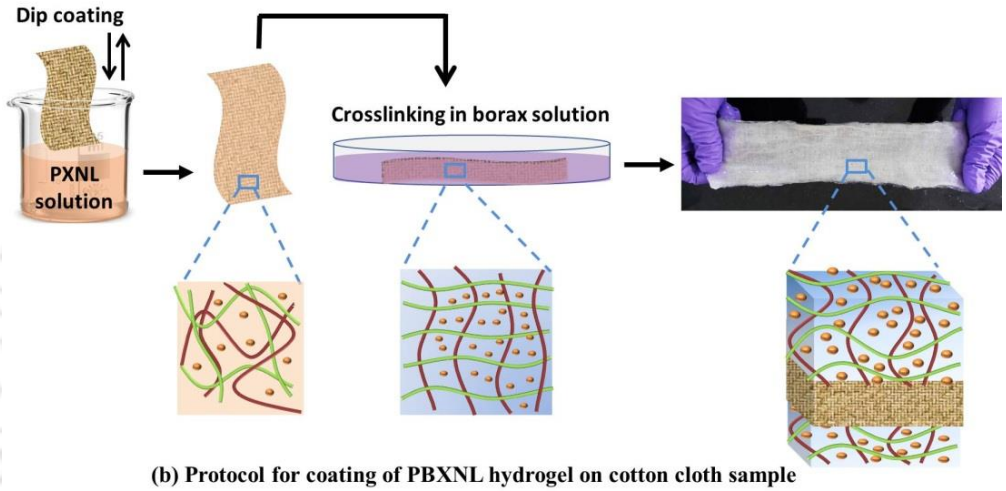

(b) Protocol for coating of PBXNL hydrogel on cotton cloth sample

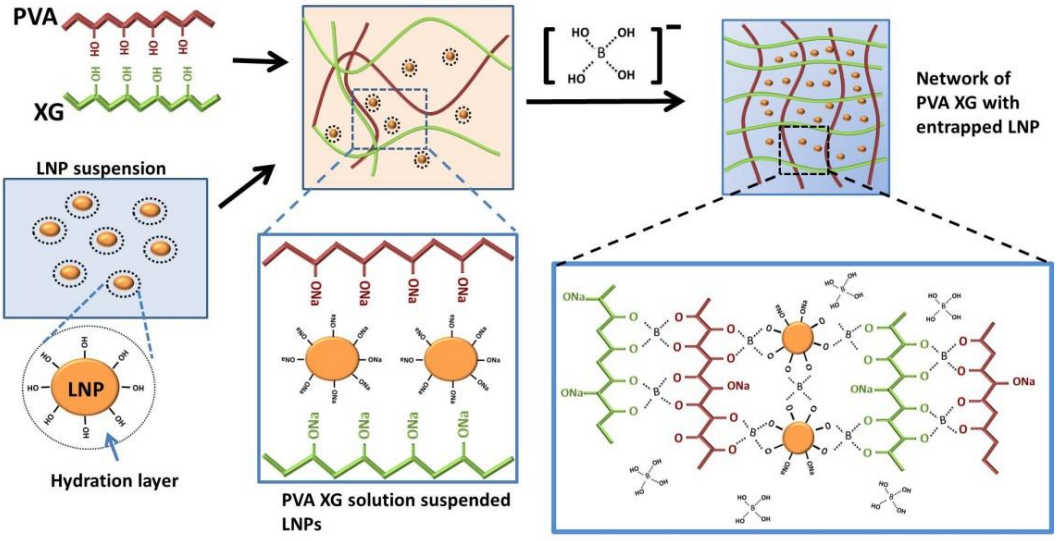

(c) Chemical structure of PBXNL hydrogel

Figure 4.1 Schematic representation of hydrogel synthesis and hydrogel coating on cotton cloth

4.2 Experimental

4.2.1 Materials

Lignin was extracted from local weed, *Arundo donax* (also known as Giant reeds) plant as described in chapter 2 section 2.2.3.[28] PVA (Mw 89,000-98,000, 99+% hydrolyzed) was purchased from Sigma-Aldrich (India) and XG was purchased from Himedia. Sodium hydroxide (≥ 99.0 %), di-sodium tetraborate (also known as borax) (≥ 98.0 %), and acetone (≥ 99.8 %) were purchased from Merck Specialities (India). Cotton cloths were procured from the local market.

4.2.2 Synthesis of lignin nanoparticles

The lignin nanoparticles were synthesized via nanoprecipitation method [29]. Initially, 1 g of air-dried lignin powder was added to 10 ml of 70% acetone followed by sonication for 30 min at 40 kHz [UC-10, Lab Companion (South Korea)]. After dissolution of lignin, the solution was added to 200 ml deionized water, followed by sonication for another 30 min. Acetone was removed from the resultant stable lignin nanoparticle suspension (LNP) and concentrated in a rotary evaporator [R300, Buchi (Switzerland)] i*n vacuo* at 50–55ºC.

4.2.3 Synthesis of PBXN, PBXNL hydrogel and hydrogel coated cotton cloth

To begin with, NaOH solution of required concentration and PVA were mixed obtain a solution with PVA concentration of 5 w/v%. The resultant mixture was stirred at 120°C for 20 min. Next, XG powder (3 w/v%) was added to PVA solution, followed by stirring at 50°C for 24 h until a uniformly mixed opaque solution (PXN) was obtained. The presence of NaOH transforms the –OH groups of PVA and XG into alcoholates (–ONa). This solution was poured into a petri dish. The borax solution was prepared by adding the desired quantity of borax powder to deionized

water. Borax dissociates in water as borate ion, $B(OH)_4^-$ and boric acid, $B(OH)_3$ (eqs. 1 and 2).

$$Na_2B_4O_7 \bullet 7H_2O \longrightarrow 2NaB(OH)_4 + 2B(OH)_3 \quad 4.1$$

$$2NaB(OH)_4 \longrightarrow 2B(OH)_4^- + 2Na^+ \quad 4.2$$

The borax solution was poured over the PXN solution in a petri dish. The alcoholates of PVA and XG rapidly engage with $B(OH)_4^-$ ions to form PBXN hydrogel that was subjected to three consecutive freeze thaw cycles (–20ºC, 20 h freeze, and 4 h thaw). This procedure is schematically represented in **Figure 4.1a**.

Similarly, to obtain PBXNL hydrogels, PVA (5% w/v) was added to NaOH solution, and the mixture was heated at 120°C for 20 min. Next, required amount of XG was added with continued stirring at 50°C for 24 h until uniformly mixed opaque PXN solution was obtained. After cooling the PXN solution, the desired quantity of LNP suspension (in v/v %) was added with stirring for 30 min. The hydration layer of LNP engages with NaOH to form alcoholates. This solution was poured into a petri dish. Further, borax solution of required concentration was poured over the solution in a petri dish for the crosslinking of the alcoholates and $B(OH)_4^-$ to obtain PBXNL hydrogel, followed by three consecutive freeze thaw cycles (–20ºC, 20 h freeze, and 4 h thaw). The compositions of various hydrogels synthesized in this study are shown in **Table 4.1**. These compositions were finalized after numerous preliminary experiments with different combinations of the PVA, XG, LNPs, and borax solutions on the basis of previous literature in the area of PVA-based fire retardant composites.

To achieve hydrogel coating on a piece of cotton cloth, the latter was dipped in PXN/PXNL solution and placed in a petri dish. The borax solution was poured on the sample until it was completely submerged. The cloth was removed after 1 h and

subjected to 3 consecutive freeze-thaw cycles to obtain hydrogel coated cotton cloth samples. All the hydrogels were washed several times with deionised water to remove the unreacted borax and NaOH. All experiments for synthesis of hydrogels were repeated 3× to assess the reproducibility of the results.

Table 4.1 Compositions of the hydrogels

Sample	PVA (w/v %)	XG (w/v %)	Borax (w/v %)	NaOH (w/v %)	LNPs (v/v %)
PX3	5	3	–	–	–
PX3B0.4	5	3	0.4	–	–
PX3B0.4N0.4	5	3	0.4	0.4	–
PX3B0.4N0.8	5	3	0.4	0.8	–
PX3B0.4N2	5	3	0.4	2	–
PX3B0.4N2L5	5	3	0.4	2	5
PX3B0.4N2L20	5	3	0.4	2	20

4.2.4 Characterization of lignin nanoparticles and hydrogels

The functional groups of the lignin nanoparticles (LNPs) and molecular structure of hydrogel samples were characterized using an FTIR spectrophotometer [Spectrum Two, PerkinElmer (USA)] over the wavenumber range of 4000–400 cm^{-1} and X-ray photoelectron spectroscopy (XPS) [PHI 5000 Versa Probe III, ULVAC]. Thermograms of dried hydrogel samples, as well as the lignin samples, were obtained using a thermogravimetric analyzer as described in chapter 2 and chapter 3 to investigate the thermal stability and properties of the samples. A crucible was filled with 8–11 mg sample and heated from 25 ºC to 600 ºC in three linear heating rates, viz. 5, 10, and 20 ºC min^{-1} under a nitrogen atmosphere (20 ml min^{-1}). KAS isoconversional method was used to obtain kinetic parameters of thermal conversion.

The particle size distribution of the LNPs was determined by using the dynamic light scattering as described in chapter 3. The zeta potential of the LNPs was evaluated by using a zeta potentiometer as described in chapter 3. The LNP suspension was sonicated for 15 min and then injected into the flow cell of the zeta potentiometer using a syringe. The electrophoretic mobility of LNP was used to determine the zeta potential. The structural and surface morphological analysis of the LNPs and freeze-dried hydrogel samples were carried out using field-emission scanning electron microscopy (FE-SEM) [Sigma 300, Zeiss (USA)] and field-emission transmission electron microscopy (FE-TEM) [2100F, Jeol (Japan)]. An energy-dispersive X-ray (EDX) [Sigma, Zeiss (USA)] analysis was conducted to determine the elemental composition of LNPs sample.

4.2.4.1 Swelling and water retention test

The formulated hydrogels were washed thoroughly, dried in oven and cut in the size (1 cm x 1 cm, thickness 0.1 ± 0.1 cm). The thicknesses of the cut samples were measured with Mitutoyo digimatic micrometer. The weight gained by the hydrogel due to absorption of water was measured gravimetrically. The initial weights of the samples were measured and referred to as Wd. The samples were immersed in 20 ml of DI water. After 1 h, the samples were taken out and after soaking off the excess water with the help of tissue; the weights of the hydrogels were measured and were denoted as Ws. The samples were reimmersed in DI water and the process was continued after an interval of 2 h for the next 24 h. The swelling ratio (SR) was calculated according to equation 4.3.

$$SR = \frac{W_s - W_d}{W_s} \times 100 \qquad 4.3$$

where, W_s and W_d denote the weight of the swollen hydrogel after time t and the

weight of the dry gel, respectively.

Similarly, water retention ability of the freshly prepared composite hydrogels (1 cm × 1 cm) was determined gravimetrically at an interval of 1 h for 24 h in an ambient atmosphere (25±2ºC, humidity 45±10 %) according to equation 4.4

$$WR = 1 - \frac{W_i - W_d}{W_i} \qquad 4.4$$

Where W_i is the weight of hydrogel at swollen state (at specified time) kept for dehydration in ambient atmosphere and W_d is the weight of the dehydrated hydrogel.

4.2.4.2 Rheological properties of the hydrogel samples

The rheological properties of hydrogel samples were determined using a rheometer [MCR 301, Anton Paar (Austria)]. A 50 mm diameter parallel plate geometry was used, keeping the gap setting at 1 mm. Oscillation shear experiments were used to investigate the viscoelastic characteristics of hydrogel over a wide range of strain and frequency. The linear viscoelastic region (LVR) was initially determined with the amplitude sweep test at a constant frequency (1 Hz) and varying strain of 0.01–100 %. Furthermore, the frequency sweep test was performed over the range of 0.01–100 Hz at constant strain (depending on the LVR).

Determination of network parameters of a hydrogel is important to understand the performance and optimize the hydrogel for coveted applications. Parameters such as crosslinking density, molecular weight between the crosslinks, and mesh size give an insight into the structure of the hydrogel network. However, these parameters are extensively influenced by the composition as well as the method of preparation of the hydrogels. For calculating the network structure parameters, rheological measurements (elastic modulus, G' and viscous modulus, G'') and swelling tests were employed. Based on rubber elasticity theory (RET) for homogeneous Gaussian chains

network parameter, the average molecular weight between crosslinks ($\overline{M_c}$), the crosslinking density (V_e) and mesh size (ξ) were determined as described in chapter 1.[29,30]

$$G' = A\frac{\rho}{\overline{M_c}}RT(V_{2r})^{2/3}(V_{2m})^{1/3} \quad 4.5$$

$$V_e = \frac{\rho}{\overline{M_c}} \quad 4.6$$

$$\xi = \left(\frac{G'N_A}{RT}\right)^{-1/3} \quad 4.7$$

where, ρ is the density of dry hydrogel and is calculated using equation (7), R is the universal gas constant, and T is the temperature. A is the pre-factor which is equal to 1 for the affine network model and $1-\frac{2}{\varphi}$ for the phantom network model. The constrained junction theory depicts that the phantom network model is followed by the real network, and number of branches originating from crosslinking site (φ) is 3[29,31,32].

$$\rho = \frac{w}{S \times t} \quad 4.8$$

where, w denotes the weight of the hydrogel, S is the cross sectional area and t is the average thickness of the hydrogels.

V_{2m} is the polymer volume fraction of crosslinked polymer in equilibrium with swollen gel and V_{2r} is the polymer volume fraction after crosslinking but before swelling. These parameters are determined as:

$$\frac{1}{V_{2m}} = 1 + \left[\frac{\rho}{\rho_w} \left(\frac{1}{Z} - 1 \right) \right] \quad 4.9$$

$$\frac{1}{V_{2r}} = 1 + \left[\frac{\rho}{\rho_w \left(\frac{1}{m} - 1 \right)} \right] \quad 4.10$$

where, ρ is the density of dry hydrogel, ρ_w is the density of water, m is the weight of the dry hydrogel, and Z is the weight of the hydrogel at equilibrium.

4.2.4.3 Experiments for determination of flammability and flame retardancy

Cone calorimeter test (CCT) and Limiting Oxygen Index (LOI) test were performed at Heat and Flame Testing Laboratory, Center of Excellence – Composites at Ahmedabad Textile Industry's Research Association (ATIRA), Gujarat.

Limiting Oxygen Index (LOI, as per ASTM D2863 standard) was determined using Paramagnetic Oxygen Analyzer. LOI represents the minimum oxygen required to ignite the sample with dimensions (100 x 10 x 1 mm^3) in the test atmosphere.

Cone calorimeter test (CCT, as per ASTM E1354 standard) was performed using FTT dual cone calorimeter to record the combustion properties of 100 mm x 100 mm dried hydrogel samples under a heat flux of 25 kW m^{-2}. This fire testing method is based on the principle that the amount of heat released during sample burning is directly related to the amount of oxygen consumed during combustion. Hence, the amount of heat generated is analogous to the fire growth rate. The total heat release rate (THR) can be determined from the test heat release rate (HRR).

Flammability of the hydrogel coated cotton fabric was investigated by open fire test and vertical burning (UL94). Sample size for vertical burning test was 100 mm × 2 mm × 0.1 mm, whereas 100 mm × 100 mm × 2 mm sample size was maintained for the open fire test. For vertical flammability test, the hydrogel coated

fabrics were kept at 40^{o}C for 2 h and burned for 10 s from the bottom in an environment at 25±2ºC and humidity 55% using a butane burner (1300^{0}C) while maintaining a flame height of 4 cm. After 10 s of burning the flame was removed and the samples were allowed to burn on its own. After the sample self-extinguishes, it was again burned for 10 s. The char length of the samples was noted at the end of the second time of burning.

4.3 Results and discussion

4.3.1 Characterization of lignin nanoparticles

Acetone is a nontoxic solvent with high hydrogen bonding capacity and easily solubilizes the lignin. Further, acetone has its solubility parameter, δ closest to that of lignin.[33] However, acetone concentration below 60% induces larger precipitation of lignin. 70% acetone was found to be optimum with the smallest amount of insoluble lignin particles. It was reported that the LNP produced via acetone fraction form a core-shell structure.[34] The hydrophobic aromatic moieties constitute the core and the hydrophilic groups of the lignin constitute the shell structure.[35,36] This results in a layer of hydration around the LNP particles making the LNPs more hydrophilic than the pristine lignin.[34] LNP produced via acetone fractionation had structural groups similar to that of pristine lignin. The FTIR analysis was carried out to affirm the functional groups in pristine lignin and LNPs. The FTIR spectra are shown in **Figure 4.2a**. The results of FTIR analysis given in **Table 4.2** confirm presence of aliphatic, aromatic, and phenolic compounds in LNPs. The nanoparticles show a reduction in the peak intensities, plausibly as a consequence of lignin molecule fractionation.[33] Consequently, the number of aliphatic groups in the lignin reduce with the generation of more active sites for interactions with XG and PVA. Further XPS analysis was

performed, to investigate the chemical state alteration of raw lignin during LNP formation. XPS total survey spectrum shows presence of C1s and O1s core level. **Figures 4.2b** and **4.2c** show the core level spectra of C1s and O1s with the fitted data of LNPs.[37,38] The spectrum clearly shows presence of C–C, C–O–C, C–OH, and C=O bonds at 284.8, 286.3 and 288 eV (**Figure 4.2b**) and aromatic–OH (A–OH) and C=O at 531.5 and 533 eV (**Figure 4.2c**), respectively. The C/O ratios based on XPS of pristine lignin and LNPs were 3.12 and 3.05 (**Table A1.1**, Appendix 1). The result of XPS analyses was in confirmation with FTIR spectra of the pristine lignin and LNPs. This essentially shows that during the process of nanoparticles formation no significant changes occurred in the chemical state of lignin and the carbon content of the pristine lignin remained well preserved in LNPs. The whole idea of LNP addition to the hydrogel is to enhance the char formation alongside xanthan gum that provides flame retardancy. Therefore, it is necessary that the chemical state of lignin remains unchanged after LNP formation process. The method used in the present study achieved this objective as seen from the C/O ratios of pristine lignin and LNP evaluated from XPS. It needs to mention that the previous studies on lignin nanoparticle synthesis have reported significant changes in the chemical state of lignin after nanoparticle formation. Myint et al. [37] have reported rise in C/O ratio of lignin from 2.5 to 3.1 during nanoparticle formation due to extraction of aromatic hydrocarbons by DMF during dissolution process. Zhang et al.[39] have reported reduction in carbon content after nanoparticle formation (using acetone–water mixture as solvent) along with higher distribution of O atoms on the surface of lignin nanoparticles.

Table 4.2 Functional groups recognized in pristine lignin and LNP.

Wavenumber (cm^{-1})	Inference
3459	O–H stretching in aromatic and aliphatic hydroxyl groups
3010	C–H stretching in aromatic compounds
2845	C–H stretching in aliphatic and aromatic carbon
1740	C=O stretching in aliphatic ester
1508	C–C stretching of aromatic skeletal
1461,1423	aromatic ring vibrations of phenyl-propane (C_9) skeleton combined with C–H in-plane deformation
1366	aliphatic C–H stretch in CH_3, O–H bending
1215	C–O stretching alkyl aryl ester
1122	C–O stretching in secondary alcohol
1032	C–O stretching in vinyl ether

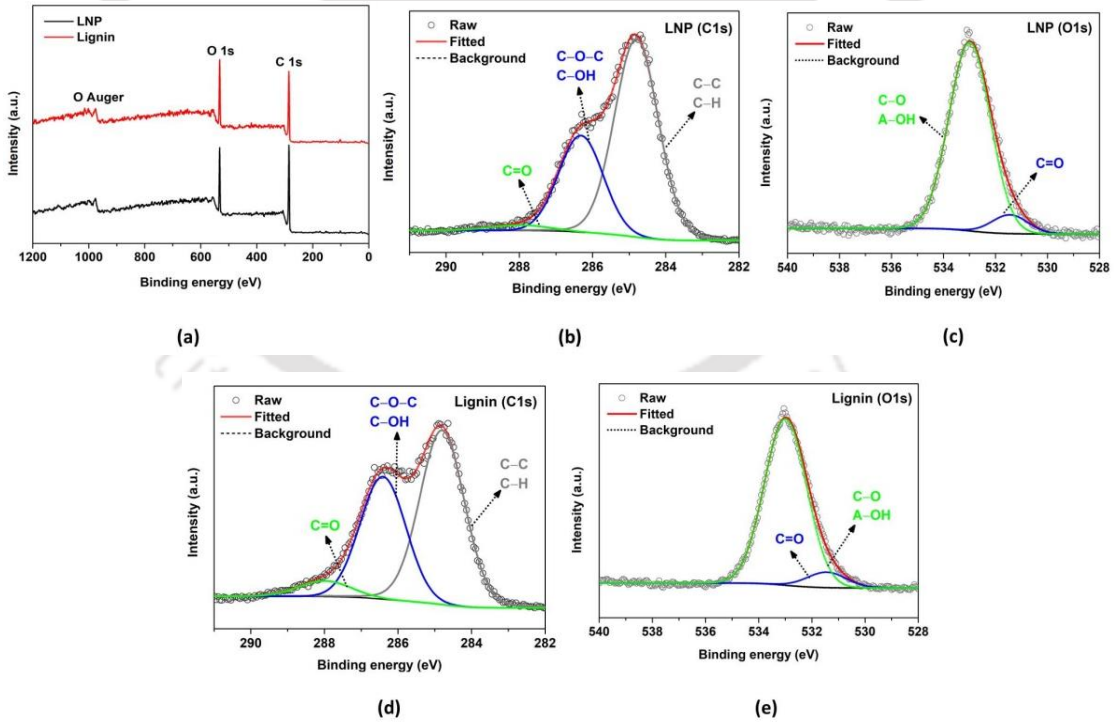

Figure 4.2 (a) XPS total survey spectra, (b) and (c) XPS spectra of C 1s and O 1s of LNPs. (d) and (e) XPS spectra of C 1s and O 1s of pristine lignin

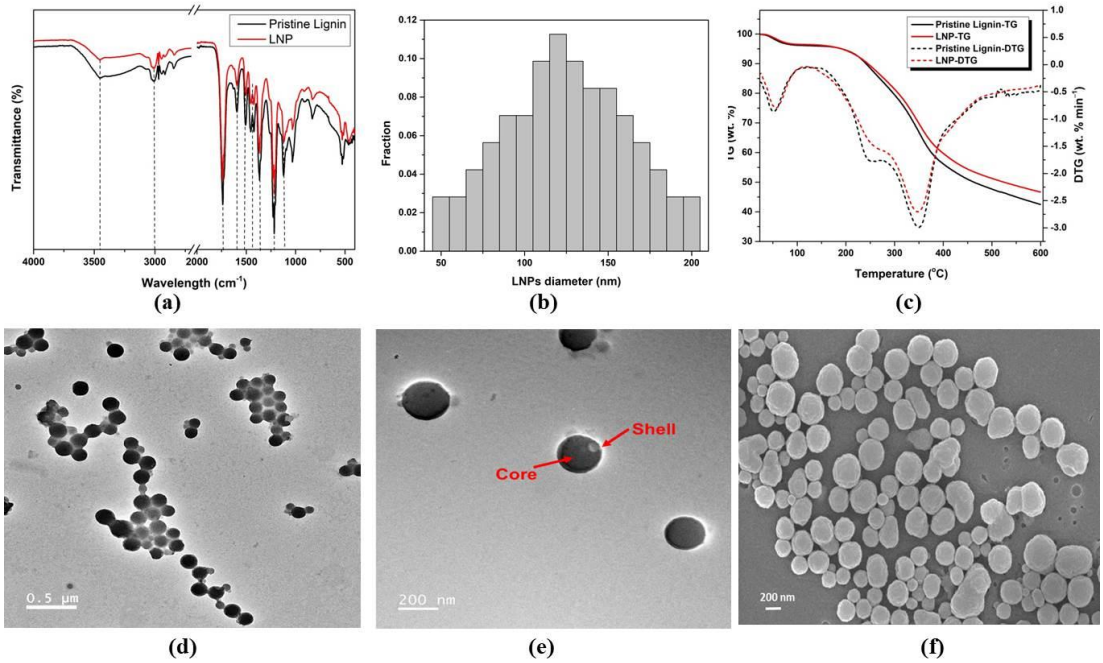

Figure 4.3 (a) FTIR spectrum of pristine lignin and LNPs, (b) Particle size distribution of lignin, (c) TGA of pristine lignin and LNP, (d) and (e) FE-TEM and (f) FE-SEM images of LNP

Figure 4.3d and 4.3e shows the FE-TEM micrographs of LNP. The shape of the particles was distinctly spherical, and ranged between 50–200 nm (**Figure 4.3b**). **Figure A1.1a** (Appendix 1) shows the FE-SEM morphology of pristine lignin. The size was observed to be much larger, with no definite shape or boundary. The EDX result confirmed high carbon and oxygen content in the lignin particles (**Figure A1.1b,** Appendix 1), possibly due to the presence of aromatic, aliphatic, and phenolic compounds (as also revealed in FTIR analysis). The zeta potential of the LNP suspension was –42 mV, which implied formation of the stable suspension and their anionic nature.[34] A well-defined core-shell nanostructure of the LNP was observed from the FE-TEM analysis (**Figure 4.3d**). An amphiphilic structure is commonly used to represent lignin. The aliphatic hydroxyl and phenolic functional groups are mainly associated with the hydrophilic part of lignin (shell part of the LNP structure), whereas aromatic functional groups are associated with the hydrophobic part of lignin

(core section of LNP structure).[40] The strong π–π interactions among the abundant aromatic rings on lignin macromolecules drove the self-assembly of lignin to form LNPs. The LNPs thus produced possess a distinctive core-shell nanostructure.[41]

The thermogravimetric (TG) and derivative thermogravimetric (DTG) curves of the pristine lignin and LNPs under a nitrogen atmosphere are shown in **Figure 4.3c**. The initial degradation of 4 % in the range of 30 – 106 ºC is mainly due to the moisture loss in the samples. In the second stage of degradation, ~17 and 15% loss were noticed in lignin and LNPs, respectively, over the temperature range of 212 – 283 ºC. This is attributed to the development of low molecular weight products as a result of propanoid side-chain cleavage.[27] Further, in the final stage of degradation (over the range of 280 – 380 ºC), ~40 and 37% losses were observed in lignin and LNPs, respectively. This loss could be attributed to the breakdown of the lignin chain, merging and reorganization of aromatic components of lignin, and ultimately char formation. The residues obtained at the end of experiments were ~42 wt% and ~46 wt% for pristine lignin and LNPs, respectively.

4.3.2 Structural characterization of the developed hydrogel

Figure 4.4a shows the FTIR spectrum of mixture of XG solution with the PVA solution and borax. As these polymer solutions were mixed, diffusion of PVA (a flexible polymer) into XG (a complex structured polymer) is expected. This damages the prevailing weak bonds and develops new association bonds, and reorganizes the complete macromolecular systems.[42] As both XG and PVA have significant number of hydroxyl groups, it is obvious to see an absorption band at 3449 cm^{-1} for –OH group.[20] The hydroxyl groups of XG and PVA may develop hydrogen bonds among them. Further, freeze thawing process strengthens the interaction among –OH group of PVA and XG. The peaks in the range of 1815 – 1630 cm^{-1} signify the stretching

vibration C=O. The peaks ranging from 1645 – 1638 cm^{-1} are attributed to high PVA concentration. Furthermore, an absorption band at 1088 cm^{-1} arises due to XG concentration. The interactions among the primary and secondary –OH groups in PVA and XG, lead to the formation of a 3-D network.

The FTIR spectrum of PX3 mixed with 0.4 w/v% borax solution revealed an alteration in the intensity of the –OH band (i.e. 3294 cm^{-1}, refer to **Figure 4.4a**). The minor shift and enlargement of the absorption band with respect to PX3 indicated the interaction of borax with PVA and XG.[43] The peaks at 1420 – 1340 cm^{-1} correspond to asymmetric stretching relaxation of B–O–B. This signifies crosslinking of polymer chains with the borate ions amid the development of tetrahedral complexes.[44] Further, the absorption at 833 and 661 cm^{-1} corresponds to B–O stretching and B–O–B associations within borate linkages, respectively.[45] **Figure 4.4b** displays the FTIR spectrum of hydrogel PX3B0.4 with various NaOH concentrations. The peaks at 3440 and 3232 cm^{-1} are ascribed to the –OH band stretching. A clear decrease in the width of peaks for wavenumber range 3695 to 2750 cm^{-1} can be observed, which affirms the interaction of NaOH with the PX3B0.4. A small peak at 2946 and 2840 cm^{-1} is possibly due to the deformation of the –CH group.[46] The shift in the peak at 1640 cm^{-1} is attributed to the C=O stretching in –COOH moiety in the polymer matrix.[47] The band at 1406 cm^{-1} signifies the breakdown of alkyl derivatives in PX hydrogel and further bending of the –OH group due to the interaction of NaOH with the polymer matrix.[47] Moreover, the absorption bands at 1221 and 1085 cm^{-1} correspond to the C–O–C linkage and C–O stretching in the polymer matrix. **Figure 4.4c** displays the FTIR spectrum of PX3B0.4N2L5 and PX3B0.4N2L20 hydrogels. The peaks at 3450 and 3332 cm^{-1}, which are relatively wider as compared to PX3B0.4 hydrogels are ascribed to –OH stretching. This can be due to the presence of LNPs in the system.

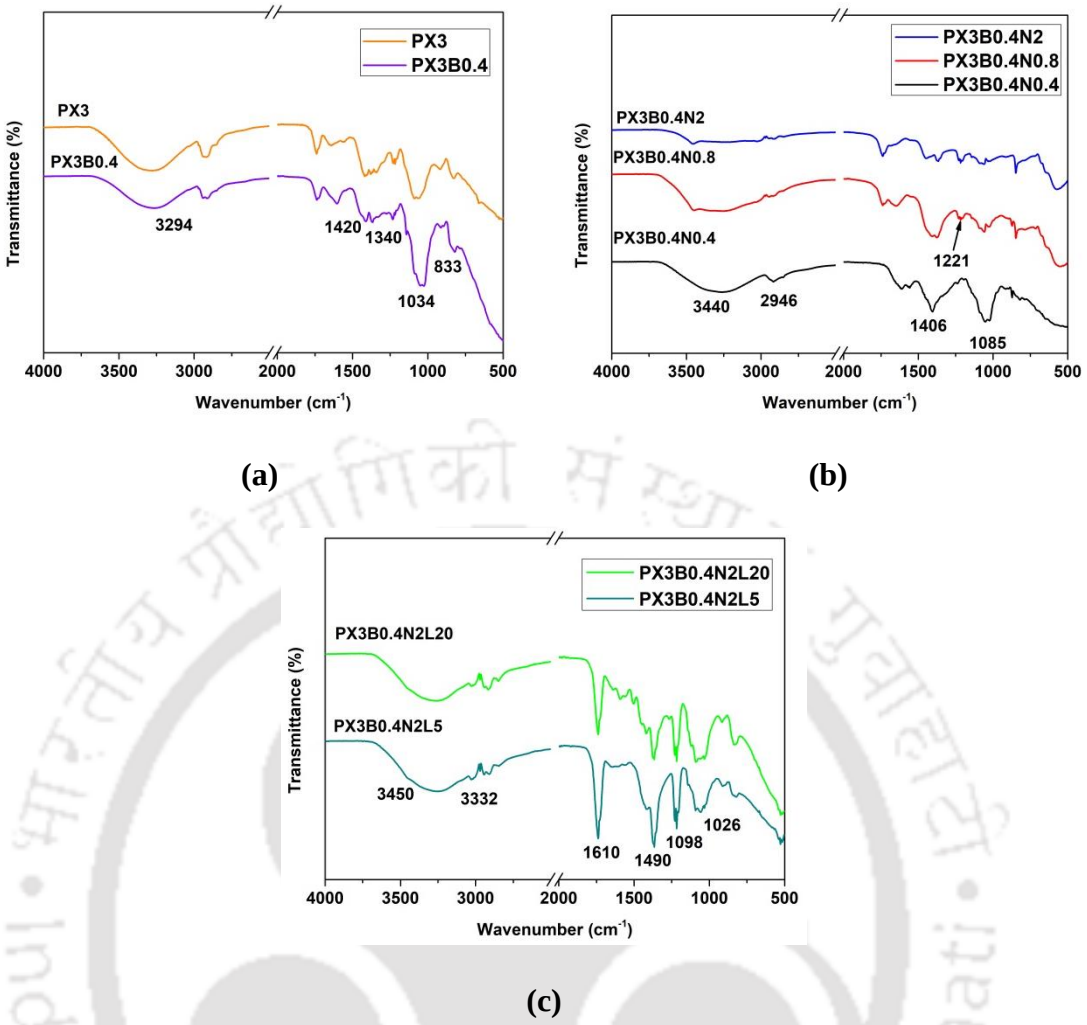

Figure 4.4 FTIR spectra of (a) PX3 and PX3B0.4 (b) PX3B0.4N0.4, PX3B0.4N0.8 and PX3B0.4N2 (c) PXB0.4N2L hydrogels

The distinct peaks from 1610 to 1490 cm^{-1} in PX3B0.4N2L5 and PX3B0.4N2L20 hydrogels are attributed to the aromatic ring and skeleton (**Figure 4.4c**). This also validates the cross-linking of LNPs and the PX3B0.4N2 network [47]. The bands from 1098 – 1026 cm^{-1} corresponds to the tensile vibration of the –OH group in the lignin. Based on **Figure 4.4c**, it is confirmed that the hydroxyl groups of the PX3B0.4N2 matrix and the aromatic hydroxyl group of lignin formed strong hydrogen bonds, which eventually promoted the development of a stable PX3B0.4N2L5 and PX3B0.4N2L20 hydrogels.

4.3.3 Rheological properties

4.3.3.1 Effect of xanthan gum

The viscoelastic behavior of the synthesized hydrogels was examined using oscillation shear tests. Initially, an amplitude sweep test was conducted in the strain range of 0.01 – 100 % and a constant frequency of 1 Hz to determine LVR of hydrogel samples. Under this region, further frequency sweep was performed without damaging the structure of the hydrogels. **Figure A1.2** (Appendix 1) shows that the G′ dominated over G″ throughout the complete strain range. Also, the increase in the elastic moduli of the PX hydrogel samples with XG concentration can be noticed in **Figure A1.2** (Appendix 1). This suggests the physical cross-linking of PVA and XG. Considering G′ > G″, the developed hydrogels confirm viscoelastic solid-like behavior. Further, a frequency sweep test was performed over 0.01 – 100 Hz at constant strain of 1 % (determined using LVR) to verify viscoelastic behavior of hydrogel. **Figure 4.5a** demonstrates the viscoelasticity of PX3 hydrogel. The trends in **Figure 4.5a** clearly depict the superiority of G′ over G″ over the entire frequency range that confirms dominating elastic nature of the hydrogel. PVA comprises of flexible chains while XG has rigid chain and complex helical structure. XG swells in water and increases the viscosity of the solution. The increment in the viscoelasticity with XG concentration is possibly due to the diffusion of XG in PVA's flexible chains. As noted earlier, both XG and PVA have ample hydroxyl groups, and the freeze-thaw process promotes inter- and intra-molecular interactions. These interactions are mostly hydrogen bonding between hydroxyl (–OH) and acetate (CH_3COO^-) groups of PVA and –OH and carboxylate (i.e., $HCOO^-$) groups of XG. Therefore, a network of hydrogen bonds connects the aforesaid functional groups to yield a composite structure with closely associated components. Borax dissociates

into borate ion, $B(OH)_4^-$ and boric acid $B(OH)_3$ (as per equation 4.1 and 4.2) in water.

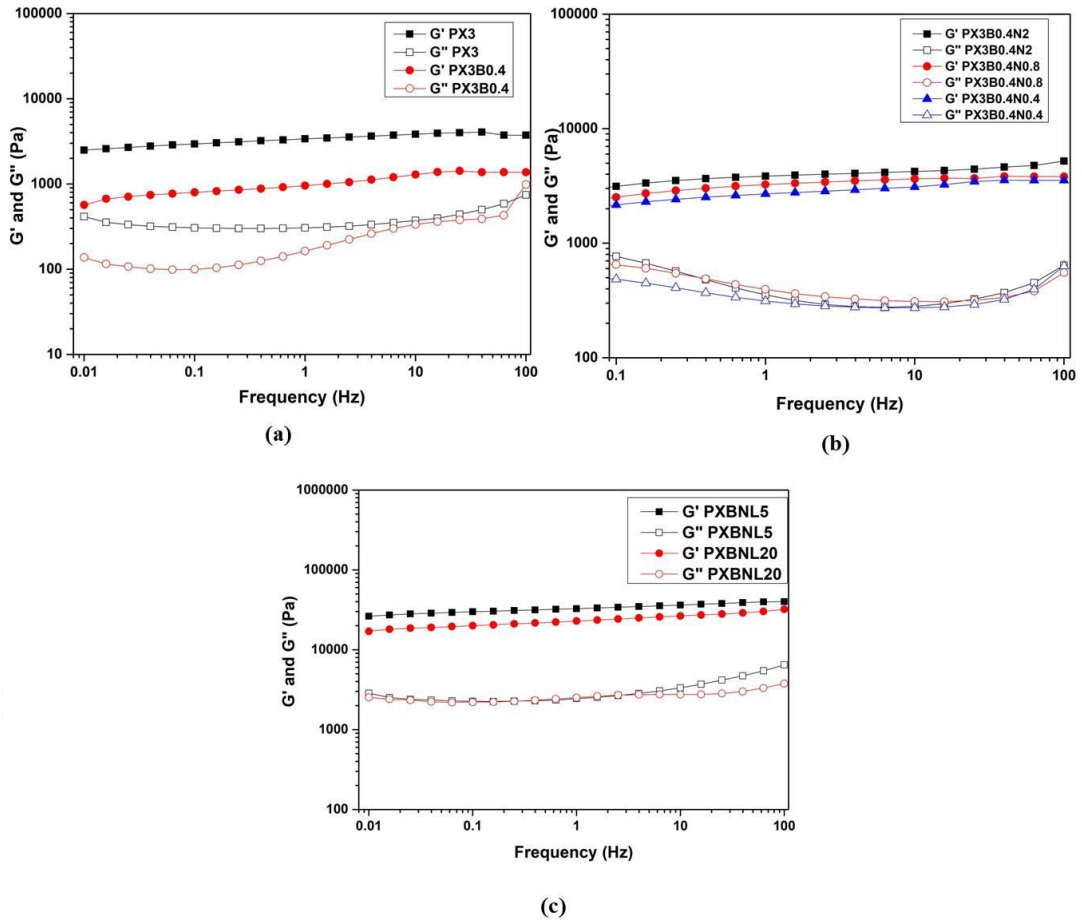

Figure 4.5 Frequency sweep of (a) PX and PXB, (b) PXBN, (c) PXBNL hydrogels

$B(OH)_4^-$ complexes through monodiol and diol-diol interactions with hydroxyl groups of PVA and XG imparting viscoelasticity to the system, as depicted in **Figure 4.1c**. Strain sweep demonstrates that the structure of PX3B0.4 remains unchanged till 1% strain even after applying shear (refer to **Figure A1.2** in Appendix 1). Similar to the strain sweep, frequency sweep shows the viscoelastic behavior of the PX3B0.4 hydrogel, which was governed by a gel-like or elastic behavior.

4.3.3.2 Effect of borax and NaOH

As expected, an enhancement in the elastic moduli of hydrogels was observed with increasing concentrations of NaOH. **Figure 4.5b** shows the influence of borax and NaOH on moduli of the PX3B0.4 hydrogel samples. $B(OH)_3$ produced during dissociation of borax in water (as per equation 4.1 and 4.2) may stick to the polymer chains that do not participate in crosslinking in the system.[47] Hence, to resolve this setback, PVA and XG are prepared in basified water (refer **Figure 4.1c**). Generally, addition of PVA and XG to basified water induces partial deprotonation of PVA, XG and LNP, which sequentially alters the –OH groups to –O–Na (alcoholates).[48] This particular phenomenon facilitates bond formation of $B(OH)_4^-$ with the polymers and LNPs. $B(OH)_4^-$ interacts with –O–Na to form O–B–O, losing Na^+ ion in the process. This association of $B(OH)_4^-$ with alcoholates established chemical bonding between PVA, XG, LNP and resulted in rapid gelation to form a constructive hydrogel network, as depicted in **Figure 4.1c**. The aforesaid phenomenon occurs when appropriate borax, XG and NaOH concentration is included in the PVA solution.[19] Hence, increment in the elastic moduli of hydrogel is observed with increasing concentrations of XG and NaOH (**Figure 4.5c**). A noteworthy improvement in the moduli can be confirmed with the inclusion of higher concentration of borax, which generates larger quantities of $B(OH)_4^-$ that interact with the alcoholates to establish greater crosslinking. Dominance of G' over G'' confirms the viscoelastic solid-like or gel-like characteristics of hydrogels. This could be ascribed to the strong molecular interactions of hydroxyl groups (which are expected to be in excess) with acetate and carboxylate functional groups. **Figures 4.5b** and **4.5c** confirm increase in the elastic modulus with NaOH concentration. However, a slight decline in elastic modulus was

observed for PX3B0.4N hydrogel (**Figure 4.5c**). Even though the inclusion of NaOH facilitated the formation of strong viscoelastic solid-like hydrogel, presence of excessive xanthan gum could hamper this facet as a result of slight degradation and uncoiling of XG helical structure in presence of NaOH.

4.3.3.3 Effect of LNPs

Figure 4.5c illustrates the viscoelasticity of the PX3B0.4N2 samples after addition of LNP. Incorporation of LNP imparts greater viscoelasticity to the hydrogel matrix. It is evident from **Figure 4.5c** that PX3B0.4N2L5 shows noteworthy improvement in the moduli of PXBN hydrogel with incorporation of LNPs. This may be due to hydration layer around LNP interacting with Na^+ ions to form alcoholates. Sequentially, these alcoholates interact with $B(OH)_4^-$ to form a strong inter and intra molecular O-B-O linkage with PVA and/or XG.[49] However, addition of 20% v/v of LNP causes slight decrement in the elastic moduli of PXBN hydrogels. This can be due to aggregation of excess LNPs in the hydrogel matrix, which hinders the association of polymers and LNPs.

4.3.4 Network parameter

The network parameters, viz. average molecular weight ($\overline{M_c}$), effective crosslink density (V_e), mesh size (ξ), shear modulus of the formulated hydrogels and swelling ability of the hydrogels were either measured experimentally or calculated. These network parameters are listed in **Table 4.3** and **Table A1.2** (Appendix 1). These depict the water absorption and swelling ability of the hydrogels. The trends in these parameters clearly demonstrate the influence of the concentrations of polymers (PVA and XG), NaOH, Borax and LNPs. A dehydrated hydrogel absorbs and swells when it comes in contact with water. Water absorption ability of the hydrogels was

measured in terms of its swelling ratio. All hydrogels swell rapidly for initial 1 h and attain equilibrium as shown in **Figure 4.6a**. This can be attributed to the hydrophilicity of the polymers. The water retention ability of the hydrogels is shown in **Figure 4.6b**. PX3B0.4N0.8 hydrogel absorbed 96–97% of water and was able to retain it for longer duration of period. This can be attributed to the appropriated degree of crosslinking where the network wasn't too loosely linked to easily evaporate the bound water nor too tightly packed to be not able to absorb water. The samples with higher amount of water absorption capacity were able to retain water for longer duration of time.

Table 4.3 Network parameters calculated from rheological measurement

Composition	G' (Pa)	$\overline{M_c}$ (kg mol^{-1})	V_e (kmol m^{-3})	ξ (nm)
PX3	3338.57	70.54	53205.08	10.72
PX3B0.4	1659.05	125.18	10774.07	13.53
PX3B0.4N0.4	2643.33	110.31	20581.09	11.58
PX3B0.4N0.8	3150.00	94.99	14762.12	10.93
PX3B0.4N2	4926.90	88.40	22246.05	9.41
PX3B0.4N2L5	33095.24	4.34	2301647.95	4.99
PX3B0.4N2L20	23428.57	12.04	870350.12	5.60

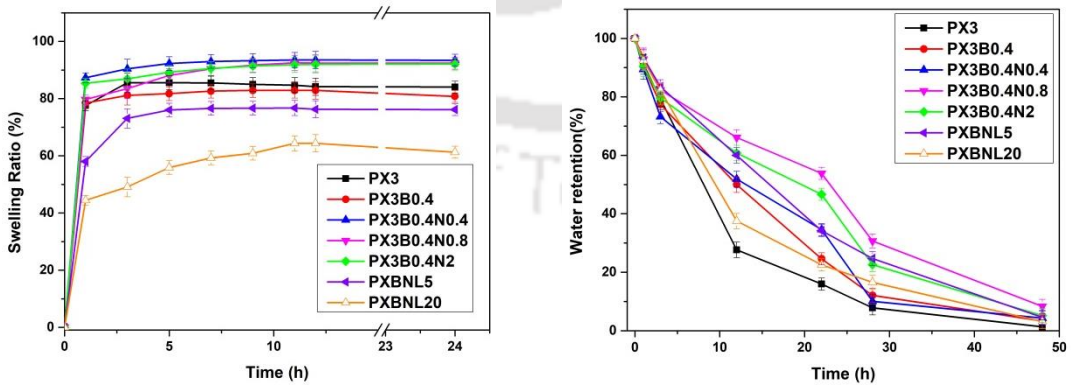

(a) **(b)**

Figure 4.6 (a) Swelling ratios and (b) water retention ability of the formulated hydrogels

Further, the porous structure (shown in **Figure 4.7**) and large mesh size of the hydrogel facilitates water absorption. To calculate V_{2m} (polymer volume fraction in swollen hydrogel), the weight of the swollen hydrogel at equilibrium was determined (equation 4.7, refer **Table A1.2** Appendix 1). It was observed that the increment in crosslinking density reduced the mesh size of the hydrogel and turned the structure of the hydrogels more compact. This hinders water molecule penetration in the network. Presence of 3 w/v % XG in PX3 hydrogel provides large number of hydroxyl and carbonyl groups to interact with hydroxyl group of PVA. Further, freeze thawing process established a rigid hydrogel network through hydrogen bonding and ice crystals formation. This rigid hydrogel network results in high elastic modulus, while simultaneously reducing the $\overline{M_c}$ and pore size due to the increasing crosslinking density (V_e) of the hydrogels. Incorporation of lower concentration of borax (0.4 w/v%) in PX3 system leads to weak physical crosslinking between PVA and XG via mono-diol and diol-diol complexation. Hence, distance between the crosslinking sites increases leading to reduction in crosslinking density. Sequentially, reduction in elastic modulus and rise in pore sizes of hydrogel is observed. Further, crosslinking of basified PVA and XG with borax instantaneously establishes covalent bonding between PVA, XG and boron atoms. This results in mechanically strong hydrogel structure with higher elastic modulus (G') and crosslinking density, and smaller $\overline{M_c}$ and pore size as shown in **Figures 4.7a** and **4.7b**. Similarly, presence of 5% v/v of LNPs further crosslinked the PX3B0.4N2 network resulting in higher elastic modulus and smaller pore structures (refer to **Figures 4.7c** and **4.7d**). These results deduced from the calculation of the network parameters determined the ability of the hydrogels to absorb and swell in water. The basis of fire retardancy in these hydrogels is its ability to absorbs and retain water. The more amount of water absorbed longer the

hydrogel will take for to ignite. Consequently, these parameters aid in evaluating the performance of the hydrogel as a flame retardant.

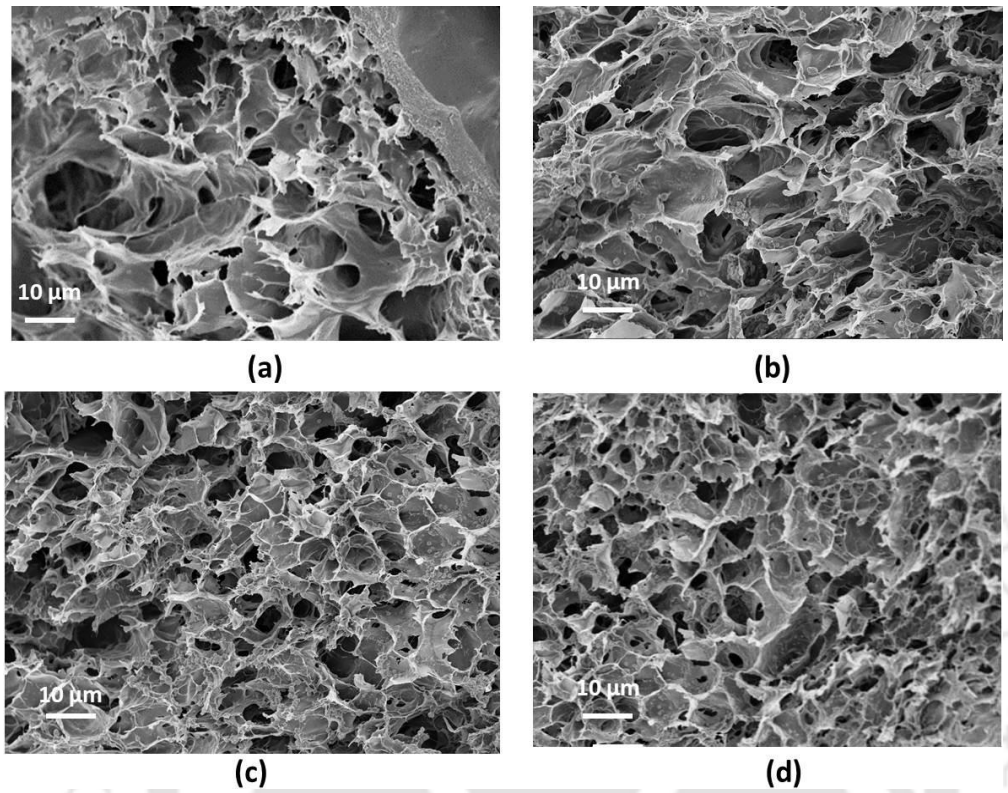

Figure 4.7 FESEM images of (a–b) PX3B0.4N2 (c–d) PX3B0.4N2L5 hydrogels. The PX3B0.4N2L5 hydrogels have smaller pore size due to greater degree of cross-linking among PVA, XG and LNPs.

4.3.5 Thermal analysis of hydrogels

The results of thermogravimetric analysis of various hydrogels synthesized in this study are summarized in **Table 4.4**. **Figure 4.8a** shows the TGA and DTG curves (representing thermal stability) of PX3 and PX3B0.4 hydrogels under a nitrogen atmosphere. The thermal degradation of the PX3 hydrogels can be distinguished in three steps. The initial degradation was below 178 ºC, which could be attributed to the moisture removal from the hydrogel.[50] The secondary degradation was observed from 214 to 366 ºC. This could be related to dehydration of the main chain of PVA, as well

as the disruption of the side chain and unfolding of the main chain of XG.[51,52] The amount of char formed at the end of the analysis (i.e. 600 ºC) was 17.09 wt.% for PX3. A similar thermal degradation trend was observed for the PX3B0.4 hydrogels. However, the shifts in the degradation temperatures, reduction in the weight loss during the second degradation step, and increment in the residue of samples at 600 ºC were observed, as depicted in **Table 4.4**. This could be attributed to the interaction of borax with PVA and XG via development of excess hydroxyl bonds.

Table 4.4 Summary of thermogravimetric analysis (TGA) results

Sample	Primary degradation	Secondary degradation		Final degradation		Residue at 600ºC (wt. %)
	Weight loss (%)	Temperature range (ºC)	Weight loss (%)	Temperature range (ºC)	Weight loss (%)	
PX3	8.15	214–366	58.64	400–487	9.50	17.09
PX3B0.4	7.07	235–350	49.38	370–486	21.06	17.35
PX3B0.4N0.4	16.92	203-306	41.95	344-509	13.75	24.49
PX3B0.4N0.8	19.76	206-298	37.85	341-506	12.54	27.00
PX3B0.4N2	27.82	192-294	28.58	353-503	8.15	32.76
PXBNL5	26.62	195-302	31.25	366-494	8.099	31.16
PXBNL20	27.33	201-285	27.91	356-503	8.02	34.61

#heating rate 10°C

Figure 4.8b shows the thermal degradation of PX3 hydrogels with different borax–NaOH concentrations. Sodium ions dehydrate the polymer matrix, and thus, the presence of NaOH in the hydrogel facilitates rapid char formation.[50] An increase in the weight loss (16 – 28%) of PXBN hydrogels can be observed during first stage of degradation. Furthermore, around 28 –41% weight loss was recorded during the secondary degradation. **Figure 4.8b** depicts NaOH induced deprotonation of PVA and

XG that shifts the degradation temperature resulting in quick ignition, and formation of high carbon content structures and aromatic char.[50] This is favorable in flame retardant materials. Similar results were observed in case of hydrogels consisting of LNPs, as shown in **Figure 4.8c**. The residues obtained for PBXNL5 and PBXNL20 were 31 and 34 wt% respectively.

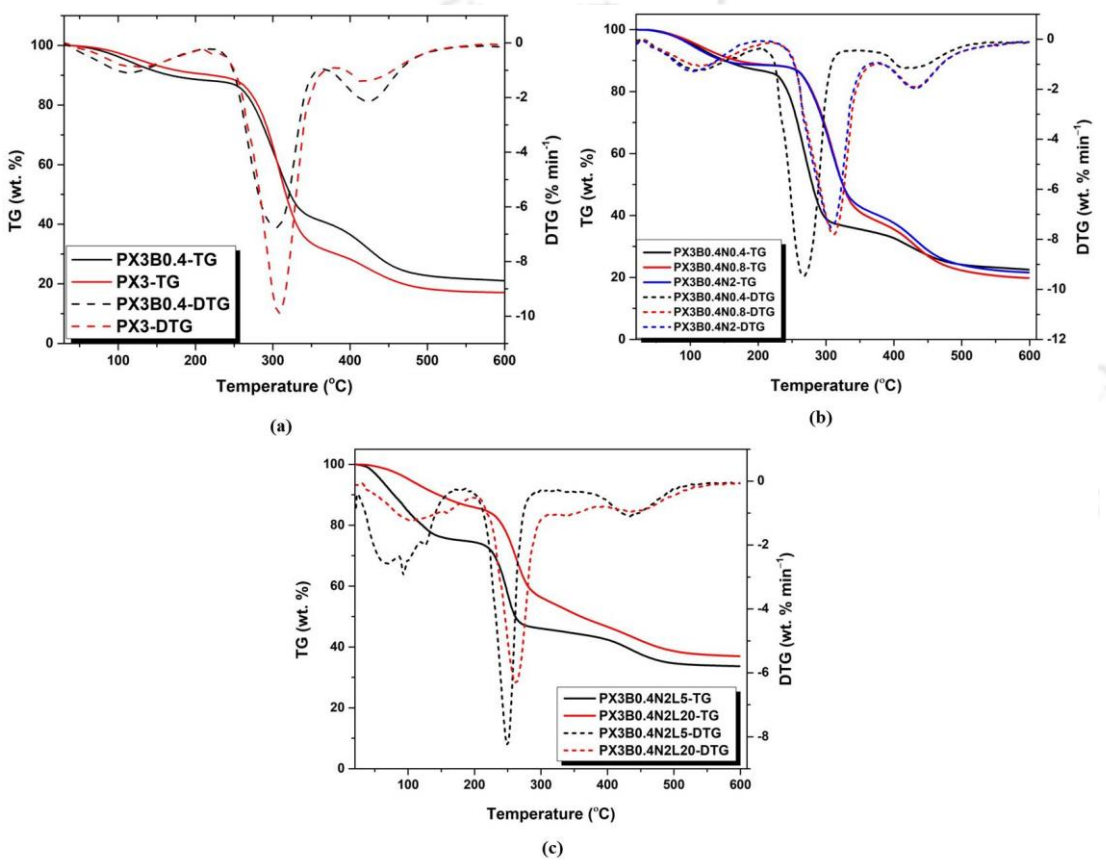

Figure 4.8 TGA and DTG curves of (a) PX3 and PX3B0.4, (b) PX3B0.4N0.4, PX3B0.4N0.8 and PX3B0.4N2, and (c) PX3B0.4N2L5 and PX3B0.4N2L20 hydrogels

4.3.6 Thermal kinetics analysis

In the previous section, thermal degradation behavior of the formulated hydrogels was discussed. The nature of complexity in hydrogel degradation, due to innumerable reactions and parameters enmeshed, compels one to gain a broader

insight into the degradation behavior of the hydrogel. Hence, the TGA data of the hydrogels was analyzed using isoconversional models to determine E_a, the kinetic parameter of activation energy, which signifies the thermal stability (or resistance to combustion) of the material. The thermograms of different hydrogels were obtained at three different heating rates (5, 10, and 20 ºC min^{-1}) in the temperature range of 30 – 600 ºC, as shown in **Figure A1.3**, Appendix 1. The thermal conversion data was analyzed using KAS method (eq. 11) [53,54] The KAS method is an integral isoconversional method for the determination of kinetic parameters of thermal conversion of biomass. The governing equation of KAS method is given below, and at any constant value of α, the activation energy can be calculated from the slope of the plot of $\ln\left(\frac{\beta}{T^2}\right)$ versus $\frac{1}{T}$.[55].

$$\ln\left(\frac{\beta_i}{T^2_{\alpha,i}}\right) = \ln\left(\frac{AR}{E_a g(\alpha)}\right) - \frac{E_\alpha}{RT_{\alpha,i}} \qquad (4.12)$$

where, β is the heating rate (K min^{-1}), T is the temperature (K), A is the pre-exponential factor, R is the molar gas constant (8.314 J $mol^{-1}K^{-1}$), and α is the degree of conversion.

Figures 4.9a and **4.9b** and **Figures A1.4a** and **A1.4b** (in Appendix 1) depict representative plots of $\ln(\beta/T^2)$ versus 1/T for the hydrogels PXB0.4N2, PXB0.4N2L20, PX3B0.4, and PX3B0.4N2L5, respectively. **Figure 4.9c** shows the fitting of equation 4.12 to the thermal conversion data (TGA analysis) of the hydrogels PXB0.4, PX3B0.4N2, PX3B0.4N2L5 and PX3B0.4N2L20 in the conversion range of 0.1 to 0.7, respectively. The complete results of the analysis are given in **Table 4.5**. Based on the variation of E_a with conversion, the degradation process can be classified into three stages. Stage I (α = 0 to 0.2) signifies the initial

degradation due to moisture loss and consequently E_a (shown in **Table 4.4**) is very low. In Stage II (α = 0.2 to 0.5), a steady rise in the value of E_a is observed. This is mainly due to substantial degradation of PVA, XG and borax linkage accompanied by incineration of polymer backbone. In stage III (α = 0.5 to 0.7), E_a of PBXNL20 is markedly higher than other hydrogels, viz. 70% and 85% higher than PX3B0.4N2 and PXBNL5, respectively, as seen in **Table 4.5**. The marked rise in E_a for the hydrogel PXBLN20 (as compared to hydrogels without LNPs) clearly indicates the influence of lignin on enhancing the thermal stability of hydrogels, which is possibly a consequence of char layer formation on the outer surface of hydrogels, which protects the inner layers from oxidation.

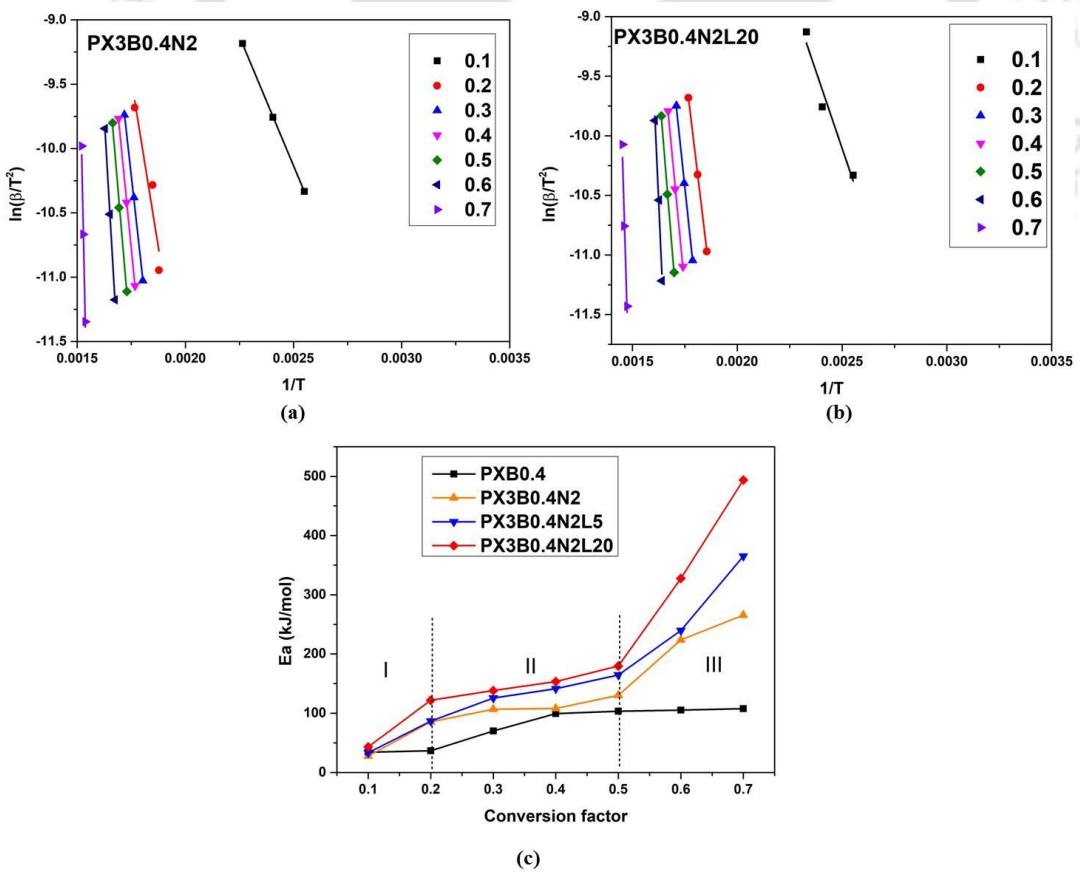

Figure 4.9 Kinetic fitting of thermograms using KAS model for (a) PX3B0.4N2 (b) PXBNL20; variation of activation energy (E_a) as a function of conversion (α).

Table 4.5 Results of activation energy calculated by KAS model for the formulated hydrogels

α	PX3B0.4		PX3B0.4N2		PX3B0.4N2L5		PX3B0.4N2L20	
	E_a	R^2	E_a	R^2	E_a	R^2	E_a	R^2
0.1	25.573	0.94	27.769	0.99	33.368	0.99	43.087	0.95
0.2	56.754	0.98	85.564	0.95	86.618	0.91	121.859	0.99
0.3	85.795	0.99	106.971	0.98	125.669	0.99	138.242	0.99
0.4	91.911	0.98	108.204	0.98	141.545	0.99	153.611	0.90
0.5	106.02	0.97	130.193	0.98	164.597	0.99	179.603	0.99
0.6	109.406	0.97	223.85	0.99	164.597	0.99	327.7	0.99
0.7	118.951	0.98	265.568	0.96	286.527	0.98	493.811	0.95

α = conversion %, E_a = activation energy kJ mol^{-1}

4.3.7 Combustion studies of hydrogel coated cotton cloth

The LOI and flammability tests were carried out to evaluate the flame retardant characteristics of PX3 hydrogel in association with borax, NaOH, and LNPs (**Figure 4.10**). The pure cotton cloth is highly flammable and also has a high flame velocity. Hence, it burns completely within seconds of the flammability test (**Figure 4.10a**). In addition, the LOI of pure cotton cloth is reported to be 20%.[55] Coating the cotton cloth with PX hydrogel hinder the process of ignition until the hydrogel dries up. **Figure 4.10b-d** shows that hydrogel coated samples do not ignite during the first 10 s due to hindrance offered by water present in the hydrogel (as previously indicated by swelling test results, **Figure 4.6a**). While igniting the samples for the second time (10 s) it was observed that the samples burn and self-extinguish leaving behind a layer of char. **Table 4.6** reports the vertical flammability test results of various hydrogels. It was observed that presence of XG induced char formation, for example 3% w/v of XG resulted in 1.9 mm length of char. Incorporation of borax (0.4% w/v) further delayed the ignition process and produced a char length of 1 mm.

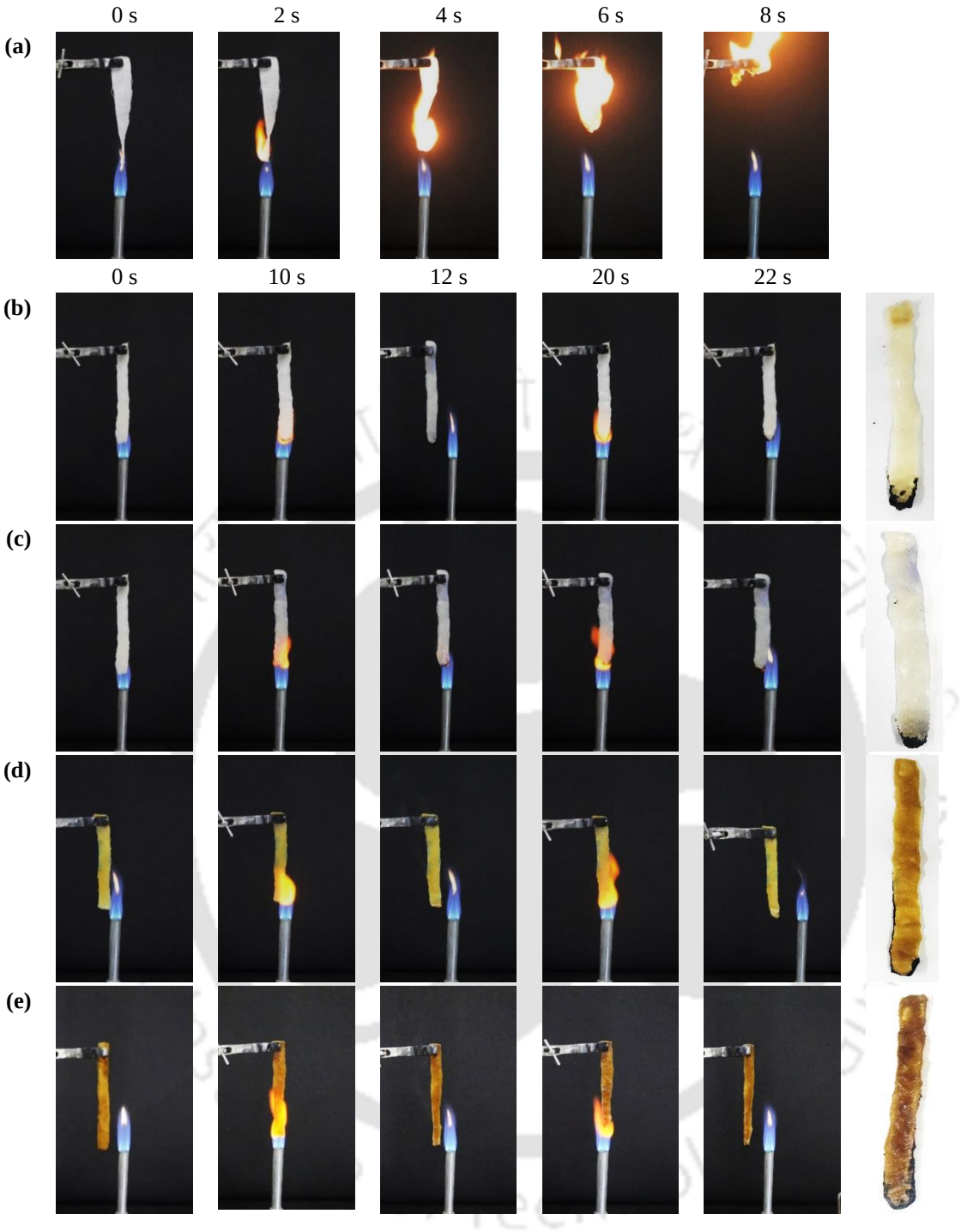

Figure 4.10 Photos showing the process of burning during UL94 (a) cotton cloth (b)PX3B0.4 (c) PX3B0.4N2 (d) PX3B0.4N2L5 (e) PX3B0.4N2L20

Similar results were obtained for hydrogels with lower concentration of LNP (5% v/v). However, higher incorporation of LNP induces rapid burning of the sample and formation of char layer. The sample self-extinguishes and the layer of char forms a

protective layer that prevents further burning of the sample. The length of char layer was 1.75 mm after 20 s burning. The LOI values of the hydrogels were as follows: PX3B0.4 = 29.75%, PX3B0.4N2 = 36.11% and PX3B0.4N2L20 = 39.39%. The LOI value of PX3B0.4N2L20 hydrogel is significantly higher than other PVA based hydrogels reported in the literature. Ye et al. [13] have reported PVA–Carrageenan hydrogels with LOI of 30%. Liu et al. [15] have reported LOI in the range of 36–37 % for PVA composites with calcium alginate and expandable graphite (30, 40 and 50 wt%). Yu et al. [2] have synthesized PVA/ Poly(N-isopropylacrylamide)/ sodium alginate hydrogels with LOI of 29%. The LOI values for the hydrogels synthesized in this study show the same trend as the activation energy (kJ mol^{-1}) and the residues (wt%) after TGA analysis, viz. PX3B0.4 = 118.951 kJ mol^{-1} and residue 17.35 wt%., PX3B0.4N2 = 265.568 kJ mol^{-1} and residue 32.76 wt%, and PX3B0.4N2L20 = 493.811 kJ mol^{-1} and residue 34.61 wt%. These results essentially show that incorporation of LNP in the PXBN hydrogels leads to significant improvement in the fire retardancy behavior of the hydrogel.

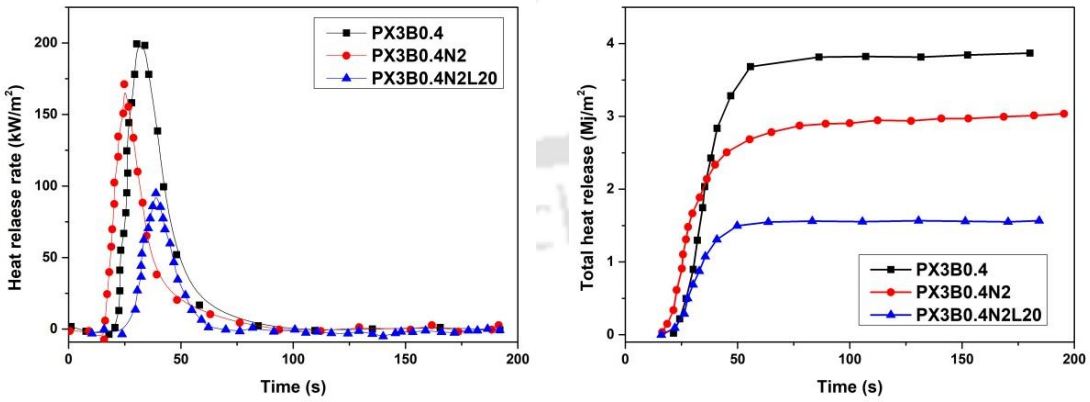

(a) **(b)**

Figure 4.11 Cone calorimeter test (CCT) result of PX3B0.4, PX3B0.4N2 and PX3B0.4N2L20 hydrogel coated cotton cloth samples (a)Heat release rate (HRR) and (b) Total heat release(THR)

Table 4.6 Vertical flammability test results of PX hydrogel composites

Material	Sample length (mm)	Total time (s)	char length (mm)	Burning characteristics
PX3	127	20	1.9	No dripping, no swelling
PX3B0.4N2	127	20	1	No dripping, no swelling
PX3B0.4N2L5	127	20	1	No dripping, no swelling
PX3B0.4N2L20	127	20	1.75	No dripping, no swelling, rapidly burns with formation of protective layer of char

Similarly, the cone calorimeter tests (CCT) revealed the amount of heat released by test samples on administering 25 kW m^{-2} heat flux. The nature of heat release, viz. heat release rate (HRR) and total heat release (THR), is calculated by the amount of oxygen consumed during the experiment (**Figures 4.11a** and **4.11b**). A single peak right after ignition is observed in HRR curve (**Figure 4.11a**), which clearly shows that oxygen consumption is higher during the initial phase of the ignition.[56] Further, a single peak may also signify the layer of char produced that prohibits the flame from further burning the surface, and hence, no development of new peaks is observed after 100 s of sample ignition. Additionally, both the HRR and THR decreased with the addition of NaOH into chemically crosslinked hydrogel system and LNPs. The trends in HRR curves concur with those of THR curves. The peak heat release rates were 201.3, 161.3 and 90.3 kW m^{-2}, and the total heat released was 3.86, 3.03 and 1.56 MJ m^{-2} for PX3B0.4, PX3B0.4N2 and PX3B0.4N2L20 samples, respectively (**Table 4.7**). The HRR and THR values observed for PX3B0.4N2L20 were much lower than the reported values of other flame retardant coating. Zhao et. al [4] reported peak HRR 269 .44 kW m^{-2} and THR value of 10.25 MJ m^{-2} for PVA –15wt% phytic acid hydrogel coated on wood samples. Kundu et al. [57] reported peak HRR of 206 kW m^{-2} for chitosan and alginate based nanocoating for

polyamide 66 fabric. Lin et al. [58] have synthesized PVA–ammonium polyphosphate composite doped with montmorillonite (MMT) clay, which drastically decreased the HRR from 576 to 156 kW m^{-2} with 15% MMT loading. Lui et al [59] have reported halogen free PVA–triphenyl phosphate (TPP) composite with peak HRR of 299 kW m^{-2}.

Table 4.7 Results of cone calorimeter tests for hydrogel samples

Sample	PHRR (kW m^{-2})	THR (MJ m^{-2})
PX3B0.4	201.3±12	3.86±2
PX3B0.4N2	161.3±17	3.03±3
PX3B0.4N2L20	90.3 ±10	1.56±4

4.4 Conclusions

This study has reported the synthesis, characterization, and testing of hydrogels comprising a biodegradable PVA matrix with two biomaterials additives, viz. xanthan gum and lignin nanoparticles. Different hydrogels synthesized in this study with combinations of the components, viz. PX3, PX3B0.4N2, PX3B0.4N2L5 and PX3B0.4N2L20, revealed enhanced structural and fire retardant properties. PX3B0.4N2 hydrogel showed better rheological properties as compared to PX3B0.4 hydrogels, which confirms a stronger gelation network induced in presence of NaOH. Addition of lignin nanoparticles facilitated tuning of the viscoelastic properties of the hydrogels. Higher concentration of lignin (20% v/v) imparted viscous nature to the hydrogel whereas a lower concentration of lignin (5% v/v) imparts elasticity to the hydrogels. These traits allowed the hydrogels to accommodate around 96% of water in their network structure. Sequentially, the water retention ability of the hydrogels also improved. However, a more compact structure of PXB0.4N2L20 resulted in low water absorption and retention. Additionally, presence of lignin nanoparticles

improved the char formation of the hydrogels, which helped in enhancing fire retardancy. The hydrogel coated cotton cloth demonstrated delayed burning process. LOI for cotton cloth improved from 20% to 39% after coating of PX3B0.4N2L20 hydrogel. The thermal degradation temperature of the formulated hydrogels was around 280 to 300 ºC, which is higher than the actual operating temperature (85º to 285 ºC) measured during the fire operations. The LOI, vertical burning, TGA, and kinetic analysis results were in accordance with the CCT's HRR and THR curves. Thus, the present study has demonstrated the potential of eco-friendly PVA-based hydrogels as effective fire retardant coatings.

References

(1) Xue, Y.; Yang, F.; Li, J.; Zuo, X.; Pan, B.; Li, M.; Quinto, L.; Mehta, J.; Stiefel, L.; Kimmey, C.; Eshed, Y.; Zussman, E.; Simon, M.; Rafailovich, M. Synthesis of an Effective Flame-Retardant Hydrogel for Skin Protection Using Xanthan Gum and Resorcinol Bis(Diphenyl Phosphate)-Coated Starch. *Biomacromolecules* **2021**, *22* (11), 4535–4543. https://doi.org/10.1021/acs.biomac.1c00804.

(2) Yu, Z.; Liu, J.; He, H.; Ma, S.; Yao, J. Flame-Retardant PNIPAAm/Sodium Alginate/Polyvinyl Alcohol Hydrogels Used for Fire-Fighting Application: Preparation and Characteristic Evaluations. *Carbohydr. Polym.* **2021**, *255* (December 2020), 117485. https://doi.org/10.1016/j.carbpol.2020.117485.

(3) Ingtipi, K.; Boro, U.; Moholkar, V. S. Lignin in Nanocomposite Hydrogels. *Micro Nanolignin Aqueous Dispersions Polym. Interact. Prop. Appl.* **2022**, 459–484. https://doi.org/10.1016/B978-0-12-823702-1.00002-5.

(4) Zhao, X.; Liang, Z.; Huang, Y.; Hai, Y.; Zhong, X.; Xiao, S.; Jiang, S. Influence of Phytic Acid on Flame Retardancy and Adhesion Performance Enhancement of Poly (Vinyl Alcohol) Hydrogel Coating to Wood Substrate. *Prog. Org. Coatings* **2021**, *161*, 106453. https://doi.org/10.1016/J.PORGCOAT.2021.106453.

(5) Ye, Q. Super-Absorbent Polymer Based Fire Retardant, Johns Hopkins

University, 2021.

(6) Asako, Y.; Otaka, T.; Yamaguchi, Y. Fire Resistance Characteristics of Materials with Polymer Gels Which Absorb Aqueous Solution of Calcium Chloride. *Numer. Heat Transf. Part A Appl.* **2004**, *45* (1), 49–66. https://doi.org/10.1080/10407780490267 38.

(7) Cao, C. F.; Yu, B.; Guo, B. F.; Hu, W. J.; Sun, F. N.; Zhang, Z. H.; Li, S. N.; Wu, W.; Tang, L. C.; Song, P.; Wang, H. Bio-Inspired, Sustainable and Mechanically Robust Graphene Oxide-Based Hybrid Networks for Efficient Fire Protection and Warning. *Chem. Eng. J.* **2022**, *439*, 134516. https://doi.org/10.1016/J.CEJ.2022.134516.

(8) Cao, C. F.; Yu, B.; Chen, Z. Y.; Qu, Y. X.; Li, Y. T.; Shi, Y. Q.; Ma, Z. W.; Sun, F. N.; Pan, Q. H.; Tang, L. C.; Song, P.; Wang, H. Fire Intumescent, High-Temperature Resistant, Mechanically Flexible Graphene Oxide Network for Exceptional Fire Shielding and Ultra-Fast Fire Warning. *Nano-Micro Lett.* **2022**, *14* (1), 1–18. https://doi.org/10.1007/s40820-022-00837-1.

(9) Li, S.; Zhou, G.; Wang, Y.; Jing, B.; Qu, Y. Synthesis and Characteristics of Fire Extinguishing Gel with High Water Absorption for Coal Mines. *Process Saf. Environ. Prot.* **2019**, *125*, 207–218. https://doi.org/10.1016/J.PSEP.2019.03.022.

(10) Liu, J.; Xiao, C. Fire-Retardant Multilayer Assembled on Polyester Fabric from Water-Soluble Chitosan, Sodium Alginate and Divalent Metal Ion. *Int. J. Biol. Macromol.* **2018**, *119*, 1083–1089. https://doi.org/10.1016/J.IJBIOMAC.2018.08.043.

(11) Illeperuma, W. R. K.; Rothemund, P.; Suo, Z.; Vlassak, J. J. Fire-Resistant Hydrogel-Fabric Laminates: A Simple Concept That May Save Lives. *ACS Appl. Mater. Interfaces* **2016**, *8* (3), 2071–2077. https://doi.org/10.1021/acsami.5b10538.

(12) Liu, X.; Xiao, C. Formation of Self-Healable Fire-Retardant Water-Soluble Chitosan/Chemically Cross-Linked Polyvinyl Alcohol/Cu(II) Gel. *Environ. Technol. Innov.* **2020**, *20*, 101087. https://doi.org/10.1016/J.ETI.2020.101087.

(13) Ye, T.; Zou, Y.; Xu, W.; Zhan, T.; Sun, J.; Xia, Y.; Zhang, X.; Yang, D. Poorly-Crystallized Poly(Vinyl Alcohol)/Carrageenan Matrix: Highly Ionic Conductive and Flame-Retardant Gel Polymer Electrolytes for Safe and Flexible Solid-State Supercapacitors. *J. Power Sources* **2020**, *475*, 228688.

https://doi.org/10.1016/J.JPOWSOUR.2020.228688.

(14) Yan, T.; Zou, Y.; Zhang, X.; Li, D.; Guo, X.; Yang, D. Hydrogen Bond Interpenetrated Agarose/PVA Network: A Highly Ionic Conductive and Flame-Retardant Gel Polymer Electrolyte. *ACS Appl. Mater. Interfaces* **2021**, *13* (8), 9856–9864. https://doi.org/https://doi.org/10.1021/acsami.0c20702.

(15) Liu, J.; Yu, Z.; He, H.; Wang, Y.; Zhao, Y. A Novel Flame-Retardant Composite Material Based on Calcium Alginate/Poly (Vinyl Alcohol)/Graphite Hydrogel: Thermal Kinetics, Combustion Behavior and Thermal Insulation Performance. *Cellulose* **2021**, *28* (13), 8751–8769. https://doi.org/https://doi.org/10.1007/s10570-021-04047-7.

(16) Banerjee, H.; Sivaperuman Kalairaj, M.; Chang, T. H.; Fu, F.; Chen, P. Y.; Ren, H. Highly Stretchable Flame-Retardant Skin for Soft Robotics with Hydrogel-Montmorillonite-Based Translucent Matrix. *Soft Robot.* **2022**, *9* (1), 98–118. https://doi.org/https://doi.org/10.1089/soro.2020.0003.

(17) Larrañeta, E.; Imízcoz, M.; Toh, J. X.; Irwin, N. J.; Ripolin, A.; Perminova, A.; Domínguez-Robles, J.; Rodríguez, A.; Donnelly, R. F. Synthesis and Characterization of Lignin Hydrogels for Potential Applications as Drug Eluting Antimicrobial Coatings for Medical Materials. *ACS Sustain. Chem. Eng.* **2018**, *6* (7), 9037–9046. https://doi.org/https://doi.org/10.1021/acssuschemeng.8b01371.

(18) Shalviri, A.; Liu, Q.; Abdekhodaie, M. J.; Wu, X. Y. Novel Modified Starch–Xanthan Gum Hydrogels for Controlled Drug Delivery: Synthesis and Characterization. *Carbohydr. Polym.* **2010**, *79* (4), 898–907. https://doi.org/10.1016/J.CARBPOL.2009.10.016.

(19) Leone, G.; Consumi, M.; Lamponi, S.; Bonechi, C.; Tamasi, G.; Donati, A.; Rossi, C.; Magnani, A. Hybrid PVA-Xanthan Gum Hydrogels as Nucleus Pulposus Substitutes. *Int. J. Polym. Mater. Polym. Biomater.* **2018**, *68* (12), 681–690. https://doi.org/10.1080/00914037.2018.1482468.

(20) Zhang, Q.; Hu, X. M.; Wu, M. Y.; Wang, M. M.; Zhao, Y. Y.; Li, T. T. Synthesis and Performance Characterization of Poly(Vinyl Alcohol)-Xanthan Gum Composite Hydrogel. *React. Funct. Polym.* **2019**, *136* (December 2018), 34–43. https://doi.org/10.1016/j.reactfunctpolym.2019.01.002.

(21) Abu Elella, M. H.; Goda, E. S.; Gab-Allah, M. A.; Hong, S. E.; Pandit, B.; Lee, S.; Gamal, H.; Rehman, A. U.; Yoon, K. R. Xanthan Gum-Derived Materials

for Applications in Environment and Eco-Friendly Materials: A Review. *J. Environ. Chem. Eng.* **2021**, *9* (1), 104702. https://doi.org/10.1016/J.JECE.2020.104702.

(22) Mandlekar, N.; Cayla, A.; Rault, F.; Giraud, S.; Salaün, F.; Guan, J. Valorization of Industrial Lignin as Biobased Carbon Source in Fire Retardant System for Polyamide 11 Blends. *Polym. 2019, Vol. 11, Page 180* **2019**, *11* (1), 180. https://doi.org/10.3390/POLYM11010180.

(23) Shukla, A.; Sharma, V.; Basak, S.; Ali, S. W. Sodium Lignin Sulfonate: A Bio-Macromolecule for Making Fire Retardant Cotton Fabric. *Cellulose* **2019**, *26* (13–14), 8191–8208. https://doi.org/DOI:10.1007/s10570-019-02668-7.

(24) Yang, H.; Shi, B.; Xue, Y.; Ma, Z.; Liu, L. L.; Liu, L. L.; Yu, Y.; Zhang, Z.; Annamalai, P. K.; Song, P. Molecularly Engineered Lignin-Derived Additives Enable Fire-Retardant, UV-Shielding, and Mechanically Strong Polylactide Biocomposites. *Biomacromolecules* **2021**, *22* (4), 1432–1444. https://doi.org/https://doi.org/10.1021/acs.biomac.0c01656.

(25) Zhang, Z.; Terrasson, V.; Guénin, E. Lignin Nanoparticles and Their Nanocomposites. *Nanomater. 2021, Vol. 11, Page 1336* **2021**, *11* (5), 1336. https://doi.org/https://doi.org/10.3390/nano11051336.

(26) He, T.; Chen, F.; Zhu, W.; Yan, N. Functionalized Lignin Nanoparticles for Producing Mechanically Strong and Tough Flame-Retardant Polyurethane Elastomers. *Int. J. Biol. Macromol.* **2022**, *209*, 1339–1351. https://doi.org/https://doi.org/10.1016/j.ijbiomac.2022.04.089.

(27) Chollet, B.; Lopez-Cuesta, J. M.; Laoutid, F.; Ferry, L. Lignin Nanoparticles as a Promising Way for Enhancing Lignin Flame Retardant Effect in Polylactide. *Materials (Basel).* **2019**, *12* (13). https://doi.org/10.3390/ma12132132.

(28) Ingtipi, K.; Moholkar, V. S. Sonochemically Synthesized Lignin Nanoparticles and Its Application in the Development of Nanocomposite Hydrogel. *Mater. Today Proc.* **2019**, *17*, 362–370. https://doi.org/10.1016/j.matpr.2019.06.443.

(29) Ben Ammar, N. E.; Saied, T. T.; Barbouche, M.; Hosni, F.; Hamzaoui, A. H.; Şen, M.; Elhouda, N.; Ammar, B.; Saied, T. T. A Comparative Study between Three Different Methods of Hydrogel Network Characterization: Effect of Composition on the Crosslinking Properties Using Sol–Gel, Rheological and Mechanical Analyses. *Polym. Bull.* **2018**, *75.9* (September), 3825–3841. https://doi.org/10.1007/s00289-017-2239-0.

(30) Richbourg, N. R.; Peppas, N. A. The Swollen Polymer Network Hypothesis: Quantitative Models of Hydrogel Swelling, Stiffness, and Solute Transport. *Prog. Polym. Sci.* **2020**, *105*, 101243. https://doi.org/10.1016/j.progpolymsci.2020.101243.

(31) Sen, M.; Yakar, A.; Güven, O. Determination of Average Molecular Weight between Cross-Links ($\bar{M}(c)$) from Swelling Behaviours of Diprotic Acid-Containing Hydrogels. *Polymer (Guildf).* **1999**, *40* (11), 2969–2974. https://doi.org/10.1016/S0032-3861(98)00251-1.

(32) Gan, Y.; Li, P.; Wang, L.; Mo, X.; Song, L.; Xu, Y.; Zhao, C.; Ouyang, B.; Tu, B.; Luo, L.; Zhu, L.; Dong, S.; Li, F.; Zhou, Q. An Interpenetrating Network-Strengthened and Toughened Hydrogel That Supports Cell-Based Nucleus Pulposus Regeneration. *Biomaterials* **2017**, *136*, 12–28. https://doi.org/10.1016/j.biomaterials.2017.05.017.

(33) Sadeghifar, H.; Wells, T.; Le, R. K.; Sadeghifar, F.; Yuan, J. S.; Jonas Ragauskas, A. Fractionation of Organosolv Lignin Using Acetone:Water and Properties of the Obtained Fractions. *ACS Sustain. Chem. Eng.* **2017**, *5* (1), 580–587. https://doi.org/https://doi.org/10.1021/acssuschemeng.6b01955.

(34) Li, X.; Shen, J.; Wang, B.; Feng, X.; Mao, Z.; Sui, X. Acetone/Water Cosolvent Approach to Lignin Nanoparticles with Controllable Size and Their Applications for Pickering Emulsions. *ACS Sustain. Chem. Eng.* **2021**, *9* (15), 5470–5480. https://doi.org/10.1021/acssuschemeng.1c01021.

(35) Sipponen, M. H.; Henn, A.; Penttilä, P.; Österberg, M. Lignin-Fatty Acid Hybrid Nanocapsules for Scalable Thermal Energy Storage in Phase-Change Materials. *Chem. Eng. J.* **2020**, *393*, 124711. https://doi.org/10.1016/J.CEJ.2020.124711.

(36) Zou, T.; Nonappa, N.; Khavani, M.; Vuorte, M.; Penttilä, P.; Zitting, A.; Valle-Delgado, J. J.; Elert, A. M.; Silbernagl, D.; Balakshin, M.; Sammalkorpi, M.; Österberg, M. Experimental and Simulation Study of the Solvent Effects on the Intrinsic Properties of Spherical Lignin Nanoparticles. *J. Phys. Chem. B* **2021**, *125* (44), 12315–12328. https://doi.org/10.1021/acs.jpcb.1c05319.

(37) Myint, A. A.; Lee, H. W.; Seo, B.; Son, W. S.; Yoon, J.; Yoon, T. J.; Park, H. J.; Yu, J.; Yoon, J.; Lee, Y. W. One Pot Synthesis of Environmentally Friendly Lignin Nanoparticles with Compressed Liquid Carbon Dioxide as an Antisolvent. *Green Chem.* **2016**, *18* (7), 2129–2146.

https://doi.org/10.1039/C5GC02398J.

(38) Choudhury, B. J.; Muigai, H. H.; Kalita, P.; Moholkar, V. S. Biomass Blend Derived Porous Carbon for Aqueous Supercapacitors with Commercial-Level Mass Loadings and Enhanced Energy Density in Redox-Active Electrolyte. *Appl. Surf. Sci.* **2022**, *601*, 154202. https://doi.org/10.1016/J.APSUSC.2022.154202.

(39) Zhang, Y.; Zhu, Y.; Jiao, M.; Zhang, J.; Chen, M.; Wang, C. Synthesis of Size-Controllable Lignin-Based Nanosperes and Its Application in Electrical Double Layer Capacitors. *ChemistrySelect* **2020**, *5* (27), 8265–8273. https://doi.org/10.1002/SLCT.202001552.

(40) Qian, Y.; Deng, Y.; Qiu, X.; Li, H.; Yang, D. Formation of Uniform Colloidal Spheres from Lignin, a Renewable Resource Recovered from Pulping Spent Liquor. *Green Chem.* **2014**, *16* (4), 2156–2163. https://doi.org/10.1039/c3gc42131g.

(41) Piccinino, D.; Capecchi, E.; Delfino, I.; Crucianelli, M.; Conte, N.; Avitabile, D.; Saladino, R. Green and Scalable Preparation of Colloidal Suspension of Lignin Nanoparticles and Its Application in Eco-Friendly Sunscreen Formulations. *ACS Omega* **2021**, *6* (33), 21444–21456. https://doi.org/10.1021/acsomega.1c02268.

(42) Brunchi, C. E.; Bercea, M.; Morariu, S.; Avadanei, M. Investigations on the Interactions between Xanthan Gum and Poly(Vinyl Alcohol) in Solid State and Aqueous Solutions. *Eur. Polym. J.* **2016**, *84*, 161–172. https://doi.org/10.1016/j.eurpolymj.2016.09.006.

(43) Lim, M.; Kwon, H.; Kim, D.; Seo, J.; Han, H.; Khan, S. B. Highly-Enhanced Water Resistant and Oxygen Barrier Properties of Cross-Linked Poly(Vinyl Alcohol) Hybrid Films for Packaging Applications. *Prog. Org. Coatings* **2015**, *85*, 68–75. https://doi.org/10.1016/j.porgcoat.2015.03.005.

(44) Al-Emam, E.; Soenen, H.; Caen, J.; Janssens, K. Characterization of Polyvinyl Alcohol-Borax/Agarose (PVA-B/AG) Double Network Hydrogel Utilized for the Cleaning of Works of Art. *Herit. Sci.* **2020**, *8* (1), 1–14. https://doi.org/10.1186/s40494-020-00447-3.

(45) Han, J.; Wang, H.; Yue, Y.; Mei, C.; Chen, J.; Huang, C.; Wu, Q.; Xu, X. A Self-Healable and Highly Flexible Supercapacitor Integrated by Dynamically Cross-Linked Electro-Conductive Hydrogels Based on Nanocellulose-

Templated Carbon Nanotubes Embedded in a Viscoelastic Polymer Network. *Carbon N. Y.* **2019**, *149*, 1–18. https://doi.org/10.1016/j.carbon.2019.04.029.

(46) Parwani, L.; Bhatnagar, M.; Bhatnagar, A.; Sharma, V. V.; Sharma, V. V. Gum Acacia-PVA Hydrogel Blends for Wound Healing. *Vegetos 2019 321* **2019**, *32* (1), 78–91. https://doi.org/10.1007/S42535-019-00009-4.

(47) Wu, L.; Huang, S.; Zheng, J.; Qiu, Z.; Lin, X.; Qin, Y. Synthesis and Characterization of Biomass Lignin-Based PVA Super-Absorbent Hydrogel. *Int. J. Biol. Macromol.* **2019**, *140*, 538–545. https://doi.org/10.1016/J.IJBIOMAC.2019.08.142.

(48) Bejenariu, A.; Popa, M.; Dulong, V.; Picton, L.; Le Cerf, D. Trisodium Trimetaphosphate Crosslinked Xanthan Networks: Synthesis, Swelling, Loading and Releasing Behaviour. *Polym. Bull.* **2009**, *62* (4), 525–538. https://doi.org/10.1007/S00289-008-0033-8.

(49) Zhang, Q.; Hu, X. M.; Wu, M. Y.; Wang, M. M.; Zhao, Y. Y.; Li, T. T. Synthesis and Performance Characterization of Poly(Vinyl Alcohol)-Xanthan Gum Composite Hydrogel. *React. Funct. Polym.* **2019**, *136*, 34–43. https://doi.org/10.1016/J.REACTFUNCTPOLYM.2019.01.002.

(50) Cheng, Z.; De Gracia, K.; Schiraldi, D. A. Sustainable, Low Flammability, Mechanically-Strong Poly(Vinyl Alcohol) Aerogels. *Polymers (Basel).* **2018**, *10* (10). https://doi.org/10.3390/POLYM10101102.

(51) Freire, T. F.; Quinaz, T.; Fertuzinhos, A.; Quyền, N. T.; de Moura, M. F. S. M.; Martins, M.; Zille, A.; Dourado, N. Thermal, Mechanical and Chemical Analysis of Poly(Vinyl Alcohol) Multifilament and Braided Yarns. *Polymers (Basel).* **2021**, *13* (21). https://doi.org/10.3390/POLYM13213644.

(52) da Silva, J. A.; Cardoso, L. G.; de Jesus Assis, D.; Gomes, G. V. P.; Oliveira, M. B. P. P.; de Souza, C. O.; Druzian, J. I. Xanthan Gum Production by Xanthomonas Campestris Pv. Campestris IBSBF 1866 and 1867 from Lignocellulosic Agroindustrial Wastes. *Appl. Biochem. Biotechnol.* **2018**, *186* (3), 750–763. https://doi.org/10.1007/S12010-018-2765-8.

(53) Li, J.; Qiao, Y.; Zong, P.; Wang, C.; Tian, Y.; Qin, S. Thermogravimetric Analysis and Isoconversional Kinetic Study of Biomass Pyrolysis Derived from Land, Coastal Zone, and Marine. *Energy and Fuels* **2019**, *33* (4), 3299–3310. https://doi.org/10.1021/ACS.ENERGYFUELS.9B00331.

(54) Muigai, H. H.; Choudhury, B. J.; Kalita, P.; Moholkar, V. S. Co–Pyrolysis of

Biomass Blends: Characterization, Kinetic and Thermodynamic Analysis. *Biomass and Bioenergy* **2020**, *143*, 105839. https://doi.org/10.1016/J.BIOMBIOE.2020.105839.

(55) Zhang, Z.; Li, X.; Ma, Z.; Ning, H.; Zhang, D.; Wang, Y. A Facile and Green Strategy to Simultaneously Enhance the Flame Retardant and Mechanical Properties of Poly(Vinyl Alcohol) by Introduction of a Bio-Based Polyelectrolyte Complex Formed by Chitosan and Phytic Acid. *Dalt. Trans.* **2020**, *49* (32), 11226–11237. https://doi.org/10.1039/D0DT02019B.

(56) Lindholm, J.; Brink, A.; Hupa, M. CONE CALORIMETER-A TOOL FOR MEASURING HEAT RELEASE RATE.

(57) Kumar Kundu, C.; Wang, W.; Zhou, S.; Wang, X.; Sheng, H.; Pan, Y.; Song, L.; Hu, Y. A Green Approach to Constructing Multilayered Nanocoating for Flame Retardant Treatment of Polyamide 66 Fabric from Chitosan and Sodium Alginate. *Carbohydr. Polym.* **2017**, *166*, 131–138. https://doi.org/10.1016/J.CARBPOL.2017.02.084.

(58) Lin, J. S.; Liu, Y.; Wang, D. Y.; Qin, Q.; Wang, Y. Z. Poly(Vinyl Alcohol)/Ammonium Polyphosphate Systems Improved Simultaneously Both Fire Retardancy and Mechanical Properties by Montmorillonite. *Ind. Eng. Chem. Res.* **2011**, *50* (17), 9998–10005. https://doi.org/10.1021/IE100674S.

(59) Liu, P.; Chen, W.; Liu, Y.; Bai, S.; Wang, Q. Thermal Melt Processing to Prepare Halogen-Free Flame Retardant Poly(Vinyl Alcohol). *Polym. Degrad. Stab.* **2014**, *109*, 261–269. https://doi.org/10.1016/J.POLYMDEGRADSTAB.2014.07.021.

भारतीय प्रौद्योगिकी संस्थान गुवाहाटी
Indian Institute of Technology Guwahati

CHAPTER 5

KAOLIN EMBEDDED CELLULOSE HYDROGEL WITH TUNABLE PROPERTIES AS GREEN FIRE RETARDANT

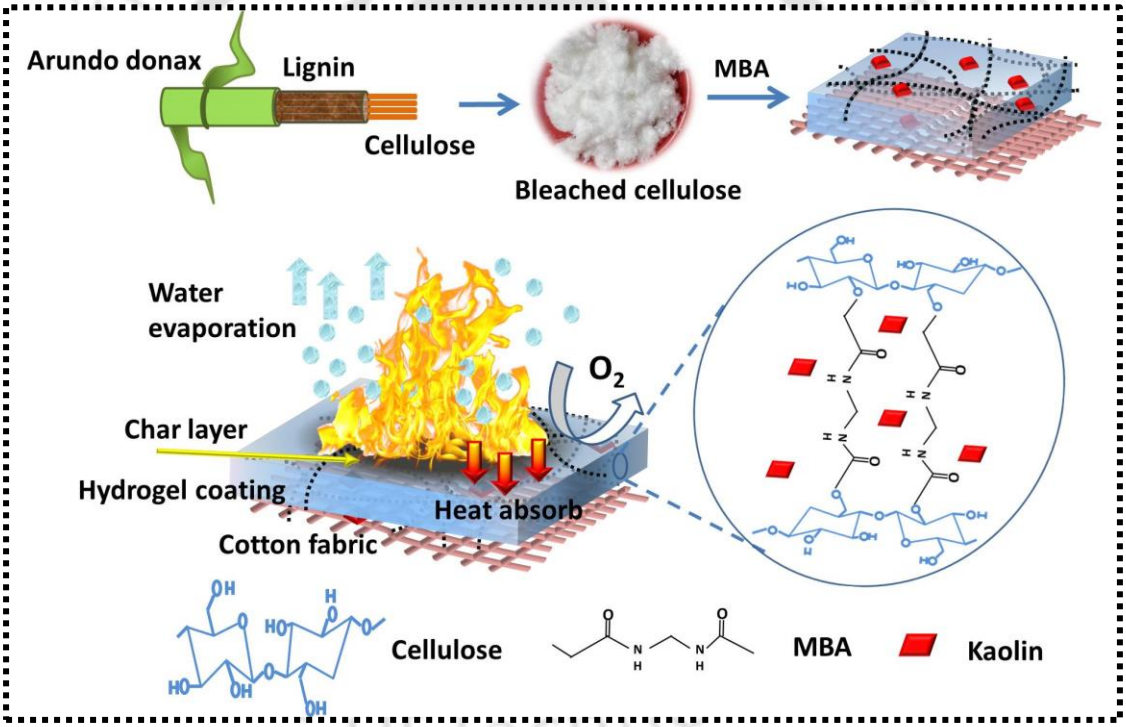

CHAPTER 5

KAOLIN EMBEDDED CELLULOSE HYDROGEL WITH TUNABLE PROPERTIES AS GREEN FIRE RETARDANT

5.1 Introduction

Every year, devastating wildfires and fire accidents in residential and industrial sectors leave a trail of destruction worldwide, resulting in enormous loss of life and extensive property damage. In addition, firefighters frequently sustain severe burns and wounds during rescue operations[1]. Therefore, extensive research has been focused on developing sustainable fireproof building materials and coatings. Considerable research efforts are also dedicated to the development of efficient firefighting gears, such as fire-resistant suits and blankets[2–5]). The conventional flame retardant coatings contain halogenated compounds, viz. polybromodiphenylether, tetrabromobisphenol A, tetrabromophthalic anhydride, and hexabromocyclododecane [6]. As a result, these flame retardants are highly toxic, spread environmental contamination, and cause adverse health issues to animals and humans. Recent research in fire retardant synthesis focuses on the use of halogen-free, green (bio-based), and sustainable materials. Hydrogels have emerged as modern, efficient coating materials with superior fire retardancy properties[7–9]). Hydrogels can absorb and retain much water in their crosslinked network[10,11]. This water essentially acts as in situ extinguisher during fire breakouts and reduces the surface temperature, which impedes the spread of fire. Also, a protective char layer is formed on the hydrogel surface after combustion, shielding the inner layers of hydrogel from further

burning[12]. In a recent study, PNIPAAm–sodium alginate–PVA-based triple network hydrogel lamination was developed to improve the fire resistance of cotton fabrics[13]. The thermal degradation temperature of these hydrogels was above 300°C, which is much higher than the actual operating temperatures during firefighting operations. Another study reported that xylan and sodium carboxymethylcellulose-based temperature-sensitive hydrogels effectively suppressed the spontaneous combustion of coal[14]. The viscosity of these gels increases with the temperature rise, forming a robust protective layer covering the coal particles and effectively isolating the coal from oxygen. Similarly, Poly acrylic acid–sodium alginate–tannic acid-based self-adhesive hydrogel was prepared to prevent the spontaneous combustion of coal[15]. Polyacrylic–polydopamine dual crosslinked hydrogel coating was also developed for fireproofing polyurethane foam[16]. This hydrogel was mechanically tough, possessed the self-quenching ability, exhibited delayed ignition, and reduced the heat release rate (HRR) and total smoke production (TSP). Another study developed a tough gelatin–montmorillonite (MMT) hydrogel as a fire retardant for hot work on oil pipelines[17].

In recent years, cellulose-based hydrogels have been investigated for applications in biomedical fields such as drug delivery, tissue engineering, wound healing, and other healthcare and hygienic products. These hydrogels are biodegradable, non-toxic, and highly biocompatible. Cellulose can also be applied in fire retardant hydrogels as it forms char after combustion in the solid phase. At low temperatures, cellulose initially degrades to form anhydrocellulose, and with the temperature rise, the rest of the cellulose gradually converts to tar and finally forms char. This char layer creates a barrier that hinders heat transfer and insulates the surface underneath, slowing down the pyrolysis process[18]. Fire retardancy of hydrogels can be enhanced by

incorporating various fillers, such as clays bentonite[19], kaolin[20], and MMT[21–23], silica[24], potassium carbonate[25], carbon nanotubes and graphene oxide. Also, cellulose can be blended with various biopolymers to perform as a fire retardant efficiently. Another study employed layer-by-layer chitosan and sodium hexametaphosphate nanocoating assembly to impart fame retardancy to cellulosic gel beads[26]. An amalgamation of nanocoating and cellulosic gel produced sufficient char, which extensively inhibited fire. In another study, a self-extinguishing phosphorus-modified methylcellulose and silica hybrid hydrogels as a fire retardant was prepared[27]. These hydrogels exhibited shorter extinguishing times than water and raw methylcellulose concoctions.

Hydrogels formulated from cellulose display excellent mechanical properties. However, the synthesis of cellulose-based hydrogels has certain bottlenecks. Cellulose comprises abundant hydroxyl groups along its rigid backbone, leading to extensive aggregation and poor solubility in water and other commonly used solvents. Hence, finding a suitable solvent for dissolution and further processing is difficult. The most widely used solvents are NaOH–urea[2829], LiOH–urea[30], NaOH–thiourea[30], and ionic liquids[31]. After dissolution, the regeneration of cellulose hydrogel requires a physical or chemical crosslinking process. The most commonly used physical mode of crosslinking is freeze-thaw[32], photocrosslinking[33], and radiation-induced crosslinking[34]. Conventionally used chemical crosslinkers are citric acid[35], glutaraldehyde[36], and epichlorohydrin[37]. Most of the aforementioned crosslinking methods are arduous, expensive, and time-consuming. Moreover, certain chemical crosslinkers are hazardous. Hence, developing a simple and efficient cross-linking method is always desired. Methylenebisacrylamide (MBA) has been effectively utilized in regeneration of cellulose from precooled alkali–urea solvent. Geng (2018)

reported a simple route for developing transparent and high swelling cellulose hydrogel using MBA[38]. Similarly, another study demonstrated the formulation of MBA-induced chemically crosslinked cellulose hydrogel in cold LiOH–urea solvent[39]. MBA induces crosslinking via basic Michael addition reaction amid double bond of the crosslinker and hydroxyl groups of cellulose.

This study reports a simple route for regenerating cellulose hydrogel on cotton fabric from a precooled NaOH–urea solvent. We have adopted a dual crosslinking method for hydrogel synthesis. The initial crosslinking was achieved via MBA-induced Michael addition reaction, and the secondary crosslinking was achieved by thermal treatment. Kaolin was infused in the hydrogel matrix. The hydrogels have been characterized for physical and chemical properties. In addition, the influence of kaolin and MBA on these properties has been examined. Finally, the flame retardant characteristics of the hydrogels have been determined using limiting oxygen index (LOI), cone calorimeter test (CCT), vertical flammability test (VFT), and open fire test (OFT). Herein, we envisaged converting low-cost and green materials (kaolin and cellulose) into high-performing fire retardants. Kaolin, being clay, inherently possesses high thermal resistance. Hence, incorporating kaolin amplifies the fire retardancy of the cellulose hydrogel, which is mainly attributed to char formation. The cellulose hydrogels tend to swell and retain water in their matrix. We contemplate that the synergistic effect of encapsulated water in the hydrogel matrix and kaolin would delay the ignition of the flammable material. It is also contemplated that the hydrogel would produce a protective char layer upon ignition, further preventing the underlying material from the ignition. Thus, our methodology of adding clay particles (kaolin) in biopolymer hydrogel introduces a conceptual framework for producing high-performance green fire retardant coatings.

5.2 Experimental section

5.2.1 Synthesis of cellulose-kaolin hydrogel

Cellulose (α cellulose content of 95%, DP 502, described in **Figure 2.7** chapter 2 and **Table A2.1**, Appendix 2) was extracted from perennial grass, *Arundo donax*[40]. The cellulose extraction procedure is described in chapter 2. NaOH pellets were purchased from Emplura. Urea and sodium chlorite was procured from Himedia, and methylene bisacrylamide and kaolin was purchased from Sigma Aldrich. Cellulose was added to precooled (–20 °C) NaOH/urea solution (13:7 ratio). The resulting solution was kept at –20 °C to dissolve the cellulose and obtain 3% w/v cellulose solutions. The required amount of kaolin was added to this solution, followed by stirring for 6 h at 80 °C to obtain a kaolin cellulose solution. Kaolin quantity in solution was varied as 0.5, 1, and 2% w/v. Lastly, MBA was added, and the solution was stirred for 6 h. The resultant solution (CMK) was poured into a petri dish and left for 24 h in an ambient atmosphere (temperature = 25±2 °C, relative humidity = 45–55%) for crosslinking. The sample obtained after 24 h was heated at 60 °C in a hot air oven for 1 h to obtain CMK hydrogel. The cellulose to MBA weight ratios (C:M) were maintained at 1:1 and 1:2, respectively. The obtained hydrogels were soaked in distilled water to remove the unreacted components. The compositions of the hydrogels formulated using the above procedure is listed in **Table 5.1**.

For preparing hydrogel-coated cotton fabric, cotton cloth was dipped in CMK solution and left in ambient conditions for 24 h (temperature = 25±2 °C, humidity = 55 %) for crosslinking and further dried at 60 °C for 1 h (**Figure 5.1**). Finally, the samples were washed with DI water (pH 6) to remove all the unreacted components (**Figure A2.1, Appendix 2**). The various compositions of the formulated hydrogels are represented in Table 1. All analyses of the hydrogel samples were performed in

triplicate.

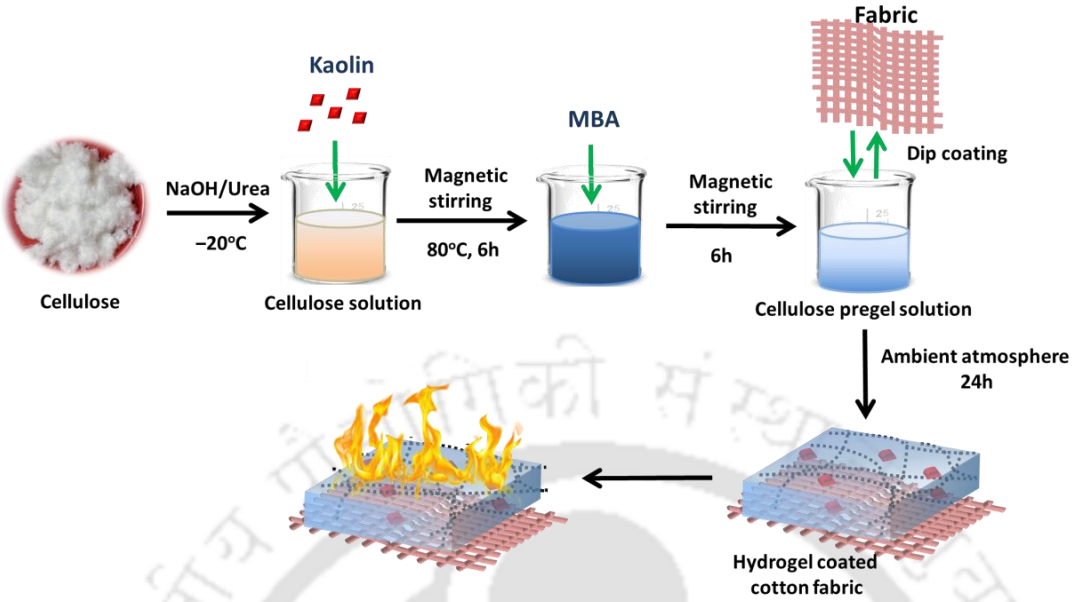

Figure 5.1 Synthesis process of kaolin cellulose hydrogel coating on cotton fabric

Table 5.1 Composition of formulated hydrogels

Sample	Cellulose (C) : MBA (M)	Kaolin (K, w/v %)
CM1	1:1	-
CM2	1:2	-
CM1K0.5	1:1	0.5
CM2K0.5	1:2	0.5
CM1K1	1:1	1
CM2K1	1:2	1
CM1K2	1:1	2
CM2K2	1:2	2

5.2.2 Structural characterization and adhesion strength of composite hydrogels

To gain insights into the interactions between various components of the hydrogels XRD, FTIR, and FE-SEM analyses were performed. X-ray diffraction (XRD) patterns of kaolin and cellulose kaolin composite were obtained using Rigaku (RINT 2500

TTRAX-III) diffractometer equipped with Cu–Kα radiation (λ = 1.5406 Å) with nickel filter. Scans were recorded in the 2θ range of 10° to 80°. Molecular interactions of the formulated hydrogels were characterized by Fourier Transform Infrared (FTIR) spectroscopy [Spectrum Two, PerkinElmer (USA)] over the wavenumber range of 4000–400 cm^{-1}. The structural and surface morphological analysis of freeze-dried hydrogel samples were carried out using Field-Emission Transmission Electron Microscope (FE-TEM) [2100F, JEOL (Japan)]. The adhesion strength between the hydrogel and cotton fabric was evaluated by performing a lap shear adhesion test according to ASTM D3163 using a universal testing machine (UTM) [Z005TNProline, ZwickRoell]. The hydrogels were coated on cotton fabrics (100 mm × 20 mm) and bonded together maintaining a coating thickness of 0.7–0.8 mm, and dried in the ambient atmosphere (25±2ºC, humidity 55%). The test sample was placed in the grips of the UTM and pulled apart at the rate of 5mm/min.The adhesion strength was calculated as follows [41,42]:

$$Adhesive\ strength = \frac{\max imum\ force\ applied}{overlap\ area} = \frac{F_{\max}}{l_o \times w} \qquad (5.1)$$

where, F_{max} is the maximum force required for detachment of the joined hydrogel coated fabric, l_o is the length and w is the width of the of the bonded section of the fabrics sample.

Rheological studies

The crosslinking of hydrogel samples was confirmed by measuring the rheological properties (elastic modulus, G' and viscous modulus, G'') via rheometer (MCR 301, Anton Paar). A 50 mm diameter parallel plate geometry was used, keeping the gap setting at 1 mm. Oscillation shear experiments were used to investigate the viscoelastic characteristics of hydrogel over a wide range of strain and frequency. Amplitude sweep test at a constant frequency (1 Hz) and varying strain of 0.01–100 % was performed to determine the linear viscoelastic region (LVR). Furthermore, the frequency sweep test was performed over the range of 0.01–100 Hz at constant strain (depending on the LVR).

5.2.3 Swelling and water retention studies

The formulated hydrogels were washed thoroughly, dried in an oven, and cut into appropriate sizes (1 cm x 1 cm, thickness 0.1 ± 0.1 cm). The thicknesses of the cut samples were measured with Mitutoyo digimatic micrometer. The weight gained by the hydrogel due to absorption of water was measured gravimetrically. The initial weights of the samples were measured and referred to as W_d. The samples were immersed in 20 ml of DI water. After 1 h, the samples were taken out, and after soaking off the excess water with the help of tissue; the weights of the hydrogels were measured and denoted as W_s. The samples were re-immersed in DI water and the process was continued after an interval of 2 h for the next 24 h. The swelling ratio (SR) and water content (WC) were calculated as:

$$SR = \frac{W_s - W_d}{W_d} \times 100 \tag{5.2}$$

$$WC = \frac{W_s - W_d}{W_s} \times 100 \tag{5.3}$$

where, W_s = weight of the swollen hydrogel (at specified time t) and W_d = weight of dry gel.

Similarly, the water retention ability of the freshly prepared composite hydrogels (1 cm × 1 cm) was determined gravimetrically at an interval of 1 h for 24 h in an ambient atmosphere (25±2 °C, humidity 45±10 %) as:

$$WR = 1 - \frac{W_i - W_d}{W_i} \tag{5.4}$$

Where W_i is the weight of hydrogel at swollen state (at a specified time) kept for dehydration in the ambient atmosphere and W_d is the weight of the dehydrated hydrogel.

Network parameters

The physical yardsticks that represent the properties of hydrogels are network parameters, viz. average molecular weight between crosslinks ($\overline{M_c}$), crosslinking density (V_e), and mesh size (ξ). These parameters were determined using rheological measurements (elastic modulus, G' and viscous modulus, G'') and swelling tests. Based on rubber elasticity

theory (RET) for homogeneous Gaussian chains network parameters, these can be calculated using the following equations: [43,44]

$$\frac{1}{V_{2m}} = 1 + \left[\frac{\rho}{\rho_w} \left(\frac{1}{Z} - 1 \right) \right] \tag{5.5}$$

$$\frac{1}{V_{2r}} = 1 + \left[\frac{\rho}{\rho_w \left(\frac{1}{m} - 1 \right)} \right] \tag{5.6}$$

$$G' = A \frac{\rho}{M_c} RT (V_{2r})^{2/3} (V_{2m})^{1/3} \tag{5.7}$$

$$V_e = \frac{\rho}{M_c} \tag{5.8}$$

$$\xi = \left(\frac{G' N_A}{RT} \right)^{-1/3} \tag{5.9}$$

$$\rho = \frac{w}{S \times t} \tag{5.10}$$

Various notations are: ρ_w = density of water, m = weight of the dry hydrogel, Z = weight of the hydrogel at equilibrium, V_{2m} = polymer volume fraction of crosslinked polymer in equilibrium with swollen gel, V_{2r} = polymer volume fraction after crosslinking but before swelling, ρ = density of dry hydrogel, R = universal gas constant, T = temperature, N_A = Avogadro number, t = thickness of the sample, A = pre-factor (with value as 1 for the affine network model and $1 - \frac{2}{\varphi}$ for the phantom network model, where φ = number of branches originating from crosslinking site). As per constrained junction theory, the phantom network model is followed by the real network and value of $\varphi = 3$ [44–46].

5.2.4 Performance evaluation of hydrogels in flame retardancy

The thermal stability of the hydrogels (and also the influence of additives viz.

MBA and Kaolin) and its efficacy in flame retardancy can be assessed using thermal analysis tests. The following tests were employed for evaluation of the thermal properties of the hydrogels: Thermogravimetry analysis (TGA), Limiting Oxygen Index (LOI), Cone Calorimeter Test (CCT), vertical burning test and open fire. These tests also indicate the flammability of the hydrogels.

Thermogravimetric analyzer [TG 209 F1 Libra, Netzsch, Germany] was employed to obtain the thermograms of dried hydrogel samples. KAS isoconversional method was used to obtain kinetic parameters of thermal conversion (or decomposition) of the hydrogels as described in chapter 4 section 4.2.4. In a typical experiment, a crucible was filled with 8–11 mg sample and heated from 30 ºC to 600 ºC in three linear heating rates, viz. 5, 10, and 20 ºC min^{-1} in nitrogen atmosphere (20 ml min^{-1}).

LOI, CCT were performed as described in chapter 4 section 4.2.4.3. Additionally, open fire test (OFT) was performed to check the efficacy of the hydrogel coated samples in dehydrated and hydrated conditions. The sample size, 100 mm × 100 mm × 2 mm was maintained for the OFT. Here, two samples of the hydrogel coated cotton cloth, one in hydrated (or native) condition and another in dehydrated form (i.e., after drying the hydrogel coated cotton cloth in an oven at 40^0C for 2 h) were ignited using butane torch flame (1300^0C) for 20 s. The flame length was maintained at 4 cm. The flammability tests were recorded in a digital camera.

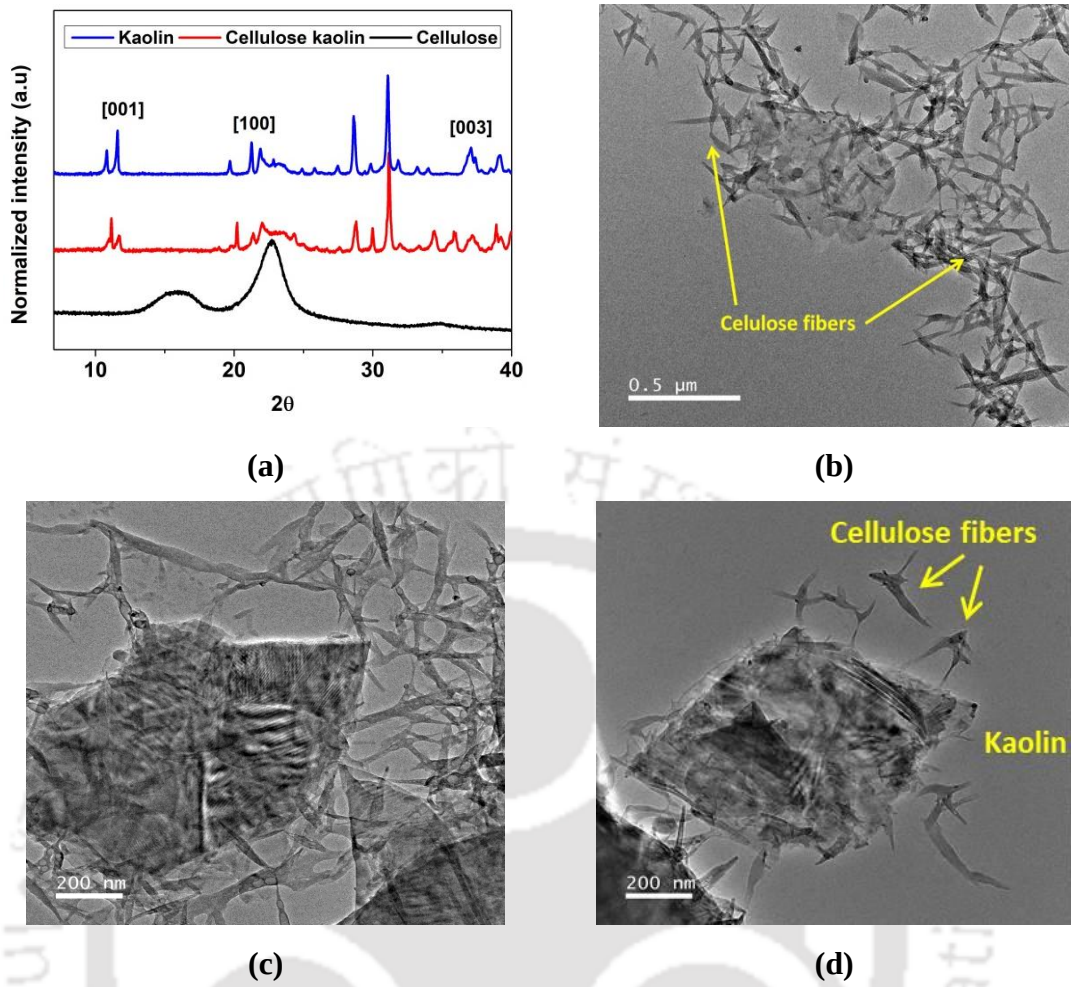

Figure 5.2 (a) XRD diffraction pattern of kaolin, cellulose and kaolin cellulose composite, (b), (c) and (d) FETEM of cellulose kaolin composite

5.3 Results and discussion

5.3.1 Structural characterization of cellulose, kaolin and composite hydrogel

Figure 5.2a presents the XRD patterns of kaolin, cellulose, and cellulose–kaolin composite. The diffraction peak at 16.3 and 22.6° belongs to (1 1 0) and (2 0 0) which are the characteristic peak of α cellulose. The diffraction peaks at 12, 21.24, and 37.12° belong to the crystalline plane (0 0 1), (1 0 0), and (0 0 3) for cellulose–kaolin composite, respectively. The XRD pattern of cellulose–kaolin composite is similar to the raw kaolin, which clearly shows the well-preserved nature of kaolin in the composite. FE-TEM micrographs give an idea regarding the dispersion of kaolin in cellulose matrix. **Figures 5.2b-**

d show well-dispersed hexagonal-shaped kaolin in the cellulose matrix, which essentially is a visual authentication to the XRD results.

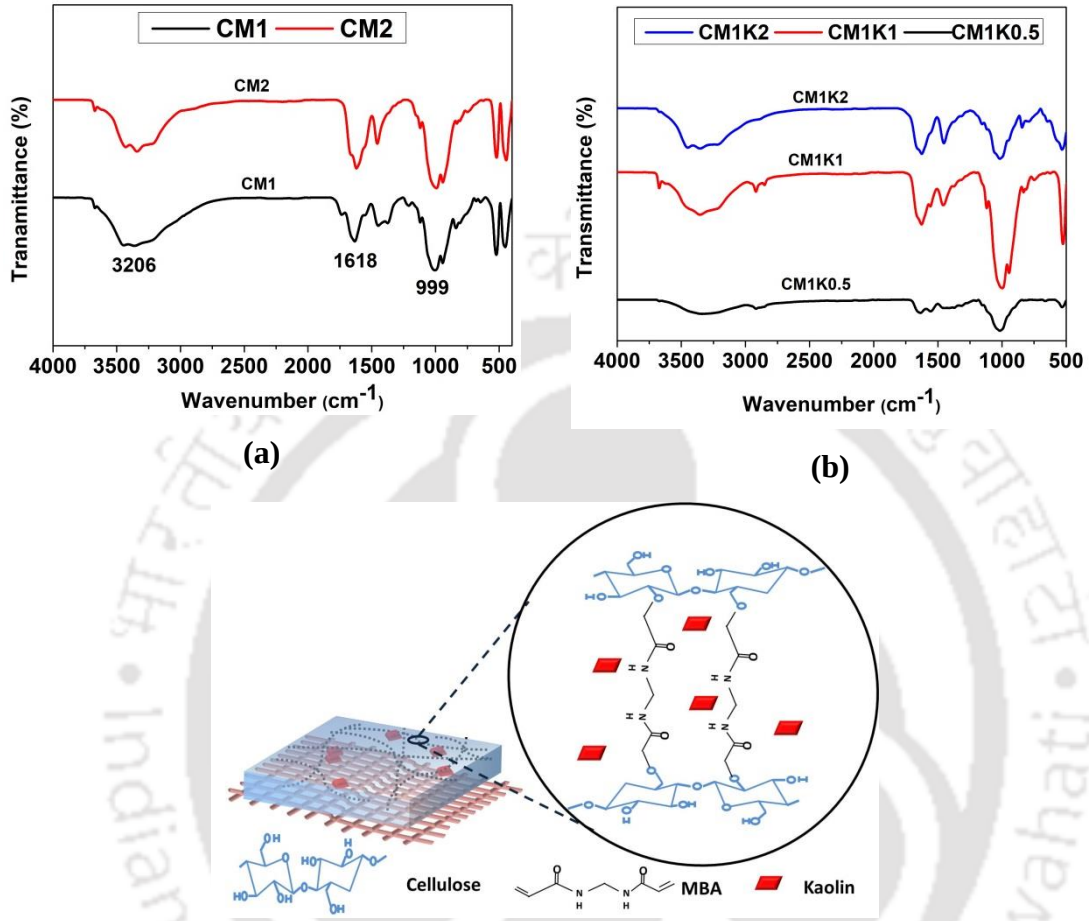

Figure 5.3 FTIR spectrum of CM hydrogels. (a) cellulose:MBA ratios of 1:1 and 1:2, respectively, and (b) CMK hydrogel (cellulose:MBA ratio 1:1) with 0.5,1 and 2 w/v% kaolin. (c) Proposed mechanism of MBA crosslinking cellulose fragments with kaolin infused.

FTIR spectra of raw cellulose, MBA and kaolin are shown in **Figure A2.2** (Appendix 2), which illustrate the characteristic peaks of various components. For raw kaolin, peaks at 3696 and 3621 cm^{-1} are due to –OH vibration bonded to Al octahedral atom on the surface or on the inter layer silicate. Peak at 1632 cm^{-1} represents the –OH vibration trapped in crystal lattice, and 1024 cm^{-1} denotes the Si–O vibration. The peaks at 3587 and 3242 cm^{-1} in cellulose FTIR spectrum are due to the –OH

stretching. Peak at 1688 cm^{-1} is attributed to C=O stretching and 1322 cm^{-1} represents the C–H bending. Similarly, for crude MBA, peak at 3487 cm^{-1} represents –OH vibration, 3206 cm^{-1} belongs to N-H stretching, 1675 cm^{-1} represent C=O stretching and 1624 cm^{-1} denotes the C=C stretching.

Figure 5.3a shows the FTIR spectra of cellulose hydrogel with cellulose to MBA ratios of 1:1 and 1:2, respectively. It could be seen that characteristic peak of MBA at 3206 cm^{-1} (due to N–H stretching) and peaks at 1650 cm^{-1}(due to –C=O stretching) intensify with increasing the concentration of MBA in the hydrogel composites. However, the peaks at 1618 cm^{-1} (due to C=C stretching) was observed to be diminished which indicates cellulose-MBA interaction via C=C. The stretching due to C=C disappears, which shows that the double bond has been consumed during the crosslinking process. Hence, a hypothetical mechanism can be conjectured from the FTIR analysis. The alkaline conditions (NaOH) initially deprotonate the hydroxyl group of the glucose group of the cellulose. This nucleophile (Michael donor) in turn reacts with MBA (Michael acceptor). This charge delocalization and break the π bond in MBA leaving the oxygen with a negative charge and a double bond which later on acquire a proton from water molecules. Hence, we proposed Michael addition reaction for the successful crosslinking of the composite hydrogel. Similarly, for 1:1 cellulose: MBA hydrogels with 0.5, 1 and, 2 % w/v of kaolin (**Figure 5.3b**), the characteristic peaks of kaolin at 3692 and 3621 cm^{-1} disappears. These findings clearly show the successful crosslinking between the constituents, and hence, the formation of hydrogel. Similar results have been observed for hydrogels with cellulose: MBA (C:M) ratio of 1:2 with different kaolin concentration (refer Appendix 2, **Figure A2.2b**). The proposed mechanism of MBA crosslinked cellulose hydrogel is shown in **Figure 5.3c**.

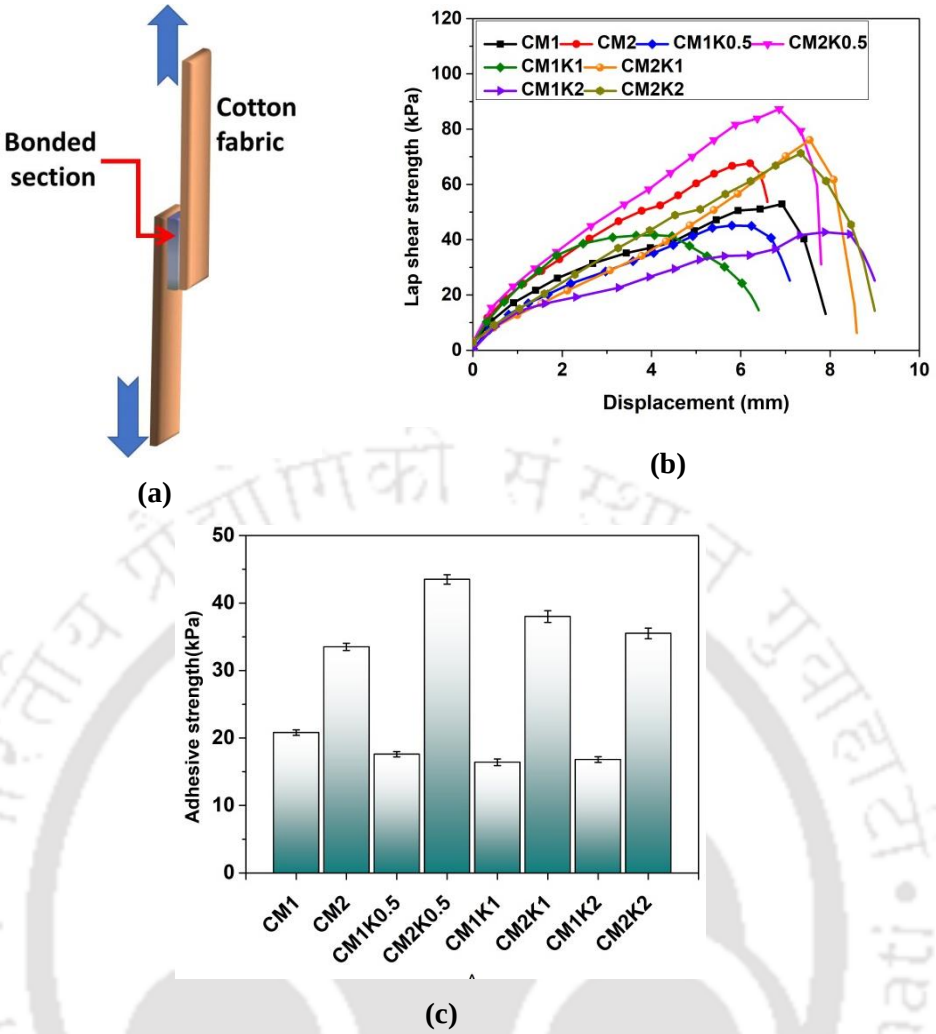

Figure 5.4. (a) Schematic illustration of the lap shear test sample. (b) Adhesion strength curve and (c) adhesion strengths of the hydrogels coated on cotton fabric.

Adhesion strength between the hydrogel and cotton fabric was assessed by the lap shear adhesion test (Figure 4a). The test results are represented in **Figures 5.4b** and **5.4c**. As shown in **Figure 5.4b**, it can be observed that coating the pregel onto the fabric allows the solution to wet the fabric and crosslink (under ambient conditions) to form hydrogel. Consequently, the resulting hydrogel strongly adheres to the fabric. The sample with a higher proportion of MBA (1:2) results in superior adhesion compared to the lower proportion of MBA. The noted adhesive strengths were 20.8 and 33.5 kPa for CM1 and CM2, respectively. The deleterious effect of kaolin can be observed in Figures 4b and 4c, with a lower proportion of MBA the amount of crosslinking achieved was inadequate to induce strong adhesion. The adhesive strengths observed were 17.6, 16.4, and 16.8 kPa for CM1K0.5, CM1K1, and

CM2K2, respectively. However, increasing the MBA content could surmount the deleterious effect of kaolin. The adhesive strengths for CM2K0.5, CM2K1, and CM2K2 were 43.5, 38, and 35.5 kPa, respectively (**Figure 5.4c**).

5.3.2 Swelling and water retention study

Swelling and water retention study for synthesized hydrogels was performed in an ambient atmosphere (25±2ºC) and humidity 55%. It was observed that all the hydrogels absorbed water and reached equilibrium within an hour of their submersion in water. MBA crosslinking via addition reaction consumed the –OH group of cellulose, and hence, prevented aggregation of cellulose when immersed in water.[38]

Figure 5.5a clearly shows the effect of MBA on the degree of swelling of the hydrogels. The degree of swelling for hydrogel with equal proportion of MBA to cellulose (1:1) was higher than hydrogels formulated with 1:2 cellulose to MBA. Relatively smaller swelling for hydrogels with 1:2 cellulose to MBA ratio is attributed to greater degree of crosslinking in presence of higher amount of MBA. **Figures 5.5b** and 5c demonstrate the swelling ratios for hydrogel samples synthesized with varying kaolin concentrations (0.5, 1 and 2% w/v). It could be seen that the swelling ratio reduces with increasing kaolin concentration for cellulose to MBA ratio of 1:1, whereas the swelling is relatively independent of kaolin concentration for cellulose to MBA ratio of 1:2. This is attributed to greater degree of crosslinking in presence of higher quantities of MBA. Comparison of the hydrogels formulated with and without kaolin (**Figures 5.5a, 5.5b** and **5.5c**) shows that presence of kaolin reduced the water absorption ability of the hydrogel.

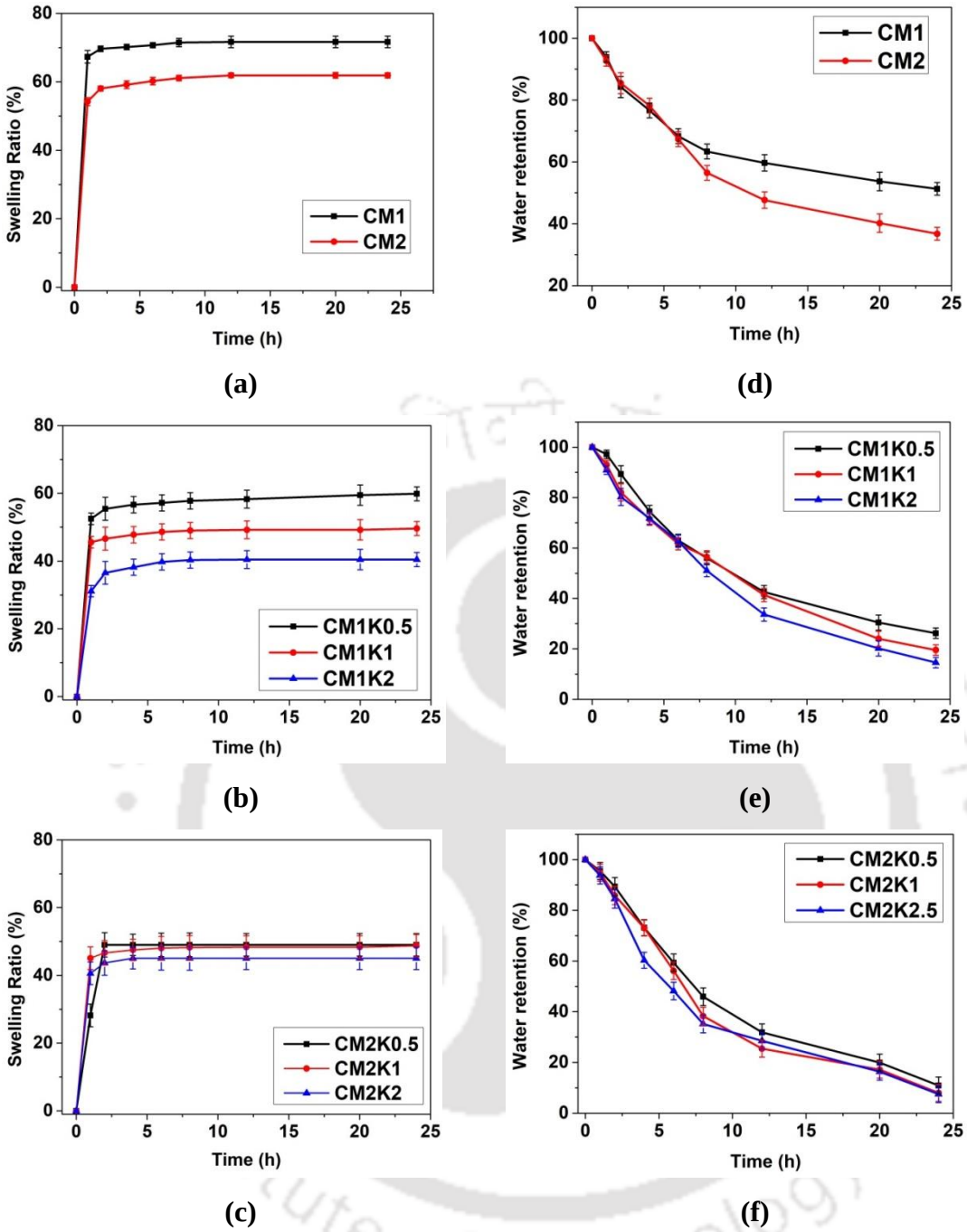

Figure 5.5 Swelling kinetics and water retention ability of (a) and (d) cellulose hydrogels for C: M ratio 1:1 and 1:2, (b) and (e) cellulose kaolin hydrogel at 1:1 C:M ratio, and lastly (c) and (f) cellulose kaolin hydrogel at 1:1 C:M ratio 1:2with 0.5, 1 and, 2 w/v% kaolin.

Low amount (0.5% w/v) of kaolin in the hydrogel allowed the crosslinking agent to establish more bonding with cellulose. Also, low water absorption behaviour of kaolin (which is hydrophobic in nature) compelled the hydrogels to lower its water

absorption performance. Hence, higher dosage of kaolin in the hydrogel resulted in low swelling of the hydrogels.

Water retention performances of the hydrogels are shown in **Figures 5.5d, 5.5e** and **5.5f**. During 24 h of experiments, the highest amount of swelling attained by C:M 1:1 ratio unveil highest amount of water retention aptitude (**Figure 5.5d**). As already discussed, kaolin absorbs lesser quantities of water, and thus, significant quantities of water remain in free form and evaporate easily.[47] Hence, increment of kaolin incorporation in the hydrogels lowers the water retention ability. In the case of hydrogel with low amount of MBA, low crosslinking density (in addition to presence of kaolin) induces low amount of water retention. the crosslinking density improves with addition of MBA, which facilitates the water retention of the hydrogels (**Figure 5.5e** and **5.5f**),[48]

5.3.3 Influence of MBA and kaolin on crosslinking of the hydrogel

Measurement of the hydrogels moduli provides an idea of its crosslinking and quantifies the degree of crosslinking. Results of the rheological studies, variation of storage modulus and loss modulus with increasing frequency is shown in Figure 4 and variation in strain % is shown in **Figure A2.3** (Appendix 2). The linear viscoelastic region (LVR) was calculated to be 1 strain% from amplitude sweep (**Figure A2.3**, Appendix 2). All the hydrogel samples showed higher elastic moduli (G'), suggesting successful crosslinking of the system. The samples projected elastic like behaviour with increasing frequency. Hence, the samples were mechanically stable and were not influenced by the increasing frequency (**Figure 5.6a, 5.6b** and **5.6c**). The strong influence of MBA and kaolin was seen in all the frequency sweep of the hydrogel. As previously discussed in section 5.3.1 (**Figure 5.2a**), MBA induced crosslinking (via addition reaction) of cellulose fragments and enhancement in its elastic moduli is

observed (**Figure 5.6a**).

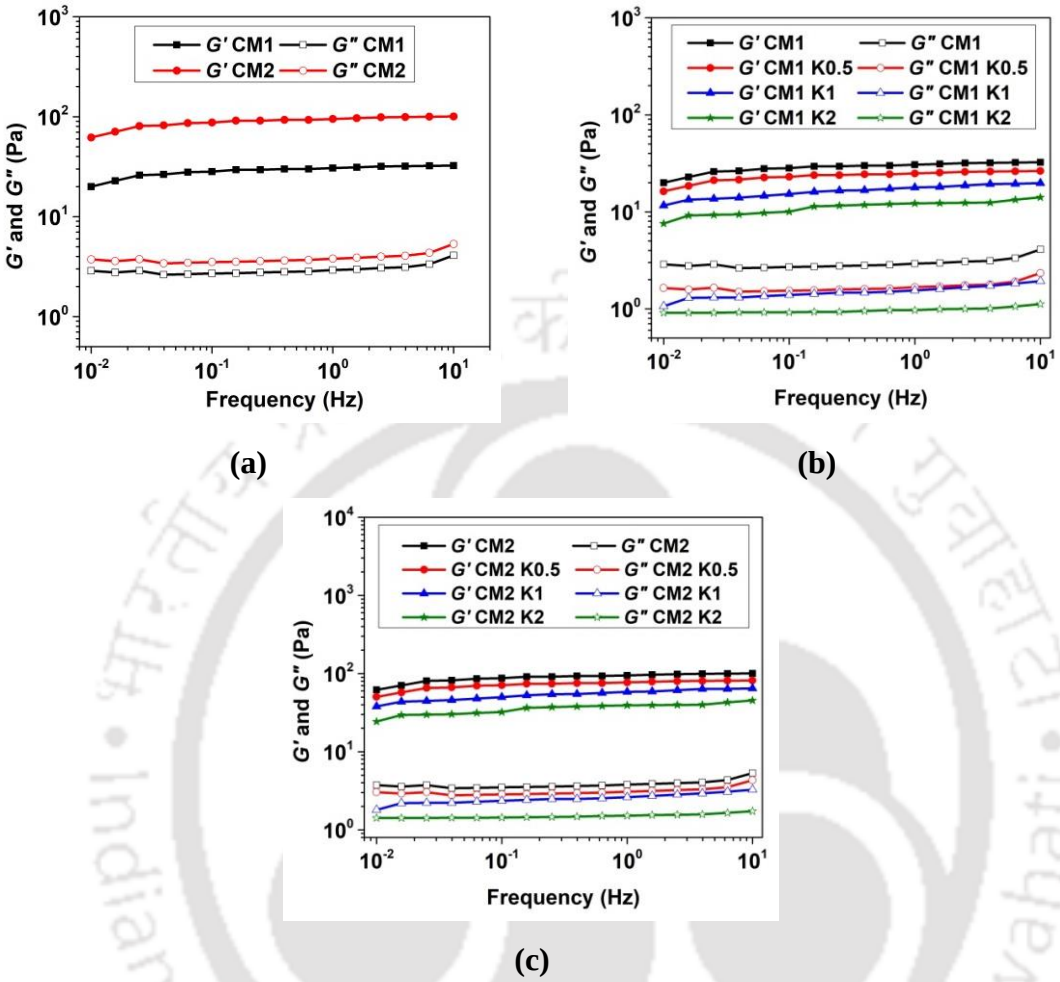

Figure 5.6 Frequency sweep of cellulose hydrogel with (a) different concentration of MBA (1:1 and 1: 2 with respect to cellulose) and kaolin (0.5, 1 and 2% w/v) with (c) 1:1 cellulose:MBA (d) 1:2 cellulose:MBA

Further, increasing the MBA ratio (with respect to cellulose) from 1:1 to 1:2 induces more crosslinking of the cellulose and hence, increment in the moduli of the hydrogel is observed. This increment of moduli (**Table 5.2**) confirms the successful crosslinking of the cellulose hydrogels. However, for CM1K0.5, CM1K1 and CM1K2 hydrogel, kaolin inclusion deteriorates the cellulose MBA bonding, which can be clearly observed from lower elastic moduli of the hydrogel systems in **Figure 5.6b** and **Table 5.2**. Also, addition of MBA at equal ratio of cellulose (1:1) was not enough

to properly bind and crosslink the cellulose fragments and kaolin particles. Hence, lesser degree of crosslinking was achieved. However, increment in MBA ratio (1:2 with respect to cellulose) induced more crosslinking and improvement in elastic moduli was seen (**Figure 5.6c**).

Table 5.2 Elastic moduli, $G^{'}$ and loss moduli, $G^{''}$ values of formulated hydrogels

Sample	$G^{'}$ (Pa)	$G^{''}$ (Pa)
CM1	28.76 ± 3.5	4.10 ± 2.0
CM1K0.5	23.38 ± 2.8	2.34 ± 2.2
CM1K1	16.40 ± 2.4	4.33 ± 5.0
CM1K2	11.17 ± 1.7	1.92 ± 3.0
CM2	89.16 ± 10.8	5.33 ± 3.0
CM2K0.5	72.49 ± 8.8	3.27 ± 1.5
CM2K1	53.77 ± 8.0	1.12 ± 2.6
CM2K2	35.90 ± 5.67	1.74 ± 3.1

5.3.4 Investigation of the internal structure of the hydrogel

Table 5.3 Evaluated mesh size (ξ), molecular weight across crosslinks, $\overline{M_c}$ and crosslinking density, V_e

Composition	Average G' (Pa)	$\overline{M_c}$ (kg mol^{-1})	V_e (kmol m^{-3})	ξ (nm)
CM1	28.76 ± 3.5	142.17±6.1	1336.44±102	52.30±4.5
CM1K0.5	23.38 ± 2.8	612.65±106	816.12±50	56.03±6.2
CM1K1	16.40 ± 2.4	701.25±99	548.47±30	63.06±6.8
CM1K2	11.17 ± 1.7	1061.73±121	444.27±15	71.67±7.0
CM2	89.16 ± 10.8	164.29±7	5072.27±200	35.87±1.0
CM2K0.5	72.49 ± 8.8	236.53±10	3523.14±175	38.43±1.5
CM2K1	53.77 ± 8.0	300.71±50	2720.79±130	42.45±2.2
CM2K2	35.90 ± 5.67	607.21±78	1197.73±100	48.57±3.3

Evaluations of network parameters provide insights to the internal structure of the hydrogels and help us reasonably justify the trends obtained in swelling test and rheological measurements. To evaluate the network parameters, average molecular weight ($\overline{M_c}$), effective crosslink density (V_e), and mesh size (ξ) of the hydrogels, elastic modulus (from rheological experiment, **Table 5.2**), thickness, and cross sectional area of the formulated hydrogels were first measured. Similarly, swelling ability and density of the hydrogel were calculated and network parameters were evaluated (**Table 5.3** and **Table A2.3**, Appendix 2).

From **Table 5.3** and **Table A2.3** (Appendix 2) the influence of crosslinker (MBA) and filler, kaolin on the internal structure of the hydrogels is clearly observed. MBA induces crosslinking, and hence, the molecular weight between crosslinks increased 142.17 kg mol^{-1} to 164.29 kg mol^{-1}(elastic moduli increment) and mesh size decreased from 52.30 to 35.87 nm respectively. However, hindrance in cellulose fragments linkage due to kaolin incorporation is vividly observed in hydrogel containing kaolin. $\overline{M_c}$ for hydrogel with 1:1 cellulose:MBA ratio increased from 612.65 kg mol^{-1} (for kaolin 0.5% w/v) to 1061.73 kg mol^{-1} (for kaolin 2% w/v), while the mesh size increased from 56 nm (for kaolin 0.5% w/v) to 71 nm (for kaolin 2% w/v), respectively. Similarly, for hydrogel with 1:2 cellulose:MBA ratio, $\overline{M_c}$ and mesh size was observed to be 607.21 kg mol^{-1} and 48.57 nm. On contrary to mesh size and $\overline{M_c}$, the increment in molecular weight between crosslinks reduce the crosslinking density (V_e) and vice versa. V_e for pristine hydrogels calculated as 1336.44kmol m^{-3} (CM1) and 5072.27 kmol m^{-3} (CM2). For hydrogels containing kaolin, the value of V_e decreased from 816.12 to 444.27 kmol m^{-3} in case of 1:1 ratio of cellulose:MBA, and 3523.14 to 1197.73 kmol m^{-3} in case of 1:2 cellulose: MBA

ratio. These results are satisfactorily advocated by the swelling ability of the hydrogels (**Figure 5.5**). In **Figure 5.5a** decrement in swelling ratio of CM2 hydrogels (higher MBA ratio than cellulose) which can be ascribed to higher crosslinking and decreased mesh size. However, kaolin incorporation (0.5, 1 and 2 w/v %) disrupt crosslinking and network formation in hydrogels to some extent. Sequentially the network formed was loosely packed with increased hydrogel mesh size. Despite increased in mesh size swelling was observed to be less owing to kaolin's property of low swelling in water [49] (**Figure 5.5b** and **5.5c**).

5.3.5 Flammability and thermal stability of the hydrogel

5.3.5.1 Thermogravimetric (TGA) analysis

Thermograms shown in **Figure 5.7** clearly depict the state (or form) of the additives (MBA and kaolin), and the influence of kaolin on the thermal properties of the hydrogel. Thermogram for MBA, cellulose and kaolin (**Figure A2.4**, Appendix 2) illustrates multiple step degradation for MBA, and single step degradation for cellulose and kaolin. The initial loss of mass up to 100ºC was ascribed to moisture. For MBA, second stage of degradation occurred from 150 – 250 ºC, followed by third stage (300 – 370 ºC) and fourth stage at 370 – 450 ºC.[38] The degradation temperature range for cellulose was 250 – 350 ºC,[50] while kaolin degraded at 445 ºC and above.[47] **Figure 5.7** and **Table A2.2** (Appendix 2) clearly show the two step degradation behaviour of the composite hydrogel. The initial weight loss can be ascribed to moisture loss. The second stage of degradation can be due to degradation of the chemical crosslinking of the hydrogels. This also confirms the successful crosslinking of the hydrogels. **Figure 5.7a** illustrates the effect on degree of crosslinking on the thermal stability of the hydrogels. With increment of MBA proportion, lesser amount of degradation is observed. However, the amount of residue obtained at the end of

experiments (600 ºC) was less compared to the hydrogel with lesser amount of MBA. This clearly shows that the presence of MBA induces crosslinking of the hydrogels but do not participate in char formation.

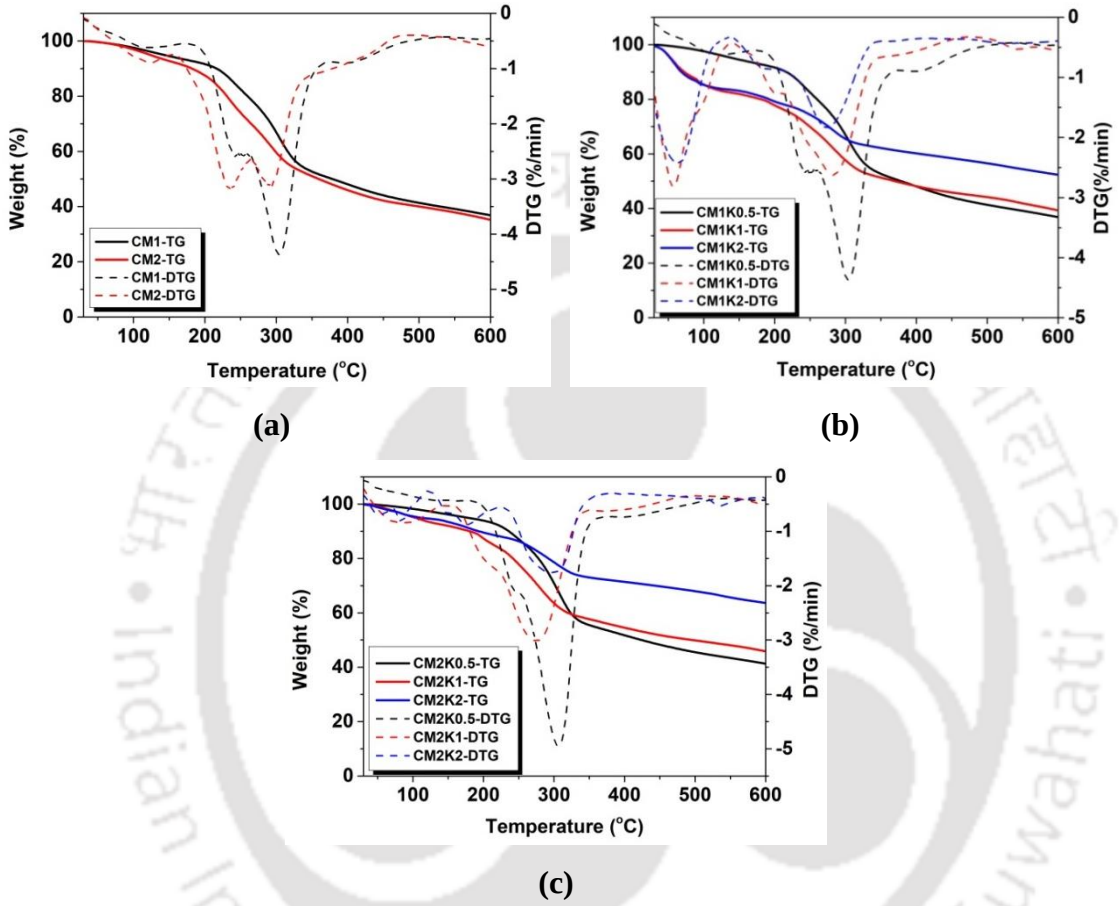

Figure 5.7 (a) TGA and DTG curves of cellulose hydrogel at 1:1 and 1:2 cellulose to MBA ratios, (b) TGA and DTG curves of hydrogels with 0.5,1 and 2% w/v kaolin at 1:1 C:M ratio, and (c) 1:2 cellulose MBA ratio

For hydrogels comprising kaolin (**Figure 5.7b** and **5.7c**) clearly states the fervent influence of kaolin in imparting thermal stability to the hydrogels. The amount of weight loss observed decreased with kaolin incorporation, 0.5 w/v % (CM1K0.5) kaolin incorporation loosed 80% of its initial weight whereas 2w/v% (CM1K2) kaolin showcased weight loss of 52%. Similar results have been observed in case of hydrogel sample with higher ratios of MBA (CM2K0.5~40.43% and CM2K2~20.96% weight

loss respectively). The hydrogels comprising 2% w/v of kaolin exhibits the highest residue retention 52.37% for CM1K2 and 63.65% for CM2K2 respectively. (**Table A2.2**, Appendix 2).

5.3.5.2 Arrhenius kinetic analysis

For ameliorate understanding of the influence of all the physical parameters (crosslinking density, mesh size, swelling and water retention ability) on degradation behaviour of the hydrogels, determination of the activation energy of the hydrogels is necessary. Based on the swelling, water retention and thermal degradation behaviour discussed extensively in previous sections (5.3.2, 5.3.3, 5.3.4 and 5.3.5.1), cellulose:MBA of 1:2 was chosen to perform the kinetic analysis.

Thermal conversion data obtained from TGA was analyzed using KAS isoconversional method to determine the activation energy, E_a. The governing equation of KAS method is given in equation 5.3.

$$\ln\left(\frac{\beta_i}{T^2_{\alpha,i}}\right) = \ln\left(\frac{AR}{E_a g(\alpha)}\right) - \frac{E_\alpha}{RT_{\alpha,i}} \qquad 5.3$$

Notations: β = heating rate (K min^{-1}), T = temperature (K), A = pre-exponential factor (s^{-1}), R = molar gas constant (8.314 J $mol^{-1}K^{-1}$). At any constant value of α (the degree of conversion), the activation energy can be calculated from the slope of the plot of $\ln\left(\frac{\beta}{T^2}\right)$ versus $\frac{1}{T}$.[51] **Figures 5.8a** and **5.8b** represents the thermograms of the CM2K1 and CM2K2 hydrogels at heating rate 5, 10 and 20 ºC/s.

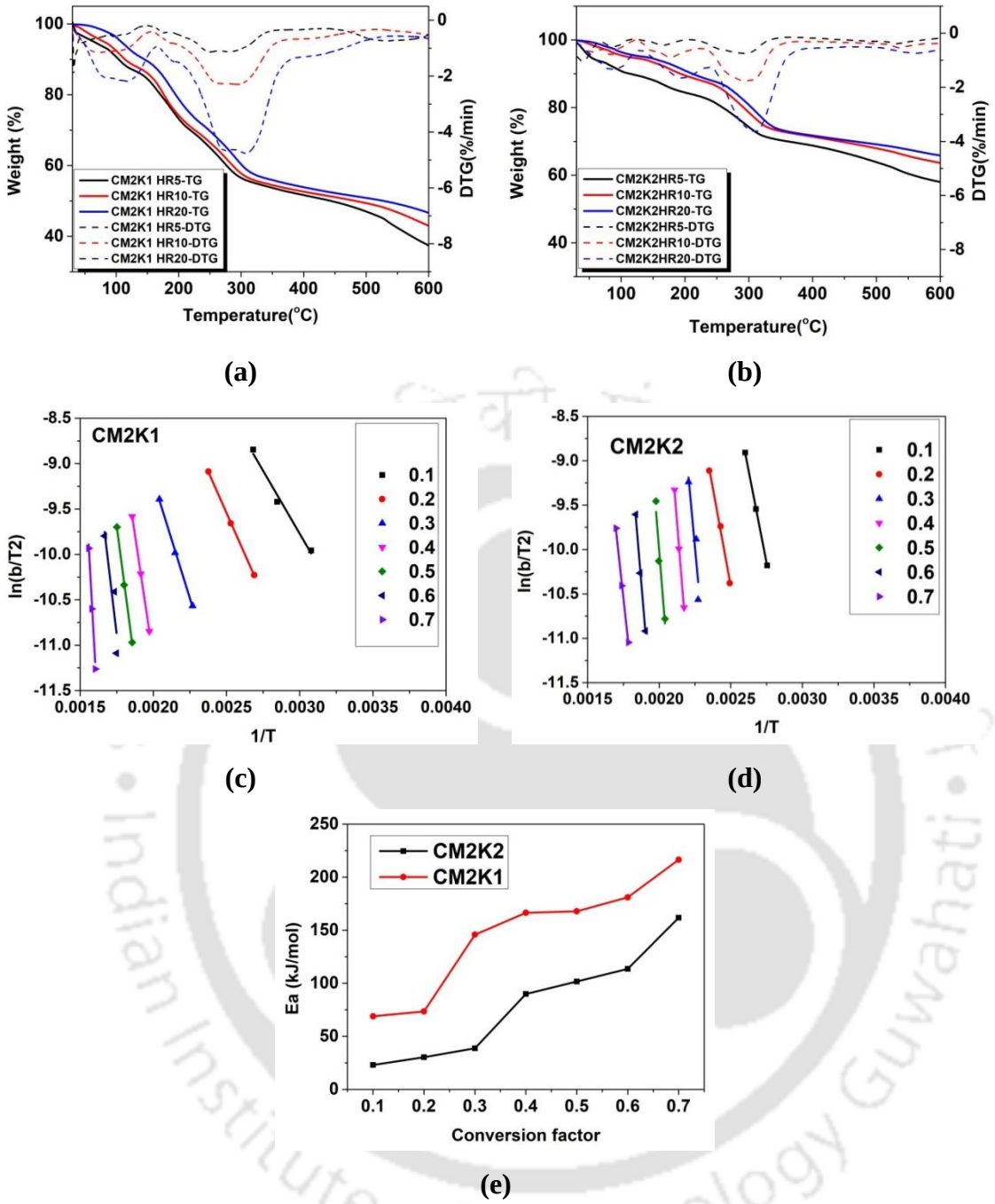

Figure 5.8 Thermograms of hydrogel CM2K1 (a) and CM2K2 (b) at HR 5,10 and 20 ºC. Arehenius plot of CM2K1 (c) and CM2K1 (d) and the Activition energy calculation using KAS method (e)

The thermal conversion data (TGA analysis) of the hydrogels CM2K1 and CM2K2 was obtained in the conversion range of 0.1 to 0.7, respectively. Figures 8c and 8d depict the representative plots of $\ln\left(\beta/T^2\right)$ versus 1/T fitting of equation 9 to

the thermal conversion data obtained from Figures 8a and 8b. The complete results of the analysis are given in **Table 5.4**.

Table 5.4 Results of activation energy calculated by KAS model

α	CM2K1		CM2K2	
	E_a	R^2	E_a	R^2
0.1	23.	0.98	69.	0.99
0.2	30.	0.99	73.	0.95
0.3	38.	0.99	146.	0.88
0.4	89.	0.99	166.	0.99
0.5	101.	0.99	167.	0.99
0.6	113.	0.85	180.	0.99
0.7	161.	0.98	216.	0.99

α = conversion %, E_a = activation energy kJ mol^{-1}

Based on the variation of E_a with conversion, the degradation process can be classified into two stages. Stage I (α = 0 to 0.2) signifies the initial degradation due to moisture loss and consequently E_a (shown in **Table 5.4**) is very low. In Stage II (α = 0.2 to 0.7), a steady rise in the value of E_a is observed. This is mainly due to substantial degradation of cellulose and MBA chemical linkage accompanied by incineration of cellulose backbones and kaolin. The rise in E_a for the kaolin (1 and 2% w/v) containing hydrogel evidently indicates the influence of kaolin on enhancing the thermal stability of hydrogels. This is possibly attributed to synergism between char layer formation due to combustion of cellulose in hydrogel with high thermal stability of kaolin. This synergism leads to delay in combustion of the hydrogel surface, and the char formed thereby protects the inner layers from oxidation.

5.3.5.3 Combustion studies of cotton cloth coated with hydrogel

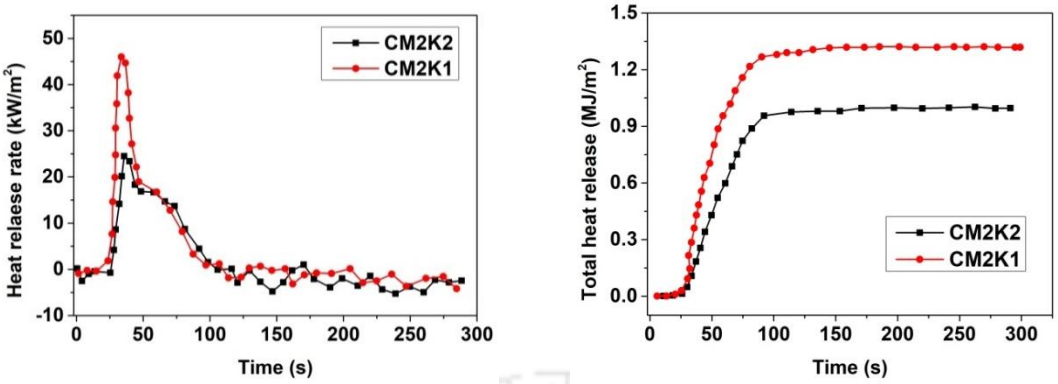

(a) **(b)**

Figure 5.9 Heat release rate(HRR) (a) and total heat release (THR) (b) of CM2K1 and CM2K2 cellulose hydrogel

Table 5.5 CCT results of the composite hydrogel

Composition	Time to ignition (s)	PHRR (kW m^{-2})	THR (MJ m^{-2})
CM2K1	23.33 ± 2.49	46 ± 5	1.3 ± 3
CM2K2	19.67 ± 1.7	26.60 ± 2	0.9 ± 2

Flammability of the hydrogels coated cotton cloth was investigated thoroughly by performing cone calorimeter test (CCT), limiting oxygen index (LOI) test, vertical flammability test (VFT), and open flame test (OFT). Results of CCT are shown in **Figure 5.9** and **Table 5.5**. On administering 25 kW m^{-2} of heat flux, the amount of heat released by the hydrogels are presented in terms of heat release rate (HRR) and total heat release rate (THR). These values are calculated based on the amount of oxygen consumed during CCT. The amount of heat released calculated for sample CM2K1 (peak HRR 46 kW m^{-2}) was higher than CM2K2 (peak HRR 25 kW m^{-2}).

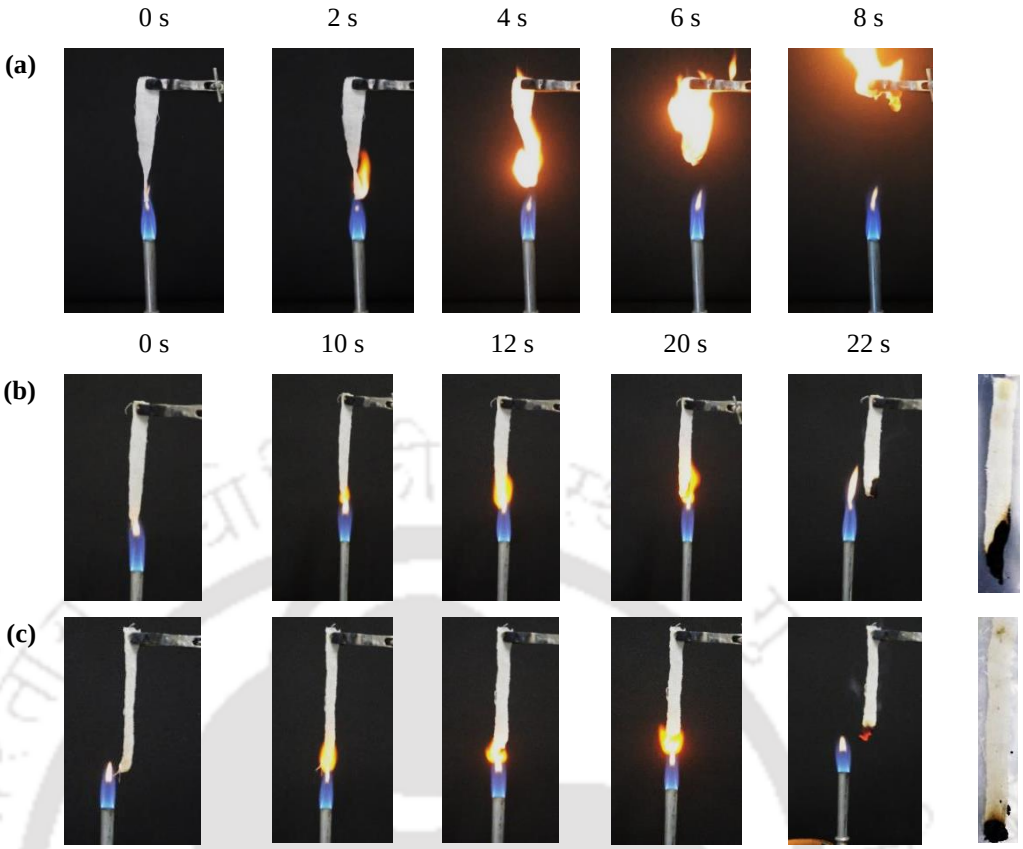

Figure 5.10 Photos showing the process of burning during UL94 (a) cotton cloth (b) CM2K1 (c) CM2K2

Similarly, THR of CM2K1 and CM12K2 was calculated to be 1.3 and 0.9 MJ m^{-2}. These values are much lower than other hydrogel composite. Xiao et al. [52] developed sodium alginate based hydrogel coating on wood possessing HRR of 113 kW m^{-2} and THR of 29.3 MJ m^{-2}. Jena et al.[22] reported HRR = 544 kW m^{-2} and THR = 59 MJ m^{-2} for guar gum graft poly butyl acrylate with 10% MMT content. The results of HRR and THR clearly showcased the influence of kaolin in the hydrogel. The high thermally stable kaolin encourage slow burning of the hydrogels and surge the time to burn the sample. Hence, the sample with 2 w/v% of kaolin (CM2K2) took longer time to burn. Further, 100s of CCT experiment revealed single peak (**Figure 5.9**) that ascertain the formation of stable layer of char after the samples burns which prohibit further burning of the samples. Results of VFT and OFT are shown in **Figure**

5.10 and **Figure 5.11**, respectively. Butane torch with flame length 4 cm was used to carry out the test on 10 cm x 1 cm (VFT samples) and 10 cm x 10 cm (OFT samples) for 20 s in ambient atmosphere (25±2ºC) with humidity 55%. The hydrogel coating was 0.2 mm for both VFT and OFT. Untreated cotton cloth is extremely combustible with high burning velocity (**Figure 5.10a** and **5.11a**) and hence, when ignited burns completely within fraction of seconds.

Cotton cloth samples coated with hydrogel when ignited delayed the process of burning. After igniting for 20s and removing the butane torch, it was observed that the samples self extinguishes leaving behind a layer of char. The length of char obtained for CM2K1 was more than CM2K2 (**Figure 5.10b** and **5.10c**). In case of open fire test (OFT), the one of the test samples were fully hydrated and the other dehydrated to investigate the efficacy of the formulated hydrogel. Post 20s ignition, on comparing the front and the back side of the hydrogel coated samples clearly give us a visual perspective of the hydrogel coating performance. The hydrogel coating formed a layer of char which not only prevented the fire from spreading but also protected the underneath material from combustion. The amount of kaolin has a huge impact on the hydrogel usage as flame retardant. The sample CM2K2 (**Figures 5.10c, 5.11b** and **5.11c**), although it wasn't able to retain much water (7% after 24h, **Figure 5.5f**), presence of high amount of kaolin prevented the spread of fire in the sample. Additionally, presence of kaolin improved the LOI of cotton cloth from 20% to 32.14% (CM2K1) and 34.37% (CM2K2).

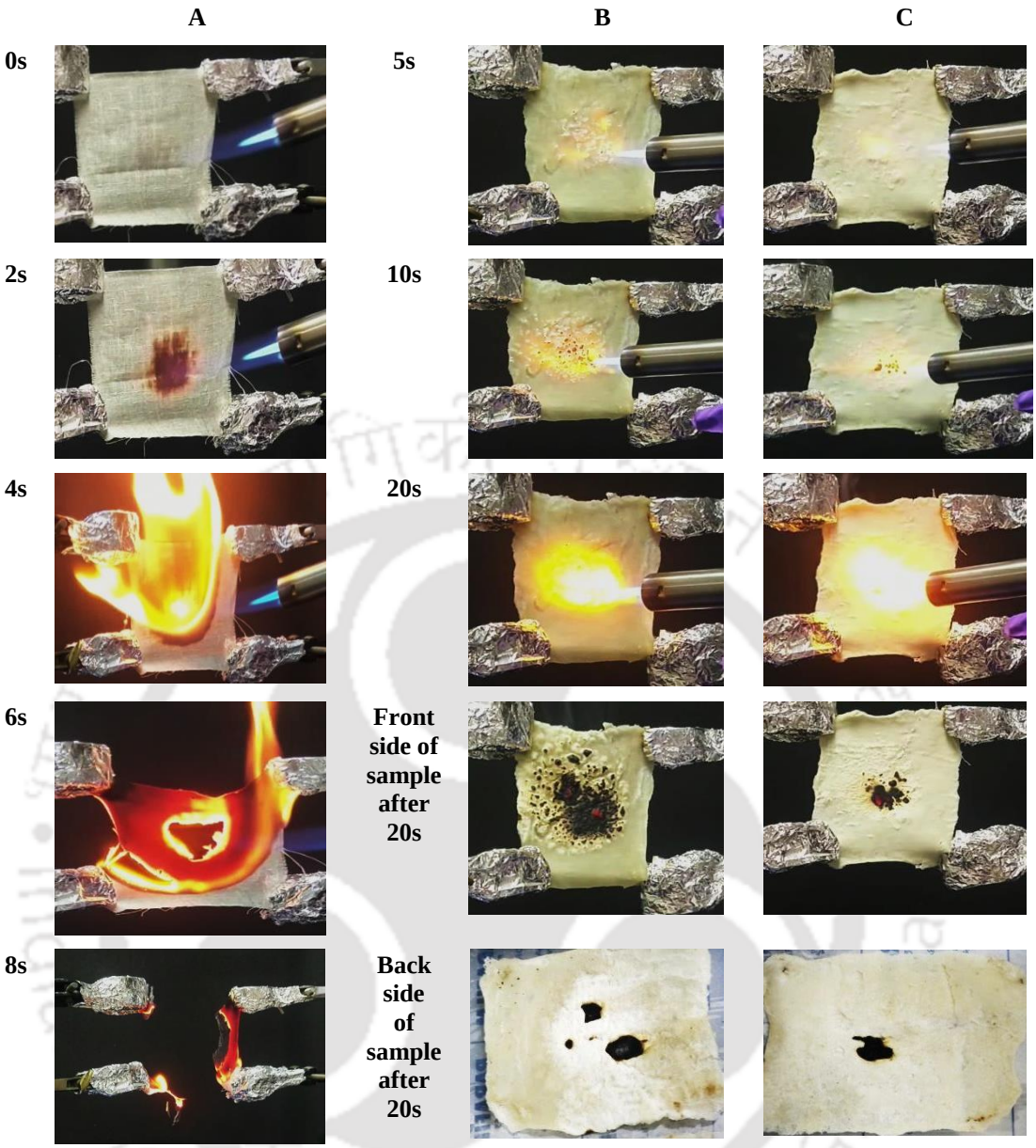

Figure 5.11 Digital images of open fire test of (A) untreated cotton cloth, (B) hydrated hydrogel coated cotton cloth and, (c) dehydrated hydrogel coating on cotton cloth

5.4 Conclusions

Herein, we have valorised the cellulose extracted from the waste perennial grass, *Arundo Donax*, to regenerate cellulose hydrogel on cotton fabric. The hydrogels synthesized could easily absorb and retained ample amount of water for 24 h (96%, for CM2 and 55% for CM2K2 hydrogels). The hydrogels synthesized exhibited fast

swelling and reached equilibrium with an hour of immersion. The TGA tests revealed 63 wt% char production after complete thermal conversion of hydrogel. Thus, the synergistic effect of water content of hydrogel matrix, the char formation and thermal resistance of kaolin effectively retards the ignition of flame propagation of the surface over which the hydrogel is applied. Additional tests also corroborated this result, viz. the hydrogels possessed low heat release rate, 26.60 kJ m^{-2} and the ignition time calculated for CM2K2 was 19.67s. The LOI of cotton cloth increased from 20% to 34.37% after hydrogel coating. This study has essentially demonstrated synthesis of an effective fire retardant hydrogel from sustainable materials, viz. cellulose and kaolin, for application on cotton fabrics as coating.

References

(1) Kahn, S. A.; Patel, J. H.; Lentz, C. W.; Bell, D. E. Firefighter Burn InjuriesPredictable Patterns Influenced by Turnout Gear. *J. Burn Care Res.* **2012**, *33* (1), 152–156. https://doi.org/10.1097/BCR.0B013E318234D8D9.

(2) Cheng, R.; Dong, K.; Liu, L.; Ning, C.; Chen, P.; Peng, X.; Liu, D.; Wang, Z. L. Flame-Retardant Textile-Based Triboelectric Nanogenerators for Fire Protection Applications. *ACS Nano* **2020**, *14* (11), 15853–15863. https://doi.org/https://doi.org/10.1021/acsnano.0c07148.

(3) He, H.; Liu, J.; Wang, Y.; Zhao, Y.; Qin, Y.; Zhu, Z.; Yu, Z.; Wang, J. An Ultralight Self-Powered Fire Alarm e-Textile Based on Conductive Aerogel Fiber with Repeatable Temperature Monitoring Performance Used in Firefighting Clothing. *ACS Nano* **2022**, *16* (2), 2953–2967. https://doi.org/https://doi.org/10.1021/acsnano.1c10144.

(4) Shakeriaski, F.; Ghodrat, M.; Rashidi, M.; Samali, B. Smart Coating in Protective Clothing for Firefighters: An Overview and Recent Improvements. *J. Ind. Text.* **2022**, *51* (5_suppl), 7428S-7454S. https://doi.org/https://doi.org/10.1177/15280837221101213.

(5) Xu, H.; Xu, P.; Wang, D.; Yang, Y.; Wang, X.; Wang, T.; An, W.; Xu, S.; Wang, Y. Z. A Dimensional Stable Hydrogel-Born Foam with Enhanced

Mechanical and Thermal Insulation and Fire-Retarding Properties via Fast Microwave Foaming. *Chem. Eng. J.* **2020**, *399*, 125781. https://doi.org/10.1016/J.CEJ.2020.125781.

(6) Yasmin, S.; Whalen, M. Flame Retardants, Hexabromocyclododecane (HCBD) and Tetrabromobisphenol A (TBBPA), Alter Secretion of Tumor Necrosis Factor Alpha (TNFα) from Human Immune Cells. *Arch. Toxicol.* **2018**, *92* (4), 1483. https://doi.org/10.1007/S00204-018-2156-5.

(7) Jiang, Z.; Dou, G. Preparation and Characterization of Chitosan Grafting Hydrogel for Mine-Fire Fighting. *ACS Omega* **2020**, *5* (5), 2303–2309. https://doi.org/https://doi.org/10.1021/acsomega.9b03551.

(8) Oliver, S.; Lei, L.; Fan, K. W.; Wang, C.; Baena, J. C.; Pham, P.; Lin, Q.; Kabir, I. I.; Wong, E. H. H.; Yuen, A. C. Y.; Boyer, C.; Yeoh, G. H. Wet or Dry Multifunctional Coating Prepared by Visible Light Polymerisation with Fire Retardant, Thermal Protective, and Antimicrobial Properties. *Cellulose* **2021**, *28* (13), 8821–8840. https://doi.org/https://doi.org/10.1007/s10570-021-04095-z.

(9) Zheng, W. J.; Cui, X. F.; Zou, W.; Chen, Q.; Zhang, H. B.; Yang, H.; Yan, J. Basalt/Polyacrylamide-Ammonium Polyphosphate Hydrogel Composites for Fire-Resistant Materials. *Macromol. Mater. Eng.* **2021**, *306* (2), 2000582. https://doi.org/10.1002/MAME.202000582.

(10) Ingtipi, K.; Boro, U.; Moholkar, V. S. Lignin in Nanocomposite Hydrogels. *Micro Nanolignin Aqueous Dispersions Polym. Interact. Prop. Appl.* **2022**, 459–484. https://doi.org/10.1016/B978-0-12-823702-1.00002-5.

(11) Ingtipi, K.; Moholkar, V. S. Sonochemically Synthesized Lignin Nanoparticles and Its Application in the Development of Nanocomposite Hydrogel. *Mater. Today Proc.* **2019**, *17*, 362–370. https://doi.org/10.1016/j.matpr.2019.06.443.

(12) Yu, Z.; Liu, J.; Suryawanshi, A.; He, H.; Wang, Y.; Zhao, Y. Thermal Insulating and Fire-Retarding Behavior of Treated Cotton Fabrics with a Novel High Water-Retaining Hydrogel Used in Thermal Protective Clothing. *Cellulose* **2021**, *28* (4), 2581–2597. https://doi.org/https://doi.org/10.1007/s10570-021-03696-y.

(13) Liu, J.; Yu, Z.; He, H.; Wang, Y.; Zhao, Y. A Novel Flame-Retardant Composite Material Based on Calcium Alginate/Poly (Vinyl Alcohol)/Graphite Hydrogel: Thermal Kinetics, Combustion Behavior and Thermal Insulation

Performance. *Cellulose* **2021**, *28* (13), 8751–8769. https://doi.org/https://doi.org/10.1007/s10570-021-04047-7.

(14) Zhou, G.; Li, S.; Meng, Q.; Tian, F.; Sun, L. Synthesis and Performance of a New Temperature-Sensitive and Super-Absorbent Fire Prevention Hydrogel Based on Ultrasonic Method. *Colloids Surfaces A Physicochem. Eng. Asp.* **2022**, *640*, 128399. https://doi.org/10.1016/J.COLSURFA.2022.128399.

(15) Shi, M.; He, Z.; Zhang, Q.; Liang, Y.; Tang, H.; Hu, X.; Xue, D.; Wang, W.; Qi, G. Preparation of a Self-Adhesive Hydrogel and Research on Its Flame-Retardant Properties. *Fuel* **2022**, *324*, 124691. https://doi.org/10.1016/J.FUEL.2022.124691.

(16) Huang, Y.; Zhou, J.; Sun, P.; Zhang, L.; Qian, X.; Jiang, S.; Shi, C. Green, Tough and Highly Efficient Flame-Retardant Rigid Polyurethane Foam Enabled by Double Network Hydrogel Coatings. *Soft Matter* **2021**, *17* (46), 10555–10565. https://doi.org/10.1039/D1SM01213D.

(17) Fan, T.; Liu, Z.; Zhao, Y.; Li, M.; Li, X. Synthesis of a Tough Montmorillonite/Hydrogel Composites for Hot Work of Long-Distance Oil Pipelines. *Compos. Sci. Technol.* **2022**, *220*, 109268. https://doi.org/10.1016/J.COMPSCITECH.2022.109268.

(18) Vahidi, G.; Bajwa, D. S.; Shojaeiarani, J.; Stark, N.; Darabi, A. Advancements in Traditional and Nanosized Flame Retardants for Polymers—A Review. *J. Appl. Polym. Sci.* **2021**, *138* (12), 50050. https://doi.org/10.1002/APP.50050.

(19) Tao, Y.; Huang, C.; Lai, C.; Huang, C.; Yong, Q. Biomimetic Galactomannan/Bentonite/Graphene Oxide Film with Superior Mechanical and Fire Retardant Properties by Borate Cross-Linking. *Carbohydr. Polym.* **2020**, *245*, 116508. https://doi.org/10.1016/J.CARBPOL.2020.116508.

(20) Cheng, W. M.; Hu, X. M.; Zhao, Y. Y.; Wu, M. Y.; Hu, Z. X.; Yu, X. T. Preparation and Swelling Properties of Poly(Acrylic Acid-Co-Acrylamide) Composite Hydrogels. *E-Polymers* **2017**, *17* (1), 95–106. https://doi.org/https://doi.org/10.1515/epoly-2016-0250.

(21) Banerjee, H.; Sivaperuman Kalairaj, M.; Chang, T. H.; Fu, F.; Chen, P. Y.; Ren, H. Highly Stretchable Flame-Retardant Skin for Soft Robotics with Hydrogel-Montmorillonite-Based Translucent Matrix. *Soft Robot.* **2022**, *9* (1), 98–118. https://doi.org/https://doi.org/10.1089/soro.2020.0003.

(22) Jena, D. K.; Sahoo, P. K. Simultaneous Improvement of Mechanical and Fire

Retardant Properties of Synthesised Biodegradable Guar Gum-g-Poly(Butyl Acrylate)/Montmorillonite Nanocomposite. *Polym. Degrad. Stab.* **2018**, *154*, 37–45. https://doi.org/10.1016/J.POLYMDEGRADSTAB.2018.05.020.

(23) Shang, K.; Ye, D. D.; Kang, A. H.; Wang, Y. T.; Liao, W.; Xu, S.; Wang, Y. Z. Robust and Fire Retardant Borate-Crosslinked Poly (Vinyl Alcohol)/Montmorillonite Aerogel via Melt-Crosslink. *Polymer (Guildf).* **2017**, *131*, 111–119. https://doi.org/10.1016/J.POLYMER.2017.07.022.

(24) Nie, Y.; Mugaanire, I. T.; Guo, Y.; Wang, R.; Hou, K.; Zhu, M. A Hybrid Hydrogel/Textile Composite as Flame-Resistant Dress. *Prog. Nat. Sci. Mater. Int.* **2021**, *31* (1), 33–40. https://doi.org/10.1016/J.PNSC.2020.11.009.

(25) Geoffroy, L.; Davesne, A. lise; Bellayer, S.; Blanchard, F.; Richard, E.; Samyn, F.; Jimenez, M.; Bourbigot, S. 3D Printed Sandwich Materials Filled with Hydrogels for Extremely Low Heat Release Rate. *Polym. Degrad. Stab.* **2020**, *179*, 109269. https://doi.org/10.1016/J.POLYMDEGRADSTAB.2020.109269.

(26) Köklükaya, O.; Karlsson, R. M. P.; Carosio, F.; Wågberg, L. The Use of Model Cellulose Gel Beads to Clarify Flame-Retardant Characteristics of Layer-by-Layer Nanocoatings. *Carbohydr. Polym.* **2021**, *255*, 117468. https://doi.org/10.1016/J.CARBPOL.2020.117468.

(27) Nabipour, H.; Shi, H.; Wang, X.; Hu, X.; Song, L.; Hu, Y. Flame Retardant Cellulose-Based Hybrid Hydrogels for Firefighting and Fire Prevention. *Fire Technol.* **2022**, *58* (4), 2077–2091. https://doi.org/https://doi.org/10.1007/s10694-022-01237-y.

(28) Dang, C.; Huang, Z.; Chen, Y.; Zhou, S.; Feng, X.; Chen, G.; Dai, F.; Qi, H. Direct Dissolution of Cellulose in NaOH/Urea/α-Lipoic Acid Aqueous Solution to Fabricate All Biomass-Based Nitrogen, Sulfur Dual-Doped Hierarchical Porous Carbon Aerogels for Supercapacitors. *ACS Appl. Mater. Interfaces* **2020**, *12* (19), 21528–21538. https://doi.org/https://doi.org/10.1021/acsami.0c01537.

(29) Wei, Q. Y.; Lin, H.; Yang, B.; Li, L.; Zhang, L. Q.; Huang, H. D.; Zhong, G. J.; Xu, L.; Li, Z. M. Structure and Properties of All-Cellulose Composites Prepared by Controlling the Dissolution Temperature of a NaOH/Urea Solvent. *Ind. Eng. Chem. Res.* **2020**, *59* (22), 10428–10435. https://doi.org/https://doi.org/10.1021/acs.iecr.9b07075.

(30) Qiu, C.; Zhu, K.; Zhou, X.; Luo, L.; Zeng, J.; Huang, R.; Lu, A.; Liu, X.; Chen,

F.; Zhang, L.; Fu, Q. Influences of Coagulation Conditions on the Structure and Properties of Regenerated Cellulose Filaments via Wet-Spinning in LiOH/Urea Solvent. *ACS Sustain. Chem. Eng.* **2018**, *6* (3), 4056–4067. https://doi.org/https://doi.org/10.1021/acssuschemeng.7b04429.

(31) Seddiqi, H.; Oliaei, E.; Honarkar, H.; Jin, J.; Geonzon, L. C.; Bacabac, R. G.; Klein-Nulend, J. Cellulose and Its Derivatives: Towards Biomedical Applications. *Cellul. 2021 284* **2021**, *28* (4), 1893–1931. https://doi.org/10.1007/S10570-020-03674-W.

(32) Seera, S. D. K.; Kundu, D.; Banerjee, T. Physical and Chemical Crosslinked Microcrystalline Cellulose-Polyvinyl Alcohol Hydrogel: Freeze–Thaw Mediated Synthesis, Characterization and in Vitro Delivery of 5-Fluorouracil. *Cellulose* **2020**, *27* (11), 6521–6535. https://doi.org/https://doi.org/10.1007/s10570-020-03249-9.

(33) Li, Z.; Wang, D.; Bai, H.; Zhang, S.; Ma, P.; Dong, W. Photo-Crosslinking Strategy Constructs Adhesive, Superabsorbent, and Tough PVA-Based Hydrogel through Controlling the Balance of Cohesion and Adhesion. *Macromol. Mater. Eng.* **2020**, *305* (1), 1900623. https://doi.org/10.1002/MAME.201900623.

(34) Ishak, W. H. W.; Ahmad, I.; Ramli, S.; Amin, M. C. I. M. Gamma Irradiation-Assisted Synthesis of Cellulose Nanocrystal-Reinforced Gelatin Hydrogels. *Nanomater. 2018, Vol. 8, Page 749* **2018**, *8* (10), 749. https://doi.org/10.3390/NANO8100749.

(35) Salihu, R.; Abd Razak, S. I.; Ahmad Zawawi, N.; Rafiq Abdul Kadir, M.; Izzah Ismail, N.; Jusoh, N.; Riduan Mohamad, M.; Hasraf Mat Nayan, N. Citric Acid: A Green Cross-Linker of Biomaterials for Biomedical Applications. *Eur. Polym. J.* **2021**, *146*, 110271. https://doi.org/10.1016/J.EURPOLYMJ.2021.110271.

(36) Zainal, S. H.; Mohd, N. H.; Suhaili, N.; Anuar, F. H.; Lazim, A. M.; Othaman, R. Preparation of Cellulose-Based Hydrogel: A Review. *J. Mater. Res. Technol.* **2021**, *10*, 935–952. https://doi.org/10.1016/J.JMRT.2020.12.012.

(37) Salleh, K. M.; Zakaria, S.; Sajab, M. S.; Gan, S.; Chia, C. H.; Jaafar, S. N. S.; Amran, U. A. Chemically Crosslinked Hydrogel and Its Driving Force towards Superabsorbent Behaviour. *Int. J. Biol. Macromol.* **2018**, *118*, 1422–1430. https://doi.org/10.1016/J.IJBIOMAC.2018.06.159.

(38) Geng, H. A One-Step Approach to Make Cellulose-Based Hydrogels of

Various Transparency and Swelling Degrees. *Carbohydr. Polym.* **2018**, *186*, 208–216. https://doi.org/10.1016/J.CARBPOL.2018.01.031.

(39) Yang, J.; Medronho, B.; Lindman, B.; Norgren, M. Simple One Pot Preparation of Chemical Hydrogels from Cellulose Dissolved in Cold LiOH/Urea. *Polym. 2020, Vol. 12, Page 373* **2020**, *12* (2), 373. https://doi.org/10.3390/POLYM12020373.

(40) Ingtipi, K.; Moholkar, V. S. Sonochemically Synthesized Lignin Nanoparticles and Its Application in the Development of Nanocomposite Hydrogel. *Mater. Today Proc.* **2019**, *17*, 362–370. https://doi.org/10.1016/J.MATPR.2019.06.443.

(41) Karami, P.; Nasrollahzadeh, N.; Wyss, C.; O'Sullivan, A.; Broome, M.; Procter, P.; Bourban, P. E.; Moser, C.; Pioletti, D. P. An Intrinsically-Adhesive Family of Injectable and Photo-Curable Hydrogels with Functional Physicochemical Performance for Regenerative Medicine. *Macromol. Rapid Commun.* **2021**, *42* (10). https://doi.org/10.1002/MARC.202000660.

(42) Wang, Y.; Yin, T.; Suo, Z. Polyacrylamide Hydrogels. III. Lap Shear and Peel. *J. Mech. Phys. Solids* **2021**, *150*, 104348. https://doi.org/10.1016/J.JMPS.2021.104348.

(43) Richbourg, N. R.; Peppas, N. A. The Swollen Polymer Network Hypothesis: Quantitative Models of Hydrogel Swelling, Stiffness, and Solute Transport. *Prog. Polym. Sci.* **2020**, *105*, 101243. https://doi.org/10.1016/j.progpolymsci.2020.101243.

(44) Ben Ammar, N. E.; Saied, T. T.; Barbouche, M.; Hosni, F.; Hamzaoui, A. H.; Şen, M.; Elhouda, N.; Ammar, B.; Saied, T. T. A Comparative Study between Three Different Methods of Hydrogel Network Characterization: Effect of Composition on the Crosslinking Properties Using Sol–Gel, Rheological and Mechanical Analyses. *Polym. Bull.* **2018**, *75.9* (September), 3825–3841. https://doi.org/10.1007/s00289-017-2239-0.

(45) Sen, M.; Yakar, A.; Güven, O. Determination of Average Molecular Weight between Cross-Links ($\bar{M}(c)$) from Swelling Behaviours of Diprotic Acid-Containing Hydrogels. *Polymer (Guildf).* **1999**, *40* (11), 2969–2974. https://doi.org/10.1016/S0032-3861(98)00251-1.

(46) Gan, Y.; Li, P.; Wang, L.; Mo, X.; Song, L.; Xu, Y.; Zhao, C.; Ouyang, B.; Tu, B.; Luo, L.; Zhu, L.; Dong, S.; Li, F.; Zhou, Q. An Interpenetrating Network-

Strengthened and Toughened Hydrogel That Supports Cell-Based Nucleus Pulposus Regeneration. *Biomaterials* **2017**, *136*, 12–28. https://doi.org/10.1016/j.biomaterials.2017.05.017.

(47) Arslan, F.; Benli, A.; Karatas, M. Effect of High Temperature on the Performance of Self-Compacting Mortars Produced with Calcined Kaolin and Metakaolin. *Constr. Build. Mater.* **2020**, *256*, 119497. https://doi.org/10.1016/J.CONBUILDMAT.2020.119497.

(48) Chang, L.; Xu, L.; Liu, Y.; Qiu, D. Superabsorbent Polymers Used for Agricultural Water Retention. *Polym. Test.* **2021**, *94*, 107021. https://doi.org/10.1016/J.POLYMERTESTING.2020.107021.

(49) Chavali, R. V. P.; Ponnapureddy, H. P. R. Swelling and Compressibility Characteristics of Bentonite and Kaolin Clay Subjected to Inorganic Acid Contamination. *https://doi.org/10.1080/19386362.2017.1299418* **2017**, *12* (5), 500–506. https://doi.org/10.1080/19386362.2017.1299418.

(50) Muthulakshmi, L.; Varada Rajalu, A.; Kaliaraj, G. S.; Siengchin, S.; Parameswaranpillai, J.; Saraswathi, R. Preparation of Cellulose/Copper Nanoparticles Bionanocomposite Films Using a Bioflocculant Polymer as Reducing Agent for Antibacterial and Anticorrosion Applications. *Compos. Part B Eng.* **2019**, *175*, 107177. https://doi.org/10.1016/J.COMPOSITESB.2019.107177.

(51) Zhang, Z.; Li, X.; Ma, Z.; Ning, H.; Zhang, D.; Wang, Y. A Facile and Green Strategy to Simultaneously Enhance the Flame Retardant and Mechanical Properties of Poly(Vinyl Alcohol) by Introduction of a Bio-Based Polyelectrolyte Complex Formed by Chitosan and Phytic Acid. *Dalt. Trans.* **2020**, *49* (32), 11226–11237. https://doi.org/10.1039/D0DT02019B.

(52) Xiao, G.; Li, F.; Li, Y.; Chen, C.; Chen, C.; Liu, Q.; Chen, W. A Novel Biomass Material Composite Hydrogel Based on Sodium Alginate. *Colloids Surfaces A Physicochem. Eng. Asp.* **2022**, *648*, 129383. https://doi.org/10.1016/J.COLSURFA.2022.129383.

CHAPTER 6

CONCLUSION AND FUTURE WORK

CHAPTER 6

CONCLUSION AND FUTURE WORK

6.1 Summary of the major outcomes

This thesis has presented investigations in the formulation of three types of hybrid composite hydrogels using biomass derived lignin nanoparticles and cellulose as hydrogel matrix. These hydrogels have potential applications as conductive hydrogels and fire retardant hydrogels. The extracted components, formulated nanoparticles, and composite hydrogels were extensively characterized using standard characterization techniques (viz. FTIR, FESEM, FETEM, and TGA). Further, the conductivity of hydrogels was measured through EIS. Fire retardant hydrogels were characterized by performing CCT, Vertical flammability tests (VFT), Open fire test (OFT), and calculating the limiting oxygen index (LOI) of the hydrogel samples. The major outcome of this thesis research can be summarized as follows:

- In Chapter 2, we successfully extracted lignin and cellulose from Arundo Donax and the extracts were of high purity. The biomass was pretreated with dilute (0.5M) HCl and then treated with alkali to extract lignin and cellulose from biomass. The pretreatment process reveals the extraction of higher purity lignin (~85%) than the sole alkaline method (~45%). The extracted components were of low sulfur and nitrogen content (confirmed by elemental analysis). Further, the extracted lignin and cellulose were characterized by FTIR, FESEM, TGA, and GPC was performed for estimation of molecular weights. FTIR confirmed the presence of chemical groups which corroborate

with the literature. FESEM images presented irregular shapes of lignin particles whereas fibers of cellulose with ~ 80 μm widths were confirmed. TGA confirmed that the residue obtained at the end of the thermal analysis was more (~40 wt.%) in the case of lignin than cellulose (~3 wt. %). The molecular weight was estimated to be M_w 3357 g mol^{-1} and 353470 g mol^{-1}, respectively. The biomass-extracted components were further blended with other biopolymers (viz. xanthan gum and chitosan) and synthetic polymer, PVA to formulate hydrogel composites which are elaborately discussed in the succeeding chapters.

- Chapter 3 reports the synthesis of physically crosslinked PVA–CS hydrogel doped with ultrasound-aided LNP-dispersed-CNTs. Initially, the microsized lignin particles (~1000 μm, MW 3357 g mol^{-1}) were reduced to 10–50 nm via sonication (250 W, 3 h). 1 wt. % CNTs were added to the resulting solution and further sonicated for 1 h. To aid the dispersion by reducing the surface tension, acetone (10 ml) was added to make the total volume of 50 ml. Lastly, LNP-dispersed-CNTs were blended with PVA–CS and freeze-thawed (–20 ^{0}C freeze and 4 h thaw) for 3 consecutive cycles to obtain PVA–CS hybrid conductive hydrogels. Further, the thermal stability of hydrogels was characterized by TGA; rheological studies were carried out to test its mechanical stability. Post addition of nanoparticles, the CS–PVA hydrogel revealed a significant increase in thermal stability. Performing EIS analysis verified conductive nature of the formulated hydrogels. Sonication of lignin particles reduced the lignin particles to nano-sized (LNP). These particles (1wt %) aided by further sonication were utilized to disperse 1wt% of MCNTs in water. Further, the resultant solution was introduced to PVA –CS solution to

obtain conductive hydrogel.

- In Chapter 4, we formulated acetone–water co-solvent produced LNPs doped PVA–xanthan gum based hydrogel which was crosslinked by borax in basified medium. The hydrogels were characterized using FTIR, FESEM, and thermogravimetric analysis. The nature of crosslinking and stability of the hydrogels was characterized by evaluating the swelling ratio, water retention ability and finally calculating the network parameters. Different hydrogels synthesized in this study with different combinations (or compositions) of the components, viz. PX3, PX3B0.4N2, PX3B0.4N2L5, and PX3B0.4N2L20 revealed enhanced structural and fire retardant properties. PX3B0.4N2 hydrogel showed better rheological properties as compared to PX3B0.4 hydrogels, which confirms a stronger gelation network induced in presence of NaOH. Addition of lignin nanoparticles facilitated the tuning of the viscoelastic properties of the hydrogels. Higher concentrations of lignin (20% v/v) imparted viscous nature to the hydrogel. These traits allowed the hydrogels to accommodate around 96% of water in their network structure. Sequentially, the water retention ability of the hydrogels also improved. However, a more compact structure of PXB0.4N2L20 resulted in low water absorption and retention. Among different hydrogels, the best combination of properties was achieved for hydrogel PX3B0.4N2L20, viz. elastic modulus (G′) = 23428.57 Pa (indicating strong elastic network), crosslinking density = 870350.12 kmol m^{-3} and mesh size of 5.60 nm. Additionally, the presence of lignin nanoparticles improved the char formation of the hydrogels (34.61 wt% for PX3B0.4N2L20), which helped in enhancing fire retardancy. The hydrogel coated cotton cloth demonstrated a delayed burning process. LOI for cotton

cloth improved from 20% to 39% after coating of PX3B0.4N2L20 hydrogel. The thermal degradation temperature of the formulated hydrogels was around 280 to 300 ºC, which is higher than the actual operating temperature (85º to 285 ºC) measured during the fire operations. Kinetic analysis of TGA data yielded the highest activation energy of 493.8 kJ mol^{-1} for hydrogel, which corroborated the LOI test results. The cone calorimeter tests of PX3B0.4N2L20 hydrogel also revealed the least peak heat release rate of 90.3 ±10 kW m^{-2} and the least total heat release rate of 1.56 ± 4 MJ m^{-2}. The LOI, vertical burning, TGA, and kinetic analysis results were in accordance with the CCT's HRR and THR curves. Thus, the present study has demonstrated the potential of eco-friendly PVA-based hydrogels as effective fire retardant coatings.

- Chapter 5 demonstrates the synthesis of cellulose kaolin based hydrogel which was crosslinked by MBA. The hydrogels synthesized could easily absorb and retain an ample amount of water for 24 h (96%, for CM2 and 55% for CM2K2 hydrogels). Hence, the swelling ability of the hydrogels varied inversely with kaolin addition. The hydrogels synthesized exhibited fast swelling and reached equilibrium within an hour of immersion. The combustion behavior was evaluated by performing cone calorimeter test (CCT), limiting oxygen Index (LOI) test, vertical flammability test (VFT), and open fire test (OFT). Hydrogels with 2% w/v kaolin revealed the lowest heat release rate (HRR) of 26.60 kJ m^{-2}, total heat release rate (THR) of 0.9 MJ $m^{-2,}$ and the highest ignition time of 19.67s. LOI of cotton fabric surged from 20% to 34.6%. Kinetic analysis using the isoconversional model yielded the highest activation energy of 216 kJ mol^{-1} for 2% w/v kaolin hydrogel, which is in concurrence

with LOI test. VFT and OFT tests validated the delay in burning process and the formation of char layers which protected the underlying layer of cotton from burning. In summary, cellulose-based hydrogels synthesized in this study are effective green fire retardant coatings for flammable materials. The TGA tests revealed 63 wt% char production after the complete thermal conversion of the hydrogel. Thus, the synergistic effect of water content of hydrogel matrix, the char formation, and the thermal resistance of kaolin effectively retards the ignition and flame propagation of the surface over which the hydrogel is applied. This study has essentially demonstrated the synthesis of an effective fire retardant hydrogel from sustainable materials, viz. cellulose, and kaolin, for application on cotton fabrics as a coating.

6.2 Scope for future research

This thesis has focused on formulating sustainable biocomposite hydrogels for application as conducting hydrogels and fire retardants. The current studies can be further investigated in the following new directions:

1. The idea of valorization of waste biomass used in this work can be further expanded. Extraction of lignin, cellulose, and hemicellulose from a single biomass may not produce an adequate amount of extracted components and a large amount of biomass is required for extraction purposes. Blends of different biomass waste can be gathered and their components extracted. Lastly, the extracted components can be valorized to formulate hydrogels.
2. In the case of formulating conductive hydrogels, increasing the conductivity is the main focus. MXene is the new material utilized to develop high-conducting hydrogels. However, a major drawback of exfoliating MXene is a

concern. Ultrasound can be utilized to obtain exfoliated MXene to produce highly conducting PVA–CS hydrogels.

3. Lignin is a high char producing component of biomass which is extensively utilized in the current work to produce lignin based fire retardants. Phosphorus and nitrogen are two functionalities that have been explored in flame retardant applications. Therefore, lignin can be modified with phosphorus and nitrogen to produce fire retardants.
4. Cellulose is highly flammable and in this work, we have transformed cellulose into cellulose hydrogel to remediate its flammability. Incorporating clay particles (kaolin) further improved the fire retardancy of cellulose. Besides kaolin, other clay particles like bentonite and montmorillonite can be incorporated to formulate hydrogel fire retardants.
5. Hemicellulose is a high char forming agent like lignin. These can be extracted from biomass and valorized in formulating high char forming fire retarding hydrogels
6. Bio based polymers and compounds such as alginate, protein, tannins, casein, and lipids can be further investigated to formulate fire retardant hydrogels.

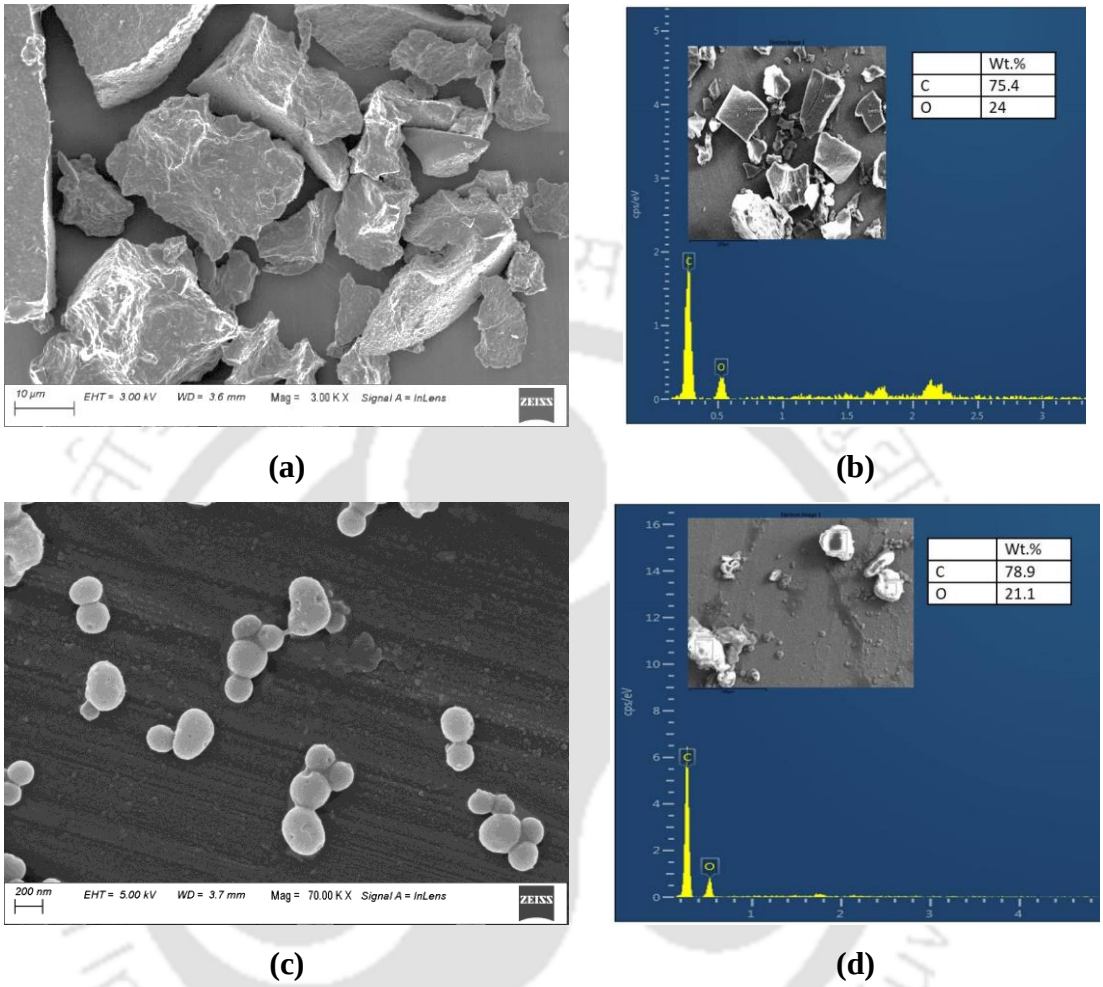

Figure A1.1 (a) FESEM and b) EDX micrographs of pristine lignin c) FESEM and d)EDX of LNPs

Table A1.1. Elemental composition analysis of pristine lignin and LNPs calculated by XPS

Sample	Elementary composition (Atomic %)		C/O
	C	O	
Pristine lignin	75.74	24.23	3.12
LNPs	75.32	24.68	3.05

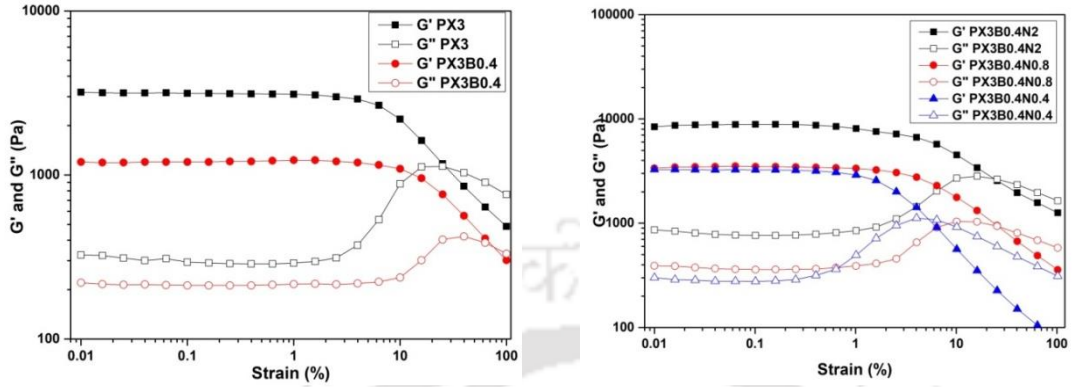

(a) **(b)**

Figure A1.2 Amplitude sweep (a) PX3 and PX3B0.4hydrogels (b) PX3B0.4N0.4, PX3B0.4N0.8 and PX3B0.4N2 hydrogels

Table A1.2 Network parameters

Composition	m (g)	S (cm^{-2})	t (mm)	ρ (g cm^{-3})	ρ_w (g cm^{-3})	w (g)	G' (Pa)	V_{2m}	V_{2r}	$(V_{2m})^{1/3}$	$(V_{2r})^{2/3}$	$\overline{M_c}$ (kg/mol)	Ve (kmol m^{-3})	ξ (nm)
PX3	0.14±0.2	1±0.1	0.13±0.1	2.73±2	1	0.61±0.2	3338.57±100	0.36±0.1	0.06±0.5	0.71±0.2	0.15±0.3	70.54±2	38737.69±20	10.72±0.2
PX3B0.4	0.13±0.1	1±0.1	0.11±0.1	12.26±1	1	0.44±0.1	1659.05± 200	0.06±0.3	0.01±0.3	0.39±0.1	0.05±0.2	125.18±5	97970.17±10	13.54±0.1
PX3B0.4N0.4	0.14±0.12	1±0.14	0.12±0.1	11.67±0.5	1	0.67±0.2	2643.34± 150	0.15±0.4	0.01±0.1	0.53±0.6	0.06±0.2	110.31±3	105766.45±50	11.59±0.14
PX3B0.4N0.8	0.14±0.2	1±0.2	0.12±0.1	11.67±0.8	1	0.69±0.2	3150.00± 50	0.16±0.2	0.01±0.9	0.54±0.4	0.06±0.1	94.99±2	122824.32±15	10.93±0.2
PX3B0.4N2	0.13±0.2	1±0.18	0.11±0.1	11.82±1	1	0.94±0.2	4926.90± 200	0.57±0.1	0.01±0.2	0.83±0.2	0.05±0.8	88.40±1	133689.37±30	9.42±0.25
PX3B0.4N2L5	0.12±0.1	1±0.1	0.12±0.1	10.00±2	1	0.23±0.1	33095.24±125	0.03±0.5	0.01±0.1	0.31±0.1	0.06±0.6	4.34±0.9	2301647.95±20	4.99±0.1
PBXN2L20	0.11±0.2	1±0.3	0.11±0.2	10.48±0.1	1	0.78±0.2	23428.57± 70	0.25±0.1	0.01±0.1	0.63±0.2	0.05±0.1	12.04±4	870350.12±10	5.60±0.13

m - dry hydrogel weight, S - cross sectional area, t – average thickness of the hydrogel film, ρ - dry gel density, ρ_w - density of water, w - weight of the swollen hydrogel, G' – elastic modulus, V_{2m}, - volume fraction of polymer at swollen state, V_{2r} - volume fraction of polymer before swelling, $\overline{M_c}$ - molecular weight between crosslink, Ve crosslnk density, ξ - mesh size

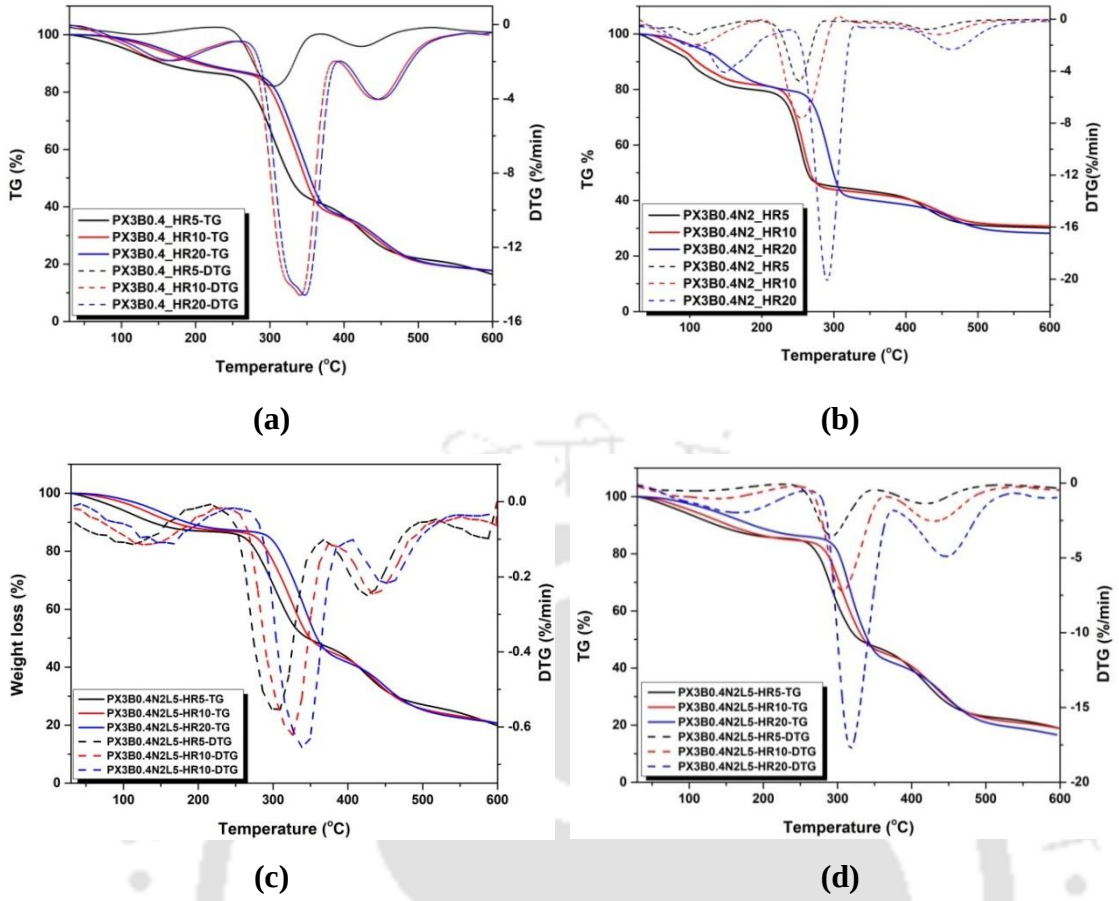

Figure A1.3 Thermograms of (a) PX3B0.4, (b) PX3B0.4N2, (c) PX3B0.4N2L5 and (d) PX3B0.4N2L20 at heating rate 5, 10 and 20 ºC

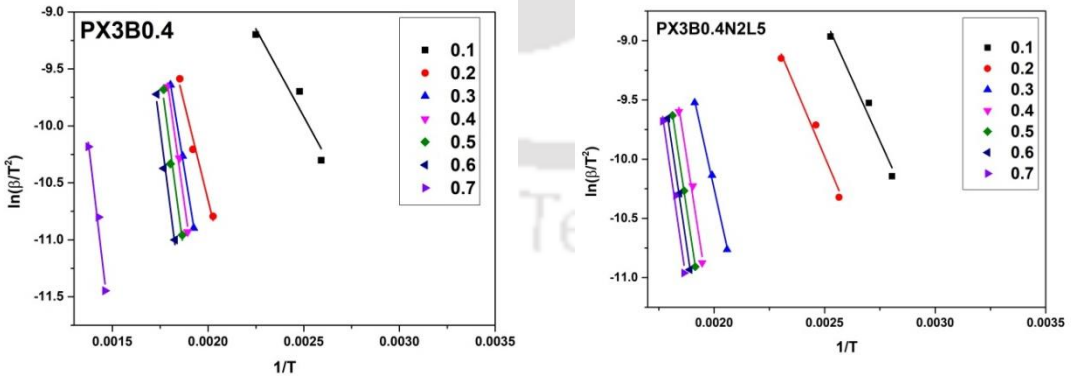

Figure A1.4 Kinetic fitting of thermograms using KAS model for (a) PX3B0.4 (b) PX3B0.4N2L5

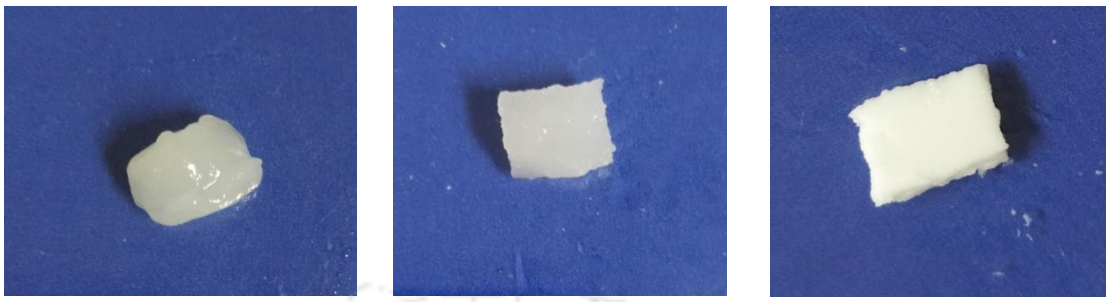

(a) **(b)** **(c)**

Figure A2.1 Formulated cellulose hydrogel (a) CM1 (b) CM2 and (c) CM2K2

Table A2.1 Number-average (M_n) and weight-average (M_W) molecular weight, degree of polymerization (DP), polydispersity index (PDI) and crystalinity index (CI) of cellulose

Sample	Mn (g/mol)	DP_n	Mw (g/mol)	DP_w	PDI	CI %
Cellulose	81571	503	353470	2182	4.3	52

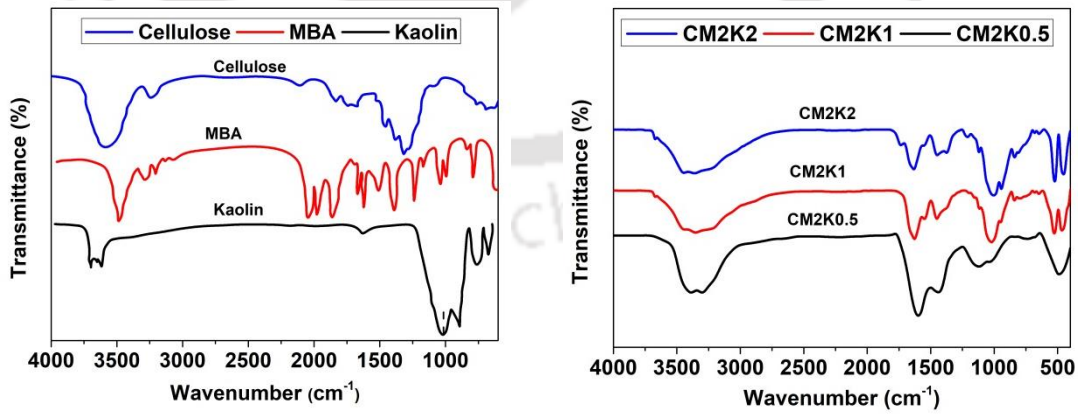

(a) **(b)**

Figure A2.2 FTIR spectrum of cellulose, (a) MBA and kaolin and (b) CMK hydrogels with C:M ratio 1:2.

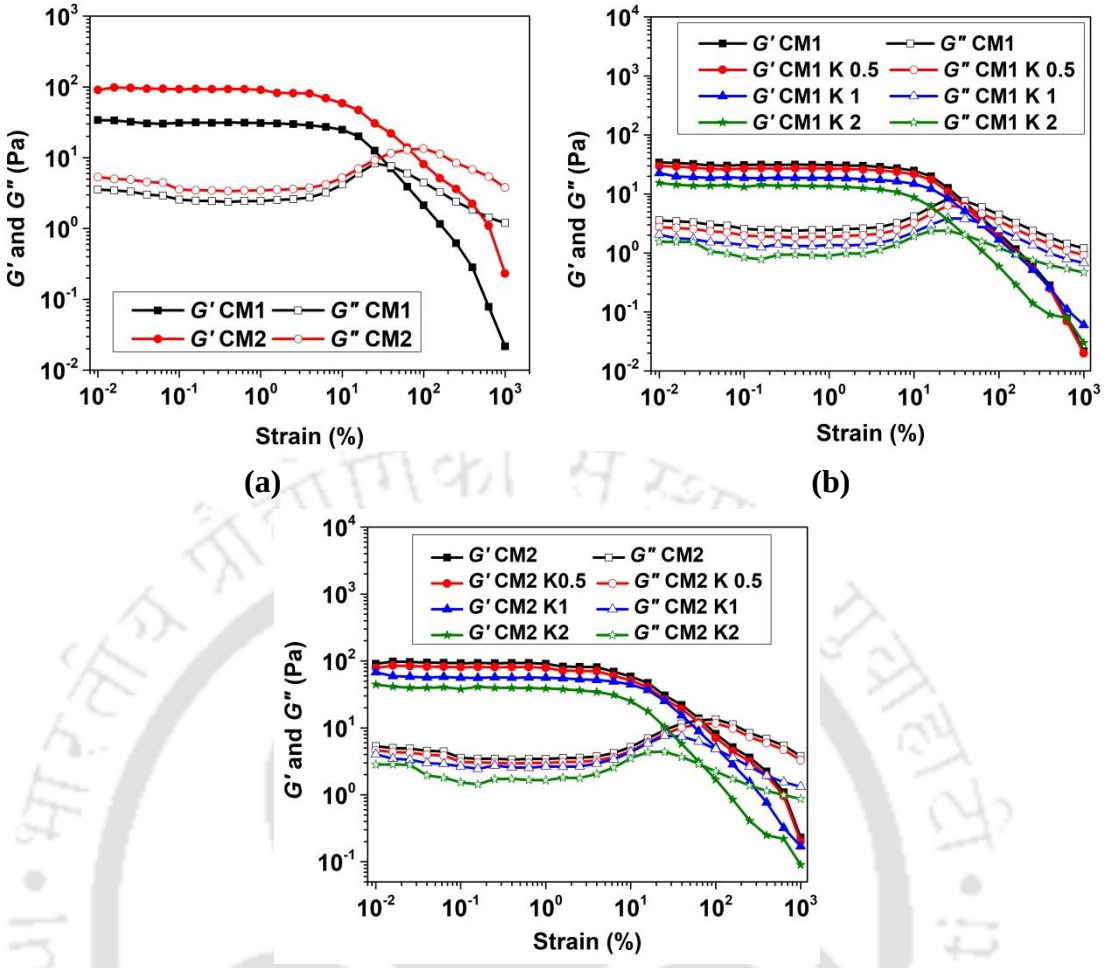

Figure A2.3 Amplitude sweep of cellulose hydrogel with varying MBA ratio (1:1 and 1:2 with respect to cellulose) and kaolin concentration (0.5, 1 and 2 w/v %)

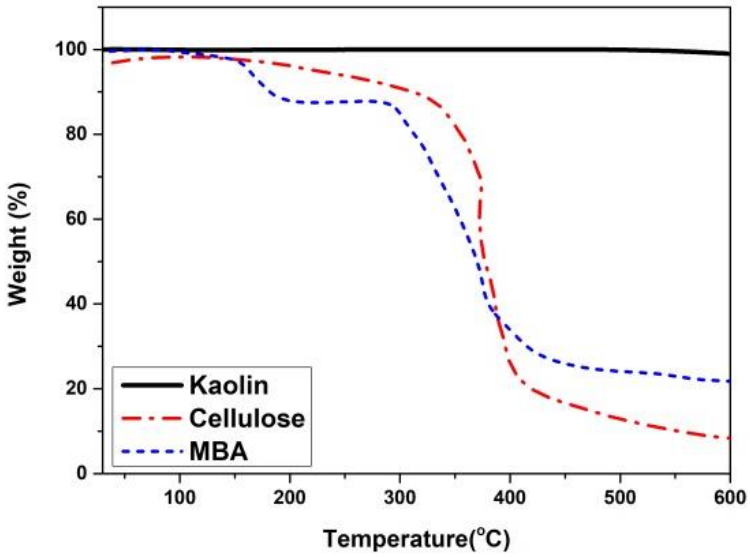

Figure A2.4 TGA curve of kaolin, cellulose and MBA

Table A2.2 Degradation range of cellulose kaolin hydrogel from TGA

Sample	Primary degradation		Secondary degradation		Residue at 600ºC (wt. %)
	Temperature range (ºC)	Weight loss (%)	Temperature range (ºC)	Weight loss (%)	
CM1K0.5	30–178	7.1	180–371	80.66	36.86
CM2K0.5	30–179	5.15	179–364	40.43	41.32
CM1K1	30–137	17.52	138–341	30.54	39.36
CM2K1	30–137	15.81	219–334	25.53	45.93
CM1K2	30–130	16.31	130–340	20.96	52.37
CM2K2	30–225	12.01	225–362	15.44	63.65

Table A2.3 Network parameters

Composition	m (mg)	S (cm^2)	t (mm)	ρ ($g\ cm^{-3}$)	ρ_w ($g\ cm^{-3}$)	w (g)	G' Pa	V_{2m}	V_{2r}	$(V_{2m})^{1/3}$	$(V_{2r})^{2/3}$	M_c ($kg\ mol^{-1}$)	V_e ($kmol\ m^{-3}$)	ξ (nm)
CM1	1±0.2	1	0.10±0.02	0.19±0.02	1	0.04±0.001	28.76± 3.5	0.18±0.01	0.01±0.01	0.56±0.01	0.05±0.01	142.17±6.1	1336.44±102	52.30±4.5
CM1K0.5	6±2.8	1	0.12±0.01	0.50±0.01	1	0.17±0.003	23.38± 2.8	0.29±0.01	0.01±0.01	0.66±0.01	0.05±0.01	612.65±106	816.12±50	56.03±6.2
CM1K1	5±1.4	1	0.13±0.01	0.38±0.02	1	0.13±0.002	16.41± 2.4	0.29±0.01	0.01±0.01	0.66±0.01	0.05±0.01	701.25±99	548.47±30	63.06±6.8
CM1K2	5±1.2	1	0.11±0.02	0.47±0.02	1	0.14±0.004	11.18± 1.7	0.25±0.01	0.01±0.01	0.63±0.01	0.05±0.01	1061.73±121	444.27±15	71.67±7.0
CM2	10±2.2	1	0.12±0.02	0.83±0.03	1	0.06±0.001	89.16± 10.8	0.07±0.01	0.01±0.01	0.41±0.01	0.05±0.01	164.29±7	5072.27±200	35.87±1.0
CM2K0.5	10±2.0	1	0.12±0.02	0.83±0.03	1	0.09±0.001	72.49± 8.8	0.11±0.01	0.01±0.01	0.48±0.01	0.05±0.01	236.53±10	3523.14±175	38.43±1.5
CM2K1	9±2.4	1	0.11±0.01	0.82±0.02	1	0.10±0.001	53.77± 8.0	0.11±0.01	0.01±0.01	0.48±0.01	0.05±0.01	300.71±50	2720.79±130	42.45±2.2
CM2K2	8±1.5	1	0.11±0.01	0.73±0.01	1	0.32±0.005	35.91± 5.7	0.40±0.01	0.01±0.01	0.74±0.01	0.05±0.01	607.21±78	1197.73±100	48.57±3.3

m – dry hydrogel weight, S – cross sectional area, t – average thickness of the hydrogel film, ρ – dry gel density, ρ_w – density of water, w – weight of the swollen hydrogel, G' – elastic modulus, V_{2m} – volume fraction of polymer at swollen state, V_{2r} – volume fraction of polymer before swelling, M_c – molecular eight between crosslink, V_e –crosslink density, ξ – mesh size

RESEARCH OUTPUT

Publications

- **K. Ingtipi**, and V. S. Moholkar. "Sonochemically synthesized lignin nanoparticles and its application in the development of nanocomposite hydrogel." Materials Today: Proceedings 17 (2019): 362-370.
- **K. Ingtipi**, B. J. Choudhury and V. S. Moholkar. “Development of NaOH-borax crosslinked PVA-Xanthan gum-Lignin hydrogel as green fire retardant coating.” Progess in Organic coating 174 (2022): 107268
- **K. Ingtipi**, B. J. Choudhury and V. S. Moholkar. “Kaolin embedded cellulose hydrogel with tunable properties as green fire retardant”. Carbohydrate Polymers 313 (2023): 120871.
- **K. Ingtipi**, B. J. Choudhury and V. S. Moholkar. “Ultrasound assisted lignin-dispersed MWCNT doped flexible PVA–Chitosan composite hydrogel”. Materials Today Communications 35 (2023): 105676.

Book chapter

- **K. Ingtipi**, U. Boro, and V. S. Moholkar. "Lignin in nanocomposite hydrogels." Micro and Nanolignin in Aqueous Dispersions and Polymers. Elsevier, 2022. 459-484.

Other publication

- B. J. Choudhury, **K. Ingtipi**, and V. S. Moholkar. "Improved energy density of reduced graphene oxide based aqueous symmetric supercapacitors in redox-active and “water-in-salt” electrolytes." Journal of Energy Storage 52 (2022): 105006.